OCS Study
BOEM 2022-038

Data Synthesis and Predictive Modeling of Deep-sea Coral and Hardbottom Habitats Offshore of the Southeastern US: Guiding Efficient Discovery and Protection of Sensitive Benthic Areas

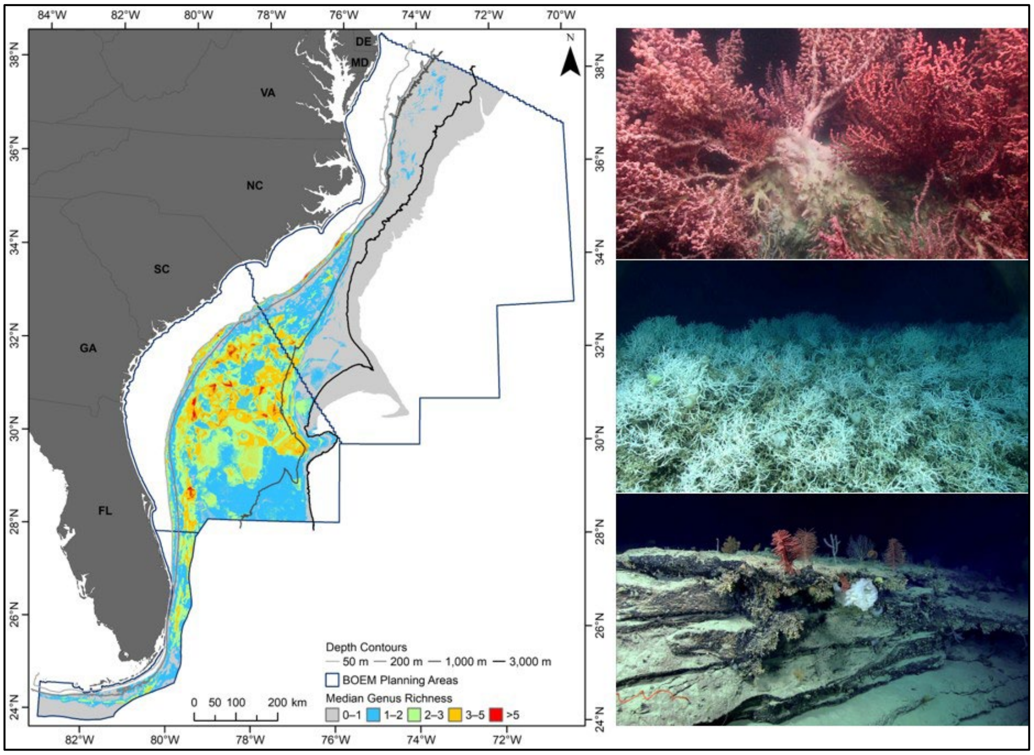

US Department of the Interior
Bureau of Ocean Energy Management
Gulf of Mexico Regional Office

OCS Study
BOEM 2022-038

Data Synthesis and Predictive Modeling of Deep-sea Coral and Hardbottom Habitats Offshore of the Southeastern US: Guiding Efficient Discovery and Protection of Sensitive Benthic Areas

Authors

Matthew Poti
Holly F. Goyert
Enrique J Salgado
Rachel Bassett
Michael Coyne
Arliss J. Winship
Peter J Etnoyer
Thomas F. Hourigan
Heather M. Coleman
John Christensen

June 2022

Prepared under BOEM Interagency Agreement M16PG00010
by
National Oceanic and Atmospheric Administration
National Centers for Coastal Ocean Science, Marine Spatial Ecology Division
1305 East-West Highway, SSMC4-N/SCI-1
Silver Spring, MD 20910

Published by

US Department of the Interior
Bureau of Ocean Energy Management
Gulf of Mexico Regional Office

DISCLAIMER

This study was funded, in part, by the US Department of the Interior, Bureau of Ocean Energy Management (BOEM), Environmental Studies Program, Washington, DC, through Interagency Agreement Number M16PG00010 with the National Oceanic and Atmospheric Administration (NOAA), National Ocean Service (NOS), National Centers for Coastal Ocean Science (NCCOS). This report has been technically reviewed by BOEM, and it has been approved for publication. The views and conclusions contained in this document are those of the authors and should not be interpreted as representing the opinions or policies of BOEM, nor does mention of trade names or commercial products constitute endorsement or recommendation for use.

REPORT AVAILABILITY

To download a PDF file of this report, go to the US Department of the Interior, Bureau of Ocean Energy Management Data and Information Systems webpage (http://www.boem.gov/Environmental-Studies-EnvData/), click on the link for the Environmental Studies Program Information System (ESPIS), and search on 2022-038. The report is also available at the National Technical Reports Library at https://ntrl.ntis.gov/NTRL/.

CITATION

Poti M, Goyert HF, Salgado EJ, Bassett R, Coyne M, Winship AJ, Etnoyer PJ, Hourigan TF, Coleman HM, Christensen J. 2022. Data synthesis and predictive modeling of deep-sea coral and hardbottom habitats offshore of the southeastern US: guiding efficient discovery and protection of sensitive benthic areas. New Orleans (LA): US Department of the Interior, Bureau of Ocean Energy Management. 224 p. Contract No.: M16PG00010. Report No.: OCS Study BOEM 2022-038.

ABOUT THE COVER

Left: Map of the predicted genus richness from the multi-taxon model developed in this study. Top right: A close view of the wall of deep-sea corals, mostly bubblegum coral (*Paragorgia* sp.), seen towards the end of dive 18 at Baltimore Canyon during Windows to the Deep 2019. Middle right: Dense fields of *Lophelia pertusa*, a common reef-building coral, found on the Blake Plateau Knolls. Middle left: The loose sediments on the top of this boulder, seen on dive 11 of the 2019 Southeastern US Deep-Sea Exploration, are rimmed by an outer layer of more durable encrusted limestone. This suggests that the feature was once taller, but is eroding over time. Bottom right: Before Windows to the Deep 2018, this section of the Blake Escarpment appeared to be an area of low slope with no distinct features. Images captured during the expedition show sponges, corals, urchins, and other organisms populating outcrops of hard substrate on the seafloor. All photos credited to NOAA Office of Ocean Exploration and Research.

ACKNOWLEDGMENTS

We dedicate this report to Brian Kinlan, our friend and colleague, who passed away before this study was completed. Brian was instrumental in the development of this study and in the use of spatial predictive models to identify potential locations of deep-sea coral habitats in support of management, research, and exploration.

We thank the many scientists who contributed their data, time, and expertise over the course of this study. Sandra Brooke (Florida State University), Erik Cordes (Temple University), Stephanie Farrington (Harbor Branch Oceanographic Institute at Florida Atlantic University), John Reed (Harbor Branch Oceanographic Institute at Florida Atlantic University), Carolyn Ruppel (United States Geological Survey, formerly Georgia Institute of Technology), George Sedberry (retired, formerly NOAA Office of National Marine Sanctuaries and South Carolina Department of Natural Resources), Timothy Snoots (South Carolina Department of Natural Resources), and Geoffrey Timms (South Carolina Department of Natural Resources) provided data and support in the development of the database of presence-absence records for deep-sea corals and hardbottom habitats compiled as part of this study. Jason Chaytor (United States Geological Survey) and Scott Harris (College of Charleston) provided bathymetry data from multibeam surveys for the compilation of bathymetry data used in the development of environmental predictors depicting depth and seafloor topography. Datasets depicting surficial sediment characteristics were developed by Christopher Jenkins (University of Colorado Boulder) for a study funded by the Bureau of Ocean Energy Management through Interagency Agreement Number M16PG0005. Sandra Brooke (Florida State University) and Martha Nizinski (NOAA National Systematics Laboratory) reviewed maps of predicted deep-sea coral occurrence and provided valuable advice and feedback. Alicia Caporaso (BOEM), Mark Mueller (BOEM), Michelle Nannen (BOEM), Stephanie Sharuga (BOEM), Mariana Steen (BOEM), and Shay Viehman (NOAA NCCOS) reviewed this report and provided helpful comments and suggestions.

This study was funded by the Bureau of Ocean Energy Management through Interagency Agreement Number M16PG00010 with the US Department of Commerce, National Oceanic and Atmospheric Administration, National Ocean Service, National Centers for Coastal Ocean Science. Michael Coyne, Holly Goyert, and Arliss Winship were supported by NOAA Contracts No. EA133C17BA0062 with CSS, Inc. Rachel Bassett and Enrique Salgado were supported by NOAA Contracts No. EA133C17BA0049 with CSS, Inc.

Contents

List of Figures

List of Tables

List of Abbreviations and Acronyms

Short Form	Long Form
arcsec	arcsecond
AUC	area under the receiver operating characteristic curve
AUV	autonomous underwater vehicle
BOEM	Bureau of Ocean Energy Management
CHAPC	Coral Habitat Area of Particular Concern
CV	coefficient of variation
DEM	digital elevation model
DOI	Department of the Interior
DSC	deep-sea coral
GEBCO	General Bathymetric Chart of the Oceans
HOV	human-occupied vehicle
HYCOM	HYbrid Coordinate Ocean Model
IDW	inverse distance weighting
m	meter
MCMC	Markov chain Monte Carlo
MLD	mixed layer depth
MODIS	Moderate Resolution Imaging Spectroradiometer
NASA	National Aeronautics and Space Administration
NCCOS	National Centers for Coastal Ocean Science
NCEI	National Centers for Environmental Information
NEPA	National Environmental Policy Act
NMFS	National Marine Fisheries Service
NMNH	National Museum of Natural History
NOAA	National Oceanic and Atmospheric Administration
NOS	National Ocean Service
OCS	Outer Continental Shelf
ROV	Remotely operated vehicle
SeaWiFS	Sea-Viewing Wide Field-of-View Sensor
USGS	US Geological Survey
VIF	variance inflation factor
VIIRS	visible infrared imaging spectroradiometer

1 Introduction

Deep-sea corals (DSCs, also known as cold-water corals or deepwater corals) and exposed hardbottom areas (hardbottom habitats) are capable of supporting diverse benthic communities. Many DSCs form complex three-dimensional structures that increase local biodiversity by providing microhabitats that are used by other species such as fishes, crustaceans, and echinoderms (Roberts et al. 2009; Buhl-Mortensen et al. 2010). Hardbottom habitats provide available surface for attachment of sessile invertebrates, including most DSCs. In addition to supporting diverse invertebrate communities, hardbottom habitats may be associated with greater diversity and abundance of large fish, particularly at sites with high relief (e.g., rocky outcrops; Quattrini et al. 2004; Kendall et al. 2009; Taylor et al. 2016). The US Department of the Interior Bureau of Ocean Energy Management (BOEM) has identified a need for information about the spatial distributions of sensitive benthic species, including DSCs, and hardbottom habitats offshore of the southeastern US within the Atlantic Outer Continental Shelf (OCS) Region. BOEM oversees the responsible development of offshore energy and mineral resources on the US OCS and needs this information to assess the potential impacts of activities that physically disturb the seafloor related to the development of these resources and to develop mitigation measures to avoid or minimize these impacts.

Ross and Nizinski (2007) and Hourigan et al. (2017b) summarized extensive research and exploration efforts to characterize DSC communities and the existing knowledge of the spatial distributions of DSC habitats offshore of the southeastern US These distributions have been greatly influenced by the Gulf Stream (and the Florida Current in the Straits of Florida), the dominant oceanographic feature in the region that has shaped the topography of the seafloor and resulted in many complex, high relief hardbottom areas. Hourigan et al. (2017b) described four major concentrations of hardbottom habitats in the region that support DSC communities: the Miami and Pourtalès Terraces and adjacent escarpments, the *Oculina* coral mounds off southeast Florida, the continental shelf and shelf break, and the continental slope and the Blake Plateau. Recent exploration and characterization of deep-sea areas in the region included two expeditions by NOAA Ship *Okeanos Explorer* (Windows to the Deep 2018; Windows to the Deep 2019) and a multi-year study by scientists from BOEM, the National Oceanic and Atmospheric Administration (NOAA), the US Geological Survey (USGS), and several research institutions (Deep SEARCH 2018; Deep SEARCH 2019).

Although considerable work has been done to characterize the distributions of DSCs and hardbottom habitats offshore of the southeastern US, much of the region remains unexplored and unmapped, and further research and exploration are needed. However, it is unlikely that more than a small fraction of deep-sea benthic habitats in the region will be surveyed because of the logistical challenges and expense of deep-sea exploration. Statistical models (i.e., species distribution models or predictive habitat models) can be an important tool for increasing the efficiency and effectiveness of mapping and exploration by identifying locations where these habitats are likely to occur.

The earliest predictive habitat models for DSCs offshore of the southeastern US were regional scale models for a group of structure-forming stony corals that included *Lophelia pertusa* (= *Desmophyllum pertusum*), *Madrepora oculata*, *Enallopsammia profunda*, *Solenosmilia variabilis*, and *Oculina varicosa* (unpublished by Davies but described in Guinotte et al. 2017). Kinlan et al. (2013) created regional scale models for three species (*Lophelia pertusa*, *Madrepora oculata*, *Enallopsammia profunda*) and one genus (*Oculina* spp.) of structure-forming stony corals and for several groups of DSCs: structure-forming stony corals, non-structure-forming stony corals (i.e., cup corals), black corals, lace corals (family Stylasteridae), sea pens, gorgonian corals, gorgonian corals in suborder Calcaxonia, gorgonian corals in suborder Holaxonia, and non-gorgonian soft corals. Mienis et al. (2014) developed two regional scale models for *Lophelia pertusa*. Though all of these regional scale models were generated with the best available data at the time and a widely used modeling approach (i.e., Maxent; Phillips et al. 2006), they have important limitations. The models all used environmental predictors depicting depth and seafloor topography that were derived from a regional bathymetry model, the 3 arc-second (approximately 90 m resolution) NOAA Coastal Relief Model, which is too coarse to resolve many of the finer scale hardbottom habitats (e.g., mounds) where DSCs have been observed. In addition, many of these models were created for broader taxonomic groups that combined taxa with different habitat requirements (e.g., depth ranges), and this may have resulted in overprediction of the extent of potential habitat for these groups (Guinotte and Davies 2014; Kinlan et al. 2020; Winship et al. 2020).

Most important, these models were all presence-background models (sometimes referred to as presence-only models) and were fit using records of DSC presence and randomly selected background (i.e., pseudo-absence) locations rather than using actual absence data. Though there have been concerns about how feasible it is to confirm absences of DSCs from underwater visual surveys and most of the earlier predictive habitat models for DSCs were presence-background models (Vierod et al. 2014), presence-background models can mistake the distribution of sampling effort for the distribution of species occurrence if they do not account for spatial bias in sampling effort (Phillips et al. 2009; Fithian et al. 2015; Winship et al. 2020). Predictions from presence-background models are typically relative measures (e.g., habitat suitability); models fit to presence-absence data provide predictions of absolute probabilities that allow direct comparison across models rather than interpretation in relative terms (Winship et al. 2020). As a result of the limitations of presence-background models, it is recommended that predictive habitat models for DSCs use presence-absence data or, if possible, abundance data (Anderson et al. 2016; Winship et al. 2020; Stephenson et al. 2021).

This study aimed to address the limitations of the earlier regional scale predictive habitat models for DSCs in the region by using presence-absence data with associated measures of sampling effort, by deriving depth and seafloor topography predictors from a compilation of bathymetry data that included available multibeam bathymetry, and by creating models primarily at the genus level. BOEM funded the NOAA National Centers for Coastal Ocean Science (NCCOS) to provide information about the spatial distributions of DSCs and hardbottom habitats offshore of the southeastern US (the Straits of Florida, South Atlantic, and Mid-Atlantic Planning Areas of the Atlantic OCS Region) to support environmental assessments and other decision documents for the review of proposed activities related to the development of offshore energy and mineral resources. The objectives of the study were (1) to compile a database of presence-absence observations of DSCs with associated measures of sampling effort and bottom type from underwater visual surveys and (2) to develop predictive models that relate the occurrence of DSCs and hardbottom habitats to spatial environmental predictors in order to predict and map their potential spatial distributions offshore of the southeastern US

This report summarizes the data and methods used in this study and its findings. This section (Section 1) outlines the management rationale for the study, provides background on the existing knowledge of DSC and hardbottom habitats offshore of the southeastern US, and defines the objectives of the study. Section 2 describes the data and methods used to compile the database of presence-absence observations of DSCs and hardbottom habitats. It also describes the set of gridded spatial environmental predictors and the occupancy modeling approach used to predict and map the potential spatial distributions for selected DSC taxa and hardbottom habitats. Section 3 presents and discusses the outputs from the occupancy models, including measures of model performance and maps of the observed and predicted spatial distributions for selected DSC taxa and hardbottom habitats. Section 4 provides conclusions about the advantages and limitations/caveats of (1) the presence-absence data, (2) the environmental predictors compiled for this study, (3) the occupancy modeling approach, and (4) the maps and data products presented in this report. It also offers guidance about how this information can be used to inform marine resource management and future research and exploration.

2 Methods

2.1 Study Area

The study area included waters between 50–3,500 m depth within BOEM's Straits of Florida, South Atlantic, and Mid-Atlantic Planning Areas and extended from Florida to Delaware (Figure 1). Locations of underwater visual surveys used to compile the presence-absence database for this study did not span this entire depth range across the study area. Therefore, the depth range of the study area extent varied with latitude. Offshore of south Florida (the Straits of Florida, the Miami and Pourtalès Terraces, and the adjacent escarpment) presence-absence data were not located shallower than approximately 150 m, so the study area was restricted to waters from 150–3,500 m depth south of 26.5 °N latitude. Similarly, the study area was restricted to continental slope waters from 200–3,500 m depth north of 34.5 °N because presence-absence data north of Cape Lookout, North Carolina, were located only on the continental slope (in submarine canyons and inter-canyons areas) and not on the continental shelf (<200 m depth).

2.2 Data Synthesis of Observations of Deep-sea Corals and Hardbottom Habitats

Relatively few records of DSC occurrence have included accurate measures of survey (i.e., sampling) effort (e.g., area surveyed) or sufficient information to infer absence of DSCs at survey locations (e.g., survey tracks with precise spatial positions linked to the observations). Therefore, consistent with this study's objectives, a comprehensive inventory of available data from field surveys conducted in the study area was compiled to obtain presence-absence observations of DSCs with associated measures of sampling effort and bottom type. Data included still images and video collected by submersible (human occupied vehicle, or HOV), remotely operated vehicle (ROV), and autonomous underwater vehicle (AUV), and records from museum collections and trawl surveys. Data were assessed for accessibility, accuracy of navigation data (i.e., spatial positions), spatial coverage, temporal range, and data quality to prioritize data in the inventory. Following this assessment, data from 20 field surveys conducted 2001–2018 were selected and analyzed to create a database of georeferenced records of DSC presence-absence with associated descriptions of bottom type (to identify hardbottom habitats) and measures of survey (i.e., sampling) effort (Table 1, Figure 2). The database included observations from submersible and ROV surveys, but did not include data from AUV surveys, museum collections, or trawl surveys. Additional information about the field surveys used to compile the database can be found in Appendix A. The presence-absence database is available as part of the data package for the study.

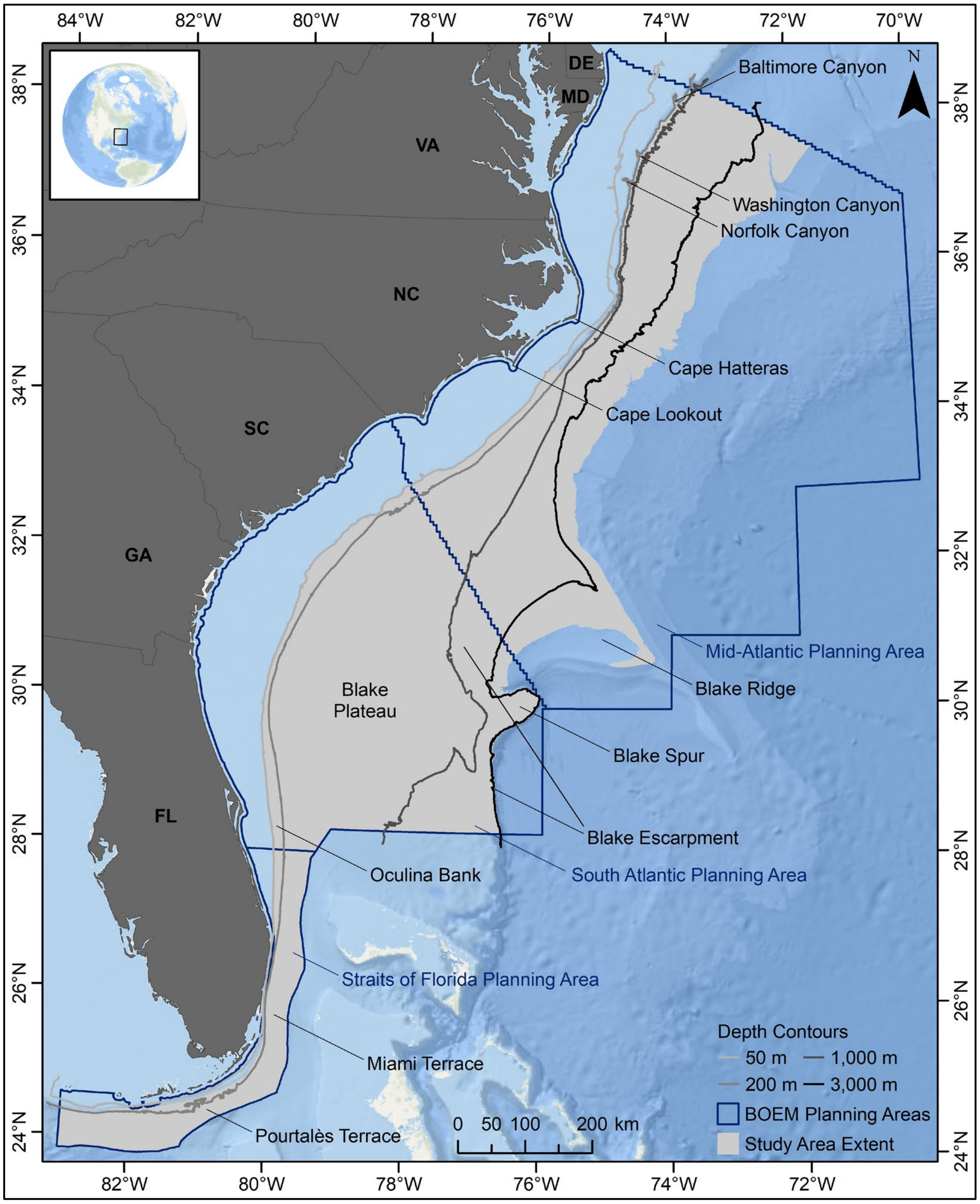

Figure 1. Study area.
The study area included waters within BOEM's Straits of Florida, South Atlantic, and Mid-Atlantic Planning Areas. The study area was restricted to depths from 150–3,500 m south of 26.5 °N, from 50–3,500 m between 26.5 °N and 34.5 °N, and from 200–3,500 m north of 34.5 °N because locations of survey data did not span the entire depth range of the planning areas.

Table 1. Field survey datasets used to create the presence-absence database of deep-sea corals and hardbottom habitats

Survey Dataset	Principal Investigator	Dives	Samples	Sites	Total Area (m^2)
Islands in the Stream 2001 Oculina Banks	Shepard, Koeing	16	41	33	8,110
Islands in the Stream 2001 NC Shelf	Ross, Sulak	10	28	16	3,987
Islands in the Stream 2001 Charleston Bump	Sedberry	3	62	36	9,987
Islands in the Stream 2002 Leg 1	Sedberry	10	166	70	19,728
Islands in the Stream 2002 Leg 2	Ross, Sulak	11	61	39	11,054
Islands in the Stream 2002 Leg 3	Pomponi, Reed	23	209	106	37,728
Windows to the Deep 2003	Ruppel, Van Dover	7	144	113	33,023
Investigating the Charleston Bump (2003)	Sedberry, Stancyk	13	193	80	25,114
Life on the Edge 2003	Ross, Baird, Sulak, Nizinski	17	202	64	25,276
Life on the Edge 2004	Ross, Baird, Sulak, Nizinski	25	202	100	27,675
Estuary to the Abyss (2004)	Sedberry, Mitchell	6	20	18	5,080
Life on the Edge 2005	Ross, Baird, Sulak, Nizinski	18	302	122	36,960
Georgetown Hole (2010)	Sedberry	5	136	66	12,533
Extreme Corals 2010	Ross, Brooke	8	356	89	13,800
Extreme Corals 2011	David, Reed	9	72	65	20,705
Florida Shelf-Edge Exploration II (2011)	Reed	13	66	13	2,409
Deepwater Canyons 2012	Ross, Brooke	20	3,673	438	64,470
Deepwater Canyons 2013	Ross, Brooke	13	3,585	264	57,920
Windows to the Deep 2018	Morrison, Sautter	17	86	84	16,300
Deep SEARCH 2018	Cordes	10	219	132	29,056

Dives = number of submersible or remotely operated vehicle dives from the dataset that were used in this study.
Samples = number of still images or video segments from the dataset that were analyzed to obtain deep-sea coral observations.
Sites = number of model grid cells containing samples from the dataset.
Total Area = sum of the survey area for all samples from the dataset.

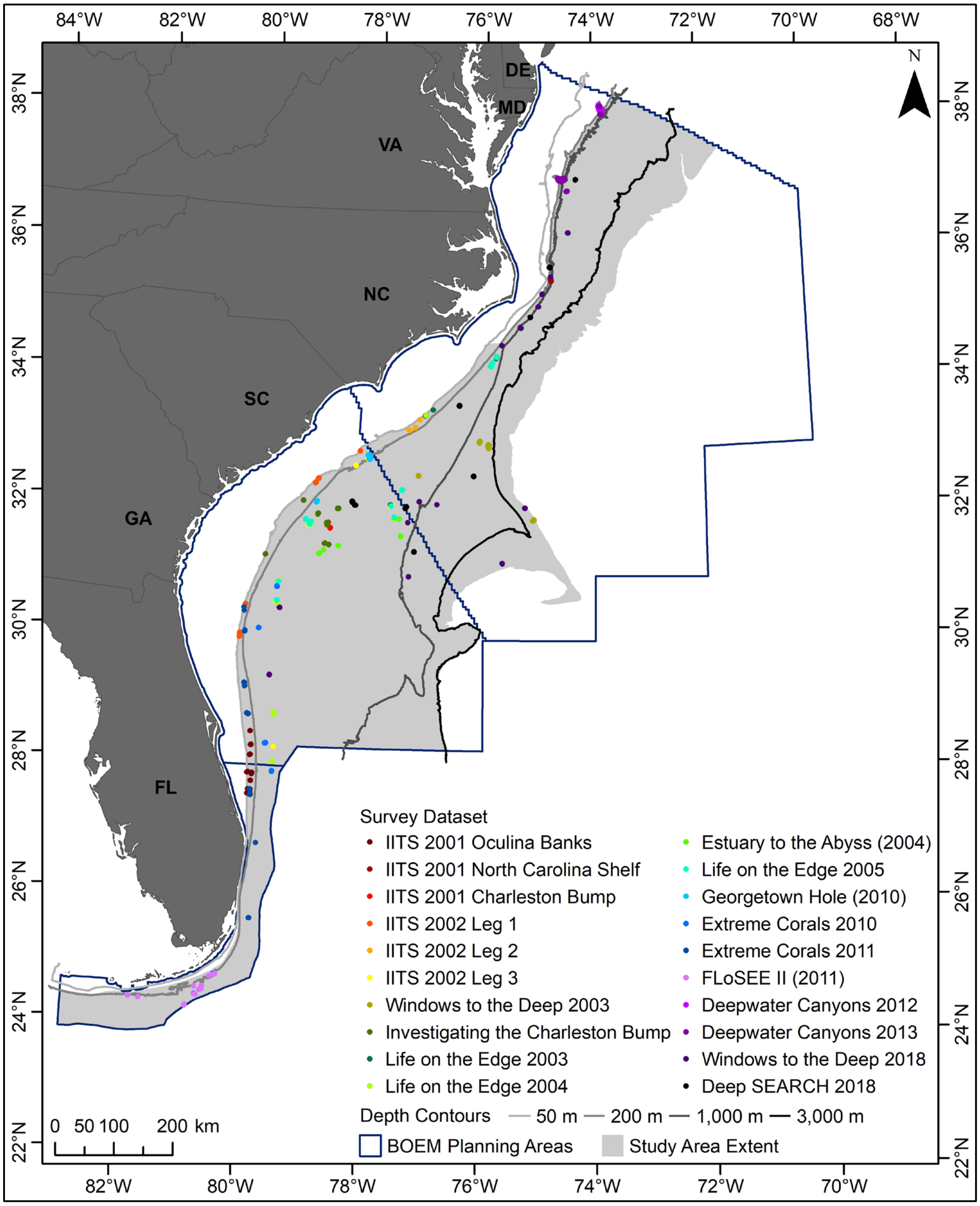

Figure 2. Locations of field survey datasets.
This map shows the locations of samples from the 20 survey datasets used to create the presence-absence database of deep-sea corals and hardbottom habitats. IITS = Islands in the Stream, FLoSEE = Florida Shelf-Edge Exploration. For additional details and maps of the sample locations for each individual dataset, see Table 1 and Appendix A.

Each observation in the database was linked to a still image or segment of video from the imagery data, hereafter referred to as a sample of the imagery data. Each sample was assigned a spatial position (i.e., the point location of a still image or midpoint of a video segment), an estimate of the areal extent of the seafloor associated with the sample (sampling effort), annotations of the DSCs observed, and a description of the bottom type. A DSC taxon was considered to be present in a sample if one or more observations of the taxon were recorded; otherwise, the taxon could be inferred as absent for the sample.

The area represented by samples ranged from approximately 1 m^2 to 827 m^2. Descriptions of bottom type identified the primary (>50% of visible seafloor) and secondary (<50% of visible seafloor) substrate type as either ‘Hard’ or ‘Soft’ to indicate whether there was exposed hard substrate available for colonization by DSCs or other benthic fauna. Values for the bottom type description (primary/secondary) included ‘Hard/Hard’, ‘Hard/Soft’, ‘Soft/Hard’, and ‘Soft/Soft.’

2.3 Selection of Deep-sea Coral Taxa for Modeling

This study focused on DSCs that form three-dimensional structure (structure-forming DSCs) that can provide microhabitats for other organisms such as fishes, crustaceans, and echinoderms since these DSCs are the most relevant to BOEM’s management activities. Though some DSC observations in the presence-absence database were identified to the species (e.g., *Lophelia pertusa*), family, or order, the majority of the observations were identified to the genus. From the list of DSC taxa recorded in the presence-absence database, the taxa of structure-forming DSCs selected for modeling included six genera of stony corals in order Scleractinia, five genera of black corals in order Antipatharia, 12 genera of gorgonian corals in order Alcyonacea, and one family of lace corals (family Stylasteridae) in order Anthoathecata (Table 2). Models were fit for genera (with the exception of the family Stylasteridae) since models for broader taxonomic groups may include taxa with different habitat requirements (e.g., depth ranges) and may overpredict the spatial extent of their distributions (Guinotte and Davies 2014; Kinlan et al. 2020; Winship et al. 2020). For the models, observations identified as Chrysogorgiidae were presumed to be *Chrysogorgia*, observations identified as Paragorgiidae were presumed to be *Paragorgia*, and observations identified as *Hypnogorgia* were presumed to be *Muricea*. However, the original scientific name entries for these observations were retained in the presence-absence database.

Table 2. Taxa selected for modeling

Taxon	Order	Family	Expected Depth Range (m)	Survey Datasets	Samples	Sites
Lophelia	Scleractinia	Caryophylliidae	250–900	16	1,144	469
Solenosmilia	Scleractinia	Caryophylliidae	300–2,000	11	318	168
Oculina	Scleractinia	Oculinidae	20–200	8	162	124
Madrepora	Scleractinia	Oculinidae	50–1,500	10	132	103
Cladocora	Scleractinia	Scleractinia incertae sedis	11–400*	1	25	23
Enallopsammia	Scleractinia	Dendrophylliidae	300–1,800	2	22	18
Stichopathes	Antipatharia	Antipathidae	20–200	9	192	101
Leiopathes	Antipatharia	Leiopathidae	150–800	12	146	110
Antipathes	Antipatharia	Antipathidae	20–200	4	90	49
Tanacetipathes	Antipatharia	Myriopathidae	50–125	4	45	24
Bathypathes	Antipatharia	Schizopathidae	300–2,000	8	44	37
Paragorgia	Alcyonacea	Paragorgiidae	400–2,500	9	921	170
Plumarella	Alcyonacea	Primnoidae	150–1,200	14	677	357
Anthothela	Alcyonacea	Anthothelidae	173–868*	6	346	98
Acanthogorgia	Alcyonacea	Acanthogorgiidae	200–1,200	7	295	75
Paramuricea	Alcyonacea	Plexauridae	50–2,500	13	208	101
Eunicella	Alcyonacea	Gorgoniidae	475–880*	7	162	89
Muricea	Alcyonacea	Plexauridae	20–125	4	126	66
Thesea	Alcyonacea	Plexauridae	50–300	6	77	38
Callogorgia	Alcyonacea	Primnoidae	30–1,000	5	52	29
Nicella	Alcyonacea	Ellisellidae	40–300	5	48	32
Chrysogorgia	Alcyonacea	Chrysogorgiidae	200–2,500	6	27	22
Acanella	Alcyonacea	Isididae	300–3,000	4	25	20
Stylasteridae	Anthoathecata	Stylateridae	100–500	13	660	330
Hardbottom	N/A	N/A	N/A	20	6,138	1,415

* denotes Expected Depth Range from Hourigan et al. (2017a) rather than from analysis of records in NMNH database.
Survey Datasets = number of datasets in the presence-absence database that included presences of the taxon.
Samples = number of samples across all survey datasets in which the taxon was present.
Sites = number of model grid cells in which the taxon was present.

Potential errors in the spatial positions or taxonomic identifications of database records were flagged and investigated using the reported depth for each sample, the depth extracted from the environmental predictor dataset representing bathymetric depth at the spatial position of the sample (see Section 2.4.2 for a description of the depth predictor), and the 'expected' depth range for each DSC taxon, calculated from the 80–95% intervals of the reported depths for each taxon in the Smithsonian National Museum of Natural History (NMNH) database. These depth ranges captured 85–100% of NMNH records while removing extreme and potentially erroneous values, providing more reliable depth ranges than those previously published (e.g., as reported in Hourigan et al. 2017a) while allowing some cushion for new discovery beyond previously published depth ranges. For each DSC taxon selected for modeling, observations in the presence-absence database that had a reported or predictor-derived depth outside the expected depth range were reviewed and in some cases were corrected or treated as absences in the models, but still retained as presences in the presence-absence database (Table 3).

Table 3. Samples for which presences were treated as absences in the models

Taxon	Samples* Treated as Absences for Taxon	Reason
Lophelia	ETTA 3467-1, ETTA 3467-1h, ETTA 3467-2, ETTA 3467-2, ETTA 3467-3	>900 m
Lophelia	JSL2_3421-2-1, JSL2_3421-2-2, JSL2_3421-2-3, JSL2_3421-2-4, JSL2_3421-3-1, JSL2_3422-3, JSL2_3422-2-1, JSL2_3422-2-2, JSL2_3422-3-2, JSL2_3423-4, JSL2_3423-6, JSL2_3423-7, JSL2_3423-2-1, JSL2_3424-2, JSL2_3424-4, JSL2_3424-3-1, JSL2_3433-2, JSL2_3434-1, JSL2_3434-2, JSL2_3434-3, JSL2_3434-4, JSL2_3434-5, JSL2_3434-7, JSL2_3434-8, JSL2_3434-2-1, JSL2_3434-2-2, JSL2_3434-2-3, JSL2_3434-3-1, JSL2_3434-3-2, JSL2_3435-1, JSL2_3435-3, JSL2_3435-4, JSL2_3435-6, JSL1_4690-1, JSL1_4690-2, JSL1_4690-3, JSL1_4690-4, J2-544-18, 201109251_T2	<200 m
Solenosmilia	JSL2_3433-3, JSL2_3433-4, JSL2_3433-7, JSL2_3433-8, JSL2_3433-3-2	<300 m
Oculina	10-100A_8	>200 m
Stichopathes	01109282_T2, 2011093001_T2, EX1806_04_1, EX1806_04_2, EX1806_04_3, T3-AL4964, T12-AL4964, T15-AL4964, T17-AL4964	>200 m
Leiopathes	EX1806_04_2, EX1806_04_3	>800 m
Leiopathes	JSL2-3289-2d, JSL2-3289-2h, JSL2-3290-3a, JSL2-3290-3c, JSL2-3290-3f, JSL2-3291-1d, JSL2-3291-1h, JSL2-3291-1k, JSL2-3291-2d, JSL2-3291-2e, JSL2-3291-2f, JSL2-3291-2g, JSL2-3291-2h, JSL2-3292-1c, JSL2-3292-1d, JSL2-3292-1e, JSL2-3292-1h, JSL2-3292-2a, JSL2-3293-1a, JSL2-3294-1b, JSL2-3295-1a, JSL2-3295-1c, JSL2-3295-1d, JSL2-3295-1e, JSL2-3295-1g, JSL2-3295-1h, JSL2-3295-1i, JSL2-3295-1j, JSL2-3295-2a, JSL2-3295-2d, JSL2-3295-2f, JSL2-3295-2g, JSL2-3296-1a, JSL2-3296-1b, JSL2-3296-1c, JSL2-3296-1h, JSL2-3296-2c, JSL2-3296-2g, JSL2-3300-1d, JSL2-3300-1h, JSL2-3300-1i, JSL2-3300-1j, JSL2-3300-1k, JSL2-3300-2b, JSL2-3300-2e, JSL2-3300-2f, JSL2-3300-2g, JSL2-3300-2h, JSL2-3300-2i, JSL2-3300-2j, JSL2-3300-2k, JSL2_3421-7, JSL2_3421-9, JSL2_3421-2-4, JSL2_3422-2-5, JSL2_3422-3-3, JSL2_3423-1, JSL2_3423-2, JSL2_3424-4, JSL2_3424-2-4, JSL2_3424-3-1	<150 m
Antipathes	JSL2_3411-1e, JSL2_3411-1f, JSL2_3411-2a, JSL2_3411-2b, JSL2_3411-2d, JSL2_3411-2j	>200 m
Tanacetipathes	10-100B_2, 10-101A_1, 201109282_T2, 201109301_T4	>125 m
Plumarella	JSL1_4691-3, JSL1_4691-4	<150 m
Anthothela	T7-AL4969	>868 m
Eunicella	JSL2-3290-3a, JSL2-3290-3c, JSL2-3291-1b, JSL2_3303_1, JSL2_3303_2, JSL2_3410-1b, JSL2_3411-1b, JSL2_3411-1d, JSL2_3411-1e, JSL2_3411-1f, JSL2_3411-2a, JSL2_3411-2b, JSL2_3411-2d, JSL2_3411-2e, JSL2_3411-2f, JSL2_3411-2g, JSL2_3411-2h, JSL2_3411-2i, JSL2_3411-2j, JSL2_3411-2k, JSL2_3411-3a, JSL2_3411-3b, JSL2_3411-3c, JSL2_3411-3d, JSL2_3412-1a, JSL2_3412-1d, JSL2_3412-1e, JSL2_3412-1f, JSL2_3412-2a, JSL2_3412-2b, JSL2_3412-2c, JSL2_3412-2f, JSL2_3412-2h, JSL2_3412-3b, 201106061_T2, 201106091_T1, 201106091_T2, 201106091_T3	<475 m
Muricea	10-101A_28, 201109282_T1, 201109282_T2	>125 m
Nicella	JSL2_3411-2f	>300 m

* identified by the field 'SegmentID' from the presence-absence database

2.4 Environmental Predictors

An initial set of 62 environmental predictor datasets representing potential drivers (or potential proxies for drivers) of the spatial distributions of DSC occurrence was compiled for the study area. The environmental predictors included measures of depth and seafloor topography, seafloor substrate, oceanography, and geography. Additional environmental predictors depicting other measures of oceanography (e.g., biological productivity, aragonite saturation, dissolved oxygen concentration) were considered, but available data for these measures generally had insufficient spatial coverage or spatial resolution. This section describes the data sources and methods used to create the environmental predictor datasets.

2.4.1 Map projection and spatial grid resolution

The environmental predictor datasets were created on a grid with a spatial resolution of 100 x 100 m in an oblique Mercator projected coordinate system (origin = 35°N 75°W, azimuth = 40°, scale = 0.9996, datum = NAD83). The spatial resolution of the grid was selected to represent the approximate length of a five minute transect by an ROV traveling at 0.5 knots, a typical sample in the presence-absence database. The projected coordinate system was chosen to minimize area distortion at the edges of the study area. The 100 x 100 m grid contained 32,073,026 grid cells in the study area.

2.4.2 Depth and seafloor topography

The depth, shape, and spatial distribution of seafloor features may have an effect on the occurrence of DSCs. Seafloor depth may be a proxy for other measures (e.g., temperature, salinity) that directly influence species distributions (Wiltshire et al. 2018). Measures of the shape and complexity of the seafloor may be useful in identifying areas of exposed hard substrate that can provide habitat (e.g., available surface for attachment) for many DSCs. A comprehensive inventory of available bathymetry data for the area offshore of the southeastern US (Appendix B) was compiled to create a single depth predictor dataset from which predictor datasets depicting measures of seafloor topography could be derived. Bathymetry data collected using multibeam sonar surveys were a priority for the inventory because coarse bathymetry data (e.g., from regional or global bathymetry models) may not be sufficient for resolving fine scale features on the seafloor that may be useful for predicting the occurrence of DSCs (Winship et al. 2020).

Bathymetry data collected by multibeam sonar were obtained from the NOAA National Centers for Environmental Information (NCEI; NCEI 2004), USGS, and the College of Charleston. These data were reviewed to identify artifacts (e.g., visible lines from a multibeam survey path) and to assess spatial coverage and spatial resolution. Some data were excluded from the inventory following this review. For example, some data had considerable gaps where the spacing between individual survey lines did not provide sufficient overlap in coverage. In addition, some data appeared to have been collected during vessel transits. These data were excluded to minimize boundary effects where the contrast in depth values with the surrounding bathymetry data could result in the identification of false seafloor features (e.g., areas incorrectly appearing to have high slope). In addition to individual bathymetry datasets, the inventory included a bathymetric terrain model created from existing bathymetry data from multibeam surveys (Andrews et al. 2016). Bathymetry data from coastal digital elevation models (DEMs; NCEI 2006), NOAA Coastal Relief Models (NCEI 1999; NCEI 2001), and the General Bathymetric Chart of the Oceans (GEBCO; Weatherall et al. 2015) were included in the inventory to use where no bathymetry data from multibeam surveys existed. At the time the inventory of bathymetry data was compiled for this study (May 7, 2021), bathymetry data from multibeam surveys were available for approximately 74% of the study area (Figure 3).

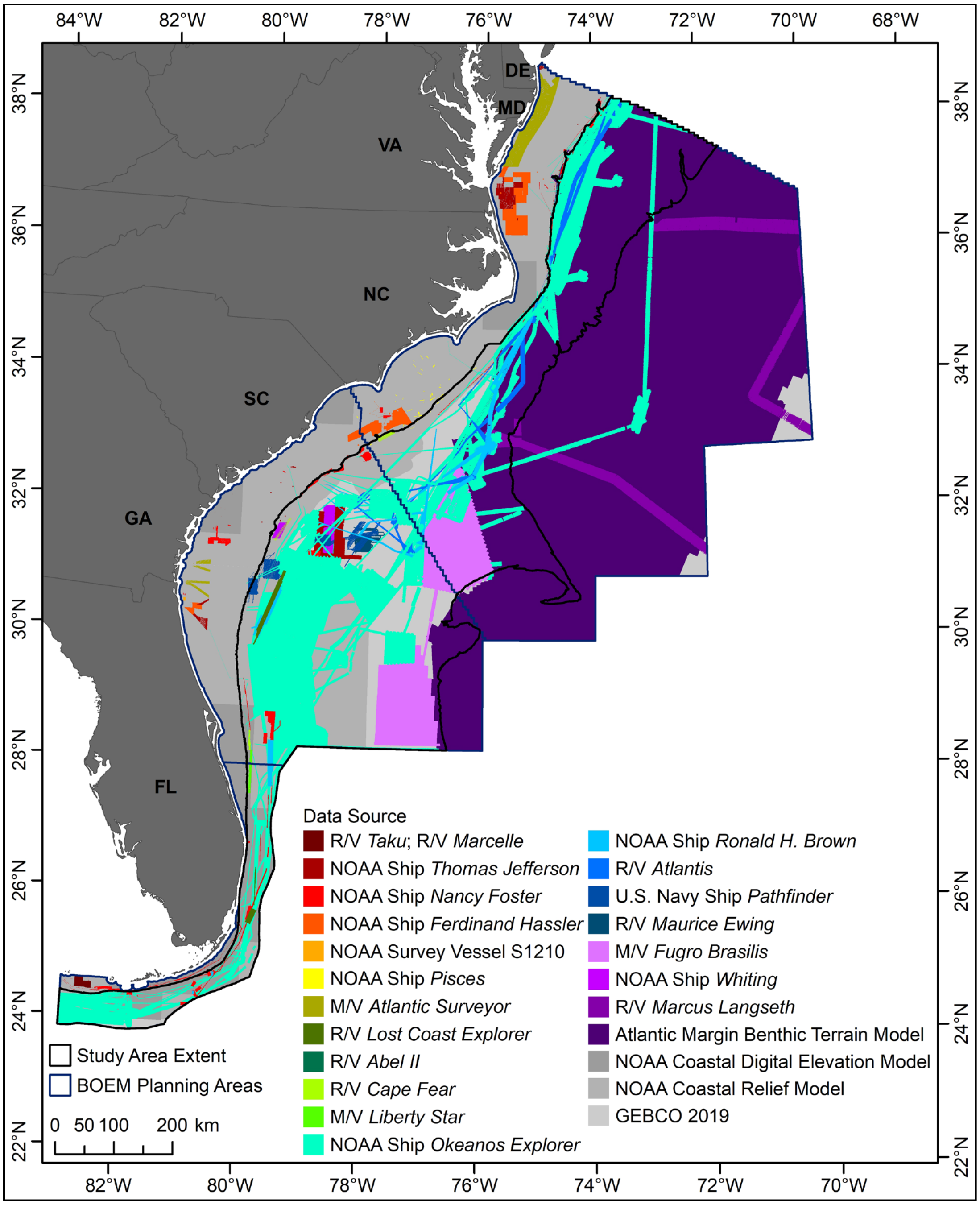

Figure 3. Coverage of available bathymetry datasets.
This map shows the footprints of the bathymetry datasets available as of May 7, 2021 that were included in the inventory used to create the merged bathymetry dataset. Datasets are symbolized by data source. For additional details about each individual dataset see Table B-1 in Appendix B.

Individual bathymetry datasets were projected and bilinearly resampled onto a 25 x 25 m grid that nested within the 100 x 100 m model grid. This spatial resolution reflected a common resolution of the multibeam bathymetry data in the inventory. Resampling of bathymetry datasets with a native spatial resolution finer than 25 x 25 m resulted in the loss of some finer scale information. Some bathymetry datasets (e.g., from multibeam surveys in deeper waters) had a native spatial resolution coarser than 25 x 25 m. Though these datasets were resampled onto the 25 x 25 m grid, they did not include information at this resolution. As a result, measures of depth and seafloor topography did not capture finer scale features in the areas represented by these coarser datasets.

A single gridded depth dataset at 25 x 25 m resolution was created by merging the projected and resampled bathymetry datasets. Where the projected and resampled bathymetry datasets overlapped, the depth value for the merged depth dataset was selected from the input dataset that had finer native spatial resolution or that was more recently collected (order reflected in Table B-1). The depth predictor dataset was generated by calculating the average depth value of the 25 x 25 m resolution merged depth dataset within each of the 100 x 100 m grid cells of the model grid (i.e., by calculating the aggregate mean).

Gridded datasets at 25 x 25 m resolution depicting 14 measures of seafloor topography (Table 4) were derived from the merged depth dataset using focal statistics functions, where the value for each grid cell was calculated from the values of the grid cells in the surrounding 3 x 3 grid cell neighborhood. These datasets were created using the ‘terra’ package (version 0.9.11; Hijmans 2020) in R (version 4.0.3; R Core Team 2020). The seafloor slope, aspect (i.e., slope direction), roughness, terrain ruggedness, and topographic position index were calculated using the ‘terrain’ function from the ‘terra’ package. Because aspect is a directional variable, the aspect dataset was converted to datasets depicting the east-west and north-south gradients of aspect by calculating the sine and cosine of aspect, respectively. Rugosity was derived as the ratio of the surface area to the area of a plane of best fit following the arc-chord ratio method, which minimizes inflated rugosity values in areas of high slope (Du Preez 2015). Several measures of seafloor curvature were computed to characterize the shape of the seafloor (e.g., whether it is convex or concave). Slope of slope was calculated using the ‘terrain’ function on the slope dataset rather than on the merged depth dataset; general curvature, total curvature, plan (i.e., planform) curvature, cross-sectional curvature, profile curvature, and longitudinal curvature were calculated following Jenness (2013). The seafloor topography predictor datasets were generated by calculating the aggregate mean of each 25 x 25 m resolution dataset within each of the 100 x 100 m grid cells of the model grid.

Because the seafloor topography predictors were derived at 100 x 100 m resolution, the model predictions did not resolve (delineate) individual seafloor features (e.g., coral mounds, scarps, or terraces) that were smaller than this. However, by deriving the initial depth and seafloor topography datasets at 25 x 25 m resolution, the intent was to capture some of the fine scale variability in seafloor topography from the available multibeam bathymetry so that the seafloor topography predictors might identify areas with extensive high relief from finer scale features (e.g., an area with numerous, smaller coral mounds).

Table 4. Environmental predictors depicting measures of depth and seafloor topography

Predictor	Description	Unit
Depth*^	Seafloor depth derived from a synthesis of bathymetry data	Meters
Slope*^	Magnitude of the maximum gradient in depth in a focal neighborhood	Degrees
East-west aspect*	Sine of the direction of seafloor slope in a focal neighborhood	Unitless
North-south aspect*	Cosine of the direction of seafloor slope in a focal neighborhood	Unitless
Roughness	Difference between the maximum depth value and minimum depth value in a focal neighborhood	Meters
Terrain ruggedness	Mean of the absolute differences in depth values between a grid cell and the surrounding grid cells in a focal neighborhood	Meters
Topographic position index	Difference between the depth value of a grid cell and the mean depth of the surrounding grid cells in a focal neighborhood	Meters
Rugosity	Ratio of the area of the contoured seafloor surface to the area of a plane of best fit that accounts for slope	Unitless
Slope of slope	Magnitude of the maximum gradient in seafloor slope in a focal neighborhood	Degrees
Total curvature	General measure of the curvature of the seafloor in a focal neighborhood	Radians/100m^2
General curvature*	General measure of the extent to which the seafloor is convex or concave in a focal neighborhood	Radians/100m
Plan curvature	Curvature of the seafloor along the line of intersection between the seafloor surface and the horizontal plane	Radians/100m
Cross-sectional curvature	Curvature of the seafloor along the line of intersection between the seafloor surface and the plane formed by the slope normal and direction of seafloor slope	Radians/100m
Profile curvature	Curvature of the seafloor along the line of intersection between the seafloor surface and the plan formed by the slope direction and the z-axis	Radians/100m
Longitudinal curvature	Curvature of the seafloor along the line of intersection between the seafloor surface and the plane formed by the slope and the slope direction	Radians/100m

Depth and seafloor topography variables were initially calculated from a 25 x 25 m synthesis of available bathymetry data. Depth and seafloor topography predictors at 100 x 100 m resolution were generated by calculating the aggregate mean of each 25 x 25 m resolution dataset within the model grid cells.
* denotes predictors included in the final predictor set for deep-sea corals.
^ denotes predictors included in the final predictor set for hardbottom habitats.

2.4.3 Seafloor substrate

Gridded datasets at 500 x 500 m resolution depicting characteristics of the seafloor substrate (Table 5) were developed by Dr. Chris Jenkins (University of Colorado Boulder). These datasets were included to account for the effects of substrate characteristics on the occurrence of DSCs. The datasets were derived from the data holdings (e.g., point data records representing seabed surveys, such as from sediment grab samples) in the dbSEABED system (dbSEABED c2007–2021). There are a substantial number of records in the dbSEABED system for the Atlantic continental margin because of its role in the USGS usSEABED project (Reid et al. 2005). Other large datasets in the dbSEABED system for the region are the USGS East Coast Sediment Texture Database (Poppe et al. 2014), the NOAA National Ocean Service (NOS) and US

Coast and Geodetic Survey (now National Geodetic Survey) Hydrographic Surveys database (NOS 2013), and the Marine Geology archive from NOAA NCEI (NCEI 2018).

The gridded datasets were created from the point sample data in the dbSEABED system using multivariate (three-dimensional) inverse distance weighting (IDW) interpolation. This approach assumes that sample data that are closer together are more similar than those that are farther apart (i.e., that they are spatially autocorrelated; Tobler 1970) and calculates values at unsampled locations using a weighted combination of the values of neighboring samples. The distance between sample data from dbSEABED was measured in three-dimensional space such that the distance weights reflected easting, northing, and depth distances. Values for the percentage gravel, percentage mud, and percentage sand were transformed using a standard log-ratio approach for compositional data (Aitchison 1986) before interpolation. Although there are considerable surficial sediment data on the Atlantic continental margin, it is important to note that there are parts of the study area (e.g., deeper waters on the continental slope) where surficial sediment samples have not been collected or sampling has been sparse. In these locations the interpolated sediment composition will not capture fine scale spatial variability and may appear to be overly generalized. The three-dimensional IDW interpolation does not provide estimates of uncertainty for the interpolated values, which would have been valuable for understanding the limitations of these predictors. The gridded datasets at 500 x 500 m from the interpolation were projected and bilinearly resampled onto the 100 x 100 m model grid to create predictor datasets for median grain size, percentage gravel, percentage mud, percentage sand, and percentage rock exposure.

Table 5. Environmental predictors depicting characteristics of seafloor substrate

Predictor	Description	Unit
Median grain size*^	Average grain size of the surficial sediments	Phi units
Percentage gravel^	Percentage composition of the gravel fraction in surficial sediments	Unitless
Percentage mud	Percentage composition of the mud fraction in surficial sediments	Unitless
Percentage sand*	Percentage composition of the sand fraction in surficial sediments	Unitless
Percentage rock exposure*^	Percentage of exposed rock on the seafloor	Unitless

Seafloor substrate measures were initially interpolated at 500 x 500 m resolution from point sample data in the dbSEABED system. Seafloor substrate predictors on the 100 x 100 m resolution model grid were created by projecting and bilinearly resampling the 500 x 500 m resolution datasets.
* denotes predictors included in the final predictor set for deep-sea corals.
^ denotes predictors included in the final predictor set for hardbottom habitats.

2.4.4 Oceanography

Gridded datasets depicting several aspects of oceanography were considered for the models to account for the direct and indirect effects of ocean productivity, ocean chemistry, and the physical state and dynamics of the ocean on the occurrence of DSCs (Table 6).

Table 6. Environmental predictors depicting measures of oceanography

Predictor	Description	Source	Unit
Surface chlorophyll-a concentration*	Satellite-derived concentration of chlorophyll-a at the ocean surface	SeaWiFS (9 x 9 km), MODIS Aqua (4 x 4 km), MODIS Terra (4 x 4 km), VIIRS (4 x 4 km)	mg/m^3
Remote sensing reflectance	Satellite-derived mean normalized water-leaving radiance at 547 nm	MODIS Aqua (4 x 4 km), MODIS Terra (4 x 4 km)	sr^{-1}
Bottom salinity*	Ocean water salinity at the seafloor	HYCOM + NCODA Global 1/12° Reanalysis	Practical Salinity Unit
Bottom temperature	Ocean water temperature at the seafloor	HYCOM + NCODA Global 1/12° Reanalysis	Degrees Celsius
Bottom east-west current velocity	East-west (u) component of ocean current velocity at the seafloor	HYCOM + NCODA Global 1/12° Reanalysis	m/s
Bottom north-south current velocity	North-south (v) component of ocean current velocity at the seafloor	HYCOM + NCODA Global 1/12° Reanalysis	m/s
Bottom current speed*^	Magnitude of ocean current speed at the seafloor	HYCOM + NCODA Global 1/12° Reanalysis	m/s
Mixed layer depth	Depth of the ocean mixed layer, in which the ocean water is fairly homogeneous because of various physical processes, derived from an ocean water temperature profile with depth	HYCOM + NCODA Global 1/12° Reanalysis	Meters

Annual and seasonal mean climatological datasets were generated for each of these environmental predictors, but only annual mean climatologies were included in the final predictor sets.
* denotes predictors included in the final predictor set for deep-sea corals.
^ denotes predictors included in the final predictor set for hardbottom habitats.

As proxies for measures of ocean productivity, gridded datasets at approximately 4 x 4 km resolution depicting long-term climatological patterns in sea surface chlorophyll-a concentration and remote sensing reflectance (water-leaving radiance at 547 nm) were created from remotely sensed ocean color data. Daily data for sea surface chlorophyll-a concentration from multiple satellite instruments were downloaded from the National Aeronautics and Space Administration (NASA) Ocean Biology Processing Group. This included data from the Sea-Viewing Wide Field-of-View Sensor (SeaWiFS) collected from 1997–2001 (NASA 2018), data from the Moderate Resolution Imaging Spectroradiometer (MODIS) instruments aboard the Aqua and Terra satellites collected from 2002–2019 (NASA 2019a; NASA 2019b), and data from the Visible Infrared Imaging Radiometer Suite (VIIRS) instrument collected from 2012–2019 (NASA 2019c). Data from MODIS and VIIRS were blended together for best spatial coverage. Data from SeaWiFS were resampled from their native resolution (approximately 9 x 9 km) to match the resolution (approximately 4 x 4 km) of the data from MODIS and VIIRS. Long-term seasonal and annual climatologies of sea surface chlorophyll-a concentration were calculated from the daily data. Daily data for remote sensing reflectance from the MODIS instruments collected from 2002–2019 (NASA 2019a; NASA 2019b) were downloaded from the NASA Ocean Biology Processing Group and used to create long-term seasonal and annual climatologies for remote sensing reflectance. Environmental predictor datasets for sea surface chlorophyll-a concentration and remote sensing reflectance were generated by projecting and bilinearly resampling the climatological datasets onto the 100 x 100 m model grid.

Gridded datasets at approximately 9 x 9 km resolution describing the physical properties of ocean water at the seafloor were derived from a global 20-year hindcast model from the HYbrid Coordinate Ocean Model (HYCOM; HYCOM Consortium 2018). Daily data for bottom ocean water salinity, bottom ocean water temperature, the east-west (u) component of bottom ocean current velocity, and the north-south (v) component of bottom ocean current velocity were used to calculate long-term seasonal and annual climatological datasets for these measures. Daily data for bottom ocean current velocity were used to derive the absolute speed of bottom ocean currents, from which long-term seasonal and annual climatological datasets for bottom ocean current speed were calculated. Daily data for ocean water temperature were used to create temperature-depth profiles (i.e., how temperature varied with water depth), from which the depth of the ocean mixed layer (i.e., mixed layer depth, MLD) was estimated as the depth at which the temperature change from the surface temperature was 0.5 °C. The daily MLD estimates were in turn used to calculate long-term seasonal and annual climatological datasets for MLD. Environmental predictor datasets for bottom salinity, bottom temperature, bottom east-west current velocity, bottom north-south current velocity, bottom current speed, and MLD were generated by projecting and bilinearly resampling the climatological datasets onto the 100 x 100 m model grid.

2.4.5 Longitude and Latitude

Environmental predictor datasets representing longitude and latitude were considered for inclusion in the models to account for the effect of location on the occurrence of DSCs since some DSC taxa were known to be restricted to specific parts of the study area. Gridded datasets on the 100 x 100 m model grid were created for longitude and latitude.

2.5 Environmental Predictor Selection

The initial set of 62 environmental predictor datasets was reduced to avoid the inclusion of highly collinear (i.e., correlated) predictors, to avoid extreme model extrapolation, and to ensure numerical convergence for successful model fitting. The Spearman rank correlation coefficient was calculated for each pair of environmental predictors using their values at all grid cells in the study area to identify and remove predictors that were highly collinear (i.e., correlated). Next, the variance inflation factor (VIF, Zuur et al. 2010) was calculated for the remaining 18 environmental predictors using their values at the sample locations in the presence-absence database. For pairs of predictors in this subset that were highly collinear (based on the Spearman rank correlation coefficient), the predictor with the highest VIF was removed, except in cases where a predictor (e.g., depth) was retained based on an a priori decision about its importance, until the remaining predictors had VIF values less than three. This process resulted in a final predictor set consisting of 12 environmental predictors: depth, slope, east-west aspect, north-south aspect, general curvature, median grain size, percentage sand, percentage rock exposure, annual mean surface chlorophyll-a concentration, annual mean bottom salinity, annual mean bottom ocean current speed, and latitude. Six environmental predictors—depth, slope, median grain size, percent gravel, percentage rock exposure, and annual mean bottom ocean current speed—were used in the model of hardbottom habitats. Appendix C contains maps of each environmental predictor that was included in the final predictor set for DSCs or hardbottom habitats.

2.6 Model Framework

2.6.1 Occupancy analysis

Occupancy models (MacKenzie et al. 2002; Kéry and Royle 2016) were fit to the presence-absence data in the database compiled for this study and the values of the selected environmental predictors at the sample locations. The estimated relationships between occurrence and the predictors from the fitted models were then used to predict the probability of occurrence at each grid cell across the entire study area, including unsampled areas. Occupancy models estimate both the probability of occurrence at a site (occupancy probability) and the probability of detecting an organism present at a site (detection probability). By accounting for detection probability, estimates of the occupancy probability at a given site are absolute, in contrast to presence-background methods (e.g., Maxent) that only provide an estimate of the relative suitability at a given site. Estimates of occupancy probability are directly comparable across taxa, which allowed the implementation of a hierarchical multi-taxon approach (i.e., a joint species distribution model). Furthermore, estimates of occupancy probability are more interpretable than relative habitat suitability and can be more useful for management (Winship et al. 2020).

2.6.2 Space-for-time substitution

Temporal replicates, where the same site is visited multiple times, are typically used to obtain repeated samples for occupancy models to estimate detection probability; however, the presence-absence database compiled for this study did not contain replicate visits to the same sites. Because DSCs are sessile, slow-growing, and can live for 10s to 1,000s of years (Prouty et al. 2017) and the field surveys represented in the database spanned a much shorter time frame than their life span, the presence-absence data in the database were well suited for the analogous ‘space-for-time substitution’ using spatial replicates assumed to be equivalent to temporal replicates (Kéry and Royle 2016). Local colonization or extinction was unlikely to occur across spatial replicates at any given site. Each model grid cell was treated as a site since the environmental predictors did not contain information at a finer resolution than the grid cell. Samples within each grid cell were treated as spatial replicates (Figure 4). Within-site variation was used advantageously—spatially replicated samples allowed the estimation of detection probability (Kéry and Royle 2016). Space-for-time substitutions have been used in occupancy modeling with other taxa, including birds (Sadoti et al. 2013; Jiménez-Franco et al. 2019) and mammals (Charbonnel et al. 2014; Srivathsa et al. 2018; Petracca et al. 2020). They have also been used to approximate historical baselines of exploited marine fauna (Lotze and Worm 2009).

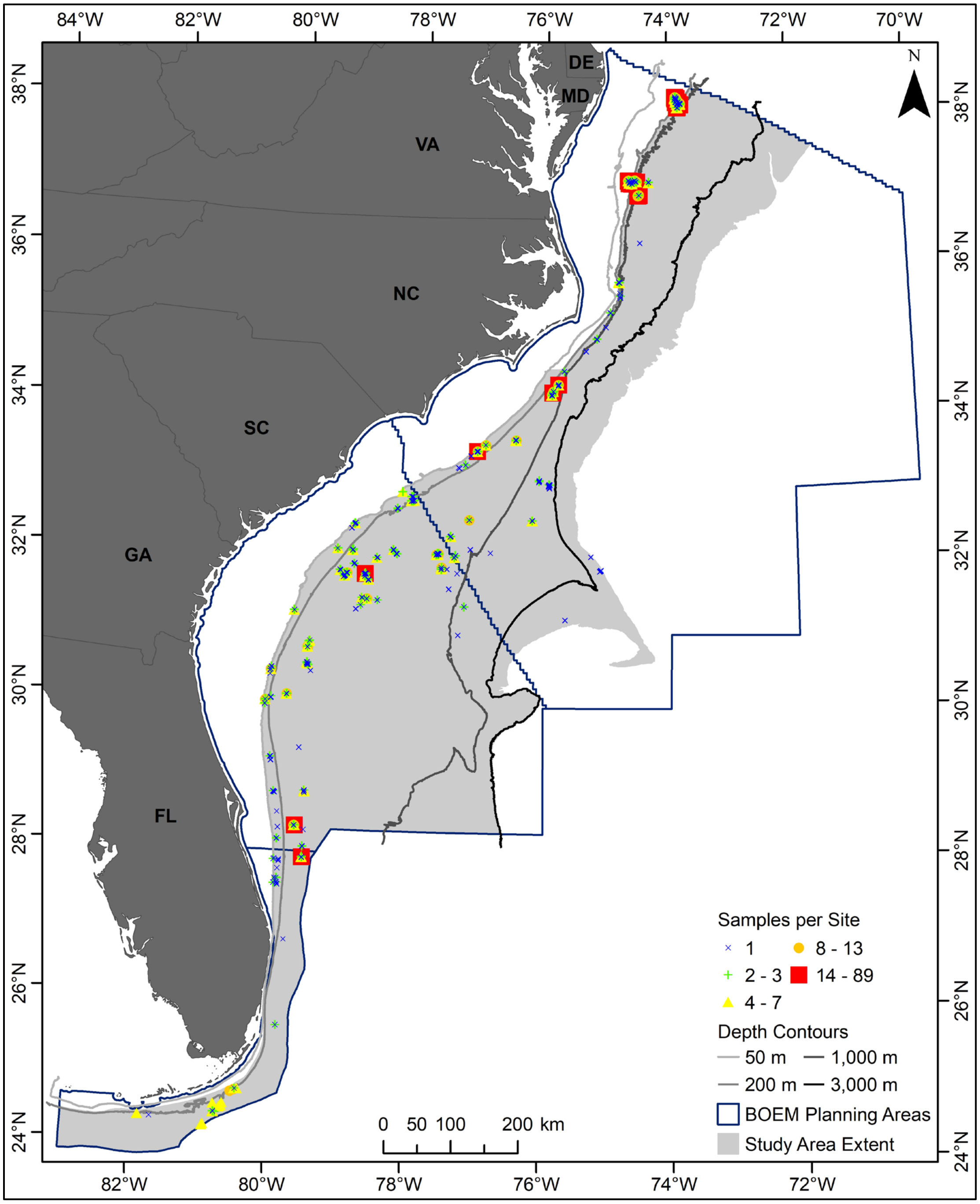

Figure 4. Spatial distribution of sampling effort.
This map shows the number of samples within each site (100 x 100 m grid cell). Samples within each grid cell were treated as spatial replicates.

By using the space-for-time substitution, estimates of detection probability are a combination of true detection probability and availability probability. Both of these probabilities account for the fact that, although an organism might have occupied a site, it could have been undetected by the observer for a couple of reasons. For example, consider a hypothetical situation where two grid cells are both occupied by corals (Figure 5). The true occupancy state of these grid cells (z) = 1. Samples are collected during a survey by taking images along a submersible's path that covers only part of the grid cell. In the first grid cell, the coral is undetected because it is obscured by a rock in the image. In the second grid cell, the coral is undetected because the submersible did not visit the part of the site where the coral was present. These two cases represent separate detection and availability processes, respectively. However, in both cases observed occurrence (y) = 0 because no corals were detected. The analysis conducted for this study could not distinguish these different types of recorded absences, thus the estimated detection probability represented a combination of the detection and availability processes, even though these processes are technically different.

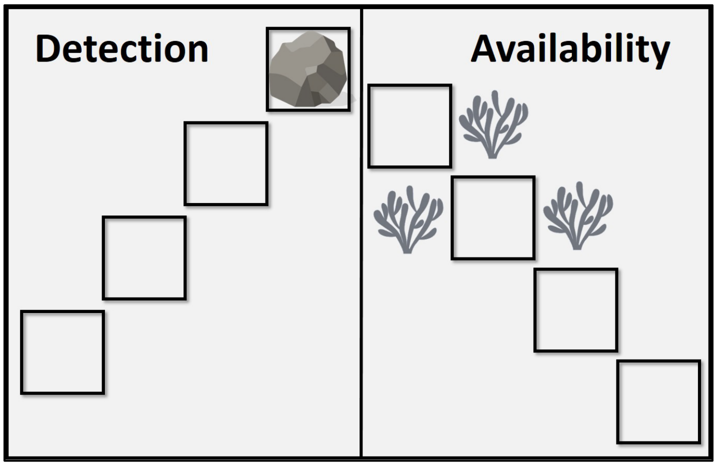

Figure 5. Illustration of detection and availability processes.
The two grid cells shown are a hypothetical subsample of the model grid, with both grid cells (sites) occupied by corals. Squares indicate spatial replicate samples (e.g., images) along a transect through these grid cells. Corals could go undetected because they are obscured by a rock in an image (left, detection process) or because they are not present at the sampled locations (right, availability process). The data would indicate absence in both grid cells, but technically these are different processes leading to recorded absence.

The issue of availability arises when using spatial replicates instead of temporal replicates in an occupancy model (Guillera-Arroita 2011). Traditionally, with temporal replicates, one would observe the entire site, or grid cell, on each visit. In this study, each spatial replicate was a subunit of the site (e.g., Figure 5). Therefore, three processes occur: detection, availability, and occupancy. These correspond to three levels of analysis: small- mid-, and large-scale, respectively (Kéry and Royle 2016). Conventionally, in a space-for-time substitution, availability is treated as part of either the observation-level (detection) or site-level (occupancy) process. Therefore, by combining availability with detection probability, the three levels can be collapsed to two: occupancy and detection. Kéry and Royle (2016) tested this approach through simulation and found that a two-level model performed equivalently to a three-level model in a space-for-time substitution framework, supporting the treatment of availability and detection probability as a single process. However, they did suggest the need for more investigation of this topic, and several subsequent studies have provided additional support for space-for-time substitutions (Srivathsa et al. 2018; Jiménez-Franco et al. 2019; Petracca et al. 2020). Hereafter, any mention of detection probability implies availability, as well.

2.6.3 Model assumptions

By distinguishing probabilities of occupancy and detection, occupancy models offer appropriate interpretation of sampled absences by distinguishing true absences (‘true negatives’) from false absences (‘false negatives’). One does not have to assume that every sampled absence is a true absence. However, occupancy models have several important assumptions (MacKenzie et al. 2002; Kéry and Royle 2016).

1. Imperfect detection. Sampled absences were not treated as true absences. False negatives were explicitly accounted for through the estimation of detection probability.
2. No false positives. DSC observations were identified only to the finest taxonomic level for which the organism could be identified with confidence.
3. Closure. The sampling time frame (i.e., temporal extent of the presence-absence data in the database compiled for this study) was short relative to the system dynamics. DSCs are sessile, slow-growing, and long-lived, so it could be assumed that their distributions remained static over this time frame. Therefore, static occupancy models were implemented, in contrast to dynamic occupancy models that relax this assumption and explicitly estimate colonization and extinction.
4. Independence of occupancy and detection probabilities. Since DSCs are sessile, there should be no behavioral response to the observer that could influence detection probability between visits.
5. Homogeneity of detection probability. The assumption that detectability was consistent throughout the study area was unlikely to be met in this study given the numerous surveys represented in the presence-absence data. To account for heterogeneity in detection probability, the survey area associated with each sample was included as an effort offset. Taxon- and site-level effects on detection probability were also included (see Section 2.7.4 for more details).

Sampling design is a further consideration in species distribution modeling. Unbalanced and non-random spatial sampling designs can bias estimates of occurrence and density, even with model-based inference (Kéry and Royle 2016; Conn et al. 2017). The compilation of presence-absence data from many different field surveys, with varying objectives and specifications, resulted in a non-random sampling design. Preferential sampling at sites with higher densities typically results in overestimates of the occupancy probability; however, occupancy models applied to such samples may result in overestimates of the detection probability and underestimates of the occupancy probability (Kéry and Royle 2016).

2.6.4 Multi-taxon occupancy analysis

Occupancy models provide estimates of absolute occupancy probabilities that are directly comparable (e.g., across taxa). For example, if the estimated occupancy probability is 0.2 for one taxon and 0.4 for another, one can reasonably estimate that the second is twice as likely to be present. These estimates are an improvement over the outputs of presence-background models, which predict relative occurrence (Kéry and Royle 2016). Occupancy models inherently provide the opportunity to model multiple taxa jointly in a hierarchical model, and to estimate taxonomic richness (i.e., combine the predicted distributions for multiple species, genera, or families into a single map). This hierarchical framework allows one to include rare taxa by the model ‘borrowing’ information from more common taxa while still allowing for heterogeneity in environmental responses among taxa (Zipkin et al. 2009). Multi-taxon occupancy models have become increasingly popular for describing the distributions of several taxa, including birds (Zipkin et al. 2009; Kéry and Royle 2008; Flanders et al. 2015; Jiménez-Franco et al. 2019) and mammals (Zipkin et al. 2010; Petracca et al. 2020). In this study, multi-taxon occupancy models were developed based on the approach of Dorazio and Royle (2005), limiting inference only to those taxa selected for modeling (Kéry and Royle 2016).

2.7 Model Structure

2.7.1 Composition of model runs

A multi-taxon hierarchical occupancy model was fit for 23 genera of structure-forming DSCs (Table 2). The multi-taxon nature of the model allowed for different spatial distributions and environmental predictor relationships across the genera. The genera included in the model did not need to have the same spatial distribution or co-occur. Because the model was hierarchical, less common genera could be included in the model by drawing information from data on more common genera. A single-taxon occupancy model was fit for lace corals in family Stylasteridae since no observations of lace coral presence in the database were recorded to genus or species. In addition to the models for DSCs, a single-taxon occupancy model was fit for hardbottom to predict and map the spatial distribution of hardbottom habitats across the study area. Samples in the database were treated as presence of hardbottom if the bottom type was identified as 'Hard/Hard', 'Hard/Soft', or 'Soft/Hard' and absence if the bottom type was identified as 'Soft/Soft.'

2.7.2 Overall structure

The occupancy models were fit in a Bayesian statistical framework and had two main components: a state process (occupancy) and an observation process (detection). The response data (i.e., dependent variable) were binary, observed presence-absence data y_{ijk} (= 0 or 1), where i = site (grid cell), j = occasion (spatial replicate), and k = genus. The expected probability of an observed presence at a given site on a given occasion was the product of occupancy and detection. The presence-absence data were assumed to be Bernoulli distributed with probability equal to the product of the estimated occupancy state and the probability of detection:

[1]
$$y_{ijk} \sim Bernoulli(z_{ik} p_{ijk})$$

where z_{ik} (= 0 or 1) is the true but unobserved state of occupancy at each sampled site and p_{ijk} is the probability of detection.

2.7.3 State process (occupancy)

The estimated occupancy state, z_{ik}, for site i and genus k was assumed to be a Bernoulli distributed variable with estimated occupancy probability, Ψ_{ik}, which was a function of the site-level environmental predictors:

[2]
$$z_{ik} \sim Bernoulli(\Psi_{ik})$$

[3]
$$cloglog(\Psi_{ik}) = \beta_{0k} + \sum_{v=1}^{n} f_{vk}(x_{vi}, \boldsymbol{\beta}_{vk})$$

where β_{0k} is the occupancy intercept for genus k, f_{vk} is a natural cubic polynomial spline for predictor variable v and genus k, n is the number of predictor variables, x_{vi} is the value of predictor variable v at site i, and $\boldsymbol{\beta}_{vk}$ is the vector of coefficients for f_{vk}. Each spline had three internal knots placed at quartiles of the predictor data, resulting in four coefficients. The natural cubic splines constrained the estimated relationships to be linear beyond the observed ranges of the predictor variables (Hastie et al. 2009). Spline basis transformations were obtained using the 'ns' function of the 'splines' package in base R (version 3.5.2; R Core Team 2018).

The genus- and predictor-specific occupancy intercepts (β_{0k}) and coefficients ($\boldsymbol{\beta}_{vk}$) were assumed to come from common normal distributions with associated mean (μ) and precision (τ) hyper-parameters:

[4]
$$\beta_{0k} \sim Normal(\mu_{\beta 0}, \tau_{\beta 0})$$

[5]
$$\boldsymbol{\beta}_{vk} \sim Normal(\mu_{\beta}, \tau_{\beta})$$

Each element of $\boldsymbol{\beta}_{vk}$ was assumed to be independent (i.e., zero multivariate normal covariance in Eq. 5). Similar to other occupancy modeling studies, normal prior probability distributions with a wide variance (mean = 0, precision = 1 x 10^{-6}) were assumed for mean hyper-parameters, and gamma prior probability distributions (shape = 0.001, rate = 0.001) were assumed for precision hyper-parameters.

2.7.4 Observation process (detection)

The probability of detection, p_{ijk}, was assumed to be a function of sampling effort, as well as site- and genus-specific effects:

$$cloglog(p_{ijk}) = \alpha_0 + \alpha_{1,i} + \alpha_{2,k} + log(effort_{ij}) \quad [6]$$

where α_0 is the intercept for detection, $\alpha_{1,i}$ is the effect of site i on detection, $\alpha_{2,k}$ is the effect of genus k on detection, and $effort_{ij}$ is the sampling effort associated with sample j from site i. Sampling effort was estimated as the area viewed for each sample (m^2), and the log of sampling effort was treated as an effort offset. Sampling effort was divided by 100 m^2 prior to the log transformation, so that presented estimates of detection probability correspond to a sample of 100 m^2. Additive site- and taxon-specific effects on the complementary log-log scale were assumed to follow normal distributions across sites and taxa, respectively (i.e., as random effects):

$$\alpha_{1,i} \sim Normal(0, \tau_{clp1}) \quad [7]$$

$$\alpha_{2,k} \sim Normal(0, \tau_{clp2}) \quad [8]$$

with means equal to 0 and estimated precision hyper-parameters, τ_{clp1} and τ_{clp2} (Pinheiro and Bates 2004). A vague normal prior probability distribution (mean = 0, precision = 1×10^{-6}) was assumed for the detection intercept, α_0, and vague gamma prior probability distributions (shape = 0.001, rate = 0.001) were assumed for the precision hyper-parameters, τ_{clp1} and τ_{clp2}.

2.8 Model Fitting and Assessment

The models were fit using JAGS (version 4.3.0), via package 'rjags' (version 4-8; Plummer 2018) in R (R Core Team 2018), which implements Markov chain Monte Carlo (MCMC) sampling. Five independent chains of 100,000 iterations each were run, following a burn-in of 100,000 updates after an adaptation phase of 100,000 iterations. Results were thinned by 100 resulting in 5,000 samples from the joint posterior probability distribution. Convergence was evaluated by visually inspecting MCMC trace plots and scatterplots of posterior samples for pairs of parameters and by calculating the Gelman-Rubin statistic ($\hat{R}$), a measure of between- and within-chain variation (Gelman and Rubin 1992). Satisfactory model convergence was assumed when $\hat{R} < 1.1$.

Model fit was assessed using the point-biserial correlation coefficient (r_{pb}) and the area under the receiver operating characteristic curve (AUC) applied to the observed presence-absence data and the corresponding model-predicted probabilities. Predicted probabilities were calculated two ways. First, predicted probabilities (P1) were calculated as the product of the estimated occupancy states (z_{ik}) and estimated detection probabilities (p_{ijk}); i.e., $z_{ik}p_{ijk}$. However, those predicted probabilities do not reflect the expected performance of the model at unsampled sites where the occupancy states and site effects on detection ($\alpha_{1,i}$) are unknown. To characterize model performance better in terms of unsampled sites, alternative predicted probabilities (P2) were calculated by substituting the estimated occupancy probability (Ψ_{ik}) for z_{ik} and adjusting the estimated detection probability by setting the estimated site-level effect ($\alpha_{1,i}$) to zero. Model performance calculated using these alternative predicted probabilities better reflects the maps of predicted occupancy probabilities. The posterior probability distributions for the performance metrics were obtained, and performance metrics were then summarized by their posterior mean values.

A model that fits the data well yields a higher point-biserial correlation. AUC compares the binary observations (presence-absence) to the continuous predicted probabilities by calculating the ratio of true positives to the inverse of false positives across a range of thresholds for the predicted probabilities. AUC ≤0.5 is no better than random, while AUC closer to 1 is desirable, being indicative of few false positives relative to true positives.

2.9 Model Predictive Performance from Validation

To assess the ability of the models to predict occurrence in unsampled areas, a spatial model validation was performed. The presence-absence data were divided into training and test subsets representing different geographic areas within the study area. Models were fit to the training data, and predictive performance was assessed with respect to the test data.

The ‘blockCV’ package (version 1.0.0; Valavi et al. 2019) in R (version 3.5.2; R Core Team 2018) was used to divide the data into the training and test subsets with approximately 70% and 30% of the data, respectively. First the study area was divided into spatial blocks (Figure 6), the size of which (95,541 m x 95,541 m) was determined from the spatial autocorrelation in the 18 predictors remaining following the first phase of environmental predictor selection (see Section 2.5). The data were then divided into 10 different subsets or ‘folds’ each composed of unique sets of spatial blocks while attempting to achieve a relatively even number of presences and absences across the folds. Seven of the folds were then chosen as the training subset with the remaining three folds making up the test subset to try to achieve a 70/30 split, with 70% of the presences and absences in the training subset and 30% of the presences and absences in the test subset. Because the multi-taxon model included multiple genera with unique spatial distributions of presences and absences, it was not possible to achieve a 70/30 split for presences and absences across all genera using the same set of folds to assign data to the training and test subsets. Therefore, seven and three folds were manually assigned to the training and test subsets, respectively, for each genus to achieve as close to a 70/30 split for presence and absence data for as many genera as possible while maintaining a substantial number of presences in both the training and test subsets for all genera. Model performance in terms of fit to the training data and prediction to the test data was assessed using the point-biserial correlation coefficient and AUC. Fit to the training data was calculated using both types of predicted probabilities (P1 and P2) while predictive performance was only assessed using the second type of predicted probabilities (P2) since there were no estimated occupancy states or site effects for the test data.

2.10 Maps of Observed and Predicted Spatial Distributions

A set of maps was created for each DSC taxon and for hardbottom habitats to depict its observed distribution from the presence-absence database and its predicted spatial distribution. The first map displays the locations of presences and absences from the presence-absence database compiled for this study. For each DSC taxon, it also includes the presence records for the taxon in the NOAA National Database for Deep-Sea Corals and Sponges (McGuinn et al. 2020; NOAA 2021). These additional records are not visible in the maps when they coincide with records also included in the presence-absence database, but in some cases the additional records identify areas where the taxon had been observed outside the spatial extent of the survey data included in the presence-absence database. The records from the NOAA National Database were not used in the models, however, because they only included information about the locations of DSC presence and could not be used to infer absence or quantify sampling effort. The second map depicts the predicted probability of occurrence (i.e., the posterior median occupancy probability) from the occupancy models. These maps indicate the expected occupancy probability based on the environmental predictor values at each grid cell, not the actual occupancy states (z). For example, if a taxon was observed in a grid cell then the actual occupancy state would be 1. Because estimates of occurrence probabilities were standardized across taxa (i.e., by accounting for absences), they are directly comparable among taxa and are estimates of absolute probability of occurrence, not relative. In addition to examining spatial patterns in the areas where DSCs or hardbottom habitats are predicted to occur, these maps can be used to identify potential targets for future exploration (e.g., an area predicted to have high probability of occurrence that has not been previously surveyed). The third map depicts the variability (i.e., uncertainty) in the predicted probability of occurrence (i.e., the posterior coefficient of variation of the occupancy probability).

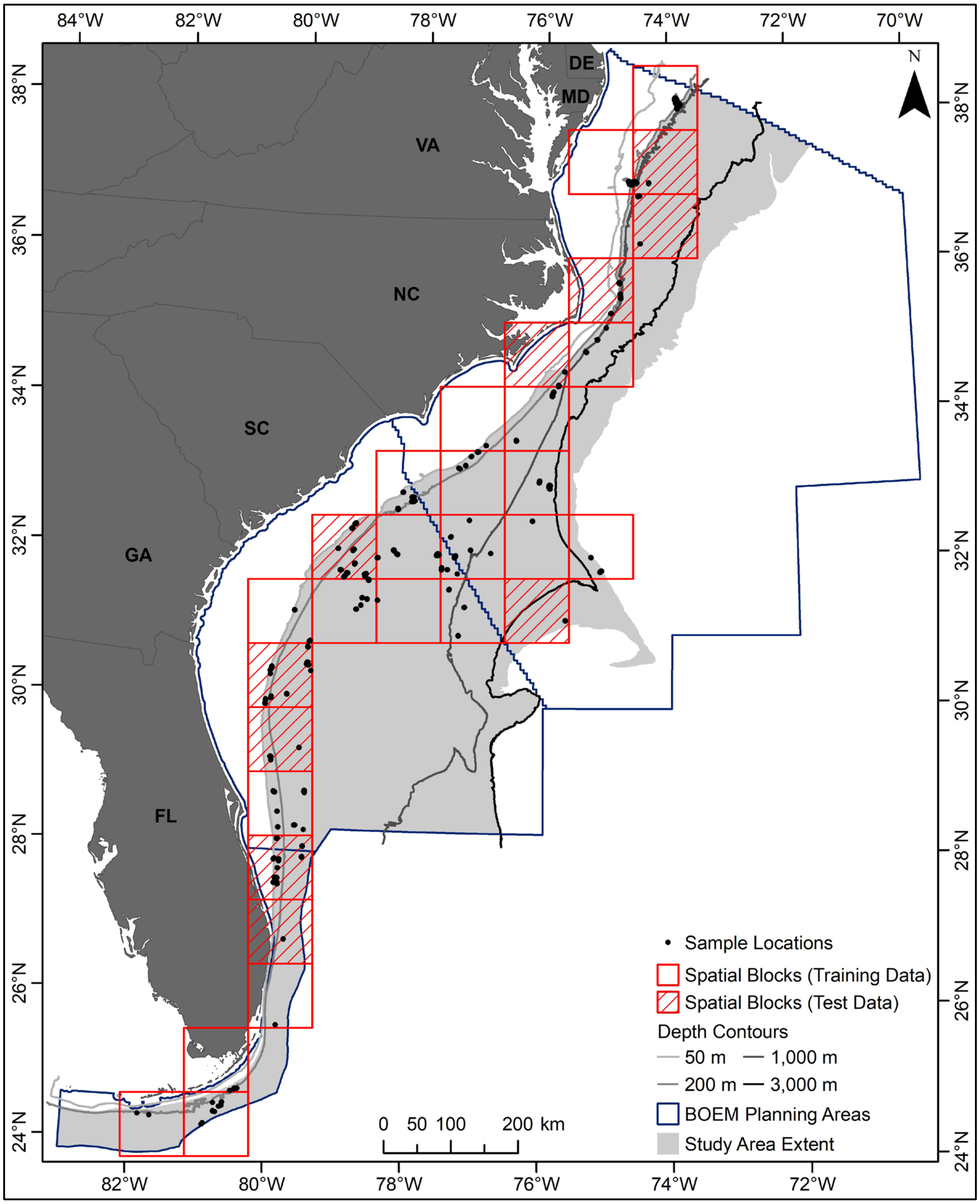

Figure 6. Example spatial blocks used in model validation.
This map shows the spatial blocks used to partition the samples into training and test subsets for validation of the multi-taxon model.

Maps of the coefficient of variation (CV) can be used to identify areas with greater variability or uncertainty (i.e., less precision) in the model predictions. It is important to note that in addition to areas of greater variability, higher values of the CV can also result from extremely low values of the predicted probability of occurrence. Therefore, maps of the CV should be interpreted in conjunction with the maps of the presence-absence records and the probability of occurrence to distinguish areas where variability was high and the taxon was predicted to occur from areas where the CV was high because the mean was extremely low.

In addition to the maps depicting the observed and predicted spatial distributions for each individual DSC taxon, maps were also created to depict the predicted genus richness (i.e., the posterior median genus richness, representing the number of genera expected at each grid cell) and corresponding variability in predicted genus richness (i.e., the posterior CV of genus richness). To create these maps, the full posterior probability distribution for genus richness was calculated, where richness was the sum of predicted occupancy probabilities (Ψ_{ik}) for the 23 genera included in the multi-taxon model (following Calabrese et al. 2014).

3 Results and Discussion

3.1 Model Fit

Point-biserial correlation coefficients ($\mathrm{r_{pb}}$) and AUC values indicated good model fit across the genera in the multi-taxon model and for Stylasteridae and hardbottom habitats when calculated using the estimated occupancy states (P1). The median correlation coefficient was 0.74 and all correlation coefficients were >0.4, while the AUC values were all >0.94 (Table 7). Performance was slightly degraded when predicted values were calculated using mean occupancy probabilities (P2) and ignoring site effects on detection, with a median correlation coefficient of 0.48 and a few AUC values <0.9 (Table 7). Taxa for which model fit was poorest in terms of the correlation between the observed presence-absence and the predicted probabilities included *Madrepora*, *Leiopathes*, *Bathypathes*, and *Anthothela*. However, all models presented in this report had sufficient model fit to be useful for informing management.

Table 7. Assessment of model fit

Taxon	Samples		$\mathrm{r_{pb}}$		AUC	
	Presence	Absence	P1	P2	P1	P2
Lophelia	1,144	8,679	0.89	0.83	0.99	0.98
Solenosmilia	318	9,505	0.69	0.44	0.99	0.95
Oculina	162	9,661	0.87	0.73	1.00	0.99
Madrepora	132	9,691	0.49	0.30	0.98	0.96
Cladocora	25	9,798	0.91	0.77	1.00	1.00
Enallopsammia	22	9,801	0.91	0.75	1.00	1.00
Stichopathes	192	9,631	0.87	0.74	1.00	0.99
Leiopathes	146	9,677	0.57	0.34	0.99	0.96
Antipathes	90	9,733	0.67	0.62	1.00	0.99
Tanacetipathes	45	9,778	0.65	0.41	1.00	0.99
Bathypathes	44	9,779	0.55	0.26	1.00	0.97
Paragorgia	921	8,902	0.71	0.50	0.97	0.90
Plumarella	677	9,146	0.84	0.72	0.99	0.98
Anthothela	346	9,477	0.43	0.24	0.94	0.85
Acanthogorgia	295	9,528	0.66	0.48	0.99	0.96
Paramuricea	208	9,615	0.78	0.41	1.00	0.86
Eunicella	162	9,661	0.82	0.53	1.00	0.98
Muricea	126	9,697	0.76	0.65	1.00	0.99
Thesea	77	9,746	0.69	0.44	1.00	0.99
Callogorgia	52	9,771	0.74	0.34	1.00	0.98
Nicella	48	9,775	0.66	0.36	1.00	0.99
Chrysogorgia	27	9,796	0.67	0.38	1.00	0.99
Acanella	25	9,798	0.83	0.47	1.00	0.99
Stylasteridae	660	9,163	0.84	0.59	0.99	0.96
Hardbottom	6,138	3,685	0.88	0.66	0.98	0.88

$\mathrm{r_{pb}}$ = point-biserial correlation coefficient.
AUC = area under the receiver operating characteristic curve.
P1: predicted probabilities were calculated as the product of the estimated occupancy states (z_{ik}) and estimated detection probabilities (p_{ijk}); i.e., $z_{ik}p_{ijk}$.
P2: predicted probabilities were calculated by substituting the estimated occupancy probability (Ψ_{ik}) for z_{ik} and adjusting the estimated detection probability by setting the estimated site-level effect ($\alpha_{1,i}$) to zero.

3.2 Model Predictive Performance from Validation

Model predictive performance when assessed on test data withheld from model fitting was generally poorer than model fit assessed on the model fit to the full dataset or the model fit to the training data, but predictive performance was still generally good overall. The median point-biserial correlation coefficient was 0.3; however, several genera (*Lophelia*, *Oculina*, *Cladocora*, *Stichopathes*, *Antipathes*, and *Muricea*) had correlation coefficients >0.6 (Table 8). Taxa for which model performance assessed on test data was poorest based on the point-biserial correlation coefficient included *Bathypathes*, *Anthothela*, *Acanthogorgia*, *Paramuricea*, *Callogorgia*, and *Acanella*. Most taxa had test AUC values >0.9, but a few genera (*Anthothela*, *Acanthogorgia*, *Paramuricea*) had test AUC values <0.6 (Table 8). It is important to note that it was not possible to achieve a 70/30 split (70% of the presences and absences in the training subset and 30% of the presences and absences in the test subset) for all genera in the multi-taxon model. This was especially true for the presences. In some cases (e.g., *Anthothela*), there were too few presences in the test data and it was difficult to assess model performance using the test data. However, based on the assessment of model fit and model performance from validation, all models presented in this report had sufficient model fit and model performance to be useful for informing management.

Table 8. Assessment of model performance from validation

Taxon	Samples (Training)		Samples (Test)		$\mathrm{r_{pb}}$ (Training)		$\mathrm{r_{pb}}$ (Test)	AUC (Training)		AUC (Test)
	Presence	**Absence**	**Presence**	**Absence**	**P1**	**P2**	**P2**	**P1**	**P2**	**P2**
Lophelia	642	6,464	502	2,215	0.86	0.73	0.81	0.99	0.95	0.97
Solenosmilia	179	6,927	139	2,578	0.65	0.36	0.34	0.97	0.87	0.98
Oculina	70	7,036	90	2,627	0.84	0.69	0.80	1.00	0.99	1.00
Madrepora	66	7,040	66	2,651	0.45	0.26	0.30	0.97	0.93	0.97
Cladocora	8	7,098	17	2,700	0.85	0.57	0.61	1.00	1.00	1.00
Enallopsammia	15	7,091	7	2,710	0.87	0.36	0.24	1.00	0.99	0.99
Stichopathes	55	7,051	137	2,580	0.84	0.62	0.77	1.00	0.98	1.00
Leiopathes	97	7,009	49	2,668	0.61	0.29	0.17	0.98	0.91	0.96
Antipathes	46	7,060	44	2,673	0.46	0.31	0.70	0.99	0.97	1.00
Tanacetipathes	37	7,069	8	2,709	0.63	0.33	0.22	0.99	0.97	1.00
Bathypathes	25	7,081	19	2,698	0.49	0.14	0.08	0.99	0.93	0.96
Paragorgia	915	6,191	6	2,711	0.62	0.51	0.29	0.96	0.91	0.76
Plumarella	437	6,669	240	2,477	0.81	0.57	0.66	0.98	0.94	0.99
Anthothela	336	6,770	10	2,707	0.50	0.31	-0.01	0.95	0.87	0.59
Acanthogorgia	173	6,933	122	2,595	0.66	0.35	-0.02	0.97	0.88	0.58
Paramuricea	156	6,950	52	2,665	0.82	0.35	0.09	1.00	0.90	0.53
Eunicella	85	7,021	77	2,640	0.80	0.41	0.10	0.99	0.96	0.98
Muricea	57	7,049	69	2,648	0.65	0.48	0.84	0.99	0.98	1.00
Thesea	48	7,058	30	2,687	0.66	0.39	0.37	0.99	0.98	0.99
Callogorgia	52	7,054	0	2,717	0.58	0.11	0.02	1.00	0.95	0.90
Nicella	18	7,088	30	2,687	0.53	0.23	0.33	0.99	0.97	0.99
Chrysogorgia	22	7,084	5	2,712	0.67	0.21	0.17	1.00	0.95	0.97
Acanella	9	7,097	16	2,701	0.81	0.28	0.00	1.00	0.98	0.80
Stylasteridae	462	7,594	198	1,569	0.88	0.73	0.54	1.00	0.98	0.93
Hardbottom	4,287	3,397	1,851	288	0.88	0.64	0.40	0.98	0.87	0.78

$\mathrm{r_{pb}}$ = point-biserial correlation coefficient.

AUC = area under the receiver operating characteristic curve.

P1: predicted probabilities were calculated as the product of the estimated occupancy states (z_{ik}) and estimated detection probabilities (p_{ijk}); i.e., $z_{ik}p_{ijk}$.

P2: predicted probabilities were calculated by substituting the estimated occupancy probability (Ψ_{ik}) for z_{ik} and adjusting the estimated detection probability by setting the estimated site-level effect ($\alpha_{1,i}$) to zero.

3.3 Probability of Detection

Detection probability was generally estimated to be higher than occupancy probability, although this was not always the case (Figures 7–9). For the multi-taxon model, detection probability and occupancy probability did not appear to be strongly correlated (e.g., higher detection probability with increasing occupancy probability). This suggests that the model may have successfully distinguished detection probability from occupancy probability.

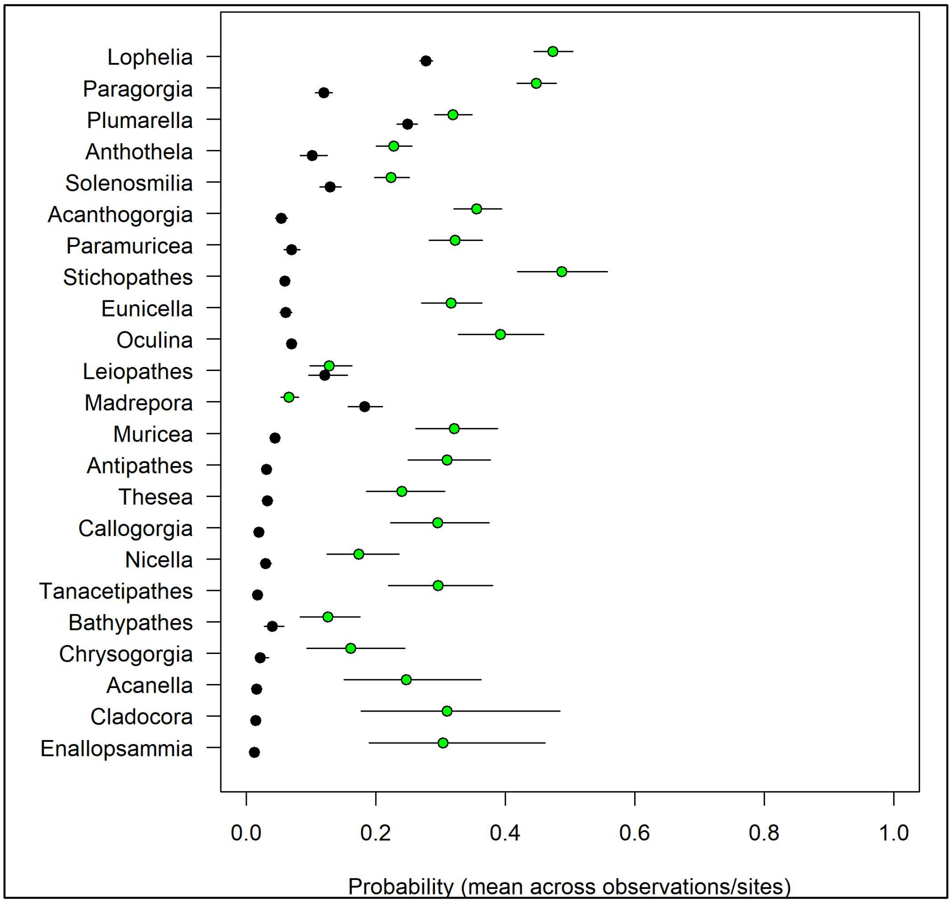

Figure 7. Probability of detection and occupancy for genera in the multi-taxon model.
In green are the posterior mean (points) and 95% credible interval (lines) for genus-specific detection probability averaged across sites and samples. In black are the posterior mean (points) and 95% credible interval (lines) for occupancy probability averaged across sites. Taxa are shown in order of decreasing frequency of occurrence (i.e., number of samples in the presence-absence database with recorded presence), with the most frequently observed genera at the top.

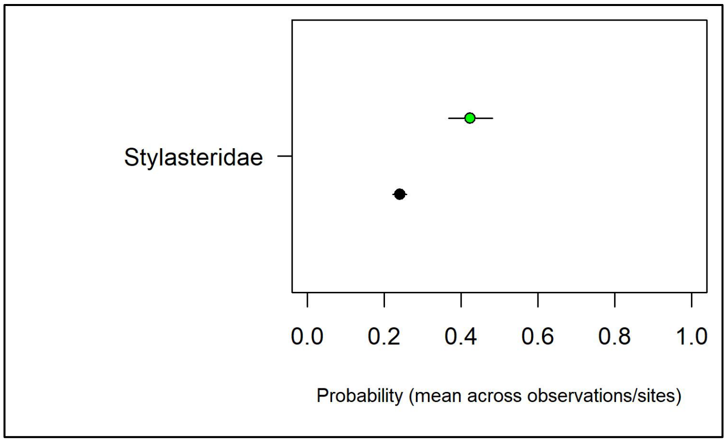

Figure 8. Probability of detection and occupancy for Stylasteridae.
In green is the posterior mean (point) and 95% credible interval (line) for detection probability averaged across sites and samples. In black is the posterior mean (point) and 95% credible interval (line) for occupancy probability averaged across sites.

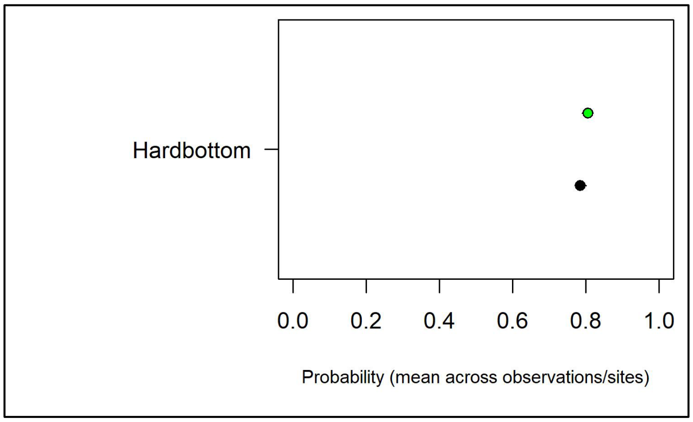

Figure 9. Probability of detection and occupancy for hardbottom habitats.
In green is the posterior mean (point) and 95% credible interval (line) for detection probability averaged across sites and samples. In black is the posterior mean (point) and 95% credible interval (line) for occupancy probability averaged across sites.

3.4 Observed and Predicted Spatial Distributions

This section describes the set of maps produced for each DSC taxon and hardbottom habitats and the maps of the predicted genus richness from the multi-taxon model (see Section 2.10 for details). Values of the median occupancy probability are referred to as very high (0.8–1), high (0.6–0.8), medium (0.4–0.6), low (0.2–0.4), and very low (0–0.2) predicted occurrence for the purpose of facilitating descriptions of the spatial patterns observed. Similarly, values of the CV of occupancy probability are referred to as very high (>25), high (10–25), medium (5–10), low (2–5), and very low (0–2). Appendix D contains the maps for each individual DSC taxon.

3.4.1 Stony corals (order Scleractinia)

The six genera of stony corals selected for the multi-taxon model included two genera (*Oculina*, *Cladocora*) typically found on the continental shelf, one genus (*Madrepora*) found across the continental shelf and slope, and three genera (*Lophelia*, *Solenosmilia*, *Enallopsammia*) typically found in deeper waters on the continental slope. *Oculina varicosa* is the most important deepwater reef-building coral on the shelf. *Lophelia pertusa* (= *Desmophyllum pertusum*), *Madrepora* spp., and *Enallopsammia profunda* contribute to reefs in deeper waters, with *Lophelia* being by far the most important of these. Unlike the other stony corals included in the multi-taxon model, *Cladocora* generally occurs in small colonies and is not known to build reef-like structures.

Oculina was present in 162 samples in the presence-absence database. These samples and additional records of *Oculina* presence in the NOAA National Database (most representing *Oculina varicosa*) were located along the continental shelf from Florida to the Carolinas (Figure D-1). There was a particularly high concentration of presences and a band of very high predicted occurrence offshore of Florida at the location known as Oculina Bank, a line of coral mound features constructed by *O. varicosa* (Figure D-1, Figure D-2). Smaller, patchy areas of medium to very high predicted occurrence were found off of the Florida Keys and along the continental shelf from northern Florida to Cape Lookout, North Carolina. Variability in the predicted occurrence of *Oculina* was very low on the continental shelf and generally highest in deeper waters (Figure D-3).

Cladocora was only present in 25 samples in the presence-absence database on the continental shelf offshore of Florida (Figure D-4). A small number of additional *Cladocora* observations in the NOAA National Database were located off of the Florida Keys (although shallower than the study area extent) and along the continental shelf from Florida to Cape Hatteras, North Carolina. Not surprisingly, given how uncommon *Cladocora* was in the study area, there were only a few small patches of medium to very high predicted occurrence on the continental shelf offshore of Florida (Figure D-5). Variability in the predicted occurrence of *Cladocora* was medium to very high throughout much of the study area, but was very low in the small area of the continental shelf where it was predicted to occur (Figure D-6).

Madrepora was present in 132 samples in the presence-absence database, and although the expected depth range for *Madrepora* spans both the continental shelf and slope, these samples were limited to the escarpment adjacent to the Pourtalès Terrace, the upper continental slope from Florida to Cape Lookout, and the Blake Plateau (Figure D-7). Many additional records of *Madrepora* presence in the NOAA National Database were found on the continental slope offshore of Florida and on the Blake Plateau, as well as on the continental shelf offshore of North Carolina. There were extensive areas of high to very high predicted occurrence along the upper continental slope from the Florida Keys to the Carolinas and patches of medium to very high predicted occurrence across the Blake Plateau (Figure D-8). The predicted occurrence of *Madrepora* was very low on the continental shelf off of Cape Lookout where there were records of *Madrepora* presence in the NOAA National Database but no samples in the presence-absence database. Variability in the predicted occurrence of *Madrepora* was highest north of Cape Hatteras and on some parts of the continental shelf, but was very low to low across much of the continental slope and on the Blake Plateau where *Madrepora* was predicted to occur (Figure D-9).

Lophelia was the most frequently observed stony coral in the presence-absence database and was present in 1,144 samples. Similar to *Madrepora*, *Lophelia* was present at samples along the upper continental slope from the Florida Keys to Cape Lookout and on the Blake Plateau, but *Lophelia* was also present in samples at Norfolk and Baltimore Canyons (Figure D-10). There were numerous additional records of *Lophelia* presence in the NOAA National Database along the upper continental slope from the Florida Keys to the Carolinas and across the Blake Plateau, including records from ROV surveys conducted by NOAA Ship *Okeanos Explorer* in 2019 that were not included in the presence-absence database. Broad areas of very high predicted occurrence for *Lophelia* spanned from the Pourtalès Terrace and the adjacent escarpment north along the upper continental slope to the Carolinas (Figure D-11). Additional smaller patches of high to very high predicted occurrence were found across the Blake Plateau. The widespread areas of predicted occurrence for *Lophelia* included parts of the study area where there were records of *Lophelia* presence in the NOAA National Database but no samples in the presence-absence database. North of Cape Hatteras, there were narrow bands of high to very high predicted occurrence in the canyon and inter-canyon areas that incise the continental slope (see inset map in Figure D-11). Variability in the predicted occurrence of *Lophelia* was generally very low, with only a few areas deeper on the continental slope having medium to high variability (Figure D-12).

Solenosmilia was present in 318 samples in the presence-absence database on the upper continental slope from Florida to South Carolina, on the Blake Plateau and the Blake Escarpment north of the Blake Spur, and at depths >1,000 m at Norfolk Canyon (Figure D-13). There were relatively few additional records of *Solenosmilia* presence in the NOAA National Database, although these did include some observations on the Pourtalès Terrace and the adjacent escarpment. Fairly large but patchy areas of high to very high predicted occurrence extended along the continental slope from the escarpment off the Miami Terrace to the Carolinas (Figure D-14). Small patches of medium to very high predicted occurrence were found around 1,000 m depth in the canyon and inter-canyon areas from Norfolk Canyon to Baltimore Canyon (see inset map in Figure D-14). There were also some large areas of high to very high predicted occurrence in deeper, unsampled areas (i.e., where there were no samples in the presence-absence database) farther offshore on the Blake Plateau, including on the Blake Spur and the Blake Escarpment. Surveys in these areas would be beneficial for ground truthing the occupancy model predictions. Variability in the predicted occurrence of *Solenosmilia* was very low on most of the continental slope where *Solenosmilia* was predicted to occur and was low to medium along the continental shelf and some deeper, unsampled areas at the northern and southern ends of the study area (Figure D-15).

Enallopsammia was only present in 22 samples in the presence-absence database. These samples were located in deeper waters on the edge of the Blake Plateau and the Blake Escarpment north of the Blake Spur and on the upper continental slope offshore of northern Florida (Figure D-16). The NOAA National Database contained numerous additional records of *Enallopsammia* presence, particularly along the upper continental slope from southeastern Florida to South Carolina. Areas with high to very high predicted occurrence were concentrated along the Blake Escarpment north of the Blake Spur with smaller patches across the Blake Plateau (Figure D-17). It is likely that the model underpredicted the occurrence of *Enallopsammia*, particularly along the upper continental slope where there were presence records in the NOAA National Database but few sample locations in the presence-absence database. Variability in the predicted occurrence of *Enallopsammia* was very low on the Blake Plateau and the Blake Escarpment where *Enallopsammia* was predicted to occur and was generally low to medium throughout the rest of the study area, with a few areas of high to very high variability (Figure D-18).

3.4.2 Black corals (order Antipatharia)

Black corals selected for the multi-taxon model included three genera (*Stichopathes*, *Antipathes*, *Tanacetipathes*) typically found on the continental shelf, one genus (*Leiopathes*) found on the outer continental shelf and upper slope, and one genus (*Bathypathes*) typically found in deeper waters on the continental slope. These genera are associated with hardbottom habitats, with the exception of some *Stichopathes* spp. that are adapted to anchor in soft sediments. While black corals do not build reefs, they do provide structure that is utilized by other species and are vulnerable to human impacts. *Leiopathes* in particular is extremely slow-growing and long-lived, reaching ages of 100s to 1,000s of years offshore of the southeastern US (Williams et al. 2007) and in the Gulf of Mexico (Prouty et al. 2011).

Stichopathes was present in 192 samples in the presence-absence database along the continental shelf from Florida to the Carolinas (Figure D-19). There were additional records of *Stichopathes* presence in the NOAA National Database along the continental shelf, including areas (e.g., off of Cape Lookout) that did not have samples in the presence-absence database. Areas of very high predicted occurrence for *Stichopathes* were found along the continental shelf from Florida to the Carolinas (Figure D-20). There were also some *Stichopathes* presence records in the NOAA National Database on the continental slope, but these records were at depths outside the expected depth range for described *Stichopathes* spp. and in areas had very low predicted occurrence. These records may represent a new genus (*Aphanostichopathes*) just described in 2021. Variability in the predicted occurrence of *Stichopathes* was very low along the continental shelf where *Stichopathes* was predicted to occur with only a few areas of high to very high variability in deeper waters at the northern and southern ends of the study area (Figure D-21).

Antipathes was present in 90 samples in the presence-absence database. Similar to *Stichopathes*, these samples were also located on the continental shelf but were less common and did not extend as far south offshore of Florida (Figure D-22). Additional records of *Antipathes* presence in the NOAA National Database were found on the continental shelf, particularly offshore of Georgia and South Carolina, and there were also a few records on the Miami and Pourtalès Terraces. Areas of very high predicted occurrence for *Antipathes* were found on the continental shelf offshore of the Carolinas, but not off of the Florida-Georgia border where there were presences in the presence-absence database and the NOAA National Database (Figure D-23). Variability in the predicted occurrence of *Antipathes* was very low on the continental shelf where it was predicted to occur but medium to very high across much of the continental slope (Figure D-24).

Tanacetipathes was even less common and was present in only 45 samples in the presence-absence database along the continental shelf from Florida to the Carolinas (Figure D-25). There were some additional *Tanacetipathes* presences along the continental shelf in the NOAA National Database. Areas of high to very high predicted occurrence for *Tanacetipathes* were smaller and patchier than for *Stichopathes* and *Antipathes*, and were primarily on the continental shelf offshore of North Carolina (Figure D-26). Like *Antipathes*, variability in the predicted occurrence of *Tanacetipathes* was very low on the continental shelf where it was predicted to occur but medium to very high across much of the continental slope (Figure D-27).

Leiopathes was present in 146 samples in the presence-absence database. These samples were located on the Pourtalès Terrace, on the upper continental slope from Florida to South Carolina, and on the Blake Plateau (Figure D-28). Some additional records of *Leiopathes* presence in the NOAA National Database were found off the Florida Keys near the Pourtalès Terrace and farther offshore on the Blake Plateau than the records in the presence-absence database. There were areas of very high predicted occurrence for *Leiopathes* on the Miami and Pourtalès Terraces, on the upper continental slope offshore of Georgia and South Carolina, and across the Blake Plateau, with additional areas of medium to high predicted occurrence in these locations as well (Figure D-29). These areas of predicted occurrence generally coincided with the presence records in the presence-absence database and NOAA National Database, but were also found in areas farther offshore on the Blake Plateau that were not represented by samples in the presence-absence database. Surveys in these areas would be beneficial for ground truthing the occupancy model predictions. Variability in the predicted occurrence of *Leiopathes* was very low in the parts of the continental slope where *Leiopathes* was predicted to occur and generally low to medium elsewhere with only a few areas with high variability in the northern part of the study area (Figure D-30).

Bathypathes was not commonly observed and was only present in 44 samples in the presence-absence database. Most of these samples were located on the upper continental slope from northern Florida to South Carolina and on the Blake Plateau and the Blake Escarpment north of the Blake Spur, but there were also samples with *Bathypathes* presence on the Pourtalès Terrace and farther north on the continental slope offshore of North Carolina (Figure D-31). Additional records of *Bathypathes* presence in the NOAA National Database were located on the continental slope offshore of the Florida Keys and southeastern Florida and on the Blake Plateau. Areas with very high predicted occurrence for *Bathypathes* were primarily farther offshore on the Blake Plateau and the Blake Escarpment, with smaller, patchy areas of medium to very high predicted occurrence on the central Blake Plateau (Figure D-32). The largest area of very high predicted occurrence was in the eastern part of the Blake Plateau, near the Blake Spur, where there were no samples in the presence-absence database and no additional records of *Bathypathes* presence in the NOAA National Database. Surveys in this area would be beneficial for ground truthing the occupancy model predictions. The predicted occurrence for *Bathypathes* was very low at some of the locations—the Pourtalès Terrace, the western and northern parts of the Blake Plateau, and the continental slope offshore of North Carolina—where there were *Bathypathes* presences in the presence-absence database, possibly because there were few presences at these locations and also records of *Bathypathes* absence. Variability in the predicted occurrence of *Bathypathes* was very low on the Blake Plateau where *Bathypathes* was predicted to occur and low to medium across the rest of the study area (Figure D-33).

3.4.3 Gorgonian corals (order Alcyonacea)

The gorgonian corals selected for the multi-taxon model included three genera (*Muricea*, *Thesea*, *Nicella*) primarily found on the continental shelf, one genus (*Callogorgia*) found across the continental shelf and upper continental slope, three genera (*Plumarella*, *Anthothela*, *Acanthogorgia*) typically found at the edge of the continental shelf and on the upper continental slope, one genus (*Eunicella*) found on the upper continental slope, one genus (*Paramuricea*) found across the continental shelf and slope, and three genera (*Paragorgia*, *Chrysogorgia*, *Acanella*) typically found across the continental slope. These genera are associated with hardbottom habitats, with the exception of *Acanella*, which can also be found in soft sediments. Gorgonians represent the most diverse group of DSCs in the region, and include a large number of genera beyond those included in the models (Hourigan et al. 2017a).

Muricea was present in 126 samples in the presence-absence database along the continental shelf from northern Florida to the Carolinas, with some additional records of *Muricea* presence in the NOAA National Database along this part of the continental shelf as well (Figure D-34). Areas of very high predicted occurrence for *Muricea* were located on the continental shelf offshore of the Carolinas, with some smaller areas of medium to very high predicted occurrence offshore of Florida and Georgia (Figure D-35). Variability in the predicted occurrence of *Muricea* was very low on the continental shelf where it was predicted to occur but was medium to very high across the rest of the study area (Figure D-36).

Thesea was present in 77 samples in the presence-absence database. These samples were located on the continental shelf from northern Florida to the Carolinas, but there were additional records of *Thesea* presence in the NOAA National Database along the continental shelf and just past the shelf break from offshore of the Florida Keys up to Cape Hatteras (Figure D-37). There were bands of very high predicted occurrence for *Thesea* along the continental shelf offshore of the Carolinas and smaller patches of medium to very high predicted occurrence off of northern Florida and Georgia (Figure D-38). There was very low predicted occurrence offshore of the Florida Keys and between Cape Lookout and Cape Hatteras, where there were records of *Thesea* presence in the NOAA National Database but no samples in the presence-absence database. It is likely the model underpredicted the occurrence of *Thesea* in these areas. Variability in the predicted occurrence of *Thesea* was very low on the continental shelf where it was predicted to occur but was medium to very high across the rest of the study area (Figure D-39).

Nicella was present in 48 samples in the presence-absence database along the continental shelf from Florida to the Carolinas, with some additional records of *Nicella* presence in the NOAA National Database on the continental shelf, particularly offshore of South Carolina (Figure D-40). A large area of very high predicted occurrence for *Nicella* was located on the continental shelf offshore of South Carolina, with smaller patches of very high predicted occurrence along the continental shelf from Florida to Cape Lookout (Figure D-41). Variability in the predicted occurrence of *Nicella* was very low on the continental shelf where it was predicted to occur but was medium to very high across the rest of the study area (Figure D-42).

Callogorgia was fairly uncommon in the presence-absence database and was present in 52 samples at just a few locations on the upper continental slope offshore of Florida, on the Blake Plateau, and near the continental shelf break offshore of South Carolina (Figure D-43). Only a few additional areas—the continental slope off the Florida Keys and the continental shelf and slope offshore of southeastern Florida—had *Callogorgia* presences in the NOAA National Database. There were some patchy areas of low to medium predicted occurrence of *Callogorgia* on the Blake Plateau and on the continental shelf off of the Carolinas, but there were no areas of high to very high predicted occurrence (Figure D-44). Variability in the predicted occurrence of *Callogorgia* was very low to low across much of the continental shelf and on the northern part of the Blake Plateau, but was medium to very high across much of the study area and highest at the northern and southern ends of the study area (Figure D-45).

Plumarella was present in 677 samples in the presence-absence database, and these sample locations were widespread, including on the Miami and Pourtalès Terraces, along the upper continental slope from Florida to the Carolinas, on the Blake Plateau, and at a few spots on the continental shelf offshore of Florida and South Carolina (Figure D-46). There were also many additional *Plumarella* presences in the NOAA National Database offshore of the Florida Keys, along the upper continental slope from southeastern Florida to South Carolina, across the central Blake Plateau, and on the continental slope between Cape Lookout and Cape Hatteras. Areas of very high predicted occurrence for *Plumarella* were extensive across the Blake Plateau, with additional areas of very high predicted occurrence on the Miami and Pourtalès Terraces and along the upper continental slope from Florida to the Carolinas (Figure D-47). Variability in the predicted occurrence of *Plumarella* was generally very low, but was medium to very high at the northern and southern ends of the study area (Figure D-48).

Anthothela was present in 346 samples in the presence-absence database on the northern Blake Plateau and at Norfolk and Baltimore Canyons, and additional *Anthothela* presences in the NOAA National Database were located on the Miami Terrace and adjacent escarpment and on the upper continental slope and western Blake Plateau offshore of northern Florida and Georgia (Figure D-49). Bands of high to very high predicted occurrence for *Anthothela* were found in the inter-canyon areas of the continental slope north of Cape Hatteras and in Norfolk, Washington, and Baltimore Canyons (see inset map in Figure D-50). Outside of these areas there were only some small and medium patches of low to medium predicted occurrence on the Pourtalès Terrace and on the western Blake Plateau. Variability in the predicted occurrence of *Anthothela* was very low across most of the Blake Plateau and in the canyon and inter-canyon areas north of Cape Hatteras, but was medium to very high along the continental shelf and in some of the deeper waters of the study area (Figure D-51).

Acanthogorgia was present in 295 samples in the presence-absence database, primarily at Norfolk Canyon but also on the western and northern Blake Plateau and on the continental slope offshore of North Carolina (Figure D-52). There were some additional *Acanthogorgia* presences in the NOAA National Database on the western and central Blake Plateau offshore of Florida and Georgia. There were narrow bands of very high predicted occurrence for *Acanthogorgia* along the continental slope and in the canyon and inter-canyon areas north of Cape Lookout, particularly in Norfolk Canyon (see inset map in Figure D-53). The predicted occurrence was only low to medium on the Blake Plateau, even where there were presences in the presence-absence database. It is likely that the model underpredicted the occurrence of *Acanthogorgia* on the Blake Plateau, possibly because the samples in the presence-absence database with *Acanthogorgia* presence were predominantly at Norfolk Canyon. Variability in the predicted occurrence of *Acanthogorgia* was very low where it was predicted to occur, but there were areas of medium to very high variability on the Blake Plateau, on the continental shelf, and at some of the deeper parts of the study area (Figure D-54).

Eunicella was present in 162 samples in the presence-absence database. These samples were located on the upper continental slope and western edge of the Blake Plateau from Florida to South Carolina and farther offshore on the Blake Plateau off of South Carolina (Figure D-55). Additional *Eunicella* presences in the NOAA National Database were located on the Miami Terrace and adjacent escarpment, along the upper continental slope from Florida to South Carolina, and across the Blake Plateau. A large area of very high predicted occurrence for *Eunicella* was found on the Blake Plateau along with smaller patches of very high predicted occurrence and additional areas of low to medium predicted occurrence across the Blake Plateau (Figure D-56). It is likely that the model underpredicted the occurrence of *Eunicella* on the

Miami Terrace and adjacent escarpment, where there were *Eunicella* presences in the NOAA National Database but very low predicted occurrence. Variability in the predicted occurrence of *Eunicella* was very low across most of the Blake Plateau, but was medium to very high on parts of the continental shelf and on the continental slope north of Cape Hatteras (Figure D-57).

Paramuricea was present in 208 samples in the presence-absence database, including samples on the continental shelf offshore of South Carolina, on the Miami and Pourtalès Terraces, on the upper continental slope from Florida to South Carolina, across the Blake Plateau north of the Blake Spur, on the continental slope offshore of North Carolina, and at Norfolk and Baltimore Canyons (Figure D-58). Additional records of *Paramuricea* presence in the NOAA National Database were found on the continental shelf and slope around the Pourtalès Terrace, on the continental slope from the Miami Terrace to central Florida, and on the Blake Plateau. There were large areas with high to very high predicted occurrence for *Paramuricea* on the central Blake Plateau and along the Blake Escarpment north of the Blake Spur (Figure D-59). Smaller patches of high to very high predicted occurrence were found on the Miami and Pourtalès Terraces and along the upper continental slope from Florida to Cape Hatteras, as well as in deeper incised parts of the continental slope near the submarine canyons (see inset map in Figure D-59). Variability in the predicted occurrence of *Paramuricea* was very low across most of the study area, except at the northern and southern ends (Figure D-60).

Paragorgia was present in 921 samples in the presence-absence database. Many of these samples were concentrated at Norfolk and Baltimore Canyons, with others found across the Blake Plateau and the Blake Escarpment north of the Blake Spur and on the upper continental slope near Cape Hatteras (Figure D-61). There were some additional records of *Paragorgia* presence in the NOAA National Database on the central Blake Plateau, the continental slope offshore of southeastern Florida, and on the Pourtalès Terrace. It is likely that the records to the north in the canyons were *Paragorgia arborea*, while the records on the Blake Plateau and farther south represented a different species. Similar to the observation data, areas of very high predicted occurrence for *Paragorgia* were concentrated north of Cape Hatteras, including a band between 200–1,000 m depth extending along much of the inter-canyon area between Hatteras and Norfolk Canyons, much of Norfolk Canyon, and smaller areas at Washington and Baltimore Canyons (see inset map in Figure D-62). Although there were observations of *Paragorgia* on the Blake Plateau, the predicted occurrence of *Paragorgia* was very low. This suggests that *Paragorgia* occurrence may be uncommon on the Blake Plateau or that the extent of *Paragorgia* occurrence in this area was underpredicted by the model. Variability in the predicted occurrence of *Paragorgia* was very low where it was predicted to occur in the canyon and inter-canyon areas of the continental slope, but was medium to high on much of the continental shelf (Figure D-63).

Chrysogorgia was only present in 27 samples in the presence-absence database but was observed on the western edge of the Blake Plateau offshore of Florida and Georgia, along the Blake Escarpment north of the Blake Spur, and in deeper waters on the continental slope offshore of North Carolina (Figure D-64). There were some additional *Chrysogorgia* presences in the NOAA National Database on the Blake Plateau and on the escarpment off of the Florida Keys. High to very high predicted occurrence for *Chrysogorgia* was limited to the Blake Escarpment north of the Blake Spur (Figure D-65). There were also areas of low to medium predicted occurrence along the Blake Escarpment and a few patches of low to medium predicted occurrence on the western Blake Plateau. Variability in the predicted occurrence of *Chrysogorgia* was very low along the Blake Escarpment, but was medium to high along the continental shelf and in some areas of the continental slope (Figure D-66).

Acanella was present in only 25 samples in the presence-absence database. These samples were located across the Blake Plateau north of the Blake Spur and in deeper waters (>1,000 m) on the continental slope offshore of North Carolina and Virginia (Figure D-67). There were additional *Acanella* presences in the NOAA National Database on this part of the continental slope at the northern end of the study area as well as numerous records of *Acanella* presence on the continental slope offshore of the Florida Keys, including some records from recent surveys conducted by NOAA Ship *Okeanos Explorer* in 2019. Areas of high to very high predicted occurrence for *Acanella* were found on the deeper continental slope offshore of Virginia and in small patches on the northern Blake Plateau and along the Blake Escarpment (Figure D-68). There were additional patches of low to medium predicted occurrence in these areas as well as on the central Blake Plateau. The predicted occurrence of *Acanella* was very low on most of the continental slope off of the Florida Keys (except for a small patch of medium predicted occurrence on the Pourtalès Terrace) where there were additional records of *Acanella* presence in the NOAA National Database. It is likely that the model underpredicted the occurrence of *Acanella* in this part of the study area. Variability in the predicted occurrence of *Acanella* was very low on the deep continental slope and parts of the Blake Plateau where it was predicted to occur and generally low to medium across the rest of the study area (Figure D-69). It is important to note that *Acanella*, unlike the other genera of structure-forming gorgonian corals selected for the multi-taxon model, can anchor in soft sediments. Because the samples in the presence-absence database generally represented hardbottom habitats (see Section 3.4.6), it is likely that the samples underrepresented the spatial extent of *Acanella* in the study area. It is also important to note that while *Acanella* was only present in 25 samples in the presence-absence database, there were 474 samples with bamboo corals present but identified only to the family level.

3.4.4 Genus richness

The genera included in the multi-taxon model included several that occur only on the continental shelf (<200 m depth), others found exclusively on the upper continental slope (200–1,000 m depth), some found more often in deeper waters (>1,000 m), and some that occur across the continental shelf and slope (Table 2). Predicted genus richness was highest (>5) on parts of the continental shelf offshore of the Carolinas and in patches across the Blake Plateau (Figure 10). There were also broad swaths with high predicted genus richness (3–5) along the continental shelf and across the Blake Plateau, with smaller areas of high predicted genus richness on the Miami and Pourtalès Terraces. Predicted genus richness was generally very low (0–1) in the deepest waters of the study area north of the Blake Spur. Variability in the predicted genus richness was generally highest (>0.5) in the deeper, unsampled (i.e., not represented by samples in the presence-absence database) parts of the study area, but was also moderate (0.3–0.5) on parts of the continental shelf and slope where the predicted genus richness was lowest (Figure 11).

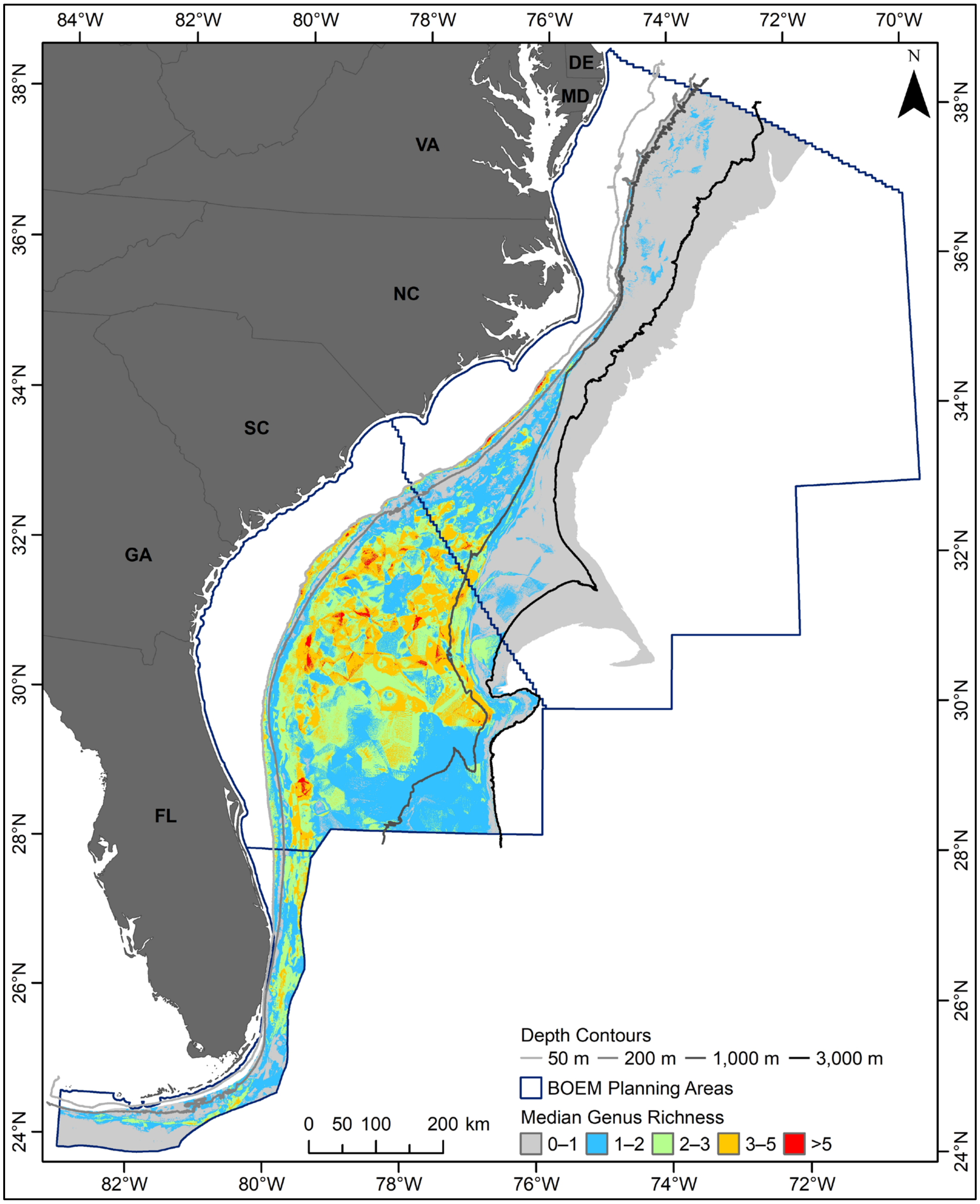

Figure 10. Predicted genus richness from the multi-taxon model.
This map shows the posterior median genus richness from the multi-taxon model.

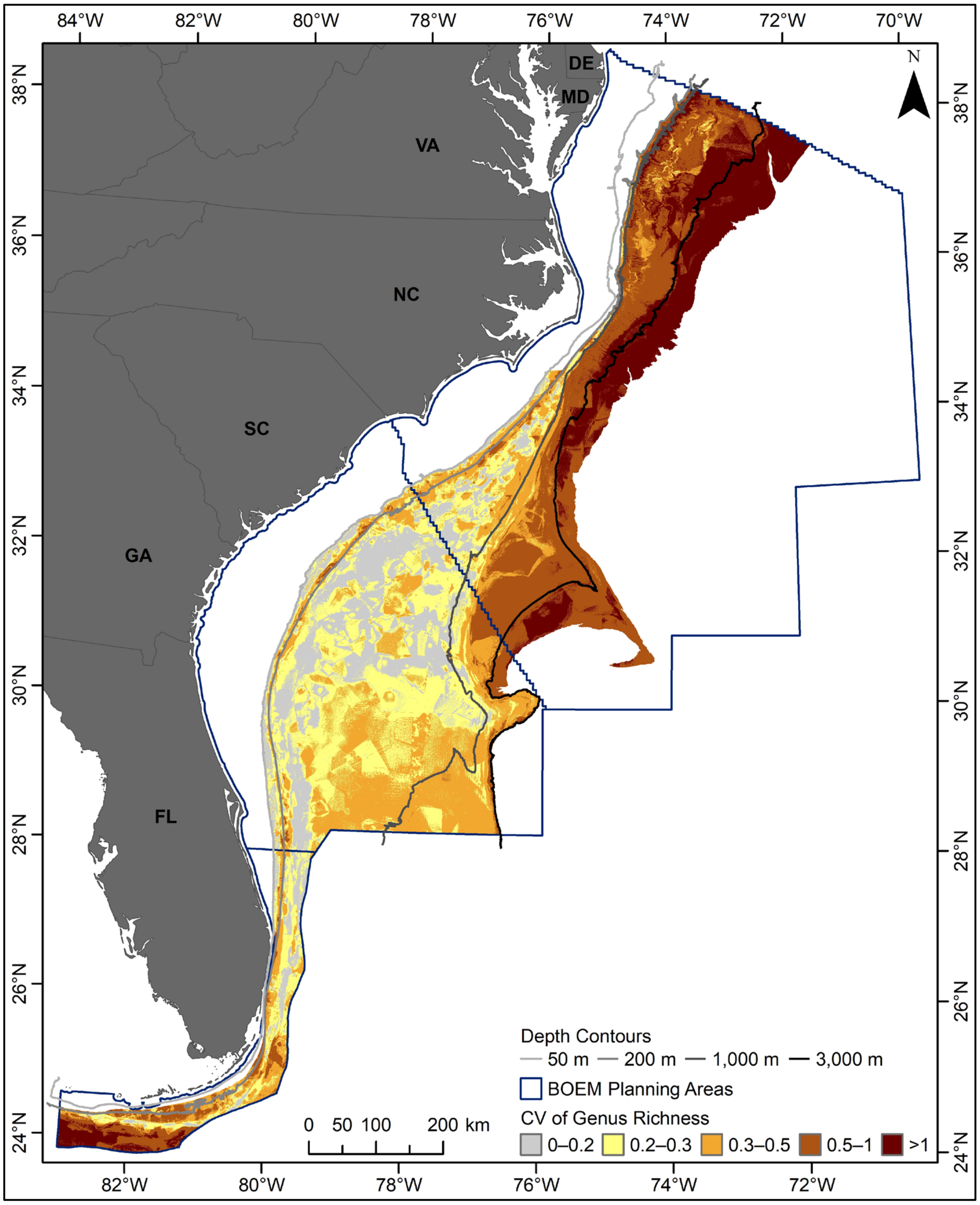

Figure 11. Variability in the predicted genus richness from the multi-taxon model.
This map shows the posterior coefficient of variation of genus richness from the multi-taxon model.

Though the map of predicted genus richness is useful for identifying areas where multiple genera of DSCs are likely to co-occur, it should be noted that the map reflects only the predicted distributions of the taxa selected for the multi-taxon model (i.e., only taxa identified to the genus level in the field surveys used to compile the presence-absence database). There are other, likely abundant, taxa (e.g., bamboo corals other than *Acanella*) that were not identified to the genus level and thus not included in the multi-taxon model. In addition, the map of the predicted genus richness does not indicate which taxa may co-occur at a given location. However, the map could be used in conjunction with the maps of predicted occurrence for individual taxa to examine potential assemblages of DSCs in a given location. For example, where there is a patch with very high predicted genus richness on the continental shelf off Cape Lookout, there is also very high predicted occurrence for *Stichopathes*, *Antipathes*, *Tanacetipathes*, *Muricea*, *Thesea*, and

Nicella. Although joint species distribution models have been used to understand community assemblages and there are also other multivariate statistical methods (e.g., ordination) that would be appropriate for assessing the composition of DSC assemblages in the study areas from the occurrence and environmental predictor data, analysis of DSC community assemblages was not the focus of this study.

3.4.5 Lace corals (family Stylasteridae, order Anthoathecata)

Lace corals in family Stylasteridae were present in 660 samples in the presence-absence database, and these samples were widespread across the study area. Samples with observations of lace corals were located on the Miami and Pourtalès Terraces, on the upper continental slope and western edge of the Blake Plateau from Florida to South Carolina, across the northern Blake Plateau, and along the continental shelf from northern Florida to the Carolinas (Figure D-70). Additional records of Stylasteridae presence in the NOAA National Database were found on the continental shelf and slope off of the Florida Keys, on the continental slope offshore of eastern Florida, and on the western and central Blake Plateau. Large swaths of very high predicted occurrence of Stylasteridae extended along the continental slope from the Florida Keys to South Carolina and across the central Blake Plateau (Figure D-71). There were also smaller patches of high to very high predicted occurrence on the continental shelf offshore of Florida and North Carolina, across the Blake Plateau, on the Blake Ridge, and on the upper continental slope offshore of North Carolina. Variability in the predicted occurrence of Stylasteridae was very low where it was predicted to occur and was only high to very high in deeper waters farther north than Stylasteridae was observed (Figure D-72).

3.4.6 Hardbottom habitats

For the purpose of modeling the occurrence of hardbottom habitats, samples in the presence-absence database were treated as presence of hardbottom if the bottom type was identified as 'Hard/Hard', 'Hard/Soft', or 'Soft/Hard' and absence if the bottom type was identified as 'Soft/Soft.' Using this definition of hardbottom presence-absence, hardbottom habitats were observed at most (n = 6,138) of the sample locations in the presence-absence database, including samples on the Miami and Pourtalès Terraces, along the continental shelf and upper slope from Florida to the Carolinas, on the Blake Plateau and Blake Escarpment north of the Blake Spur, on the Blake Ridge, and in the canyon and inter-canyon areas of the continental slope north of Cape Hatteras (Figure 12). Not surprisingly, given the extent of hardbottom occurrences in the presence-absence database, there were wide swaths of very high predicted occurrence at all of these locations where hardbottom habitats were observed as well as in areas where there were no samples in the presence-absence database along the continental shelf, along the upper continental slope from Florida to Cape Hatteras, and across the Blake Plateau (Figure 13). The area where hardbottom habitats were least likely to occur based on the model prediction (or at least where areas of high predicted occurrence were patchier) was deeper waters on the continental slope north of the Blake Escarpment. Variability in the predicted occurrence of hardbottom habitats was very low throughout the study area compared to the variability in predicted occurrence for DSC taxa (Figure 14). Although the map of the predicted occurrence of hardbottom habitats provides a general characterization of the spatial extent of hardbottom habitats in the study area, finer scale characterization of seafloor habitats will likely require additional information about the occurrence of hardbottom habitats beyond what can be provided by observations from visual field surveys focused on DSC habitats. Additional field surveys on soft bottom areas would be beneficial to provide information about where hardbottom is absent. Because underwater visual surveys are expensive and may limit the spatial coverage of identified hardbottom habitats, other methods of sampling the seafloor (e.g., sediment grab samples) may also be useful. It is also important to note that the study area did not include a large portion of the continental shelf <50 m depth where there are likely to be areas of hardbottom habitats that are not associated with DSCs.

3.5 Environmental Predictor Effects

It is difficult to make inferences about the ecological drivers of the occurrence of DSCs and hardbottom habitats from the models presented in this report. Plots of the marginal effects of each environmental predictor on the predicted occurrence are sometimes used to examine the relationships between the predicted occurrence and each individual environmental predictor. These plots depict how the predicted occurrence varies across the range of environmental predictor values while holding each of the other environmental predictors at its mean value from the sample locations. For example, the predicted occurrence of *Lophelia* was highest within its expected depth range of 250–900 m (Figure 15). Marginal effects plots for the other taxa are included in Appendix E. Marginal plots in which the predicted occurrence is very low (i.e., near zero) across the range of predictor values may reflect that the taxon had a very low probability of occurrence in the study area (i.e., it was uncommon) or that the effect of a specific environmental predictor was not significant for the taxon.

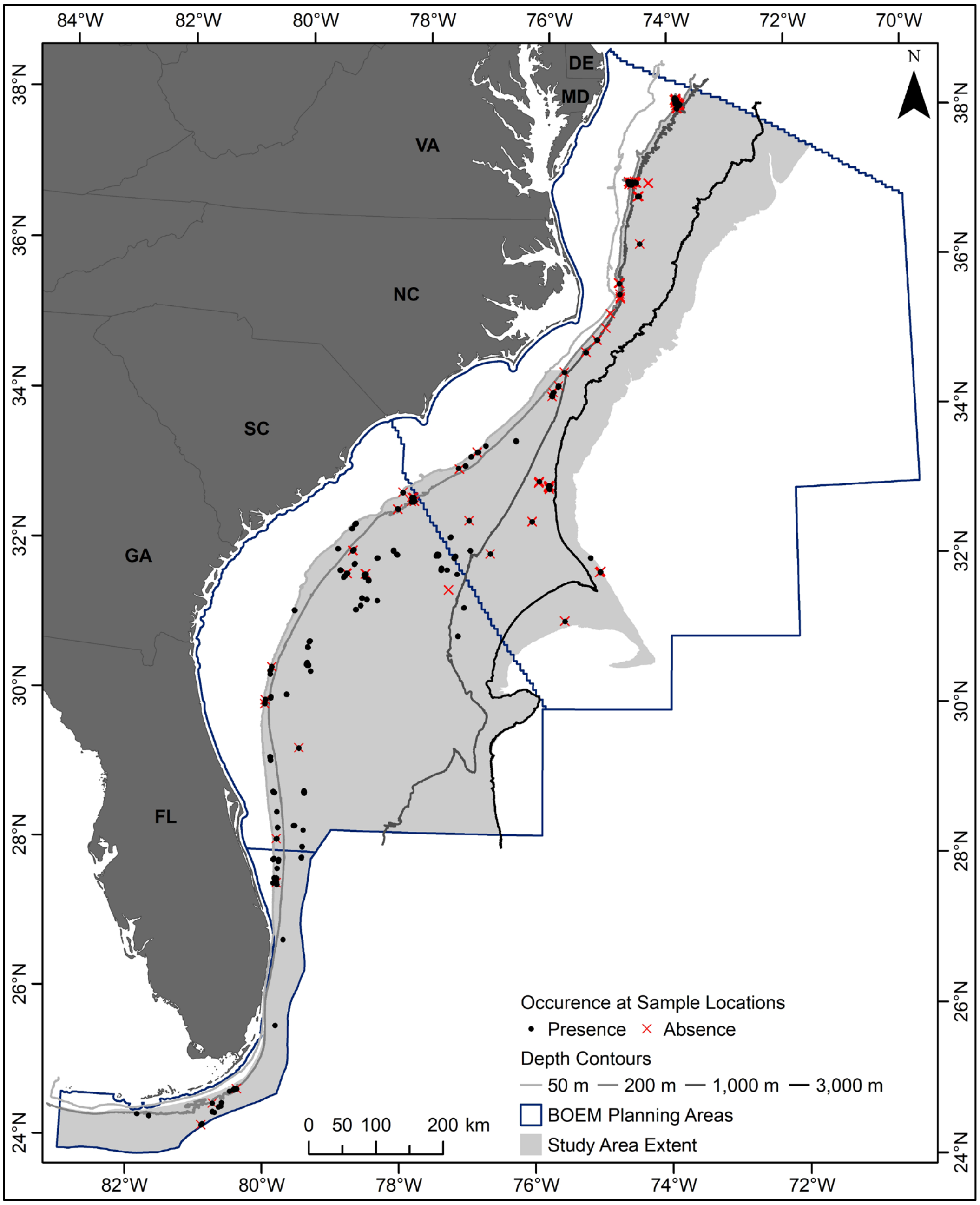

Figure 12. Occurrence records for hardbottom habitats.
This map shows the observed occurrence (presence-absence) of hardbottom habitats at sample locations in the presence-absence database compiled for this study.

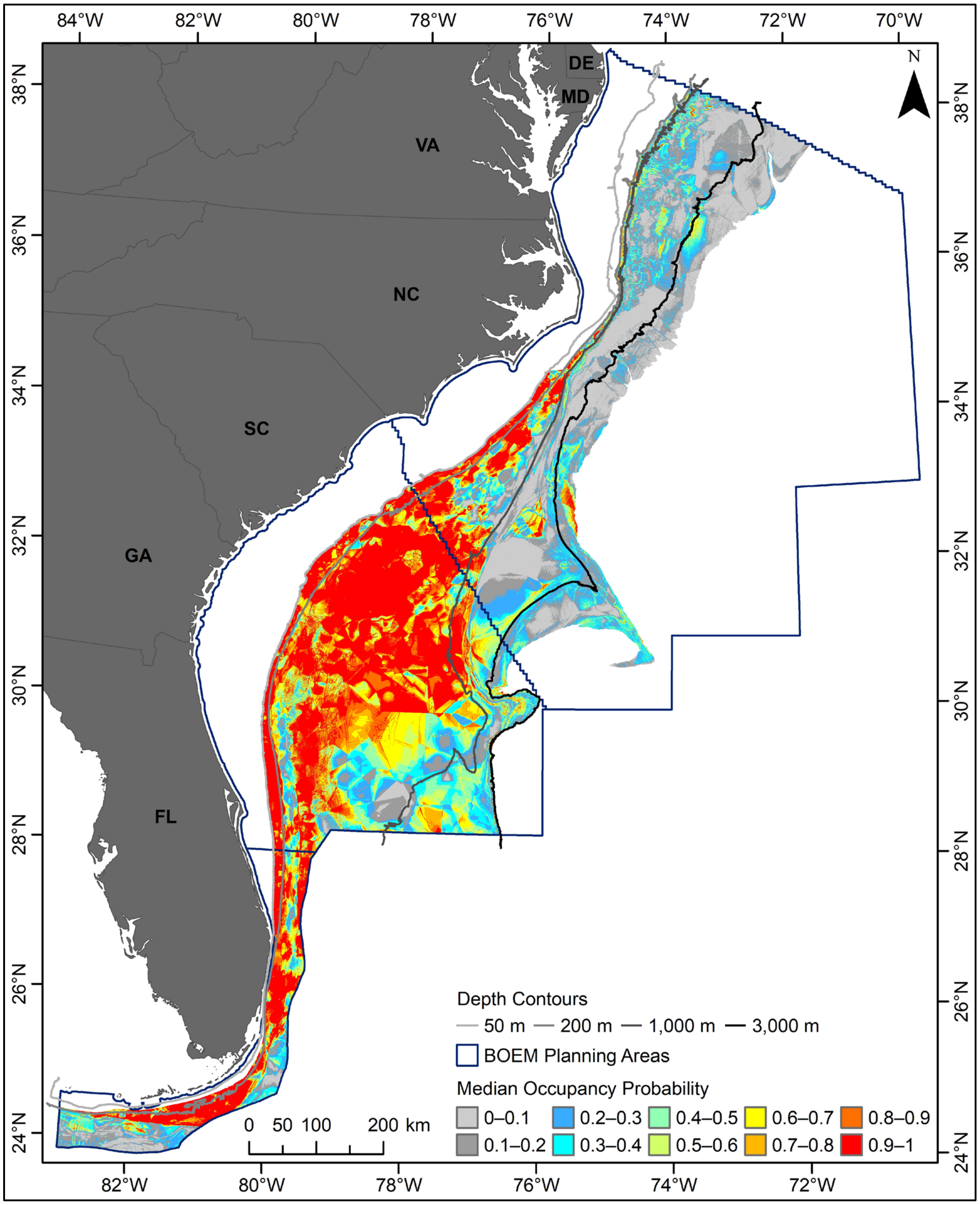

Figure 13. Predicted occurrence of hardbottom habitats.
This map shows the posterior median occupancy probability for hardbottom habitats.

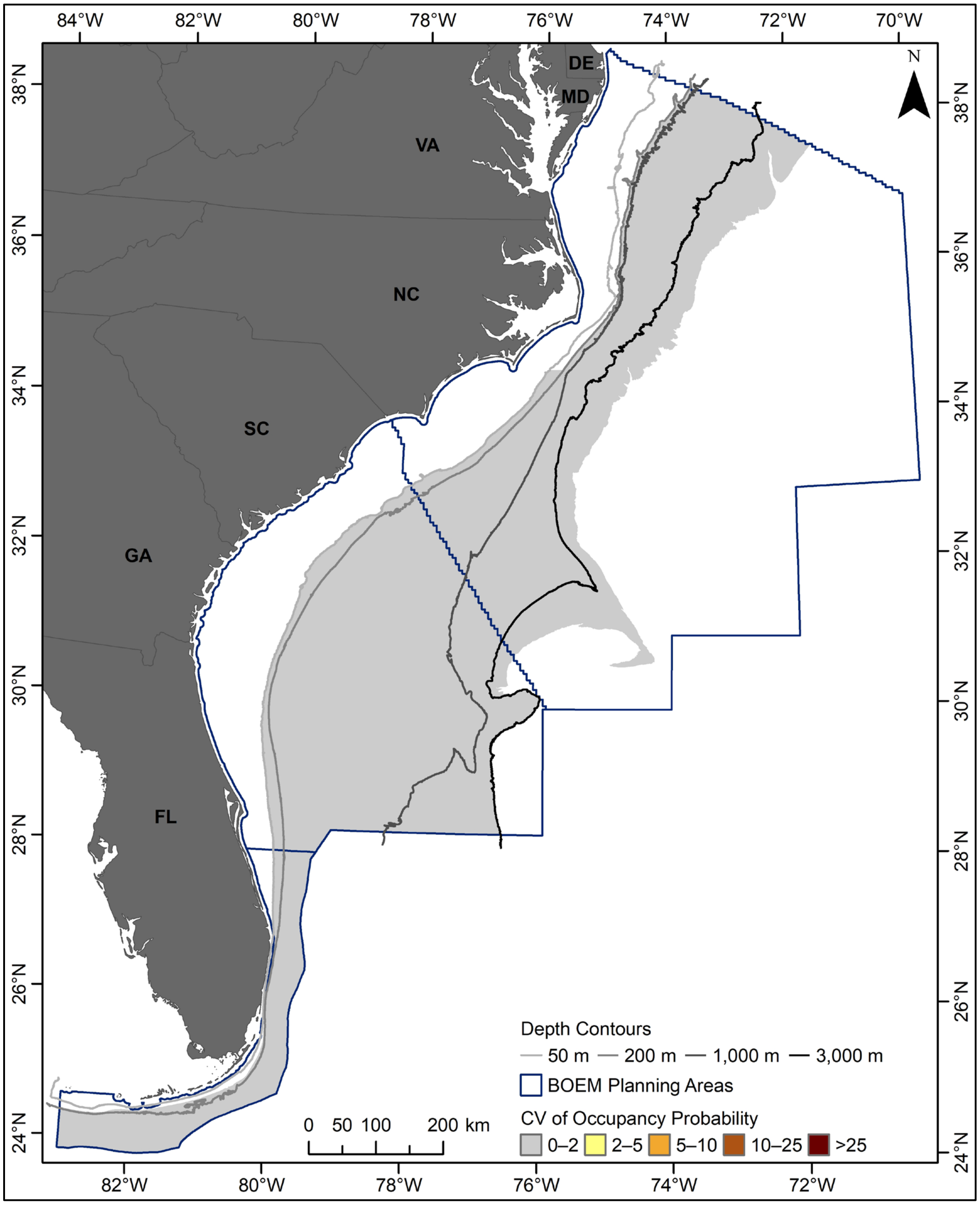

Figure 14. Variability in the predicted occurrence of hardbottom habitats.
This map shows the posterior coefficient of variation of occupancy probability for hardbottom habitats.

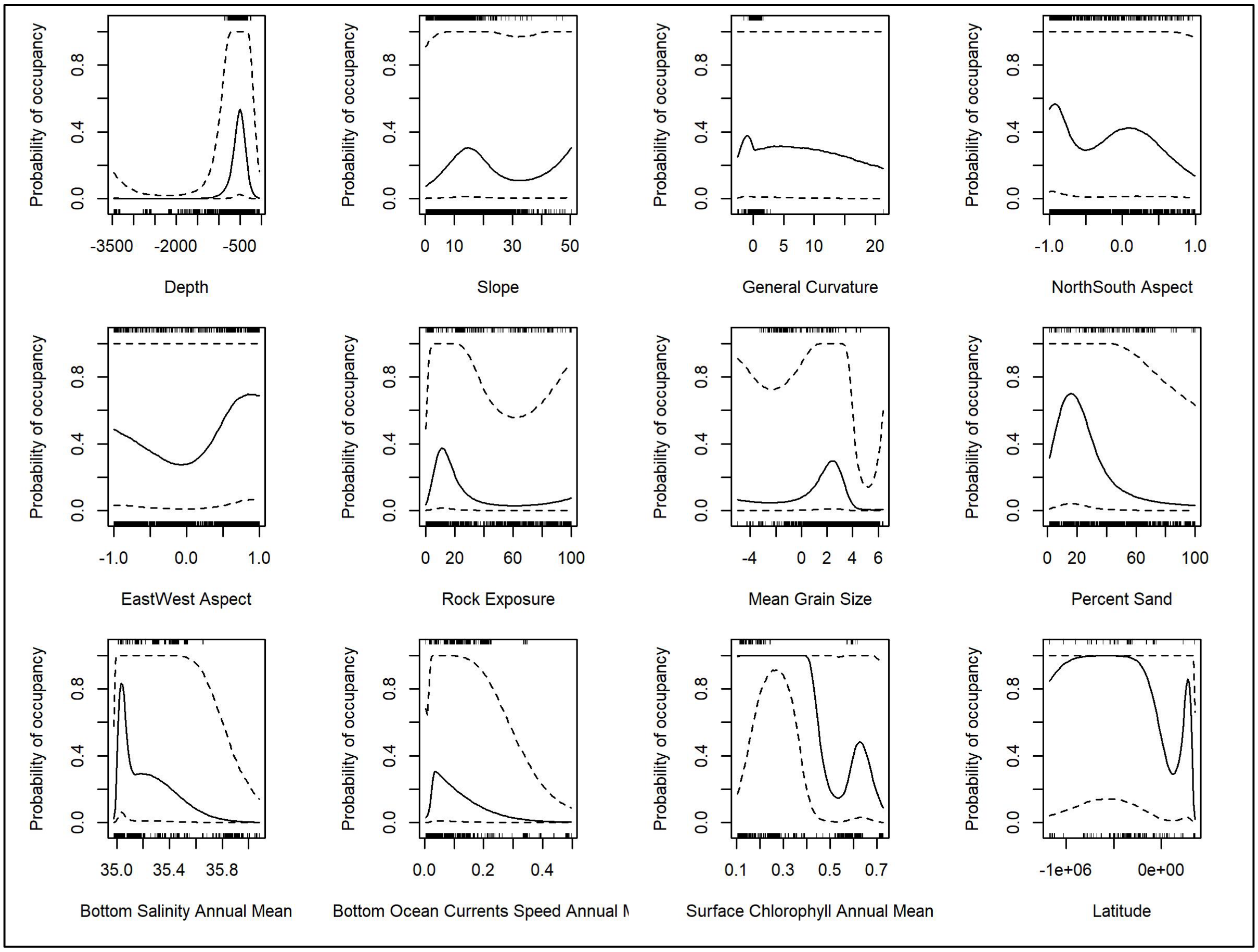

Figure 15. Marginal effects of the predictors on the predicted occurrence of *Lophelia*.
The y-axes show the predicted occurrence for *Lophelia* for values of each environmental predictor (the x-axes). The solid line depicts the posterior median occupancy probability, while the dashed lines depict the 95% credible interval. Tick marks at the top and bottom (i.e., rug plots) of each plot indicate the sampled predictor values at which *Lophelia* was observed to be present (top) or absent (bottom). The marginal effects plots should be interpreted with caution because they illustrate the estimated effects of each predictor while all others are set at their mean value (i.e., each plot ignores the realized range of effects from all predictors).

4 Conclusion

This study provided maps and data products that will be used by BOEM to inform and support environmental risk assessments, environmental impact statements, and other decision-support documents related to the review of proposed offshore energy development offshore of the southeastern US. In addition, these maps and data products can also be used to guide future ocean exploration and research in the region to aid in the discovery of previously unknown sensitive benthic areas. The maps and data products can also be used to inform other management decisions in the region (e.g., related to fisheries).

Data from 20 field surveys were compiled and analyzed to create a new database containing observations of DSC and hardbottom habitat occurrence (presence-absence). This database was then used in statistical models that related the occurrence of selected DSC taxa and hardbottom habitats to spatial environmental predictors in order to predict and map their potential spatial distributions across the study area offshore of the southeastern US.

The data and methods used to create the database and models provide several improvements over the earlier regional scale predictive habitat models for DSCs for this region. First, and most significant, the models developed in this study incorporated absence data with associated measures of sampling effort. This allowed the models to predict absolute probabilities of occurrence rather than the relative measures of habitat suitability provided by presence-background models (Winship et al. 2020). The occupancy models attempted to distinguish true from false absences, thereby accounting for imperfect detection and providing estimates of the true probability of occurrence (Kéry and Royle 2016). Second, the models used environmental predictors representing depth and seafloor topography that were derived from a compilation of bathymetry data, including data from multibeam sonar surveys that covered approximately 74% of the study area, rather than a regional bathymetry model. This compilation of bathymetry data and data from many of the multibeam surveys were not available when the earlier predictive habitat models were developed. These predictors do a better job resolving fine scale hardbottom or mound features on the seafloor that may be useful for predicting the occurrence of DSCs (Winship et al. 2020). As a result, maps of the predicted probabilities of occurrence were generated at a finer spatial resolution (100 x 100 m) and with finer delineation of seafloor features associated with predicted occurrence of DSCs than the earlier predictive habitat models (e.g., Kinlan et al. 2013). Third, the models were created for DSC genera rather than for broader taxonomic groups for which models may overpredict the extent of potential habitat (Guinotte and Davies 2014; Kinlan et al. 2020; Winship et al. 2020). Fourth, modeling multiple genera jointly in a hierarchical model (i.e., the multi-taxon model) allowed for the inclusion of rare taxa and facilitated the estimation of taxonomic richness by combining the predicted distributions for multiple genera (Zipkin et al. 2009). Finally, the precision (i.e., variability) of the predicted occurrence was estimated and mapped for each taxon, providing a measure of the confidence or uncertainty associated with the predicted occurrence at any given location.

Although the data and methods used in this study improved on the existing regional predictive habitat models for the study area, challenges and limitations remain, particularly with respect to sampling design. Ideally, occupancy models are fit to well-balanced data where each field survey collects observations at every site, with similar numbers of replicate samples (i.e., images or video segments from a visual survey) per site. Such a systematic survey is not yet feasible at the regional scale and resolution of this study and would be challenging even at a local scale for the deep sea given the cost and logistical challenges of conducting surveys with submersibles and ROVs. Because the presence-absence database compiled in this study depended on existing, available data from previously conducted field surveys, with varying objectives and specifications, this resulted in a non-random sampling design. There was considerable variability in sampling effort across the study area, where parts of the study area (e.g., the central and eastern Blake Plateau) had few or no surveys in the presence-absence database. As a result of the substantial heterogeneity and data imbalance in the samples compiled into the presence-absence database, it was sometimes challenging for the models to estimate detection and occupancy probabilites. Model predictions should therefore be interpreted with proper attention to the associated measures of uncertainty (i.e., the CV of the occupancy probabilities). Future models would benefit from observation data collected using a more systematic survey design.

Another challenge is the selection of the appropriate spatial scale and resolution for the analysis of deep-sea biota (Scales et al. 2017; Frishkoff et al. 2019). If the analysis is conducted at too coarse a spatial resolution, fine scale habitat information that could be useful for estimating species-environment relationships may be lost (e.g., the ability to resolve seafloor features like coral mounds). On the other hand, some environmental predictors may not be available at fine spatial resolution (e.g., those derived from satellite remote sensing). Furthermore, conducting the analysis at too fine a spatial resolution could result in fewer spatial replicates, reducing the power to estimate detectability. Bathymetry data collected by multibeam sonar should be used when possible to create environmental predictors depicting depth and seafloor topography in order to resolve the fine scale seafloor features that may provide habitat for DSCs (Winship et al. 2020). There has been extensive multibeam mapping within the study area, covering approximately 74% of the area at the time bathymetry data were compiled for this study. However, much of the continental shelf and upper continental slope and parts of the Blake Plateau have not been mapped. Recent mapping surveys by NOAA Ship *Okeanos Explorer* in 2021 have helped fill in gaps in the multibeam coverage on the Blake Plateau. Collection of additional multibeam bathymetry data in these areas would enable better characterization of the seafloor. The inventory of existing high resolution bathymetry (Table B-1) and map of its coverage (Figure 3) could be used to identify priority areas for mapping surveys.

This report provides maps with information about the observed and predicted distributions of individual DSC taxa (primarily genera) and hardbottom habitats across the study area. For each taxon, the maps show the presence or absence of the taxon at sample locations in the presence-absence database compiled in this study and the predicted occurrence (posterior median occupancy probability) and variability in the predicted occurrence (posterior CV of the occupancy probability) across the study area on the 100 x 100 m resolution model grid. In addition, there are maps that show the predicted genus richness (i.e., the number of genera expected to occur at each grid cell) and variability in the predicted genus richness for the 23 genera included in the multi-taxon model.

The information in these maps and the associated data products can be used in the planning and review of proposed activities related to the development of offshore energy and mineral resources by identifying areas where the predicted occurrence for a sensitive taxon of interest or the predicted genus richness was below a specific threshold to minimize the impacts of the activities. Convsersely, if the predicted occurrence or predicted genus richness are above a specific threshold, an area may need to be considered for protection. In either case, targeted field surveys in these areas should be conducted to validate model predictions. It is also important to note that while the genera modeled in this study included many of the most abundant structure-forming coral species, they do not include all taxa that may be vulnerable to anthropogenic impacts.

The maps and data products can also be used to inform future exploration of potential DSC and hardbottom habitats and the collection of data to validate (i.e., ground truth) the model predictions with independent data. Areas where the predicted occurrence of a key taxon or the predicted genus richness was high but sampling effort was low should be given high priority for exploration. For example, exploration would be beneficial in the deeper waters (around 1,000 m) on the Blake Plateau near the Blake Spur where there were several taxa (*Madrepora*, *Lophelia*, *Solenosmilia*, *Enallopsammia*, *Bathypathes*, *Plumarella*, *Paramuricea*) with high to very high predicted occurrence but no samples in the presence-absence database. For model validation, the field surveys should be designed based on the model predictions (e.g., Anderson et al. 2016; Rooper et al. 2018). In general, the use of a stratified survey design for even sampling of environmental gradients is strongly recommended (Hirzel and Guisan 2002; Williams and Brown 2019) and would benefit future modeling efforts in the region.

The analyses and products presented in this report were not designed to replace, but rather to inform, additional analysis required by law under the National Environmental Policy Act (NEPA) and other environmental statutes[1]

---

[1] . For more information about how these products may be used, please see the BOEM Environmental Studies Program (https://www.boem.gov/environmental-studies) or the BOEM Office of Public Affairs (https://www.boem.gov/newsroom).

References

Aitchison J. 1986. The statistical analysis of compositional data. London (GB): Chapman and Hall.

Anderson OF, Guinotte JM, Rowden AA, Clark MR, Mormede S, et al. 2016. Field validation of habitat suitability models for vulnerable marine ecosystems in the South Pacific Ocean: implications for the use of broad-scale models in fisheries management. Ocean Coast Manag. 120:110–126.

Andrews BD, Chaytor JD, ten Brink US, Brothers DS, Gardner JV, et al. 2016. Bathymetric terrain model of the Atlantic margin for marine geological investigations, version 2.0 [dataset]. Reston (VA): US Department of the Interior, US Geological Survey. Report No.: US Geological Survey Open-File Report 2012-1266. [accessed 2021 Sept 2]. https://pubs.er.usgs.gov/publication/ofr20121266.

Buhl-Mortensen L, Vanreusel A, Gooday AJ, Levin LA, Priede IG, et al. 2010. Biological structures as a source of habitat heterogeneity and biodiversity on the deep ocean margins. Mar Ecol. 31(1):21–50.

Calabrese JM, Certain G, Kraan C, Dormann CF. 2014. Stacked species distribution models and adjusting bias by linking them to macroecological models. Glob Ecol Biogeogr. 23(1):99–112.

Charbonnel A, D'Amico F, Besnard A, Blanc F, Buisson L, et al. 2014. Spatial replicates as an alternative to temporal replicates for occupancy modelling when surveys are based on linear features of the landscape. J Appl Ecol. 51(5):1425–1433.

Conn PB, Johnson DS, Boveng PL. 2015. On extrapolating past the range of observed data when making statistical predictions in ecology. PLoS One. 10(10):e0141416.

Conn PB, Thorson JT, Johnson DS. 2017. Confronting preferential sampling when analyzing population distributions: diagnosis and model-based triage. Methods Ecol Evol. 8(11):1535–1546.

dbSEABED: information integration system for marine substrates. c2007–2021. Boulder (CO): Institute of Arctic and Alpine Research, University of Colorado Boulder; [updated 2021 Jul 21; accessed 2021 Sept 2]. https://instaar.colorado.edu/~jenkinsc/dbseabed/.

Deep SEARCH 2018: deep sea exploration to advance research on coral/canyon/seep habitats. 2018. Silver Spring (MD): National Oceanic and Atmospheric Administration, Office of Ocean Exploration and Research; [accessed 2021 Sept 2]. https://oceanexplorer.noaa.gov/explorations/18deepsearch/.

Deep SEARCH 2019: deep sea exploration to advance research on coral/canyon/seep habitats. 2019. Silver Spring (MD): National Oceanic and Atmospheric Administration, Office of Ocean Exploration and Research; [accessed 2021 Sept 2]. https://oceanexplorer.noaa.gov/explorations/19deepsearch/.

Dorazio RM, Royle JA. 2005. Estimating size and composition of biological communities by modeling the occurrence of species. J Am Stat Assoc. 100(470):389–398.

Dorazio RM, Royle JA, Söderström B, Glimskär A. 2006. Estimating species richness and accumulation by modeling species occurrence and detectability. Ecology. 87(4):842–854.

Du Preez C. 2015. A new arc-chord ratio (ACR) rugosity index for quantifying three-dimensional landscape structural complexity. Landsc Ecol. 30:181–192.

Fithian W, Elith J, Hastie T, Keith DA. 2015. Bias correction in species distribution models: pooling survey and collection data for multiple species. Methods Ecol Evol. 6:424–438.

Flanders NP, Gardner B, Winiarski KJ, Paton PWC, Allison T, et al. 2015. Key seabird areas in southern New England identified using a community occupancy model. Mar Ecol Prog Ser. 533:277–290.

Frishkoff LO, Mahler DL, Fortin M-J. 2019. Integrating over uncertainty in spatial scale of response within multispecies occupancy models yields more accurate assessments of community composition. Ecography. 42(12):2132–2143.

Gelman A, Rubin DB. 1992. Inference from iterative simulation using multiple sequences. Stat Sci. 7(4):457–472.

Guillera-Arroita G. 2011. Impact of sampling with replacement in occupancy studies with spatial replication. Methods Ecol Evol. 2(4):401–406.

Guinotte JM, Davies AJ. 2014. Predicted deep-sea coral habitat suitability for the US West Coast. PLoS One. 9(4):e93918.

Guinotte JM, Georgian S, Kinlan BP, Poti M, Davies AJ. 2017. Predictive habitat modeling for deep-sea corals in US waters. In: Hourigan TF, Etnoyer PJ, Cairns SD, editors. The state of deep-sea coral and sponge ecosystems of the United States. Silver Spring (MD): National Oceanic and Atmospheric Administration, National Marine Fisheries Service. 467 p. Report No.: NOAA Technical Memorandum NMFS-OHC-4.

Hastie T, Tibshirani R, Friedman J. 2009. Basis expansions and regularization. In: The elements of statistical learning. New York (NY): Springer. p. 139–189.

Hijmans RJ. 2020. terra: spatial data analysis. R package version 0.9-11; [accessed 2021 Sept 2]. https://CRAN.R-project.org/package=terra.

Hirzel A, Guisan A. 2002. Which is the optimal sampling strategy for habitat suitability modelling? Ecol Modell. 157(2):331–341.

Hourigan TF, Cairns SD, Reed J, Ross SW. 2017a. Deep-sea coral taxa in the US Southeast region: depth and geographic distribution. In: Hourigan TF, Etnoyer PJ, Cairns SD, editors. The state of deep-sea coral and sponge ecosystems of the United States. Silver Spring (MD): National Oceanic and Atmospheric Administration, National Marine Fisheries Service. 467 p. Report No.: NOAA Technical Memorandum NMFS-OHC-4.

Hourigan TF, Reed J, Pomponi S, Ross SW, David AW, Harter S. 2017b. State of deep-sea coral and sponge ecosystems of the southeast United States. In: Hourigan TF, Etnoyer PJ, Cairns SD, editors. The state of deep-sea coral and sponge ecosystems of the United States. Silver Spring (MD): National Oceanic and Atmospheric Administration, National Marine Fisheries Service. 467 p. Report No.: NOAA Technical Memorandum NMFS-OHC-4.

HYCOM Consortium. 2018. HYCOM + NCODA Global 1/12° Reanalysis [dataset]; [accessed 2021 Sept 2]. https://www.hycom.org/dataserver/gofs-3pt0/reanalysis.

Jenness J. 2013. DEM surface tools. Flagstaff (AZ): Jenness Enterprises; [accessed 2021 Sept 2]. http://www.jennessent.com/arcgis/surface_area.htm.

Jiménez-Franco MV, Kéry M, León-Ortega M, Robledano F, Esteve MA, Calvo JF. 2019. Use of classical bird census transects as spatial replicates for hierarchical modeling of an avian community. Ecol Evol. 9(2):825–835.

Kendall MS, Bauer LJ, Jeffrey CFG. 2009. Influence of hard bottom morphology on fish assemblages of the continental shelf off Georgia, southeastern USA. Bull Mar Sci. 84(3):265–286.

Kéry M, Royle JA. 2008. Hierarchical Bayes estimation of species richness and occupancy in spatially replicated surveys. J Appl Ecol. 45(2):589–598.

Kéry M, Royle JA. 2016. Applied hierarchical modeling in ecology: analysis of distribution, abundance and species richness in R and BUGS, volume 1: prelude and static models. Boston (MA): Academic Press. 808 p.

Kinlan BP, Poti M, Hourigan T, Dorfman D, Caldow C. 2013. Predictive models of deep-sea coral habitat suitability in the US Southeast region [dataset]. Silver Spring (MD): National Oceanic and Atmospheric Administration, National Centers for Coastal Ocean Science; [accessed 2021 Sept 2]. https://nccospublicstor.blob.core.windows.net/projects-attachments/35/DSC_PredictiveModeling_US_Southeast.zip.

Kinlan BP, Poti M, Drohan AF, Packer DB, Dorfman DS, et al. 2020. Predictive modeling of suitable habitat for deep-sea corals offshore the northeast United States. Deep Sea Res Part I. 158:103229.

Lotze HK, Worm B. 2009. Historical baselines for large marine mammals. Trends Ecol Evol. 24(5):254–262.

MacKenzie DI, Nichols JD, Lachman GB, Droege S, Royle JA, et al. 2002. Estimating site occupancy rates when detection probabilities are less than one. Ecology. 83(8):2248–2255.

McGuinn RP, Hourigan TF, Cross SL, Dornback LM, Etnoyer PJ, et al. 2020. NOAA's national database for deep-sea corals and sponges: 2020 status update. Silver Spring (MD): National Oceanic and Atmospheric Administration, National Marine Fisheries Service, Office of Habitat Conservation, Deep Sea Coral Research and Technology Program. 56 p. Report No.: NOAA Technical Memorandum NMFS-OHC-007.

Mienis F, Duineveld GCA, Davies AJ, Lavaleye MMS, Ross SW, et al. 2014. Cold-water coral growth under extreme environmental conditions, the Cape Lookout area, NW Atlantic. Biogeosciences. 11:2543–2560.

[NASA] National Aeronautics and Space Administration Ocean Biology Processing Group. 2018. Sea-Viewing Wide Field-of-View Sensor Ocean Color Data [dataset]. Greenbelt (MD): National Aeronautics and Space Administration, Goddard Space Flight Center, Ocean Biology Processing Group; [accessed 2021 Sept 2]. https://oceandata.sci.gsfc.nasa.gov/directaccess/SeaWiFS/.

[NASA] National Aeronautics and Space Administration Ocean Biology Processing Group. 2019a. Moderate Resolution Imaging Spectroradiometer Aqua Ocean Color Data [dataset]. Greenbelt (MD): National Aeronautics and Space Administration, Goddard Space Flight Center, Ocean Biology Processing Group; [accessed 2021 Sept 2]. https://oceandata.sci.gsfc.nasa.gov/directaccess/MODIS-Aqua/.

[NASA] National Aeronautics and Space Administration Ocean Biology Processing Group. 2019b. Moderate Resolution Imaging Spectroradiometer Terra Ocean Color Data [dataset]. Greenbelt (MD): National Aeronautics and Space Administration, Goddard Space Flight Center, Ocean Biology Processing Group; [accessed 2021 Sept 2]. https://oceandata.sci.gsfc.nasa.gov/directaccess/MODIS-Terra/.

[NASA] National Aeronautics and Space Administration Ocean Biology Processing Group. 2019c. Visible Infrared Imaging Radiometer Suite Ocean Color Data [dataset]. Greenbelt (MD): National Aeronautics and Space Administration, Goddard Space Flight Center, Ocean Biology Processing Group; [accessed 2021 Sept 2]. https://oceandata.sci.gsfc.nasa.gov/directaccess/VIIRS-SNPP/.

[NCEI] National Centers for Environmental Information. 1999. US Coastal Relief Model – Southeast Atlantic [dataset]. Stennis Space Center (MS): National Oceanic and Atmospheric Administration, National Centers for Environmental Information; [accessed 2021 Sept 2]. https://www.ncei.noaa.gov/metadata/geoportal/rest/metadata/item/gov.noaa.ngdc.mgg.dem:305/html.

[NCEI] National Centers for Environmental Information. 2001. US Coastal Relief Model – Florida and East Gulf of Mexico [dataset]. Stennis Space Center (MS): National Oceanic and Atmospheric Administration, National Centers for Environmental Information; [accessed 2021 Sept 2]. https://www.ncei.noaa.gov/metadata/geoportal/rest/metadata/item/gov.noaa.ngdc.mgg.dem:307/html.

[NCEI] National Centers for Environmental Information. 2004. Multibeam bathymetry database. Stennis Space Center (MS): National Oceanic and Atmospheric Administration, National Centers for Environmental Information; [updated 2021 Aug 19; accessed 2021 Sept 2]. https://www.ngdc.noaa.gov/mgg/bathymetry/multibeam.html.

[NCEI] National Centers for Environmental Information. 2006. Coastal digital elevation models (DEMs) [dataset]. Stennis Space Center (MS): National Oceanic and Atmospheric Administration, National Centers for Environmental Information; [accessed 2021 Sept 2]. https://www.ngdc.noaa.gov/mgg/coastal/coastal.html.

[NCEI] National Centers for Environmental Information. 2018. Marine geology: stewardship and services for geosample data from Earth's ocean floor and lakebeds [dataset]. Stennis Space Center (MS): National Oceanic and Atmospheric Administration, National Centers for Environmental Information; [accessed 2021 Sept 2]. https://www.ngdc.noaa.gov/mgg/geology/.

[NOAA] National Oceanic and Atmospheric Administration Deep Sea Coral Research and Technology Program. 2021. NOAA National Database for Deep-Sea Corals and Sponges, version 20210414-0 [dataset]. Silver Spring (MD): National Oceanic and Atmospheric Administration, National Marine Fisheries Service, Office of Habitat Conservation, Deep Sea Coral Research and Technology Program; [accessed 2021 July 27]. https://deepseacoraldata.noaa.gov/.

[NOS] National Ocean Service. 2013. NOAA/NOS and US Coast and Geodetic Survey seabed descriptions from hydrographic surveys [dataset]. Stennis Space Center (MS): National Oceanic and Atmospheric Administration, National Centers for Environmental Information; [accessed 2021 Sept 2]. https://www.ngdc.noaa.gov/geosamples/survey.jsp.

Petracca LS, Funston PJ, Henschel P, Cohen JB, Maclennan S, Frair JL. 2020. Modeling community occupancy from line transect data: a case study with large mammals in post-war Angola. Anim Conserv. 23(4):420–433.

Phillips SJ, Anderson RP, Schapire RE. 2006. Maximum entropy modeling of species geographic distributions. Ecol Modell. 190(3–4):231–259.

Phillips SJ, Dudik M, Elith J, Graham CH, Lehman J, Leathwick J, Ferrier S. 2009. Sample selection bias and presence-only distribution models: implications for background and pseudo-absence data. Ecol Appl. 19(1):181–197.

Pinheiro J, Bates D. 2004. Mixed-effect models in S and S-Plus. New York (NY): Springer. 528 p.

Plummer M. 2018. rjags: Bayesian graphical models using MCMC. R package version 4-8; [accessed 2021 Sept 2]. https://CRAN.R-project.org/package=rjags.

Poppe LJ, McMullen KY, Williams SJ, Paskevich VF, editors. 2014. USGS east-coast sediment analysis: procedures, database, and GIS data, version 3.0 [dataset]. Reston (VA): US Department of the Interior, US Geological Survey. Report No.: US Geological Survey Open-File Report 2005-1001. [accessed 2021 Sept 2]. https://woodshole.er.usgs.gov/openfile/of2005-1001/.

Prouty NG, Roark EB, Buster NA, Ross SW. 2011. Growth-rate and age distribution of deep-sea black corals in the Gulf of Mexico. Mar Ecol Prog Ser. 423:101–115.

Prouty NG, Roark EB, Andrews AH, Robinson LF, Hill T, et al. 2017. Age, growth rates, and paleoclimate studies in deep-sea corals of the US In: Hourigan TF, Etnoyer PJ, Cairns SD, editors. The state of deep-sea coral and sponge ecosystems of the United States. Silver Spring (MD): National Oceanic and Atmospheric Administration, National Marine Fisheries Service. 467 p. Report No.: NOAA Technical Memorandum NMFS-OHC-4.

Quattrini AM, Ross SW, Sulak KJ, Necaise AM, Casazza TL, Dennis GD. 2004. Marine fishes new to continental United States waters, North Carolina, and the Gulf of Mexico. Southeast Nat. 3(1):155–172.

R Core Team. 2018. R: a language and environment for statistical computing, version 3.5.2. Vienna (AT): R Foundation for Statistical Computing; [accessed 2021 Sept 2]. https://www.R-project.org/.

R Core Team. 2020. R: a language and environment for statistical computing, version 4.0.3. Vienna (AT): R Foundation for Statistical Computing; [accessed 2021 Sept 2]. https://www.R-project.org/.

Reid JM, Reid JA, Jenkins CJ, Hastings ME, Williams SJ, Poppe LJ. 2005. usSEABED: Atlantic coast offshore surficial sediment data release, version 1.0 [dataset]. Reston (VA): US Department of the Interior, US Geological Survey. Report No.: US Geological Survey Data Series 118. [accessed 2021 Sept 2]. https://pubs.usgs.gov/ds/2005/118/.

Roberts JM, Wheeler AJ, Freiwald A, Cairns S. 2009. Cold-water corals: the biology and geology of deep-sea coral habitats. New York (NY): Cambridge University Press. 351 p.

Rooper CN, Wilborn R, Goddard P, Williams K, Towler R, Hoff GR. 2018. Validation of deep-sea coral and sponge distribution models in the Aleutian Islands, Alaska. ICES J Mar Sci.75(1):199–209.

Ross SW, Nizinski MS. 2007. State of deep coral ecosystems in the US Southeast region: Cape Hatteras to southeastern Florida. In: Lumsden SE, Hourigan TF, Bruckner AW, Dorr G, editors. The state of deep coral ecosystems of the United States. Silver Spring (MD): National Oceanic and Atmospheric

Administration, National Marine Fisheries Service. 365 p. Report No.: NOAA Technical Memorandum CRCP-3.

Sadoti G, Zuckerberg B, Jarzyna MA, Porter WF. 2013. Applying occupancy estimation and modelling to the analysis of atlas data. Divers Distrib. 19(7):804–814.

Scales KL, Hazen EL, Jacox MG, Edwards CA, Boustany AM, Oliver MJ, Bograd SJ. 2017. Scale of inference: on the sensitivity of habitat models for wide-ranging marine predators to the resolution of environmental data. Ecography. 40(1):210–220.

Srivathsa A, Puri M, Kumar NS, Jathanna D, Karanth KU. 2018. Substituting space for time: empirical evaluation of spatial replication as a surrogate for temporal replication in occupancy modelling. J Appl Ecol. 55(2):754–765.

Stephenson F, Rowden AA, Anderson OF, Pitcher CR, Pinkerton MH, Peterson G, Bowden DA. 2021. Presence-only habitat suitability models for vulnerable marine ecosystem indicator taxa in the South Pacific have reached their predictive limit. ICES J Mar Sci. fsab162.

Taylor JC, Paxton AB, Voss CM, Summers B, Buckel CA, Vander Pluym J, Ebert EB, Viehman TS, Fegley SR, Pickering EA, et al. 2016. Benthic habitat mapping and assessment in the Wilmington-East Wind Energy Call Area. Sterling (VA): US Department of the Interior, Bureau of Ocean Energy Management. 150 p. Report No.: BOEM 2016-003 and NOAA Technical Memorandum 196.

Tobler WR.1970. A computer movie simulating urban growth in the Detroit region. Econ Geogr. 46:234–240.

Valavi R, Elith J, Lahoz-Monfort JJ, Guillera-Arroita G. 2019. blockCV: an R package for generating spatially or environmentally separated folds for k-fold cross-validation of species distribution models. Methods Ecol Evol. 10(2):225–232.

Vierod ADT, Guinotte JM, Davies AJ. 2014. Predicting the distribution of vulnerable marine ecosystems in the deep sea using presence-background models. Deep Sea Res Part II. 99:6–18.

Weatherall P, Marks KM, Jakobsson M, Schmitt T, Tani S, Arndt JE, Rovere M, Chayes D, Ferrini V, Wigley R. 2015. A new digital bathymetric model of the world's oceans. Earth Space Sci. 2(8):331–345.

Williams B, Risk M, Ross S, Sulak K. 2007. Stable isotope records from deep-water antipatharians: 400-year records from the southeastern coast of the United States of America. Bull Mar Sci. 81(3):437–447.

Williams BK, Brown ED. 2019. Sampling and analysis frameworks for inference in ecology. Methods Ecol Evol. 10(11):1832–1842.

Wiltshire KH, Tanner JE, Althaus F, Sorokin SJ, Williams A. 2018. Predicting environmental suitability for key benthic species in an ecologically and environmentally important deep-sea environment. Deep Sea Res Part II. 157–158:121–133.

Windows to the Deep 2018: exploration of the southeast US continental margin. 2018. Silver Spring (MD): National Oceanic and Atmospheric Administration, Office of Ocean Exploration and Research; [accessed 2021 Sept 2]. https://oceanexplorer.noaa.gov/okeanos/explorations/ex1806/.

Windows to the Deep 2019: exploration of the deep-sea habitats of the southeastern United States. 2019. Silver Spring (MD): National Oceanic and Atmospheric Administration, Office of Ocean Exploration and Research; [accessed 2021 Sept 2]. https://oceanexplorer.noaa.gov/okeanos/explorations/ex1903/.

Winship AJ, Thorson JT, Clarke ME, Coleman HM, Costa B, Georgian SE, Gillett D, Grüss A, Henderson MJ, Hourigan TF, et al. 2020. Good practices for species distribution modeling of deep-sea corals and sponges for resource management: data collection, analysis, validation, and communication. Front Mar Sci. 7:303.

Zipkin EF, DeWan A, Royle JA. 2009. Impacts of forest fragmentation on species richness: a hierarchical approach to community modelling J Appl Ecol. 46(4):815–822.

Zipkin EF, Royle JA, Dawson DK, Bates S. 2010. Multi-species occurrence models to evaluate the effects of conservation and management actions. Biol Conserv. 143(2):479–484.

Zuur AF, Ieno EN, Elphick CS. 2010. A protocol for data exploration to avoid common statistical problems. Methods Ecol Evol. 1(1):3–14.

Appendix A: Survey Datasets Included in the Synthesis of Deep-sea Coral and Hardbottom Habitat Observations

A.1 Islands in the Stream 2001 Oculina Banks

Data provider: NOAA Central Library

Principal investigators: Andrew Shepard, Chris Koeing

Year: 2001

Vessel: R/V *Seward Johnson*

Vehicle (Vehicle type): *Clelia* (HOV)

Observation types: submersible transects, video, specimens

BOEM planning areas: Straits of Florida, South Atlantic

Depth range: 62–99 m

Dives: 16

Samples: 41

Sites: 33

Total area: 8,110 m^2

Recorded taxa (included in models): *Oculina*, *Stichopathes*

The Islands in the Stream 2001 expedition included three legs in the South Atlantic Bight: Oculina Banks, North Carolina Shelf, and Charleston Bump. The Oculina Banks leg of the expedition assessed the condition of *Oculina* corals and associated reef fish and evaluated efforts to reestablish coral habitat and reef fish populations[2]..

---

[2] For additional information, see the expedition website (https://oceanexplorer.noaa.gov/explorations/islands01/)

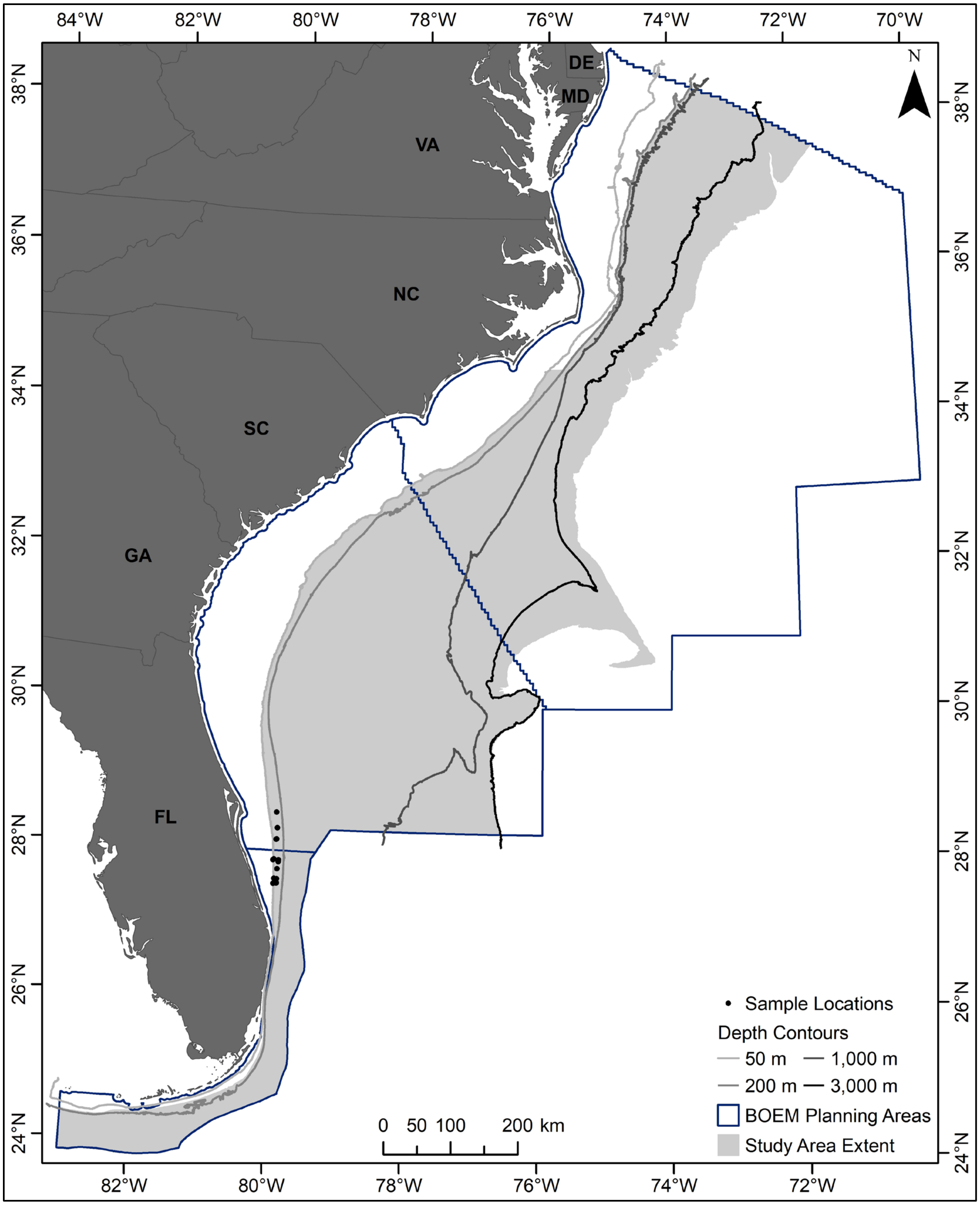

Figure A-1. Locations of samples from the Islands in the Stream 2001 Oculina Banks dataset.

A.2 Islands in the Stream 2001 North Carolina Shelf

Data provider: NOAA Central Library

Principal investigators: Steve Ross, Ken Sulak

Year: 2001

Vessel: R/V *Seward Johnson*

Vehicle (Vehicle type): *Johnson Sea Link II* (HOV)

Observation types: submersible transects, video, specimens

BOEM planning area: Mid-Atlantic

Depth range: 360–853 m

Dives: 10

Samples: 28

Sites: 16

Total area: 3,987 m^2

Recorded taxa (included in models): *Lophelia*, *Oculina*, *Stichopathes*, *Thesea*

The Islands in the Stream 2001 expedition included three legs in the South Atlantic Bight: Oculina Banks, North Carolina Shelf, and Charleston Bump. The North Carolina Shelf leg of the expedition explored three sites on the continental shelf offshore of North Carolina: 1) an area known as 'The Point' where three major ocean currents converge to create a hotspot of productivity, 2) the Lophelia Banks, an area of extensive DSC reefs off Cape Lookout, NC, and 3) the Cape Fear Terrace, an area of extensive hardbottom features including rocky outcrops, ledges, and pinnacles[3].

---

[3] For additional information, see the expedition website (https://oceanexplorer.noaa.gov/explorations/islands01/).

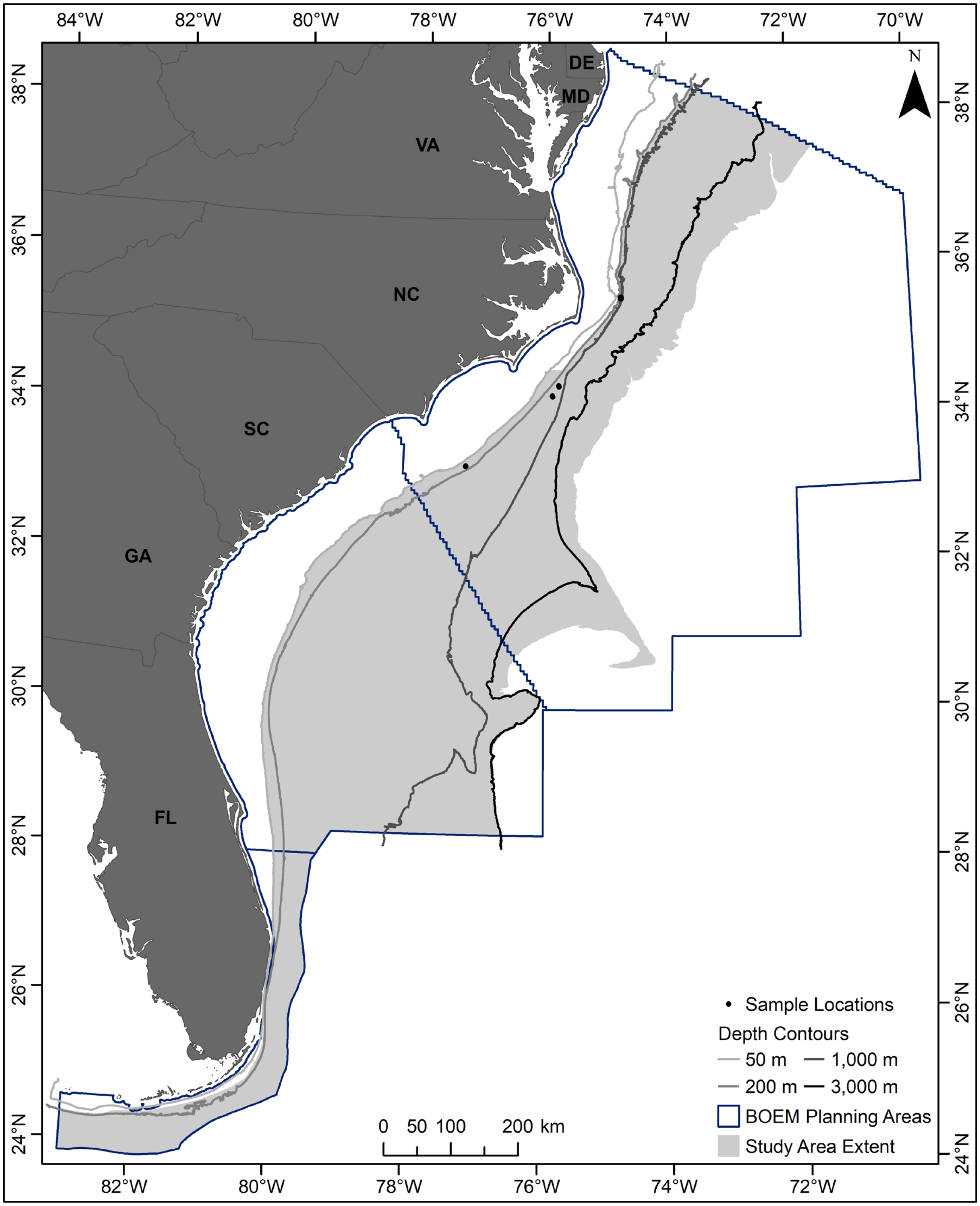

Figure A-2. Locations of samples from the Islands in the Stream 2001 North Carolina Shelf dataset.

A.3 Islands in the Stream 2001 Charleston Bump

Data provider: NOAA Central Library

Principal investigator: George Sedberry

Year: 2001

Vessel: R/V *Seward Johnson*

Vehicle (Vehicle type): *Johnson Sea Link II* (HOV)

Observation types: submersible transects, video, specimens

BOEM planning area: South Atlantic

Depth range: 476–570 m

Dives: 3

Samples: 62

Sites: 36

Total area: 9,987 m^2

Recorded taxa (included in models): *Lophelia*, *Solenosmilia*, *Leiopathes*, *Plumarella*, *Paramuricea*, *Eunicella*, *Callogorgia*, Stylasteridae

The Islands in the Stream 2001 expedition included three legs in the South Atlantic Bight: Oculina Banks, North Carolina Shelf, and Charleston Bump. The Charleston Bump leg of the expedition explored the area around Charleston Bump, a rocky outcrop offshore of South Carolina on the Blake Plateau that rises from >700 m depth to 375 m. The Bump deflects the flow of the Gulf Stream offshore, causing the formation of eddies and gyres (Charleston Gyre) and resulting in upwelling. The rocky seafloor around the Bump is characterized by scarps, ridges, and overhangs[4].

---

[4] For additional information, see the expedition website (https://oceanexplorer.noaa.gov/explorations/islands01/).

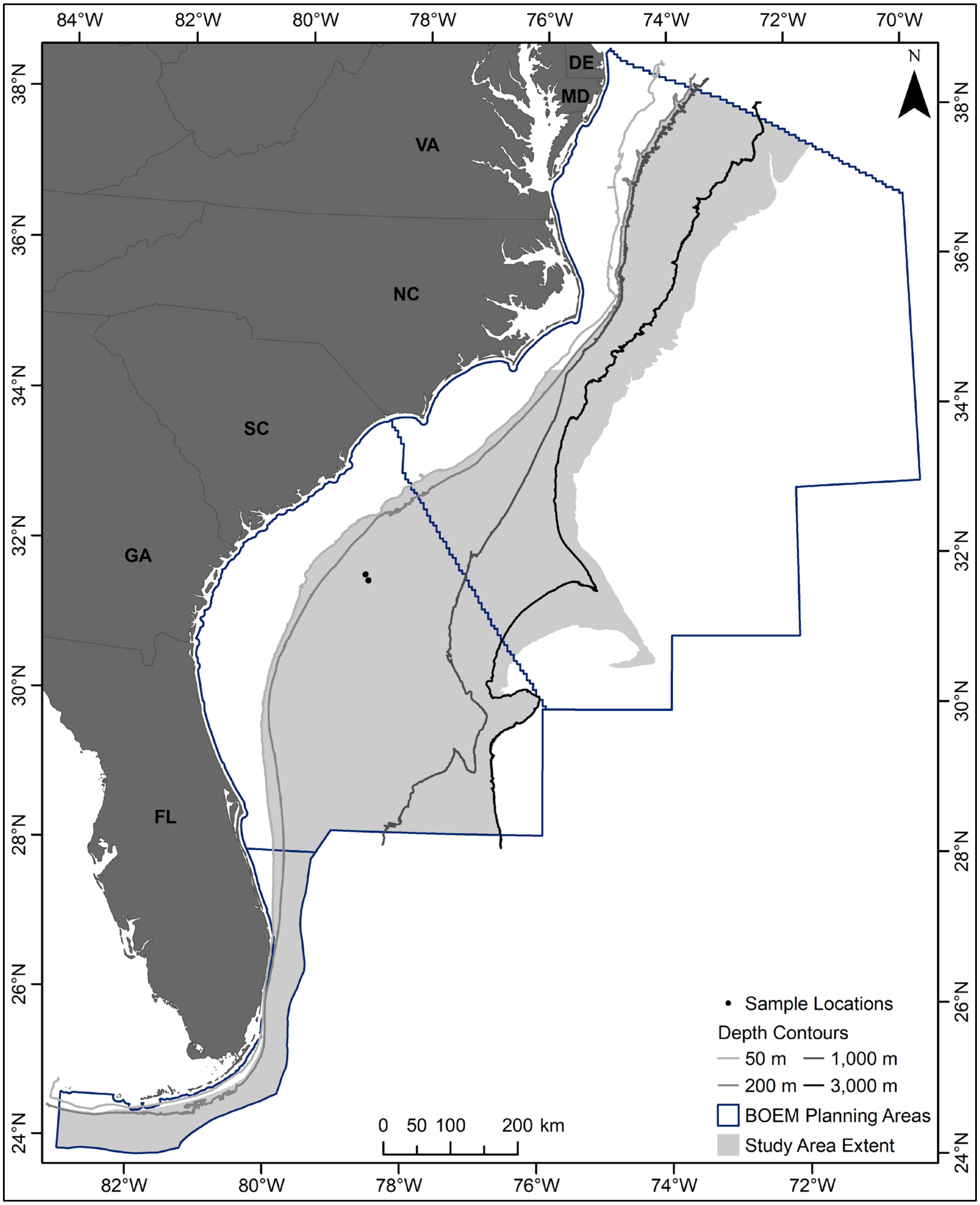

Figure A-3. Locations of samples from the Islands in the Stream 2001 Charleston Bump dataset.

A.4 Islands in the Stream 2002 Leg 1

Data provider: NOAA Central Library

Principal investigator: George Sedberry

Year: 2002

Vessel: R/V *Seward Johnson*

Vehicle (Vehicle type): *Johnson Sea Link II* (HOV)

Observation types: submersible transects, video, specimens

BOEM planning area: South Atlantic

Depth range: 43–205 m

Dives: 10

Samples: 166

Sites: 70

Total area: 19,728 m^2

Recorded taxa (included in models): *Oculina*, *Stichopathes*, *Leiopathes*, *Antipathes*, *Plumarella*, *Eunicella*, *Muricea*, *Thesea*, *Callogorgia*, *Nicella*, Stylasteridae

The Islands in the Stream 2002 expedition included four investigations carried out across three legs to learn more about high-relief areas along the continental shelf break and slope from Florida to North Carolina. The goal of the first leg was to discover and explore spawning locations of reef fishes in the area and to describe how underlying features and oceanographic processes interact to provide habitat for associated species. Scientists used a submersible to collect video and still images of the shelf-edge reefs and sediment, rocks, and marine organisms for further analysis. Side-scan sonar was used to determine characteristics of bottom topography at scales larger than the submersible could explore. The results supported protective management strategies to sustain the exploited fish species that utilize these spawning locations[5].

---

[5] For additional information, see the expedition website (https://oceanexplorer.noaa.gov/explorations/02sab/).

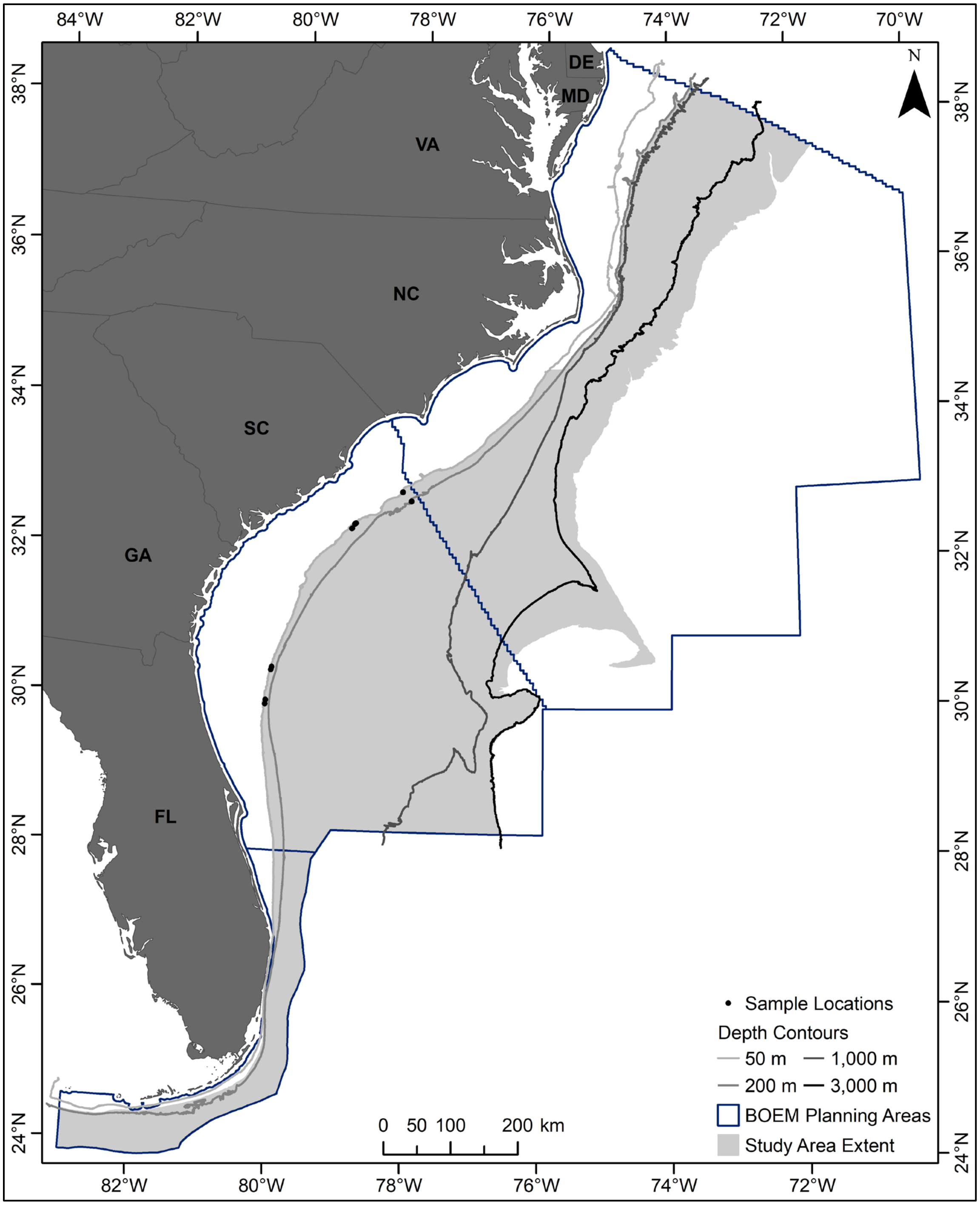

Figure A-4. Locations of samples from the Islands in the Stream 2002 Leg 1 dataset.

A.5 Islands in the Stream 2002 Leg 2

Data provider: NOAA Central Library

Principal investigators: Steve Ross, Ken Sulak

Year: 2002

Vessel: R/V *Seward Johnson*

Vehicle (Vehicle type): *Johnson Sea Link II* (HOV)

Observation types: submersible transects, video, specimens

BOEM planning area: Mid-Atlantic

Depth range: 59–452 m

Dives: 11

Samples: 61

Sites: 39

Total area: 11,054 m^2

Recorded taxa (included in models): *Lophelia*, *Oculina*, *Madrepora*, *Stichopathes*, *Tanacetipathes*, *Eunicella*, *Thesea*, *Nicella*, Stylasteridae

The Islands in the Stream 2002 expedition included four investigations carried out across three legs to learn more about high-relief areas along the continental shelf break and slope from Florida to North Carolina. The focus of the second leg was to explore two major types of unique and biologically productive habitats along the North Carolina coast, both of which have experienced an increase in commercial and recreational fishing activities as well as increasing interest in hydrocarbon exploration and development. These habitats were: 1) outer shelf hardgrounds in water depths from 80–200 m that are characterized by rocky outcrops, hardbottom pavement pinnacles, and sand channels and 2) reef banks of stony corals (e.g., *Lophelia pertusa*) found on the middle continental shelf in water depths from 400–500 m[6].

---

[6] For additional information, see the expedition website (https://oceanexplorer.noaa.gov/explorations/02sab/).

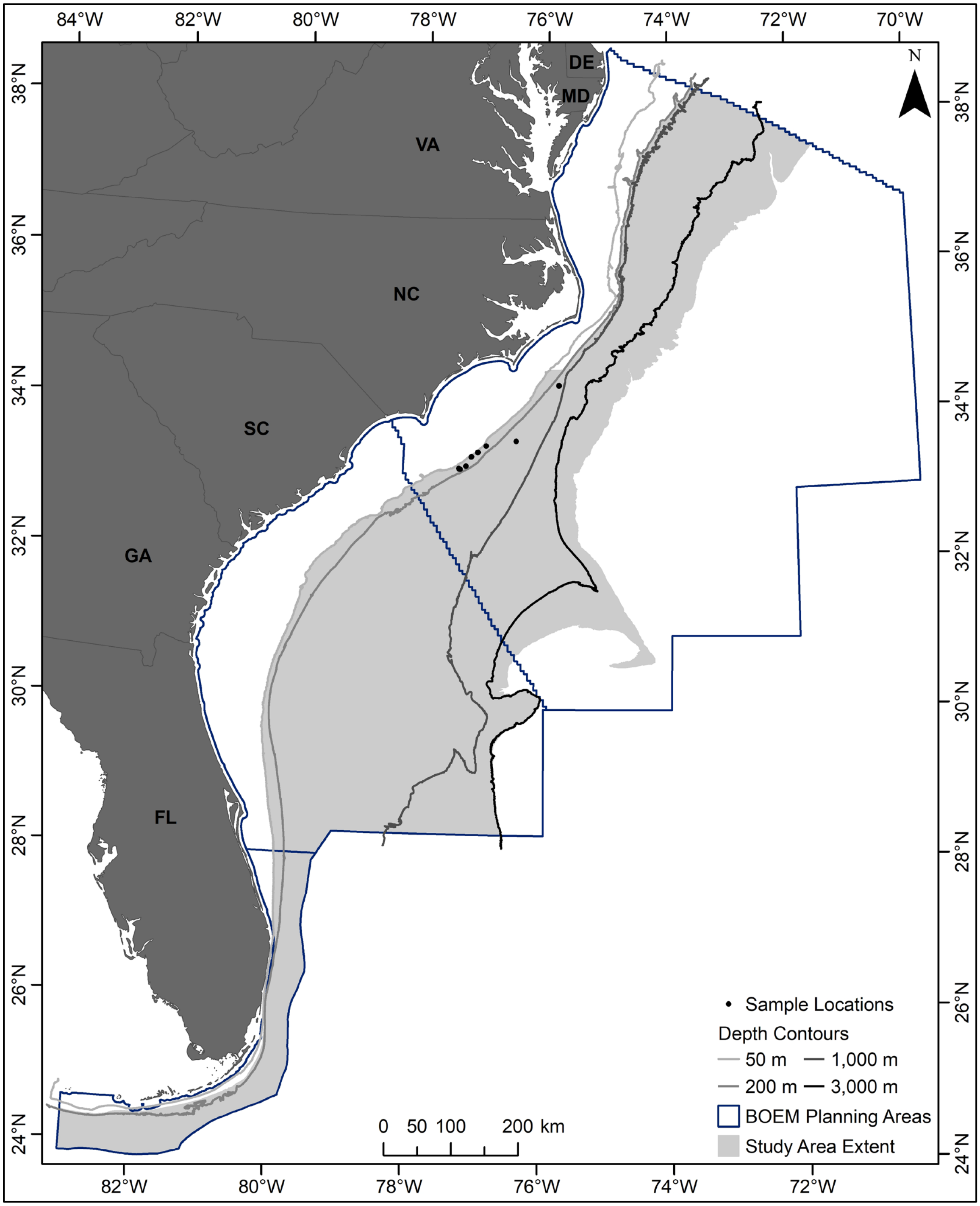

Figure A-5. Locations of samples from the Islands in the Stream 2002 Leg 2 dataset.

A.6 Islands in the Stream 2002 Leg 3

Data provider: NOAA Central Library

Principal investigators: Shirley Pomponi, John Reed

Year: 2002

Vessel: R/V *Seward Johnson*

Vehicle (Vehicle type): *Johnson Sea Link II* (HOV)

Observation types: submersible transects, video, specimens

BOEM planning area: South Atlantic

Depth range: 189–764 m

Dives: 23

Samples: 209

Sites: 106

Total area: 37,728 m^2

Recorded taxa (included in models): *Lophelia*, *Solenosmilia*, *Madrepora*, *Leiopathes*, *Bathypathes*, Paragorgiidae, *Plumarella*, *Anthothela*, *Paramuricea*, *Eunicella*, *Callogorgia*, Stylasteridae

The Islands in the Stream 2002 expedition included four investigations carried out across three legs to learn more about high-relief areas along the continental shelf break and slope from Florida to North Carolina. The third leg consisted of two different projects, each with its own objectives. Many of the objectives of each project were met concurrently during submersible dives. The first project, Pharmaceutical Discovery, sought to explore currently untapped sources of new drugs that may be applied to the development of compounds used to study, diagnose, or treat human diseases. The second project, Vision and Bioluminescence, explored the visual physiology and environment of deep-sea benthic fauna, focusing on bioluminescence[7].

---

[7] For additional information, see the expedition website (https://oceanexplorer.noaa.gov/explorations/02sab/).

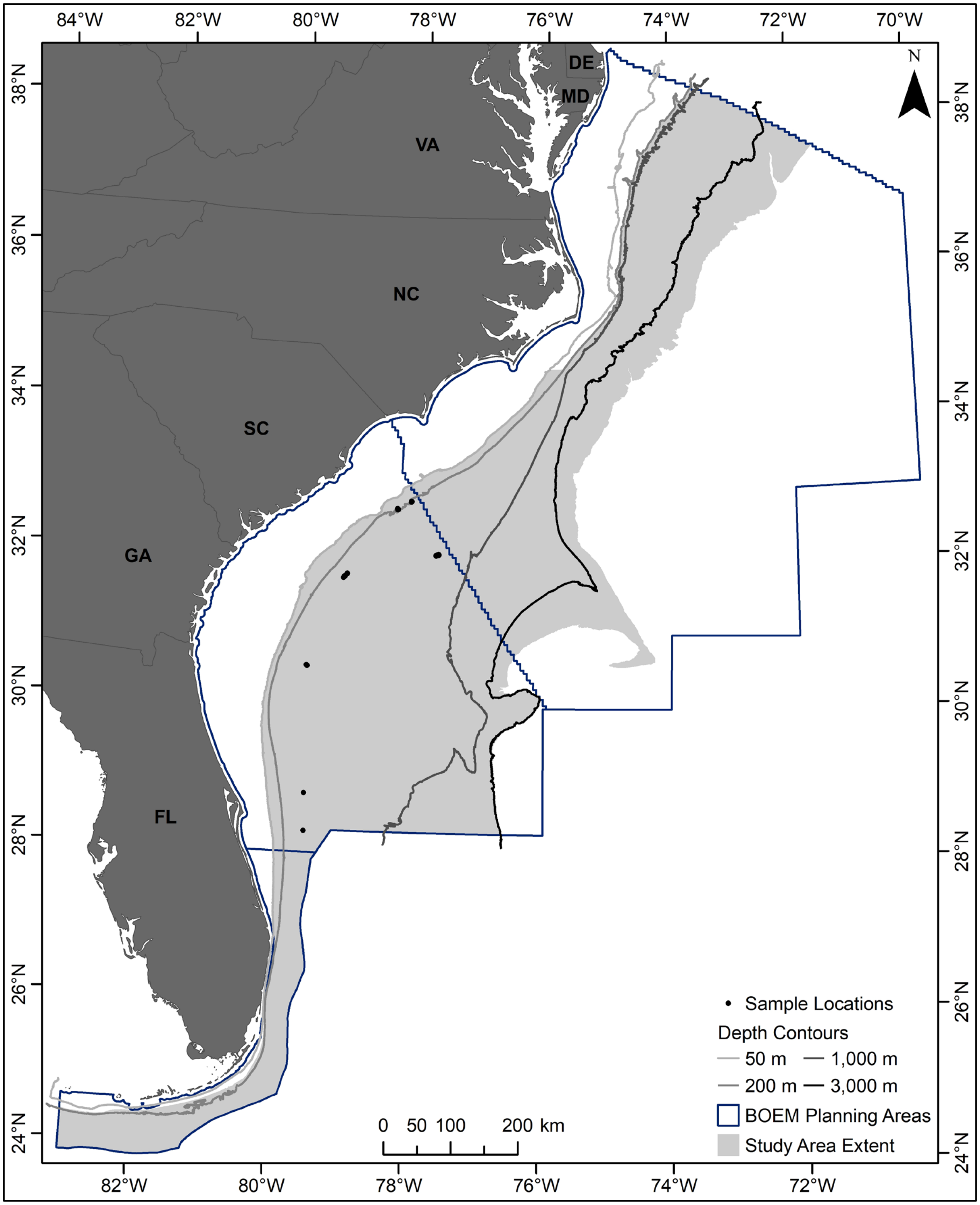

Figure A-6. Locations of samples from the Islands in the Stream 2002 Leg 3 dataset.

A.7 Windows to the Deep 2003

Data provider: Georgia Institute of Technology

Principal investigators: Carolyn Ruppel, Cindy Van Dover

Year: 2003

Vessel: R/V *Atlantis*

Vehicle (Vehicle Type): *Alvin* (HOV)

Observation types: submersible transects, video, specimens

BOEM planning area: Mid-Atlantic

Depth range: 2,113–3457 m

Dives: 7

Samples: 144

Sites: 113

Total area: 33,023 m^2

Recorded taxa (included in models): None

The goal of the Windows to the Deep 2003 expedition was to explore the Blake Ridge and Carolina Rise for new methane seeps and cold seep communities using an integrated biological, chemical, and geophysical approach. Exploration was focused on three areas: 1) the Blake Ridge Diapir, 2) the Cape Fear Diapir and surrounding region, and 3) the Blake Ridge in the vicinity of a large sediment wave field. All surveys were conducted deeper than 2,000 m. Sparse fauna were found in habitats dominated by soft sediment communities[8].

---

[8] For additional information, see the expedition website (https://oceanexplorer.noaa.gov/explorations/03windows/).

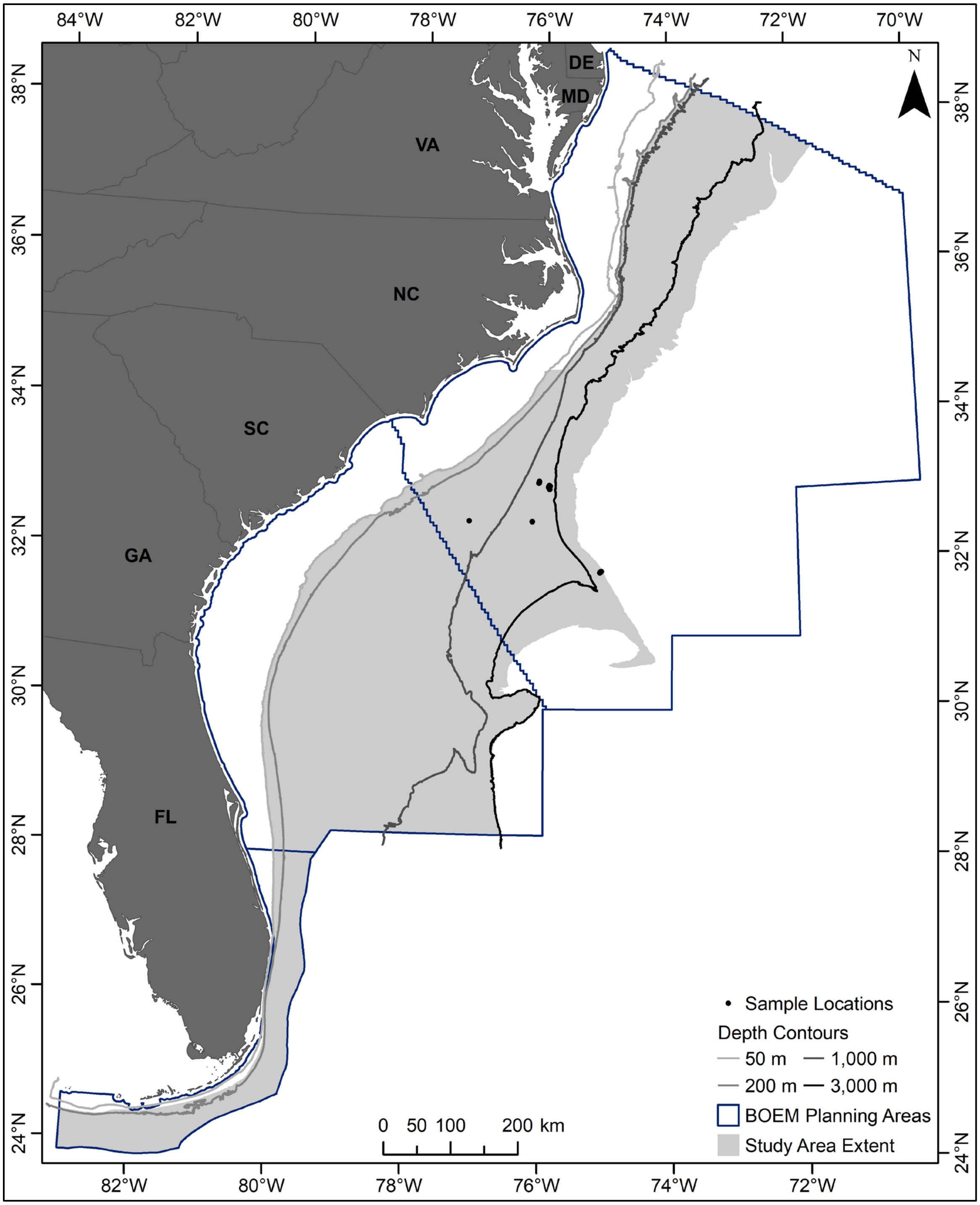

Figure A-7. Locations of samples from the Windows to the Deep 2003 dataset.

A.8 Investigating the Charleston Bump

Data provider: NOAA Central Library

Principal investigators: George Sedberry, Steve Stancyk

Year: 2003

Vessel: R/V *Seward Johnson*

Vehicle (Vehicle type): *Johnson Sea Link II* (HOV)

Observation types: submersible transects, video, specimens

BOEM planning area: South Atlantic

Depth range: 45–584 m

Dives: 13

Samples: 193

Sites: 80

Total area: 25,114 m^2

Recorded taxa (included in models): *Lophelia*, *Solenosmilia*, *Oculina*, *Madrepora*, *Leiopathes*, *Antipathes*, *Bathypathes*, Paragorgiidae, *Plumarella*, *Anthothela*, *Paramuricea*, *Eunicella*, *Muricea*, *Thesea*, *Nicella*, *Acanella*, Stylasteridae

The Charleston Bump was first described in the 1970s when it was documented that it deflected the Gulf Stream offshore. This deflection and the resulting eddies, gyres, and upwelling help concentrate plankton, fishes, and other organisms along thermal fronts downstream from the Bump, increasing overall productivity. The Investigation the Charleston Bump expedition focused on describing small habitat features created by the interaction of currents and erosion resistant features. Emphasis was given to characterizing the fauna associated with steep rocky scarps, scour depressions, and other hardbottom areas. The objectives were to map, explore, and describe deep reef habitats, including characterizing how they are used by marine organisms[9].).

---

[9] For additional information, see the expedition website (https://oceanexplorer.noaa.gov/explorations/03bump/

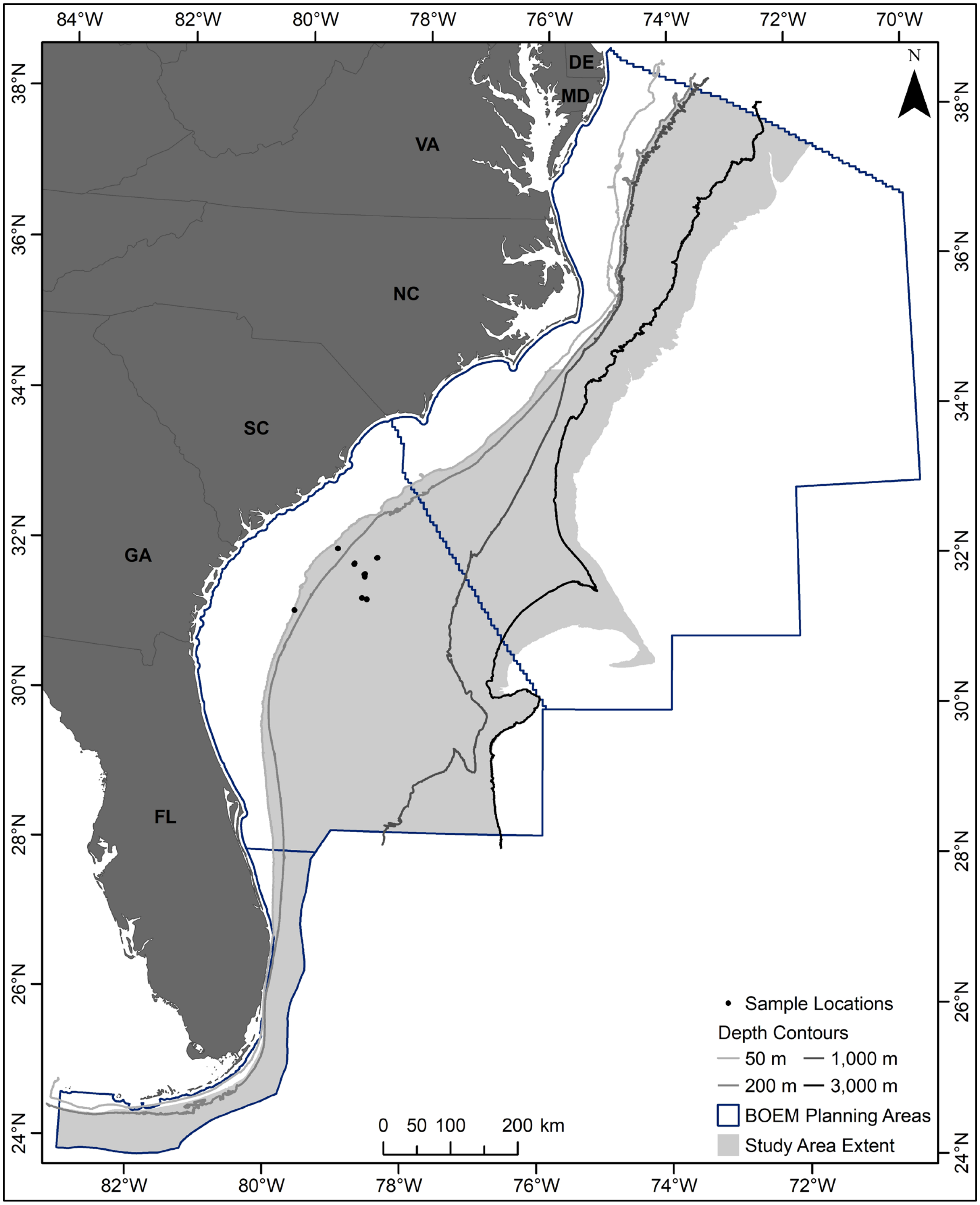

Figure A-8. Locations of samples from the Investigating the Charleston Bump dataset.

A.9 Life on the Edge 2003

Data provider: NOAA Central Library

Principal investigators: Steve Ross, Liz Baird, Ken Sulak, Martha Nizinski

Year: 2003

Vessel: R/V *Seward Johnson*

Vehicle (Vehicle type): *Johnson Sea Link II* (HOV)

Observation types: submersible transects, video, specimens

BOEM planning areas: South Atlantic, Mid-Atlantic

Depth range: 70–640 m

Dives: 17

Samples: 202

Sites: 64

Total area: 25,276 m^2

Recorded taxa (included in models): *Lophelia*, *Solenosmilia*, *Madrepora*, *Stichopathes*, *Leiopathes*, *Antipathes*, *Tanacetipathes*, *Bathypathes*, Paragorgiidae, *Plumarella*, *Acanthogorgia*, *Paramuricea*, *Eunicella*, *Muricea*, *Thesea*, *Callogorgia*, *Nicella*, Chrysogorgiidae, *Acanella*, Stylasteridae

The goal of the Life on the Edge expeditions (2003–2005) was to explore and ultimately compare and contrast the closely associated ecosystems of the hard grounds on the outer continental shelf and mid-slope DSC (*Lophelia*) banks offshore from the Carolinas to southeastern Florida. The objective was to document the locations and areal extent of unexplored deep reef habitats (80–700 m), especially on a small scale, as well as to document the biodiversity of deep reef fauna by quantifying habitats, species associations, and behaviors. The 2004 and 2005 expeditions would continue to define the benthic fish and invertebrate community structures, classify reef and off reef habitat zones, and document faunal affinities. Specimens were collected to age DSCs and amplify and sequence their DNA for phylogenetic, phylogeographic, and community genetics[10].

---

[10] For additional information about the 2003 expedition, see the expedition website (https://oceanexplorer.noaa.gov/explorations/03edge/).

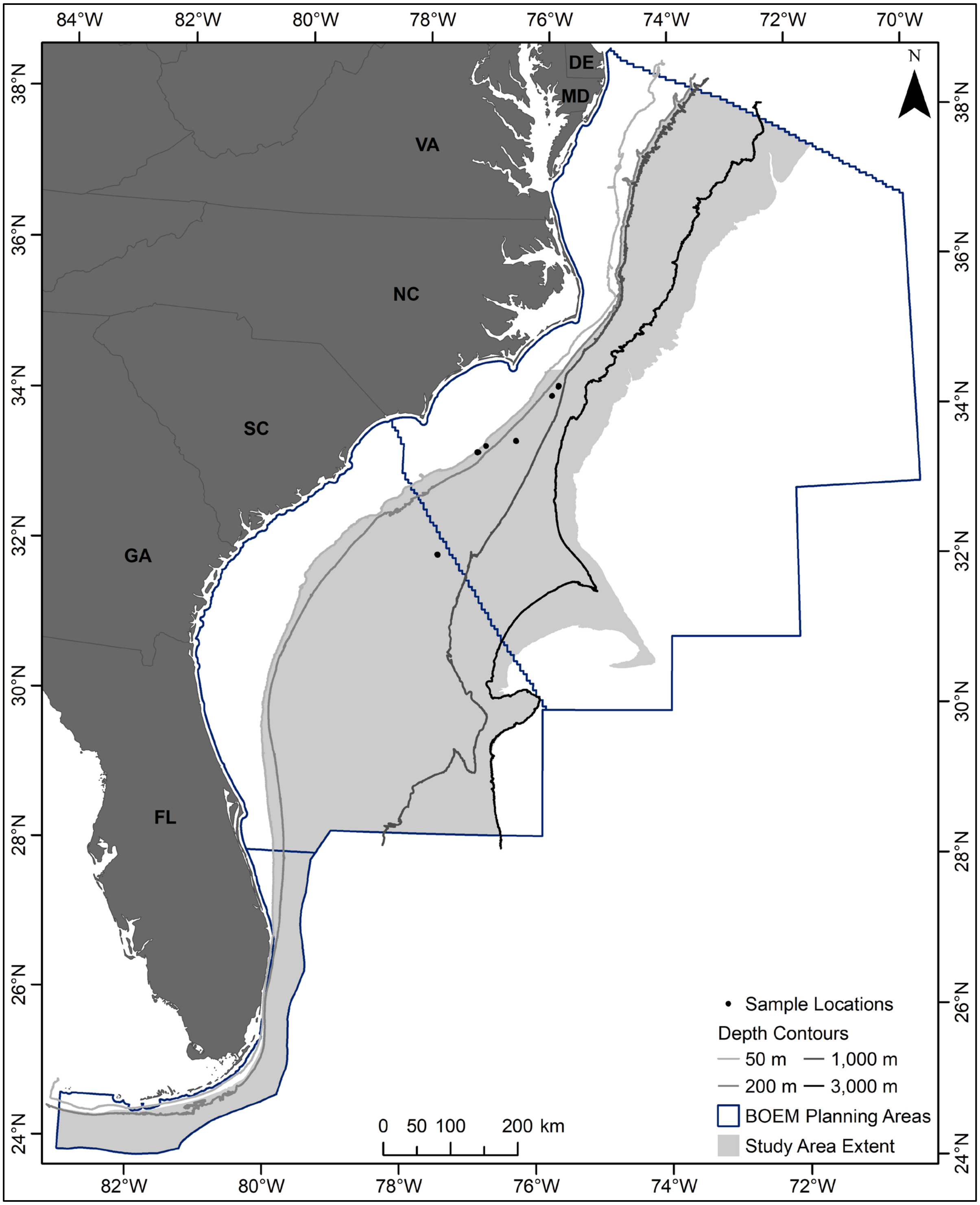

Figure A-9. Locations of samples from the Life on the Edge 2003 dataset.

A.10 Life on the Edge 2004

Data provider: NOAA Central Library

Principal investigators: Steve Ross, Liz Baird, Ken Sulak, Martha Nizinski

Year: 2004

Vessel: R/V *Seward Johnson*

Vehicle (Vehicle type): *Johnson Sea Link I* (HOV)

Observation types: submersible transects, video, specimens

BOEM planning areas: South Atlantic, Mid-Atlantic

Depth range: 76–783 m

Dives: 25

Samples: 202

Sites: 100

Total area: 27,675 m^2

Recorded taxa (included in models): *Lophelia*, *Solenosmilia*, *Oculina*, *Madrepora*, *Stichopathes*, *Leiopathes*, *Antipathes*, *Tanacetipathes*, *Bathypathes*, Paragorgiidae, *Plumarella*, *Acanthogorgia*, *Paramuricea*, *Eunicella*, *Thesea*, *Callogorgia*, Chrysogorgiidae, Stylasteridae

The goal of the Life on the Edge expeditions (2003–2005) was to explore and ultimately compare and contrast the closely associated ecosystems of the hard grounds on the outer continental shelf and mid-slope DSC (*Lophelia*) banks offshore from the Carolinas to southeastern Florida. The objective was to document the locations and areal extent of unexplored deep reef habitats (80–700 m), especially on a small scale, as well as to document the biodiversity of deep reef fauna by quantifying habitats, species associations, and behaviors. The 2004 and 2005 expeditions would continue to define the benthic fish and invertebrate community structures, classify reef and off reef habitat zones, and document faunal affinities. Specimens were collected to age DSCs and amplify and sequence their DNA for phylogenetic, phylogeographic, and community genetics[11].

---

[11] For additional information about the 2004 expedition, see the expedition website (https://oceanexplorer.noaa.gov/explorations/04edge/).

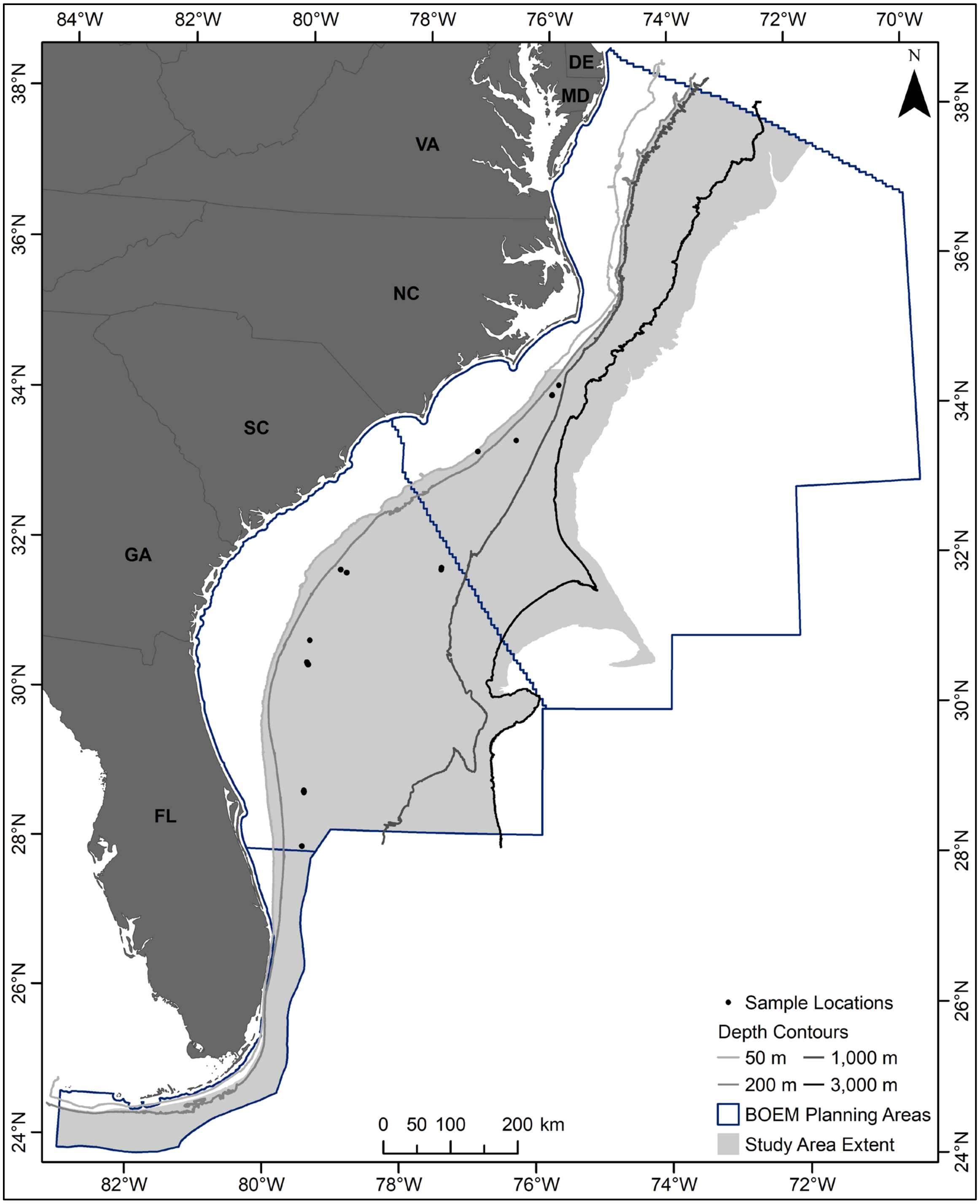

Figure A-10. Locations of samples from the Life on the Edge 2004 dataset.

A.11 Estuary to the Abyss

Data providers: Project Oceanica, College of Charleston

Principal investigators: George Sedberry, Mark Mitchell

Year: 2004

Vessel: R/V *Seward Johnson*

Vehicle (Vehicle type): *Johnson Sea Link II* (HOV)

Observation types: submersible transects, video, specimens

BOEM planning area: South Atlantic

Depth range: 526–909 m

Dives: 6

Samples: 20

Sites: 18

Total area: 5,080 m^2

Recorded taxa (included in models): *Lophelia*, *Solenosmilia*, *Leiopathes*, *Plumarella*, *Anthothela*, *Paramuricea*, *Eunicella*, Stylasteridae

The Estuary to the Abyss expedition focused on the habitats and fauna in the deeper (>400 m), relatively unexplored waters along the Latitude 31°30' Transect, a line that extends from the Georgia coast to the edge of the continental shelf. The research built upon shallow water (10–400 m) data previously collected in a variety of habitats along the transect[12].

---

[12] For additional information about the expedition, see the expedition website (https://oceanexplorer.noaa.gov/explorations/04etta/).

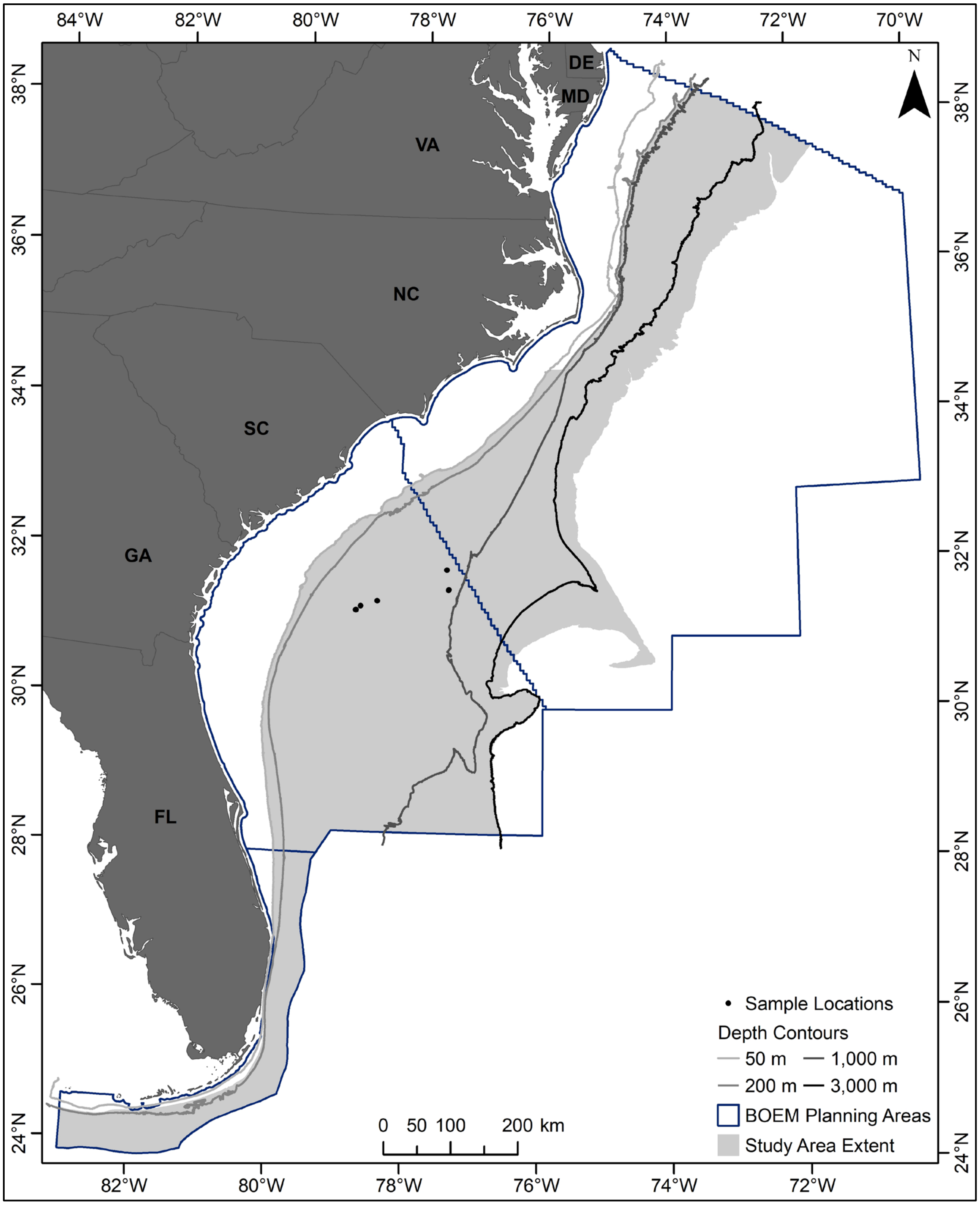

Figure A-11. Locations of samples from the Estuary to the Abyss dataset.

A.12 Life on the Edge 2005

Data provider: NOAA Central Library

Principal investigators: Steve Ross, Liz Baird, Ken Sulak, Martha Nizinski

Year: 2005

Vessel: R/V *Seward Johnson*

Vehicle (Vehicle type): *Johnson Sea Link I* (HOV)

Observation types: submersible transects, video, specimens

BOEM planning areas: South Atlantic, Mid-Atlantic

Depth range: 365–705 m

Dives: 18

Samples: 302

Sites: 122

Total area: 36,960 m^2

Recorded taxa (included in models): *Lophelia*, *Solenosmilia*, *Madrepora*, *Leiopathes*, *Bathypathes*, Paragorgiidae, *Plumarella*, *Acanthogorgia*, *Paramuricea*, Chrysogorgiidae, Stylasteridae

The goal of the Life on the Edge expeditions (2003–2005) was to explore and ultimately compare and contrast the closely associated ecosystems of the hard grounds on the outer continental shelf and mid-slope DSC (*Lophelia*) banks offshore from the Carolinas to southeastern Florida. The objective was to document the locations and areal extent of unexplored deep reef habitats (80–700 m), especially on a small scale, as well as to document the biodiversity of deep reef fauna by quantifying habitats, species associations, and behaviors. The 2004 and 2005 expeditions would continue to define the benthic fish and invertebrate community structures, classify reef and off reef habitat zones, and document faunal affinities. Specimens were collected to age DSCs and amplify and sequence their DNA for phylogenetic, phylogeographic, and community genetics[13].

---

[13] For additional information about the 2004 expedition, see the expedition website (https://oceanexplorer.noaa.gov/explorations/05coralbanks/).

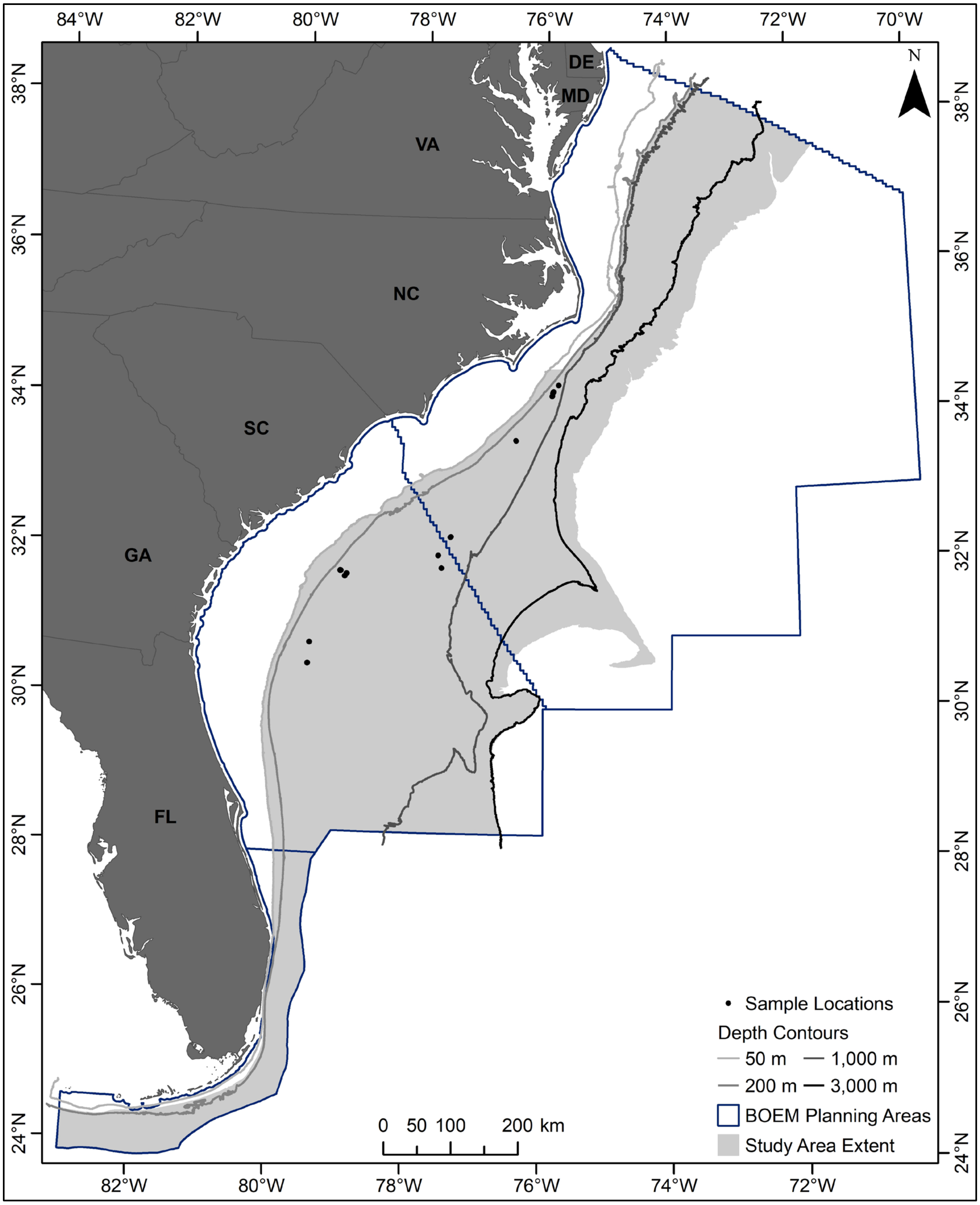

Figure A-12. Locations of samples from the Life on the Edge 2005 dataset.

A.13 Georgetown Hole

Data provider: Gray's Reef National Marine Sanctuary

Principal investigator: George Sedberry

Year: 2010

Vessel: NOAA Ship *Pisces*

Vehicle (Vehicle type): Phantom DS4 (ROV)

Observation types: ROV transects, video, specimens

BOEM planning area: South Atlantic

Depth range: 165–408 m

Dives: 5

Samples: 136

Sites: 66

Total area: 12,533 m^2

Recorded taxa (included in models): *Lophelia*, *Oculina*, *Tanacetipathes*, *Plumarella*, *Muricea*

The Georgetown Hole expedition intended to observe and sample DSC banks at depths of 400–500 m offshore of Georgia, but currents were too strong to deploy the ROV. Instead, ROV dives were conducted at depths of 150–250 m at Georgetown Hole, a site that had been previously explored and was known to have complex hardbottom features[14].

---

[14] For additional information about the expedition, see the expedition website (https://sanctuaries.noaa.gov/missions/2010coral_east/mission_summary.html).

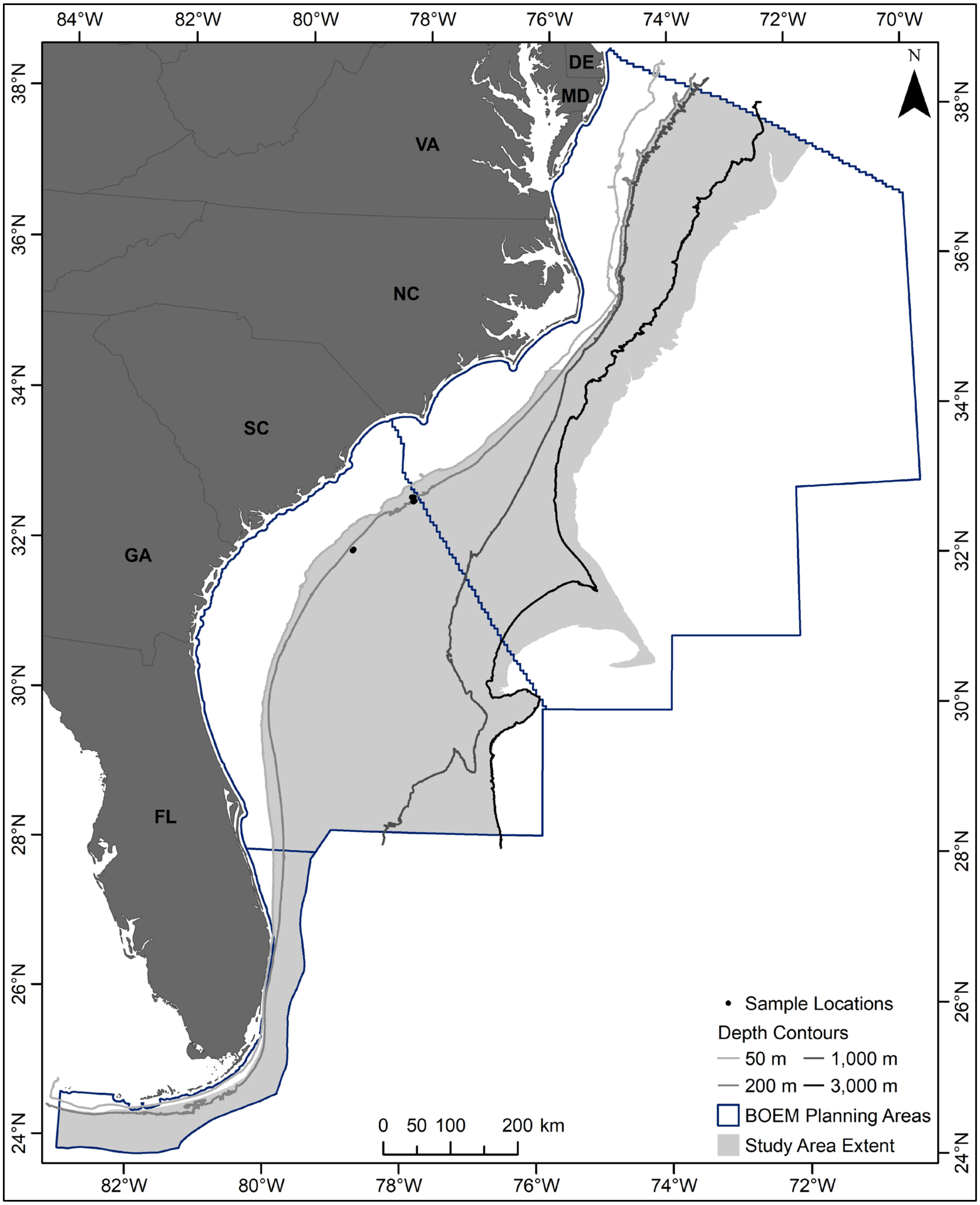

Figure A-13. Locations of samples from the Georgetown Hole dataset.

A.14 Extreme Corals 2010

Data provider: NOAA Central Library

Principal investigators: Steve Ross, Sandra Brooke

Year: 2010

Vessel: NOAA Ship *Ronald H. Brown*

Vehicle (Vehicle type): *Jason II* (ROV)

Observation types: ROV transects, video, specimens

BOEM planning areas: Straits of Florida, South Atlantic

Depth range: 161–709 m

Dives: 8

Samples: 356

Sites: 89

Total area: 13,800

Recorded taxa (included in models): *Lophelia*, *Solenosmilia*, *Madrepora*, *Leiopathes*, *Plumarella*, Chrysogorgiidae, Stylasteridae

The NOAA Deep Sea Coral Research and Technology Program sponsored the Extreme Corals 2010 expedition. The objectives of the expedition were: 1) to document coral and sponge habitats, 2) to describe habitat associations, community structure, and distributions of coral habitats, 3) to examine growth, reproduction, feeding, and energetics of major structure-forming corals, 4) to determine trophodynamics of communities associated with reef and off reef habitats, 5) to collect samples for paleoecology (coral age, growth, and historical temperature and productivity), 6) to describe the physical environment of reefs, 7) to collect water samples near corals and in the water column for aragonite saturation analysis, 8) to collect live corals for multiple analyses and experiments, 9) to collect sponges for taxonomy, genetics, and habitat characterization, 10) to collect samples for population connectivity, and 11) to perform education/outreach activities[15].

---

[15] For additional information about the expedition, see the cruise report (https://safmc.net/wp-content/uploads/2016/06/Coral_AppK_RonBrownCruiseReport_Nov2010_20Jan11.pdf).

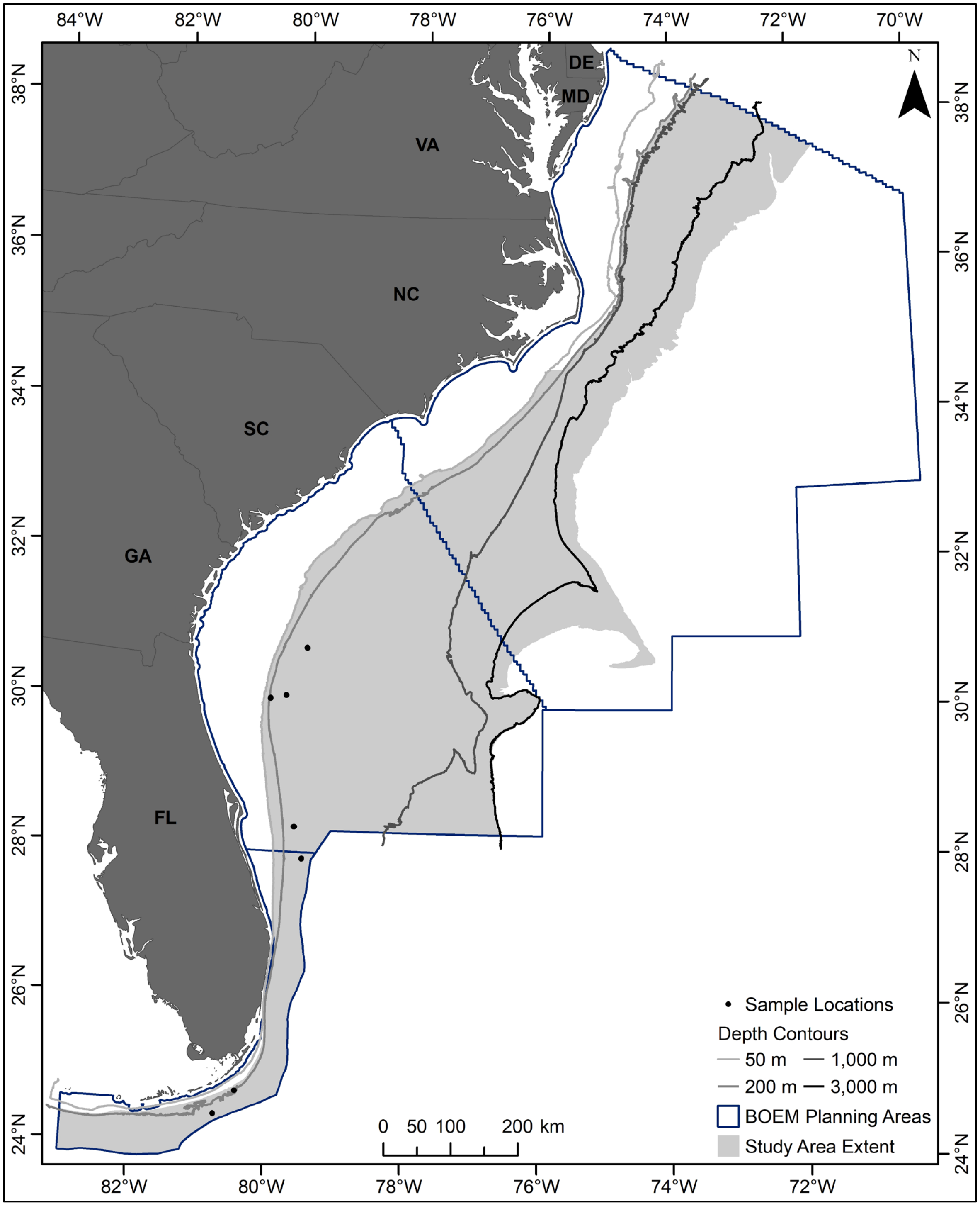

Figure A-14. Locations of samples from the Extreme Corals 2010 dataset.

A.15 Extreme Corals 2011

Data provider: Harbor Branch Oceanographic Institute

Principal investigator: Andy David, John Reed

Year: 2011

Vessel: NOAA Ship *Pisces*

Vehicle (Vehicle type): Phantom (ROV)

Observation type: ROV transects, video, specimens

BOEM planning areas: Straits of Florida, South Atlantic

Depth range: 56–375 m

Dives: 9

Samples: 72

Sites: 65

Total area: 20,705 m^2

Recorded taxa (included in models): *Lophelia*, *Oculina*, *Cladocora*, *Stichopathes*, *Tanacetipathes*, *Plumarella*, *Paramuricea*, *Eunicella*, *Muricea*, *Nicella*, Stylasteridae

The Extreme Corals 2011 expedition was part of an ongoing study of DSC habitats offshore of the southeastern US Primary research objectives of the multi-year science plan included mapping and characterizing coral and fish populations inside and adjacent to new managed areas. The focus of the 2011 expedition was to explore hard grounds out to 550 m depth off of south Florida with an emphasis on assessing areas that are coral/sponge habitat and areas that were still open to bottom fishing activities within the managed areas[16].

---

[16] For additional information about the expedition, see the cruise report (https://www.ncei.noaa.gov/data/oceans/coris/library/NOAA/DSCRTP/Grants/NA09OAR4320073/2011_Pisces_CIOERT_Cruise-SEADESII_Report-FINAl_2-28-2013.pdf).

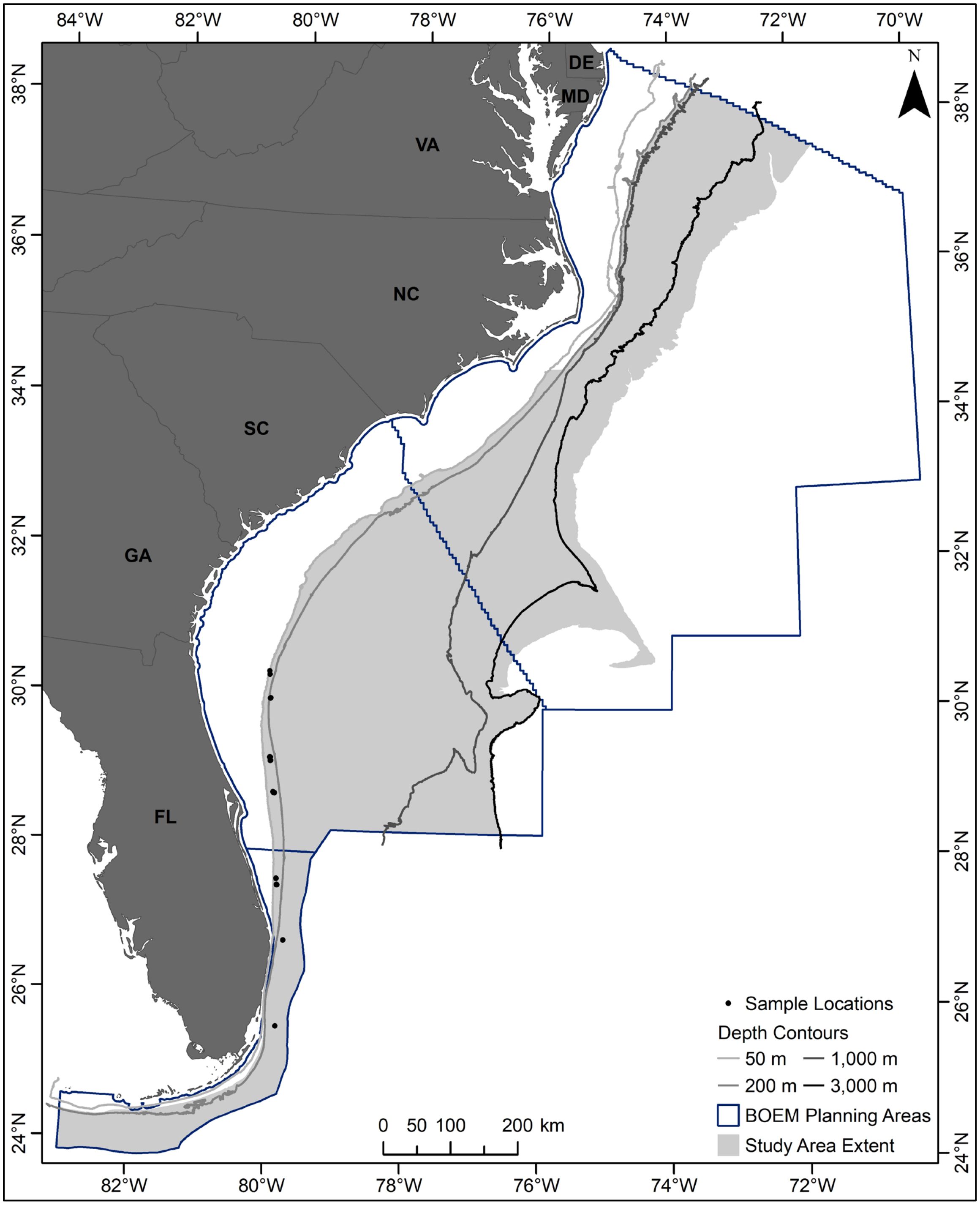

Figure A-15. Locations of samples from the Extreme Corals 2011 dataset.

A.16 Florida Shelf-Edge Exploration II

Data provider: Harbor Branch Oceanographic Institute

Principal investigator: John Reed

Year: 2011

Vessel: NOAA Ship *Nancy Foster*

Vehicle (Vehicle type): *Kraken 2* (ROV)

Observation type: ROV transects, video, specimens

BOEM planning area: Straits of Florida

Depth range: 154–573 m

Dives: 13

Samples: 66

Sites: 13

Total area: 2,409 m^2

Recorded taxa (included in models): *Lophelia*, *Madrepora*, *Stichopathes*, *Leiopathes*, *Tanacetipathes*, *Bathypathes*, *Plumarella*, *Paramuricea*, *Muricea*, Stylasteridae

The Florida Shelf-Edge Exploration (FLoSEE) II expedition included seven days of ROV surveys funded in part by the NOAA Deep Sea Coral Research and Technology Program to explore and sample DSC and sponge ecosystems. Surveys were conducted at the newly designated Deepwater Coral Habitat Areas of Particular Concern (CHAPC) and East Hump Marine Protected Area on the Pourtalès Terrace to provide a general description and collect images of the habitat and biota. The expedition also focused on education and outreach activities to promote knowledge of ocean ecosystems and challenges of exploring deep ocean frontiers[17].

---

[17] For additional information about the expedition, see the cruise report (http://fau.digital.flvc.org/islandora/object/fau%3A6349).

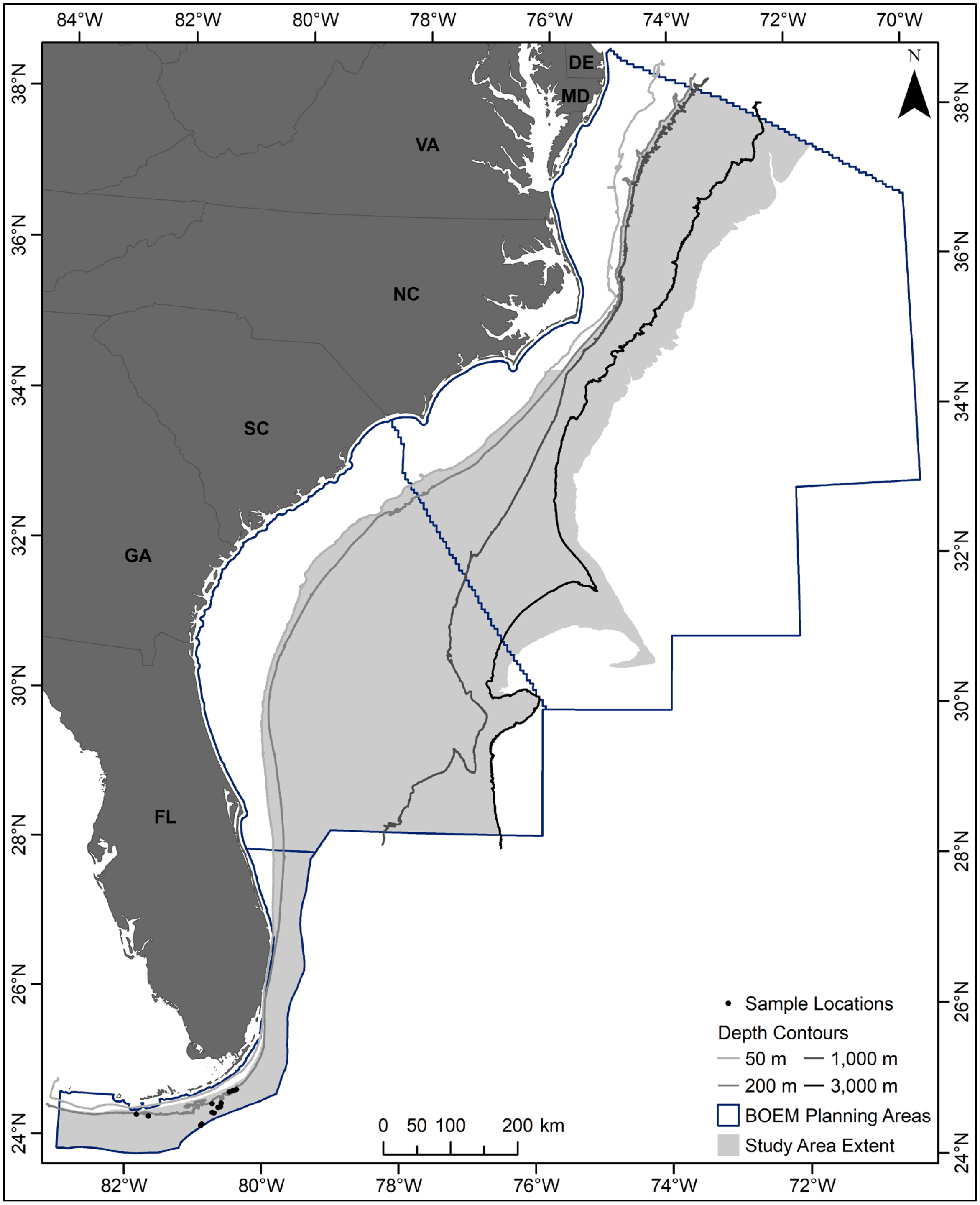

Figure A-16. Locations of samples from the Florida Shelf-Edge Exploration II dataset.

A.17 Deepwater Canyons 2012

Data provider: Florida State University

Principal investigators: Steve Ross, Sandra Brooke

Year: 2012

Vessel: NOAA Ship *Nancy Foster*

Vehicle (Vehicle type): *Kraken 2* (ROV)

Observation types: ROV transects, video, specimens

BOEM planning area: Mid-Atlantic

Depth range: 276–1,003 m

Dives: 20

Samples: 3,673

Sites: 438

Total area: 64,470 m^2

Recorded taxa (included in models): *Lophelia*, Paragorgiidae, *Anthothela*, *Acanthogorgia*, *Paramuricea*

The Deepwater Canyons 2012 expedition was part of the multi-year Mid-Atlantic Deepwater Canyons project, funded by BOEM, the NOAA Office of Ocean Exploration and Research, and USGS. The goal of this project was to explore and characterize hard bottom communities (including DSCs), soft bottom communities, and shipwreck sites in the submarine canyons offshore of Virginia and Maryland[18].

---

[18] . For additional information about the expedition, see the expedition website (https://oceanexplorer.noaa.gov/explorations/12midatlantic/).

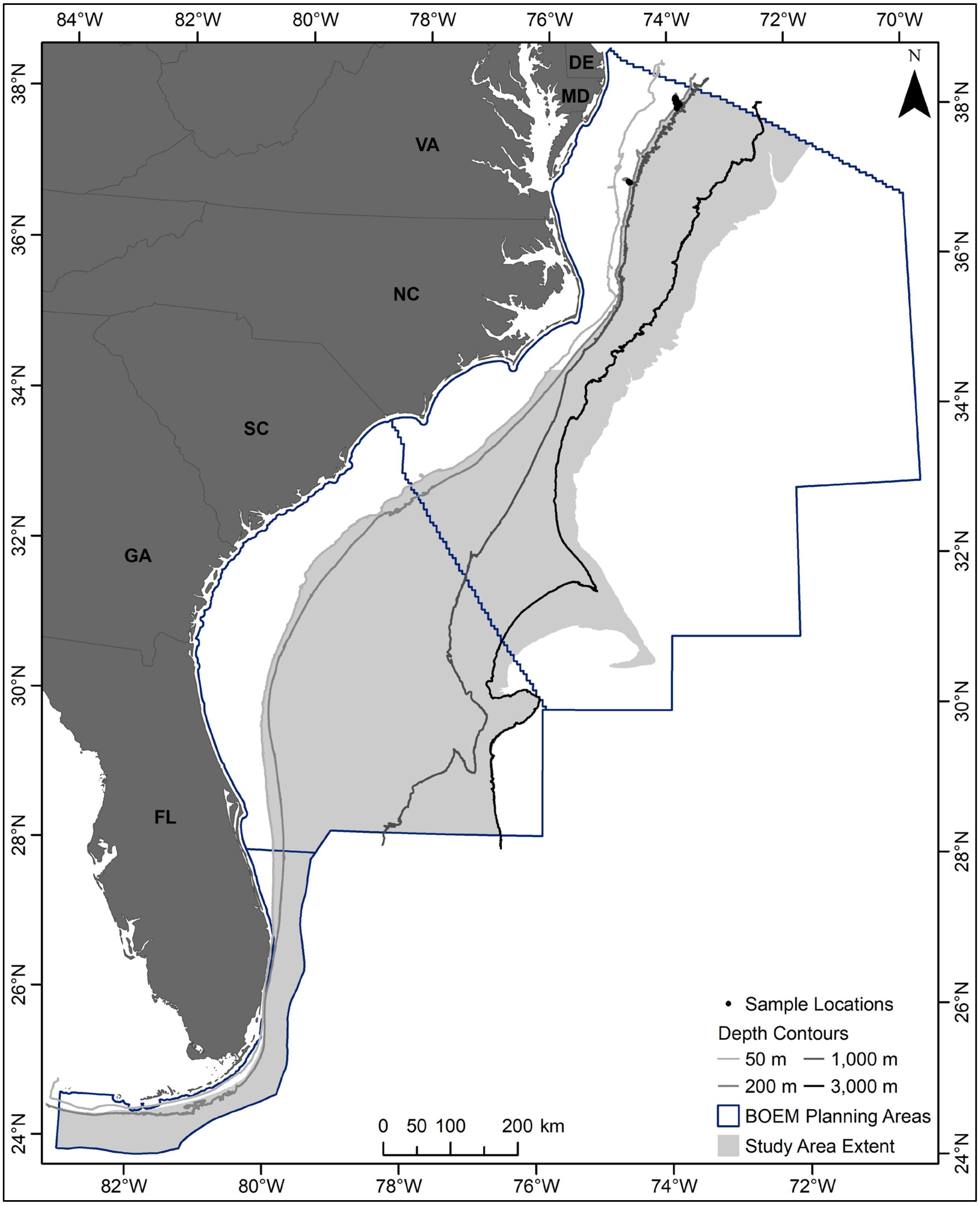

Figure A-17. Locations of samples from the Deepwater Canyons 2012 dataset.

A.18 Deepwater Canyons 2013

Data provider: Florida State University

Principal investigators: Steve Ross, Sandra Brooke

Year: 2013

Vessel: NOAA Ship *Ronald H. Brown*

Vehicle (Vehicle type): *Jason II* (ROV)

Observation types: ROV transects, video, specimens

BOEM planning area: Mid-Atlantic

Depth range: 290–1,612

Dives: 13

Samples: 3,585

Sites: 264

Total area: 57,920 m^2

Recorded taxa (included in models): *Lophelia*, *Solenosmilia*, Paragorgiidae, *Anthothela*, *Acanthogorgia*, *Paramuricea*

The Deepwater Canyons 2013 expedition was part of the multi-year Mid-Atlantic Deepwater Canyons project, funded by BOEM, the NOAA Office of Ocean Exploration and Research, and USGS. The goal of this project was to explore and characterize hard bottom communities (including DSCs), soft bottom communities, and shipwreck sites in the submarine canyons offshore of Virginia and Maryland.[19]

---

[19] . For additional information about the expedition, see the expedition website (https://oceanexplorer.noaa.gov/explorations/13midatlantic/).

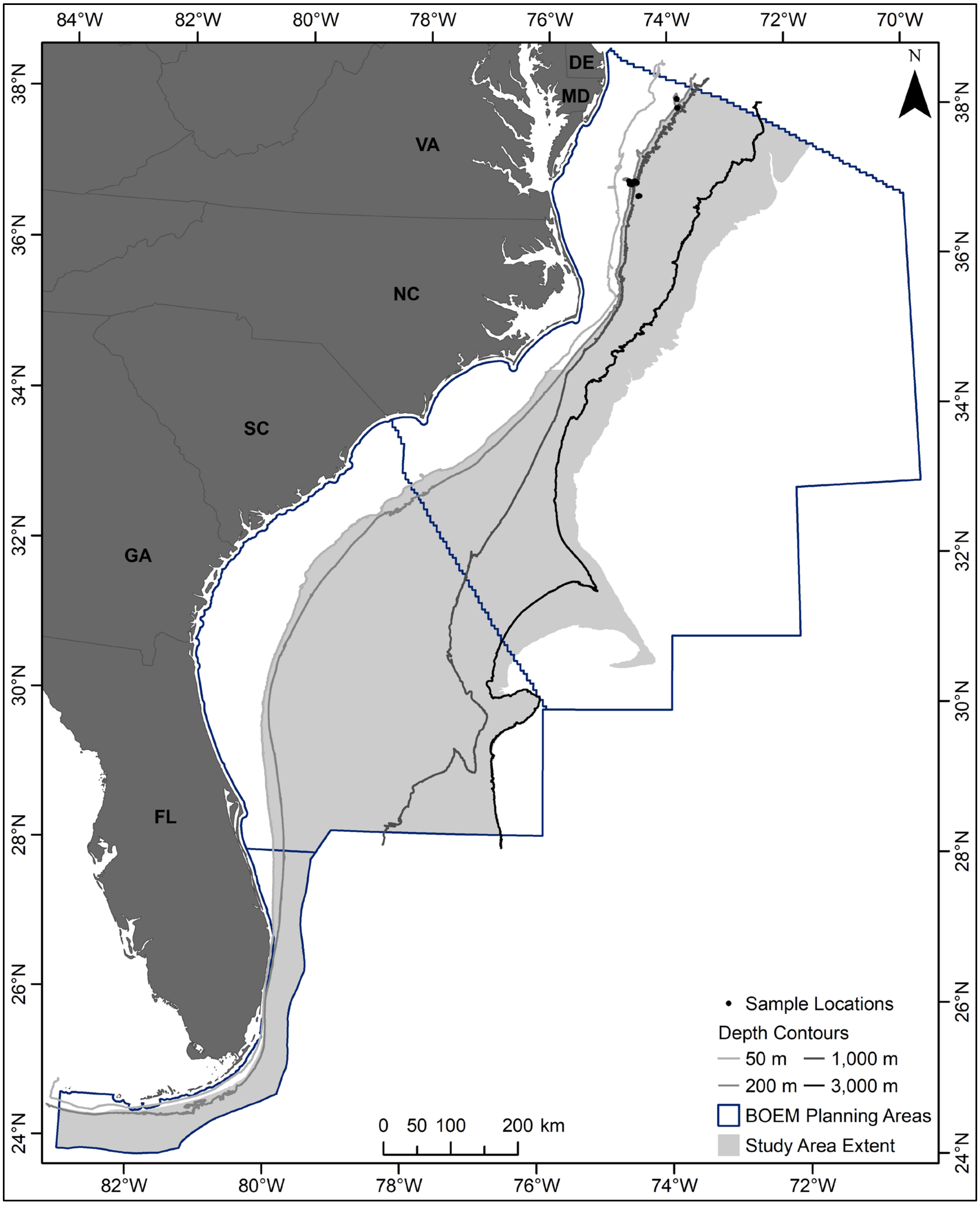

Figure A-18. Locations of samples from the Deepwater Canyons 2013 dataset.

A.19 Windows to the Deep 2018

Data provider: NOAA Office of Ocean Exploration and Research

Principal investigator(s): Cheryl Morrison, Leslie Sautter

Year: 2018

Vessel: NOAA Ship *Okeanos Explorer*

Vehicle (Vehicle type): *Deep Discoverer* (ROV)

Observation type: ROV transects, video, specimens

BOEM planning areas: South Atlantic, Mid-Atlantic

Depth range: 303–3,419 m

Dives: 17

Samples: 86

Sites: 84

Total area: 16,300 m^2

Recorded taxa (included in models): *Lophelia*, *Solenosmilia*, *Madrepora*, *Enallopsammia*, *Stichopathes*, *Leiopathes*, *Bathypathes*, Paragorgiidae, *Plumarella*, *Anthothela*, *Acanthogorgia*, *Paramuricea*, *Eunicella*, Chrysogorgiidae, *Acanella*

The Windows to the Deep 2018 expedition was a two-part, 36-day telepresence-enabled expedition to explore and collect data on unknown or poorly understood areas identified by the ocean management and scientific communities. Scientists explored a diversity of features with mapping and ROV surveys targeting DSC and sponge communities, maritime heritage sites, a landslide feature, and possible cold seeps. Extensive scarp, mound, and large *Lophelia*, *Madrepora*, and *Enallopsammia* reef habitats were observed, along with a wide diversity of fishes[20].

---

[20] For additional information about the expedition, see the expedition website (https://oceanexplorer.noaa.gov/okeanos/explorations/ex1806/).

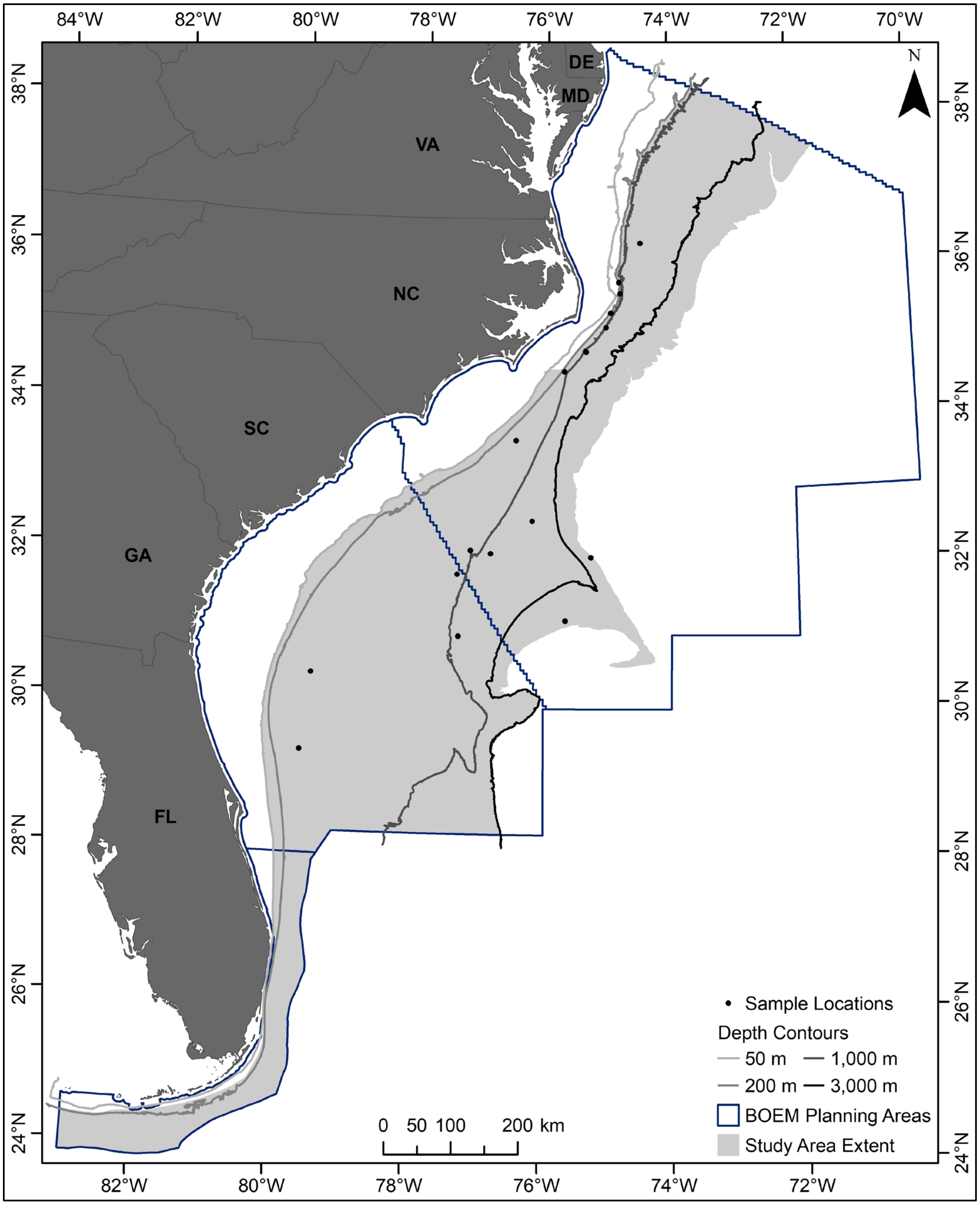

Figure A-19. Locations of samples from the Windows to the Deep 2018 dataset.

A.20 Deep SEARCH 2018

Data provider: Temple University

Principal investigator: Erik Cordes

Year: 2018

Vessel: R/V *Atlantis*

Vehicle (Vehicle Type): *Alvin* (HOV)

Observation types: submersible transects, video, specimens

BOEM planning areas: South Atlantic, Mid-Atlantic

Depth range: 363–2,169

Dives: 10

Samples: 219

Sites: 132

Total area: 29,056 m^2

Recorded taxa (included in models): *Lophelia*, *Solenosmilia*, *Madrepora*, *Enallopsammia*, *Stichopathes*, *Leiopathes*, *Bathypathes*, Paragorgiidae, *Plumarella*, *Anthothela*, *Acanthogorgia*, *Paramuricea*, Chrysogorgiidae, *Acanella*, Stylasteridae

The purpose of the Deep SEARCH 2018 expedition was to collect critical baseline information about deep water habitats offshore of the US Mid- and South Atlantic. The expedition was the third in the multi-year, multi-agency Deep Sea Exploration to Advance Research on Coral/Canyon/Cold Seep Habitats (Deep SEARCH) project. The goals of the expedition were to explore and characterize biological communities, examine their sensitivity to natural and human disturbances, and describe the oceanographic, geological, geochemical, and acoustic conditions associated with each habitat type[21]

---

[21] . For additional information about the expedition, see the expedition website (https://oceanexplorer.noaa.gov/okeanos/explorations/ 18deepsearch/).

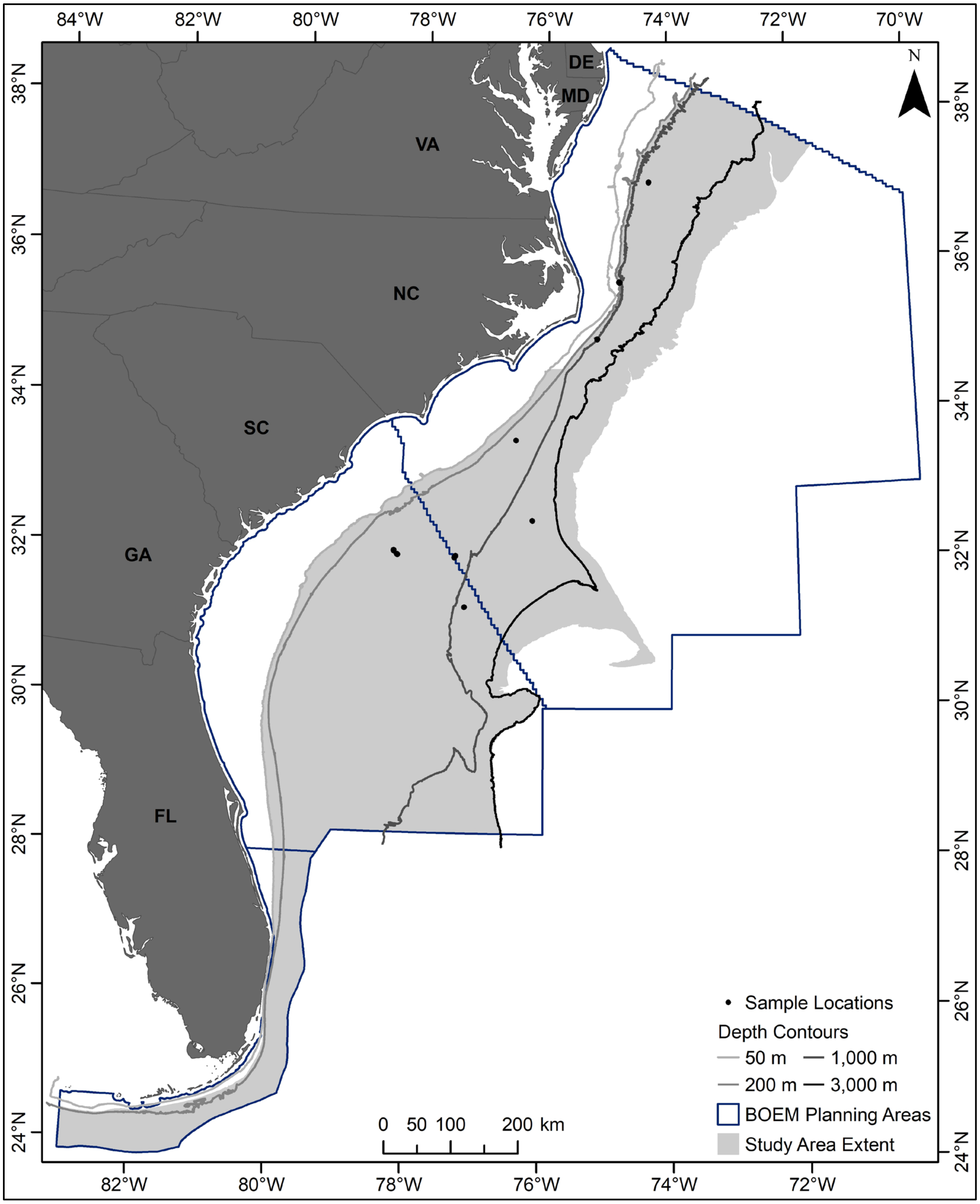

Figure A-20. Locations of samples from the Deep SEARCH 2018 dataset.

Appendix B: Inventory of Bathymetry Datasets

Table B-1. Compilation of bathymetry datasets included in the merged bathymetry dataset

Dataset	Data Source and/or Vessel	Year	Native Resolution	Data Provider
H13163_MB_2m_MLLW_Combined	eTrac, Inc.; R/V *Taku*, R/V *Marcelle*	2019	2 m	NCEI
H13161_MB_2m_MLLW_Combined	eTrac, Inc.; R/V *Taku*, R/V *Marcelle*	2019	2 m	NCEI
H13160_MB_2m_MLLW_Combined	eTrac, Inc.; R/V *Taku*, R/V *Marcelle*	2019	2 m	NCEI
F00720_MB_1m_MLLW_1of1	NOAA Ship *Thomas Jefferson*	2018	1 m	NCEI
NF-17-08_Leg2_North_4m_NAD83_UTM17N	NOAA Ship *Nancy Foster*	2017	4 m	NCEI
F00697_MB_2m_MLLW_1of1_NAD83_UTM17N	NOAA Ship *Ferdinand Hassler*	2016	2 m	NCEI
F00679_MB_2m_MLLW_Combined	NOAA Ship *Ferdinand Hassler*	2016	2 m	NCEI
H12934_MB_4m_MLLW_combined	NOAA Ship *Ferdinand Hassler*	2016	4 m	NCEI
H12932_MB_4m_MLLW_Combined	NOAA Ship *Ferdinand Hassler*	2016	4 m	NCEI
H12931_MB_2m_MLLW_Combined_1of1	NOAA Ship *Ferdinand Hassler*	2016	2 m	NCEI
H12930_MB_4m_MLLW_combined	NOAA Ship *Ferdinand Hassler*	2016	4 m	NCEI
H12929_MB_2m_MLLW_1of1	NOAA Ship *Ferdinand Hassler*	2016	2 m	NCEI
H12895_MB_2m_MLLW_1of1	NOAA Ship *Ferdinand Hassler*	2016	2 m	NCEI
H12894_MB_2m_MLLW_1of1	NOAA Ship *Ferdinand Hassler*	2016	2 m	NCEI
H12893_MB_2m_MLLW_1of1	NOAA Ship *Ferdinand Hassler*	2016	2 m	NCEI
H12859_MB_2m_MLLW_combined	NOAA Ship *Ferdinand Hassler*	2016	2 m	NCEI
H12858_MB_2m_MLLW_Combined	NOAA Ship *Ferdinand Hassler*	2016	2 m	NCEI
H12843_MB_2m_MLLW_Combined	NOAA Ship *Ferdinand Hassler*	2015	2 m	NCEI
H12841_MB_2m_MLLW_1of1	NOAA Ship *Ferdinand Hassler*	2015	2 m	NCEI
H12840_MB_2m_MLLW_Combined	NOAA Ship *Ferdinand Hassler*	2015	2 m	NCEI
H12839_MB_4m_MLLW_Combined	NOAA Ship *Ferdinand Hassler*	2015	4 m	NCEI
H12794_MB_1m_MLLW_1of1	NOAA Ship *Thomas Jefferson*	2015	1 m	NCEI

Dataset	**Data Source and/or Vessel**	**Year**	**Native Resolution**	**Data Provider**
W00411_MB_1m_MLLW_1of1	NOAA Ship *Nancy Foster*	2015	1 m	NCEI
NF-14-07-FKNMS_MarquesasRock_2m_NAD83_UTM17N	NOAA Ship *Nancy Foster*	2014	2 m	NCEI
NF-14-07-FKNMS_SatanShoal_1m_UTM17N	NOAA Ship *Nancy Foster*	2014	1 m	NCEI
NF-14-06-EPA_Palm_Beach_5m_NAD83_UTM17N	NOAA Ship *Nancy Foster*	2014	5 m	NCEI
NF-14-04-EFH_North_1m	NOAA Ship *Nancy Foster*	2014	1 m	NCEI
NF-14-04-EFH_South_1m	NOAA Ship *Nancy Foster*	2014	1 m	NCEI
NF-14-03-GRNMS_1m	NOAA Ship *Nancy Foster*	2014	1 m	NCEI
F00636_MB_1m_MLLW_1of1	NOAA Navigation Response Team 2	2014	1 m	NCEI
H12668_MB_50cm_MLLW_1of1	NOAA Ship *Ferdinand Hassler*	2014	50 cm	NCEI
W00290_MB_4m_MLLW_combined	NOAA Ship *Pisces*	2014	4 m	NCEI
H12572_MB_4m_MLLW_Combined	NOAA Ship *Thomas Jefferson*	2013	4 m	NCEI
H12570_MB_4m_MLLW_Combined	NOAA Ship *Thomas Jefferson*	2013	4 m	NCEI
H12561_MB_2m_MLLW_combined	Leidos; M/V *Atlantic Surveyor*	2013	2 m	NCEI
H12560_MB_2m_MLLW_combined	Leidos; M/V *Atlantic Surveyor*	2013	2 m	NCEI
H12559_MB_2m_MLLW_Combined	Leidos; M/V *Atlantic Surveyor*	2013	2 m	NCEI
W00391_MB_1m_MLLW_1of1	NOAA Ship *Nancy Foster*	2013	1 m	NCEI
H12505_MB_1m_MLLW_1of1	NOAA Ship *Ferdinand Hassler*	2012	1 m	NCEI
H12504_MB_1m_MLLW_Combined	NOAA Ship *Ferdinand Hassler*	2012	1 m	NCEI
H12503_MB_1m_MLLW_Combined	NOAA Ship *Ferdinand Hassler*	2012	1 m	NCEI
H12502_MB_1m_MLLW_1of1	NOAA Ship *Ferdinand Hassler*	2012	1 m	NCEI
H12501_MB_1m_MLLW_1of1	NOAA Ship *Ferdinand Hassler*	2012	1 m	NCEI
H12423_MB_1m_MLLW_Combined	NOAA Ship *Ferdinand Hassler*	2012	1 m	NCEI
H12397_MB_2m_MLLW_1of1	Leidos; M/V *Atlantic Surveyor*	2012	2 m	NCEI
H12396_MB_2m_MLLW_Combined	Leidos; M/V *Atlantic Surveyor*	2012	2 m	NCEI
H12395_MB_2m_MLLW_Combined	Leidos; M/V *Atlantic Surveyor*	2012	2 m	NCEI
H12394_MB_2m_MLLW_Combined	Leidos; M/V *Atlantic Surveyor*	2012	2 m	NCEI
W00383_MB_2m_MLLW_1of1	NOAA Ship *Nancy Foster*	2012	2 m	NCEI
NF-11-05-CSC_Bulls_2m	NOAA Ship *Nancy Foster*	2011	2 m	College of Charleston

Dataset	Data Source and/or Vessel	Year	Native Resolution	Data Provider
D00158_MB_4m_MLLW_1of2	NOAA Ship *Ferdinand Hassler*	2011	4 m	NCEI
F00607_MB_4m_MLLW_Combined	NOAA Ship *Ferdinand Hassler*	2011	4 m	NCEI
H12346_MB_1m_MLLW_Combined	NOAA Ship *Ferdinand Hassler*	2011	1 m	NCEI
H12341_MB_2m_MLLW_Combined	NOAA Ship *Thomas Jefferson*	2011	2 m	NCEI
H12339_MB_1m_MLLW_Combined	Leidos; M/V *Atlantic Surveyor*	2011	1 m	NCEI
H12338_MB_1m_MLLW_Combined	Leidos; M/V *Atlantic Surveyor*	2011	1 m	NCEI
H12337_MB_4m_MLLW_Combined	Leidos; M/V *Atlantic Surveyor*	2011	4 m	NCEI
H12336_MB_4m_MLLW_Combined	Leidos; M/V *Atlantic Surveyor*	2011	4 m	NCEI
H12309_MB_2m_MLLW_Combined	NOAA Ship *Thomas Jefferson*	2011	2 m	NCEI
H12307_MB_2m_MLLW_Combined	NOAA Ship *Thomas Jefferson*	2011	2 m	NCEI
H12306_MB_2m_MLLW_Combined	NOAA Ship *Thomas Jefferson*	2011	2 m	NCEI
H12160_MB_4m_MLLW_Combined	Leidos; M/V *Atlantic Surveyor*	2011	4 m	NCEI
W00419_MB_2m_MLLW_1of1	NOAA Ship *Nancy Foster*	2011	2 m	NCEI
LCE2010_Jacksonville_3m	R/V *Lost Coast Explorer*	2010	3 m	NOAA NCCOS
LCE2010_MiamiNorth_3m	R/V *Lost Coast Explorer*	2010	3 m	NOAA NCCOS
LCE2010_MiamiSouth_3m	R/V *Lost Coast Explorer*	2010	3 m	NOAA NCCOS
NF1015_ARF_EastGraysReef_1m	NOAA Ship *Nancy Foster*	2010	1 m	NCEI
NF1015_ARF_Seamap_N_GraysReef_2_South_0d5m	NOAA Ship *Nancy Foster*	2010	1 m	NCEI
NF1004_GRNMS_TowerOuterEast_1m_interp	NOAA Ship *Nancy Foster*	2010	1 m	NCEI
NF1004_GRNMS_TowerInnerEast_1m_interp	NOAA Ship *Nancy Foster*	2010	1 m	NCEI
NF1004_GRNMS_TowerInnerWest_1m_interp	NOAA Ship *Nancy Foster*	2010	1 m	NCEI
NF1004_GRNMS_TowerOurterWest_1m_interp	NOAA Ship *Nancy Foster*	2010	1 m	NCEI
H12203_MB_4m_MLLW_Combined	NOAA Ship *Thomas Jefferson*	2010	4 m	NCEI
H12202_MB_2m_MLLW_1of1	NOAA Ship *Thomas Jefferson*	2010	2 m	NCEI
H12201_MB_4m_MLLW_combined	NOAA Ship *Thomas Jefferson*	2010	4 m	NCEI
H12200_MB_4m_MLLW_combined	NOAA Ship *Thomas Jefferson*	2010	4 m	NCEI
H12161_MB_1m_MLLW_Combined	Leidos; M/V *Atlantic Surveyor*	2010	1 m	NCEI

Dataset	**Data Source and/or Vessel**	**Year**	**Native Resolution**	**Data Provider**
H12098_MB_4m_MLLW_combined	Leidos; M/V *Atlantic Surveyor*	2010	4 m	NCEI
H12097_MB_2m_MLLW_combined	Leidos; M/V *Atlantic Surveyor*	2010	2 m	NCEI
H12096_MB_1m_MLLW_Combined	Leidos; M/V *Atlantic Surveyor*	2010	1 m	NCEI
H12095_MB_4m_MLLW_combined	Leidos; M/V *Atlantic Surveyor*	2010	4 m	NCEI
H12094_MB_4m_MLLW_Combined	Leidos; M/V *Atlantic Surveyor*	2010	4 m	NCEI
H12093_MB_4m_MLLW_Combined	Leidos; M/V *Atlantic Surveyor*	2010	4 m	NCEI
H12092_MB_4m_MLLW_combined	Leidos; M/V *Atlantic Surveyor*	2010	4 m	NCEI
H12091_MB_1m_MLLW_combined	Leidos; M/V *Atlantic Surveyor*	2010	1 m	NCEI
H12003_MB_4m_MLLW_Combined	Leidos; M/V *Atlantic Surveyor*	2010	4 m	NCEI
H12002_MB_1m_MLLW_Combined	Leidos; M/V *Atlantic Surveyor*	2010	1 m	NCEI
NF0905GRNMS_WestAnchorLedge_1m_Cube	NOAA Ship *Nancy Foster*	2009	1 m	NCEI
NF0905GRNMS_EastAnchorLedge_1m_Cube	NOAA Ship *Nancy Foster*	2009	1 m	NCEI
NF0905GRNMS_EW_Tower_1m_CUBE_Interpolated	NOAA Ship *Nancy Foster*	2009	1 m	NCEI
F00585_MB_2m_MLLW_1of1	NOAA Ship *Thomas Jefferson*	2009	2 m	NCEI
H12099_MB_4m_MLLW_combined	Leidos; M/V *Atlantic Surveyor*	2009	4 m	NCEI
H12037_MB_1m_MLLW_1of1	NOAA Ship *Thomas Jefferson*	2009	1 m	NCEI
H12001_MB_1m_MLLW_Combined	Leidos; M/V *Atlantic Surveyor*	2009	1 m	NCEI
H11899_4m_MLLW_5of5	Ocean Surveys, Inc.; R/V *Abel II*	2009	4 m	NCEI
H11898_MB_4m_MLLW_combined	Ocean Surveys, Inc.; R/V *Abel II*	2009	4 m	NCEI
H11897_2m_MLLW_5of6	Ocean Surveys, Inc.; R/V *Abel II*	2009	2 m	NCEI
H11897_4m_MLLW_6of6	Ocean Surveys, Inc.; R/V *Abel II*	2009	4 m	NCEI
NF-08-16-CSC_docrxn_1m	NOAA Ship *Nancy Foster*	2008	1 m	College of Charleston
H11992_MB_1m_MLLW_1of1	Leidos; M/V *Atlantic Surveyor*	2008	1 m	NCEI
H11874_MB_2m_MLLW_combined	Leidos; M/V *Atlantic Surveyor*	2008	2 m	NCEI
H11873_MB_2m_MLLW_combined	Leidos; M/V *Atlantic Surveyor*	2008	2 m	NCEI
H11872_MB_1m_MLLW_Combined	Leidos; M/V *Atlantic Surveyor*	2008	1 m	NCEI
H11821_2m_MLLW_1of10	NOAA Ship *Thomas Jefferson*	2008	2 m	NCEI
H11821_2m_MLLW_2of10	NOAA Ship *Thomas Jefferson*	2008	2 m	NCEI

Dataset	**Data Source and/or Vessel**	**Year**	**Native Resolution**	**Data Provider**
H11821_2m_MLLW_3of10	NOAA Ship *Thomas Jefferson*	2008	2 m	NCEI
W00394_MB_2m_MLLW_1of1	NOAA Ship *Nancy Foster*	2008	2 m	NCEI
NF0710_OEBox1_5m	NOAA Ship *Nancy Foster*	2007	5 m	College of Charleston
NF0710_OEBox2_5m	NOAA Ship *Nancy Foster*	2007	5 m	College of Charleston
NF0710_OEBox9_5m	NOAA Ship *Nancy Foster*	2007	5 m	College of Charleston
NF0710_OEBox10_5m	NOAA Ship *Nancy Foster*	2007	5 m	College of Charleston
NF0710_OEBox35_5m	NOAA Ship *Nancy Foster*	2007	5 m	College of Charleston
H11650_1m_MLLW_Combined	Leidos; M/V *Atlantic Surveyor*	2007	1 m	NCEI
H11649_1m_MLLW_Combined	Leidos; M/V *Atlantic Surveyor*	2007	1 m	NCEI
H11648_1m_MLLW_Combined	Leidos; M/V *Atlantic Surveyor*	2007	1 m	NCEI
H11647_1m_MLLW_Combined	Leidos; M/V *Atlantic Surveyor*	2007	1 m	NCEI
NF-07-03-CSC_DocRx_2m	NOAA Ship *Nancy Foster*	2007	2 m	College of Charleston
NF-07-03-CSC_Meanders_1m	NOAA Ship *Nancy Foster*	2007	1 m	College of Charleston
H11568_2m_MLLW_Combined	NOAA Ship *Thomas Jefferson*	2006	2 m	NCEI
H11555_1m_MLLW_1of6	Leidos; M/V *Atlantic Surveyor*	2006	1 m	NCEI
H11554_1m_MLLW_1of1	Leidos; M/V *Atlantic Surveyor*	2006	1 m	NCEI
H11303_2m_MLLW_Combined	NOAA Ship *Thomas Jefferson*	2006	2 m	NCEI
South_Atlantic_Bight_2005_Chapman1m	R/V *Cape Fear*	2005	1 m	NOAA NMFS
South_Atlantic_Bight_2005_Georgia2m	R/V *Cape Fear*	2005	2 m	NOAA NMFS
South_Atlantic_Bight_2005_ncMPA2m	R/V *Cape Fear*	2005	2 m	NOAA NMFS
South_Atlantic_Bight_2005_Oculina1m	R/V *Cape Fear*	2005	1 m	NOAA NMFS

Dataset	**Data Source and/or Vessel**	**Year**	**Native Resolution**	**Data Provider**
H11302_2m_MLLW_Combined	NOAA Ship *Thomas Jefferson*	2003	2 m	NCEI
H11301_MB_1m_MLLW_1of1	NOAA Ship *Thomas Jefferson*	2005	1 m	NCEI
OculinaNorth5m	Harbor Branch Oceanographic Institute; M/V *Liberty Star*	2002	5 m	NCEI
OculinaSouth5m	Harbor Branch Oceanographic Institute; M/V *Liberty Star*	2002	5 m	NCEI
EX1805_MB_FNL_Area6-10m_WGS84-interp	NOAA Ship *Okeanos Explorer*	2018	10 m	NCEI
EX1804_MB_FNL_10m_EastFlorida_WGS84	NOAA Ship *Okeanos Explorer*	2018	10 m	NCEI
NF-17-08_Leg2_South_10m_NAD83_UTM17N	NOAA Ship *Nancy Foster*	2017	10 m	NCEI
RB1008_Bathy_10m	NOAA Ship *Ronald H. Brown*	2010	10 m	NCEI
NF-09-13-DSC_Bathy_10m	NOAA Ship *Nancy Foster*	2009	10 m	NOAA NCCOS
W00232_MB_8m_MLLW_Combined	NOAA Ship *Nancy Foster*	2009	8 m	NCEI
W00397_MB_8m_MLLW_Combined	NOAA Ship *Nancy Foster*	2008	8 m	NCEI
NF0709-GRNMS_North_10m	NOAA Ship *Nancy Foster*	2007	10 m	NCEI
NF0709-GRNMS_South_10m	NOAA Ship *Nancy Foster*	2007	10 m	NCEI
NF0709-GRNMS_RegA_10m	NOAA Ship *Nancy Foster*	2007	10 m	NCEI
NF0709-GRNMS_RegB_10m	NOAA Ship *Nancy Foster*	2007	10 m	NCEI
EX1904_MB_FNL_VAtoNY_20m_WGS84	NOAA Ship *Okeanos Explorer*	2019	20 m	NCEI
EX1805_MB_FNL_Area1_20m_WGS84	NOAA Ship *Okeanos Explorer*	2018	20 m	NCEI
EX1805_MB_FNL_Area4_15m_WGS84_interpolated	NOAA Ship *Okeanos Explorer*	2018	15 m	NCEI
EX1805_MB_FNL_Area5-15m_WGS84_interpolated	NOAA Ship *Okeanos Explorer*	2018	15 m	NCEI
F00693_MB_VR_MLLW	NOAA Ship *Thomas Jefferson*	2017	Variable	NCEI
W00406_MB_16m_MLLW_Combined_NAD83_UTM17N	NOAA Ship *Nancy Foster*	2015	16 m	NCEI
W00424_MB_16m_MLLW_Combined	NOAA Ship *Nancy Foster*	2011	16 m	NCEI
EX1907_MB_FNL_North_25m_WGS84	NOAA Ship *Okeanos Explorer*	2019	25 m	NCEI
EX1907_MB_FNL_South_25m_WGS84	NOAA Ship *Okeanos Explorer*	2019	25 m	NCEI
EX1906_MB_FNL_North_25m_WGS84	NOAA Ship *Okeanos Explorer*	2019	25 m	NCEI
EX1906_MB_FNL_South_30m_WGS84	NOAA Ship *Okeanos Explorer*	2019	30 m	NCEI
EX1903L2_MB_FNL_North_25m_WGS84	NOAA Ship *Okeanos Explorer*	2019	25 m	NCEI

Dataset	Data Source and/or Vessel	Year	Native Resolution	Data Provider
EX1903L2_MB_FNL_South_25m_WGS84	NOAA Ship *Okeanos Explorer*	2019	25 m	NCEI
EX1903L1_MB_FNL_BlakePlateau_25m_WGS84	NOAA Ship *Okeanos Explorer*	2019	25 m	NCEI
EX1903L1_MB_FNL_KeyWestTransit_25m_WGS84	NOAA Ship *Okeanos Explorer*	2019	25 m	NCEI
EX1902_MB_FNL_25m_WGS84	NOAA Ship *Okeanos Explorer*	2019	25 m	NCEI
RB1903EM122_25mCube	NOAA Ship *Ronald H. Brown*	2019	25 m	USGS
AT41_25mEdits	R/V *Atlantis*	2018	25 m	USGS
EX1812_MB_FNL_30m_ASPIRE_Prioirty1_WGS84	NOAA Ship *Okeanos Explorer*	2018	30 m	NCEI
EX1806_MB_FNL_South_Shallow_30m_WGS84	NOAA Ship *Okeanos Explorer*	2018	30 m	NCEI
EX1805_MB_FNL_Area2_30m_WGS84	NOAA Ship *Okeanos Explorer*	2018	30 m	NCEI
EX1804_MB_FNL_30m_SouthFlorida_WGS84	NOAA Ship *Okeanos Explorer*	2018	30 m	NCEI
EX1710_MB_FNL_30m_Florida_WGS84	NOAA Ship *Okeanos Explorer*	2017	30 m	NCEI
EX1404L2_MB_FNL_25m_WGS84	NOAA Ship *Okeanos Explorer*	2014	25 m	NCEI
EX1403_MB_FNL_Stetson_Mesa_30m_WGS84	NOAA Ship *Okeanos Explorer*	2014	30 m	NCEI
EX1205L1_MB_FNL_HatterasTransverseCanyon_30m_WGS84	NOAA Ship *Okeanos Explorer*	2012	30 m	NCEI
EX1205L1_MB_FNL_CapeFearDiapir_BlakeRidgeDiapir_30m_WGS84	NOAA Ship *Okeanos Explorer*	2012	30 m	NCEI
EX1205L1_MB_FNL_800M_ISOBATH_30m_WGS84	NOAA Ship *Okeanos Explorer*	2012	30 m	NCEI
EX1203_FloridaEastCoast_MultibeamBathymetry_30m_WGS84	NOAA Ship *Okeanos Explorer*	2012	30 m	NCEI
EX1106_MB_FNL_SWilm_Balt_Canyons_25m_WGS84	NOAA Ship *Okeanos Explorer*	2011	25 m	NCEI
EX1106_MB_FNL_PamlicoCanyon_25m_WGS84	NOAA Ship *Okeanos Explorer*	2011	25 m	NCEI
EX1106_MB_FNL_KellerCanyon_25m_WGS84	NOAA Ship *Okeanos Explorer*	2011	25 m	NCEI
NF-11-04-NC_All_25m	NOAA Ship *Nancy Foster*	2011	25 m	University of North Carolina Wilmington
H11680_30m_MLLW_Combined	NOAA Ship *Thomas Jefferson*	2007	30 m	NCEI
South_Atlantic_Bight_2006_DeepCoralBump_30mBathy	NOAA Ship *Nancy Foster*	2006	30 m	NOAA NCCOS
PAT0503_DeepCoralWest1_Bathy30m	US Navy Ship *Pathfinder*	2003	30 m	NOAA NCCOS
PAT0503_DeepCoralNortheast1_Bathy30m	US Navy Ship *Pathfinder*	2003	30 m	NOAA NCCOS

Dataset	**Data Source and/or Vessel**	**Year**	**Native Resolution**	**Data Provider**
PAT0503_DeepCoralNortheast2_Bathy30m	US Navy Ship *Pathfinder*	2003	30 m	NOAA NCCOS
H11071A_DeepCoral_Bathy_30m	NOAA Ship *Thomas Jefferson*	2003	30 m	NCEI
EW9702_NWDeepCoral_30m	US Navy; R/V *Maurice Ewing*	1997	30 m	NOAA NCCOS
EW9702_NEDeepCoral_30m	US Navy; R/V *Maurice Ewing*	1997	30 m	NOAA NCCOS
EX1805_MB_FNL_Area3_35m_WGS84	NOAA Ship *Okeanos Explorer*	2018	35 m	NCEI
H12977_MB_VR_MLLW	NOAA Ship *Ferdinand Hassler*	2017	Variable	NCEI
KR-OER19-01_Area1A_50m	M/V Fugro Brasilis	2019	50 m	NCEI
KR-OER19-01_Area1B_50m	M/V Fugro Brasilis	2019	50 m	NCEI
EX1812_MB_FNL_50m_PostBahamasTransit_WGS84	NOAA Ship *Okeanos Explorer*	2018	50 m	NCEI
EX1806_MB_FNL_North_50m_WGS84	NOAA Ship *Okeanos Explorer*	2018	50 m	NCEI
EX1806_MB_FNL_South_Deep_50m_WGS84	NOAA Ship *Okeanos Explorer*	2018	50 m	NCEI
EX1803_MB_FNL_50m_EasternGoMex_WGS84	NOAA Ship *Okeanos Explorer*	2018	50 m	NCEI
H13095_MB_VR_MLLW	NOAA Ship *Ferdinand Hassler*	2018	Variable	NCEI
H13094_MB_VR_MLLW	NOAA Ship *Ferdinand Hassler*	2018	Variable	NCEI
EX1711_MB_FNL_50m_Florida_WGS84	NOAA Ship *Okeanos Explorer*	2017	50 m	NCEI
F00695_MB_VR_MLLW_1of1	NOAA Ship *Ferdinand Hassler*	2017	Variable	NCEI
H12984_MB_VR_MLLW	NOAA Ship *Ferdinand Hassler*	2017	Variable	NCEI
EX1404L3_MB_FNL_West_50m_WGS84	NOAA Ship *Okeanos Explorer*	2014	50 m	NCEI
EX1403_MB_FNL01_50m_WGS84	NOAA Ship *Okeanos Explorer*	2014	50 m	NCEI
EX1403_MB_FNL03_50m_WGS84	NOAA Ship *Okeanos Explorer*	2014	50 m	NCEI
EX1402L1_MB_FNL_01_50m_WGS84	NOAA Ship *Okeanos Explorer*	2014	50 m	NCEI
EX1402L1_MB_FNL_02_50m_WGS84	NOAA Ship *Okeanos Explorer*	2014	50 m	NCEI
EX1402L1_MB_FNL_03_50m_WGS84	NOAA Ship *Okeanos Explorer*	2014	50 m	NCEI
EX1302_MB_FNL_01_50m_WGS84	NOAA Ship *Okeanos Explorer*	2013	50 m	NCEI
EX1302_MB_FNL_02_50m_WGS84	NOAA Ship *Okeanos Explorer*	2013	50 m	NCEI
EX1206_MB_FNL_MidAtlantic_Survey_50m_WGS84	NOAA Ship *Okeanos Explorer*	2012	50 m	NCEI
EX1205L1_MB_FNL_ALL_50m_WGS84	NOAA Ship *Okeanos Explorer*	2012	50 m	NCEI

Dataset	**Data Source and/or Vessel**	**Year**	**Native Resolution**	**Data Provider**
EX1204_MB_FNL_01_50m_WGS84	NOAA Ship *Okeanos Explorer*	2012	50 m	NCEI
EX1201_MB_FNL_50m_WGS84	NOAA Ship *Okeanos Explorer*	2012	50 m	NCEI
EX1106_MB_FNL_03_50m_WGS84	NOAA Ship *Okeanos Explorer*	2011	50 m	NCEI
EX1106_MB_FNL_04_50m_WGS84	NOAA Ship *Okeanos Explorer*	2011	50 m	NCEI
EX1106_MB_FNL_05_50m_WGS84	NOAA Ship *Okeanos Explorer*	2011	50 m	NCEI
EX1106_MB_FNL_06_50m_WGS84	NOAA Ship *Okeanos Explorer*	2011	50 m	NCEI
EX1106_MB_FNL_07_50m_WGS84	NOAA Ship *Okeanos Explorer*	2011	50 m	NCEI
EX1104_MB_FNL_04_50m_WGS84	NOAA Ship *Okeanos Explorer*	2011	50 m	NCEI
PAT0503_DeepCoralWest2_Bathy50m	US Navy Ship *Pathfinder*	2003	50 m	NOAA NCCOS
H11174_Whiting_2002_50m	NOAA Ship *Whiting*	2002	50 m	College of Charleston
H11071_DeepCoral_Bathy_50m	NOAA Ship *Whiting*	2001	50 m	NCEI
H10947_DeepCoral_Bathy_50m	NOAA Ship *Whiting*	2000	50 m	NCEI
F00716_MB_VR_MLLW	NOAA Ship *Ferdinand Hassler*	2018	Variable	NCEI
MGL1407_100m_bathy	R/V *Marcus Langseth*	2014	100 m	NCEI
EX1202L1_Geo_OverAll_100m	NOAA Ship *Okeanos Explorer*	2012	100 m	NCEI
EX1105_Overall_100m_WGS84	NOAA Ship *Okeanos Explorer*	2012	100 m	NCEI
AMBath100m_V2	Various	2016	100 m	USGS
EX1203_Overview_MultibeamBathymetry_200m_WGS84	NOAA Ship *Okeanos Explorer*	2012	200 m	NCEI
Cape_Hatteras_DEM_2006_thirdarcsec_MHW_WGS84	NCEI	2006	1/3 arcsec	NCEI
Myrtle_Beach_DEM_2006_thirdarcsec_MHW_WGS84	NCEI	2006	1/3 arcsec	NCEI
Savannah_DEM_2006_thirdarcsec_MHW_WGS84	NCEI	2006	1/3 arcsec	NCEI
Central_Florida_DEM_2014_thirdarcsec_NAVD88_WGS84	NCEI	2014	1/3 arcsec	NCEI
Palm_Beach_DEM_2010_thirdarcsec_NAVD88_WGS84	NCEI	2010	1/3 arcsec	NCEI
Miami_DEM_2014_thirdarcsec_WGS84	NCEI	2014	1/3 arcsec	NCEI
Key_West_DEM_2011_thirdarcsec_NAVD88_WGS84	NCEI	2011	1/3 arcsec	NCEI
Southern_Florida_F010_DEM_2018_thirdarcsec_MLLW_WGS84	NCEI	2018	1/3 arcsec	NCEI
NOAA_CRM_Southeast_Atlantic_3arcsec_WGS84	NCEI	1998	3 arcsec	NCEI
NOAA_CRM_Florida_and_East_Gulf_of_Mexico_3arcsec_WGS84	NCEI	2001	3 arcsec	NCEI

Dataset	Data Source and/or Vessel	Year	Native Resolution	Data Provider
GEBCO_2019	GEBCO	2019	15 arcsec	GEBCO

Appendix C: Maps of the Environmental Predictors

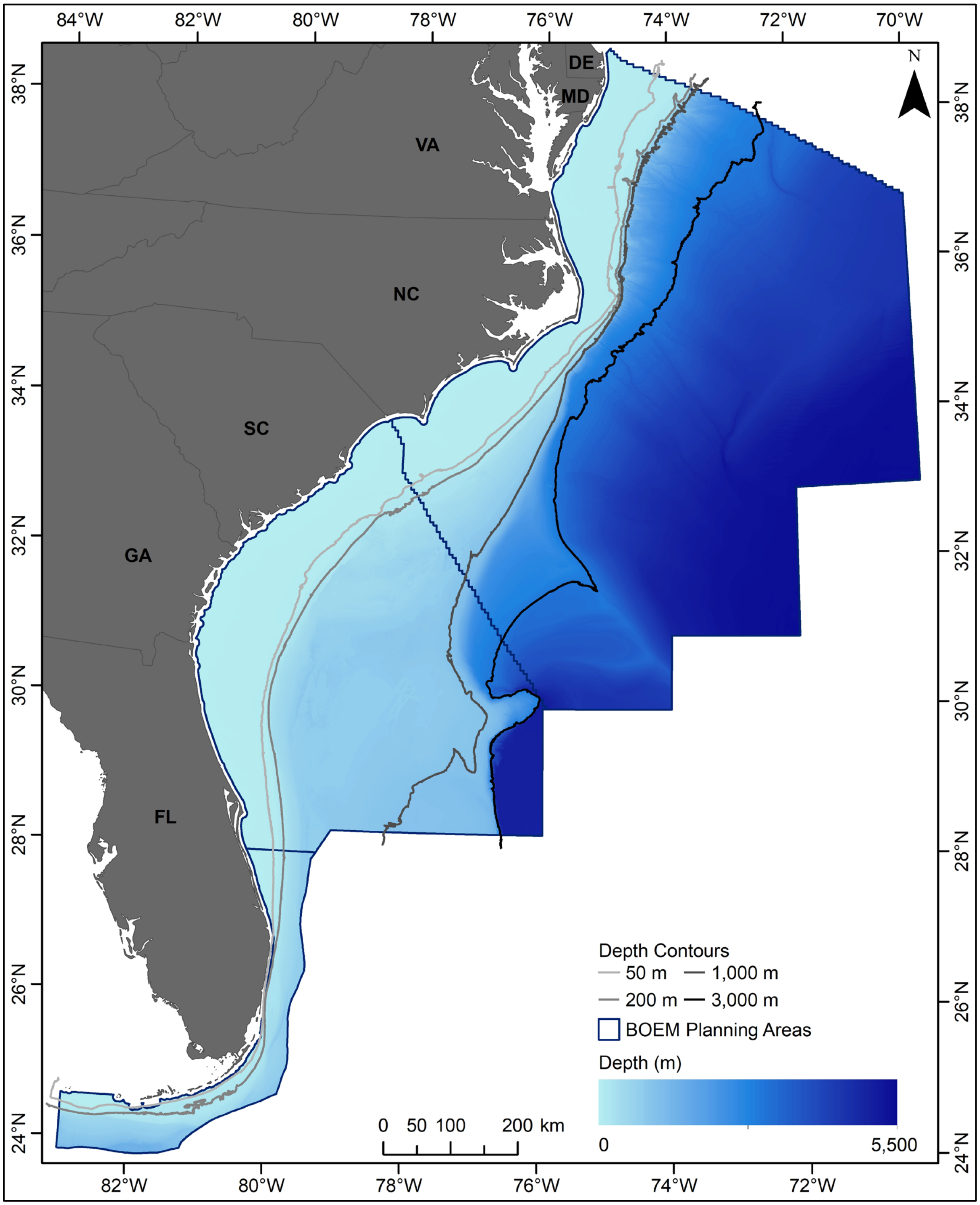

Figure C-1. Depth of the seafloor, 100 x 100 m resolution.

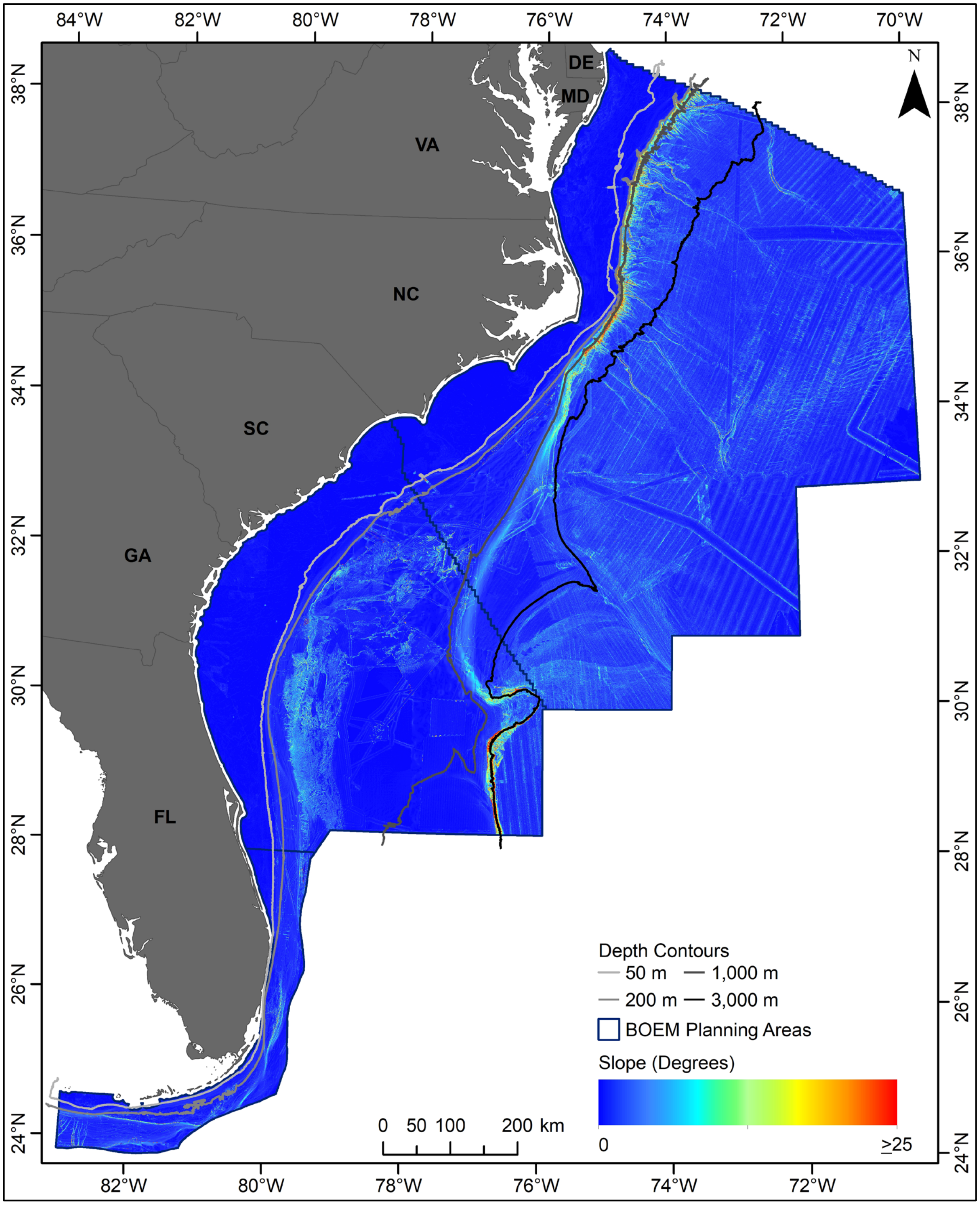

Figure C-2. Slope of the seafloor, 100 x 100 m resolution.

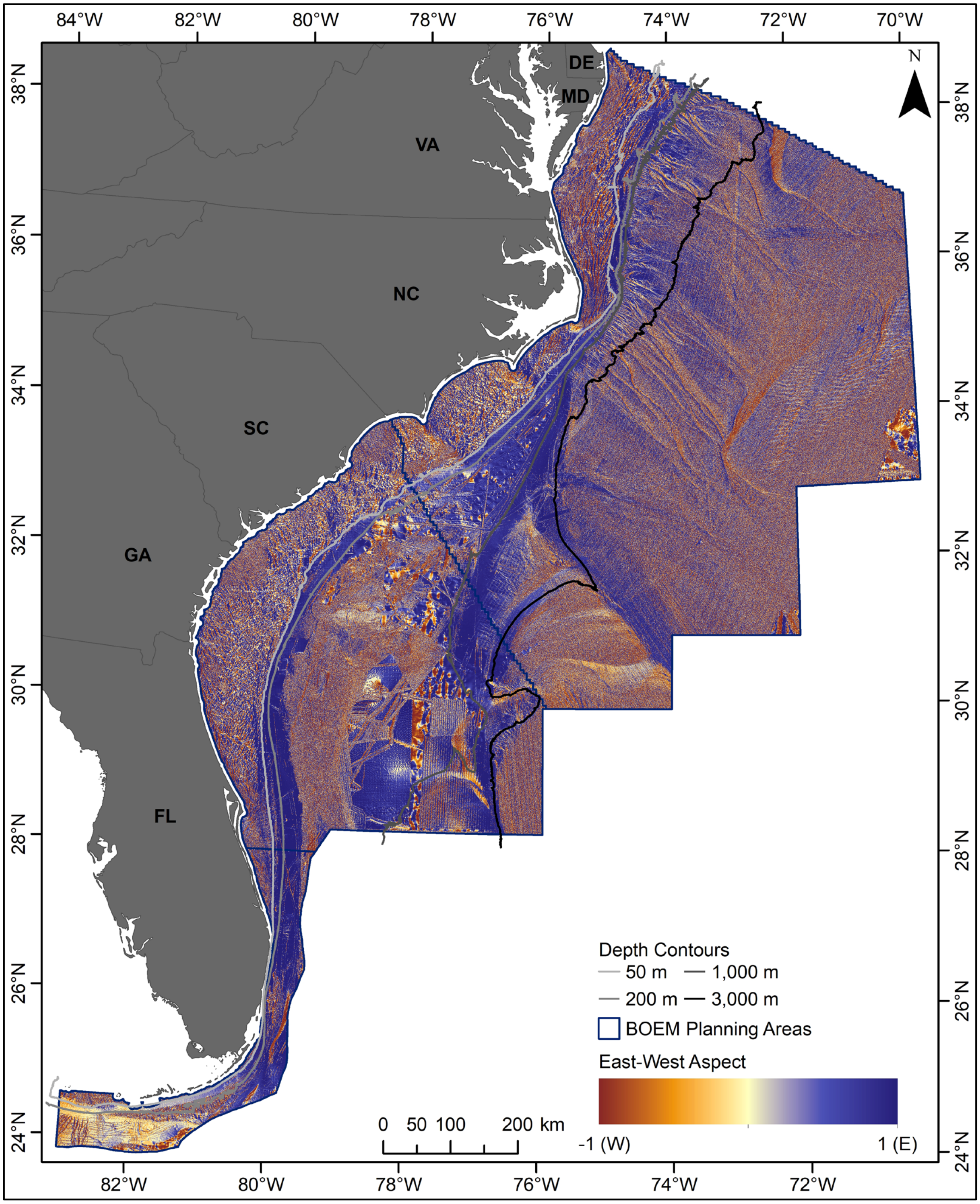

Figure C-3. East-west aspect (sine of seafloor slope direction), 100 x 100 m resolution.

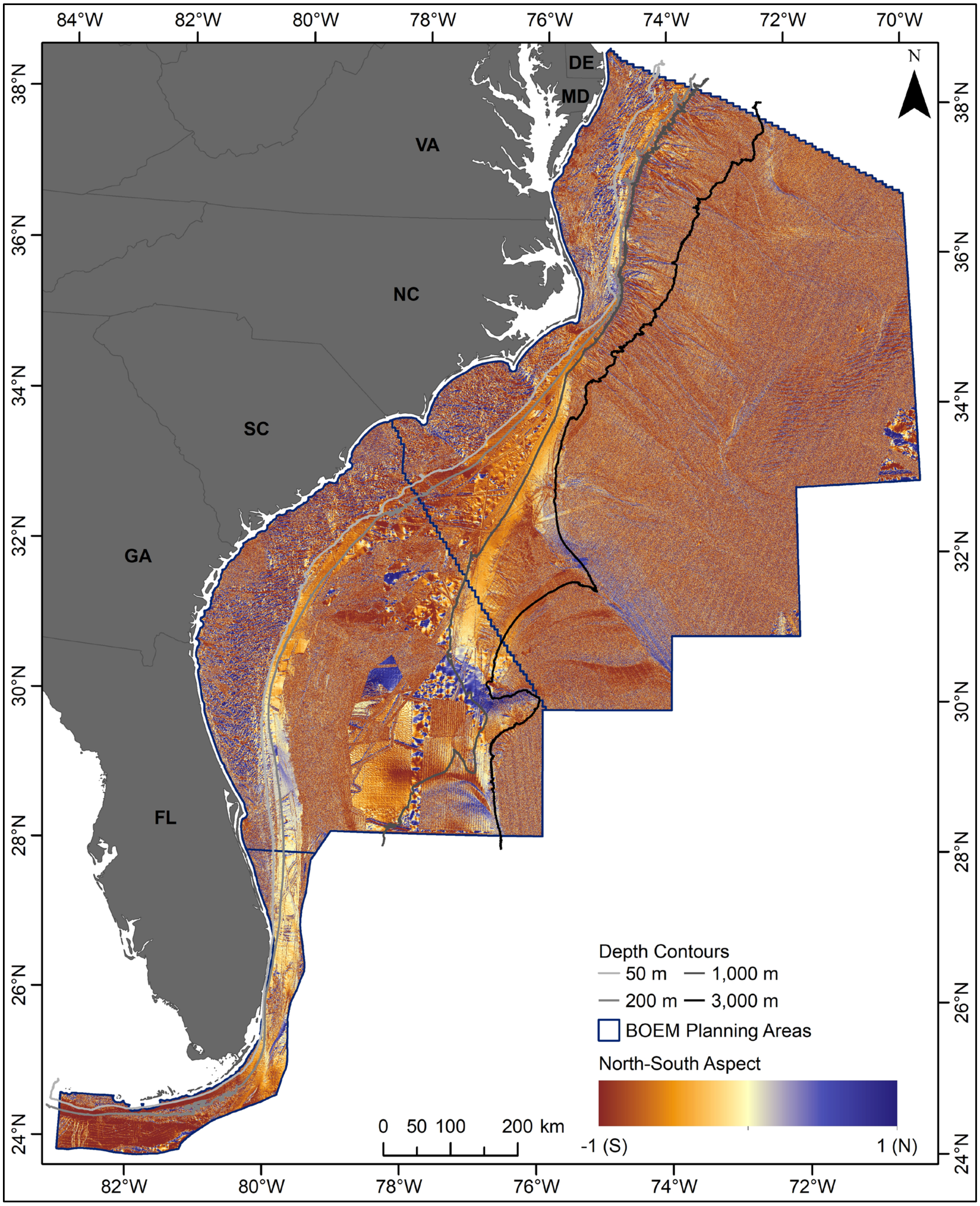

Figure C-4. North-south aspect (cosine of seafloor slope direction), 100 x 100 m resolution.

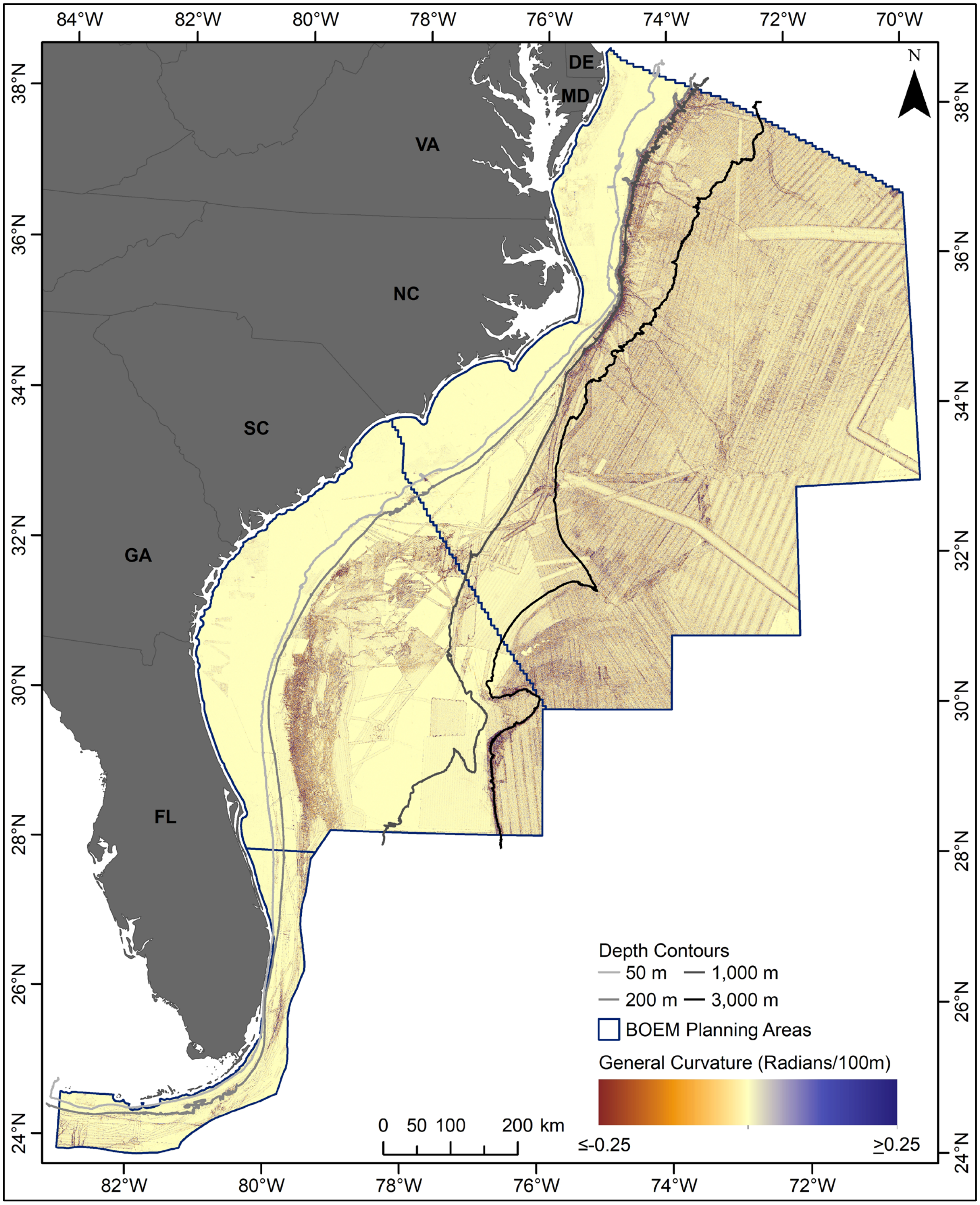

Figure C-5. General curvature of the seafloor, 100 x 100 m resolution.

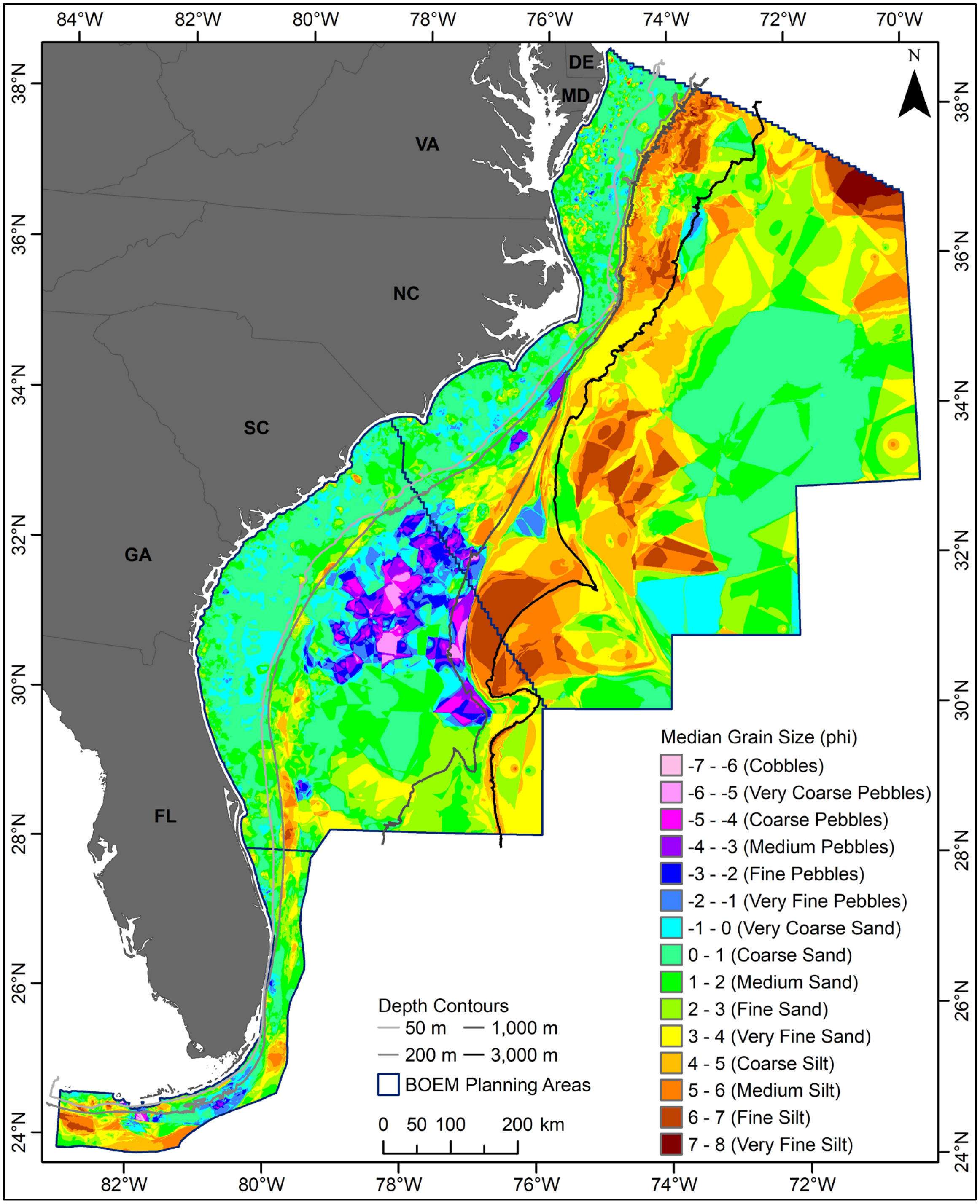

Figure C-6. Surficial sediment median grain size, 100 x 100 m resolution.

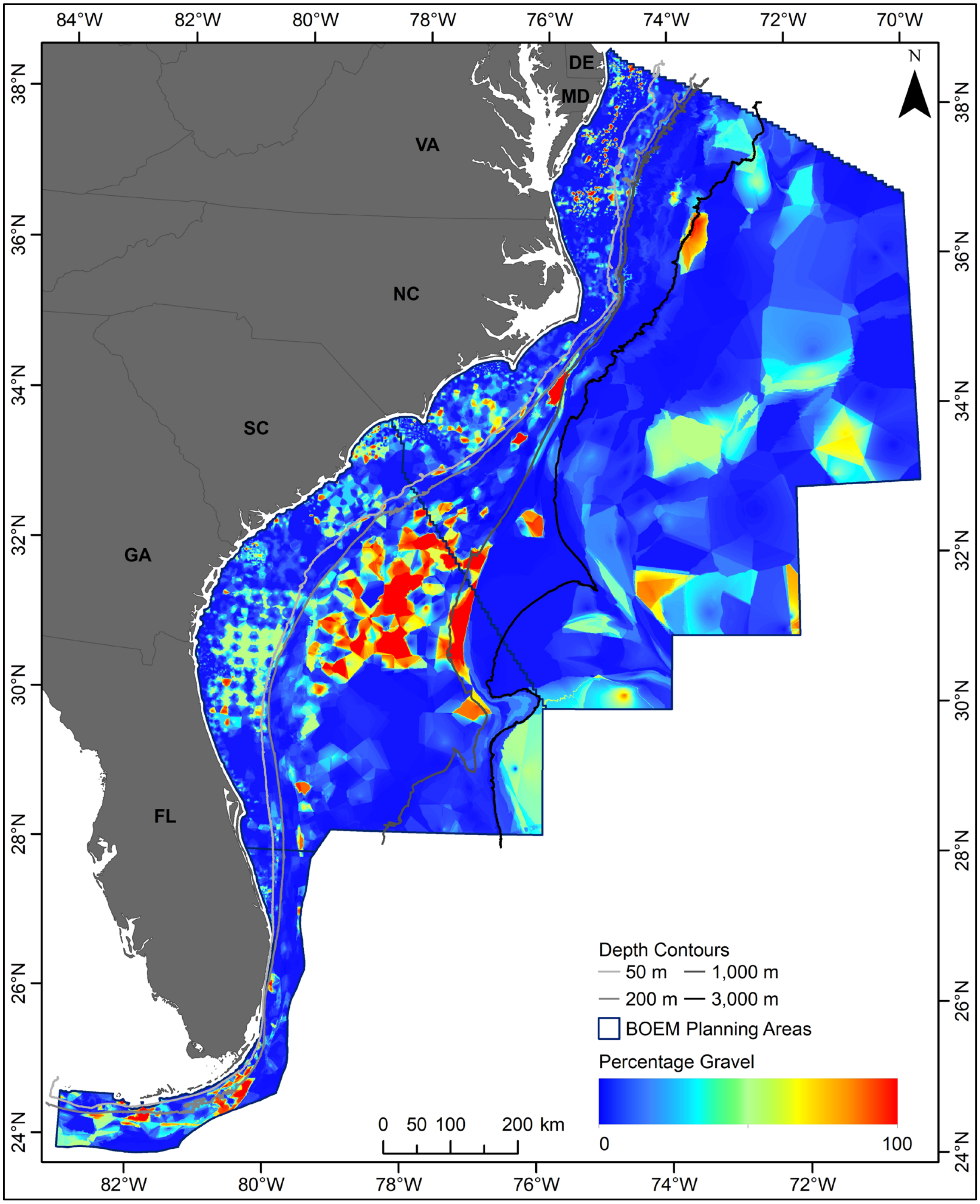

Figure C-7. Surficial sediment percentage gravel, 100 x 100 m resolution.

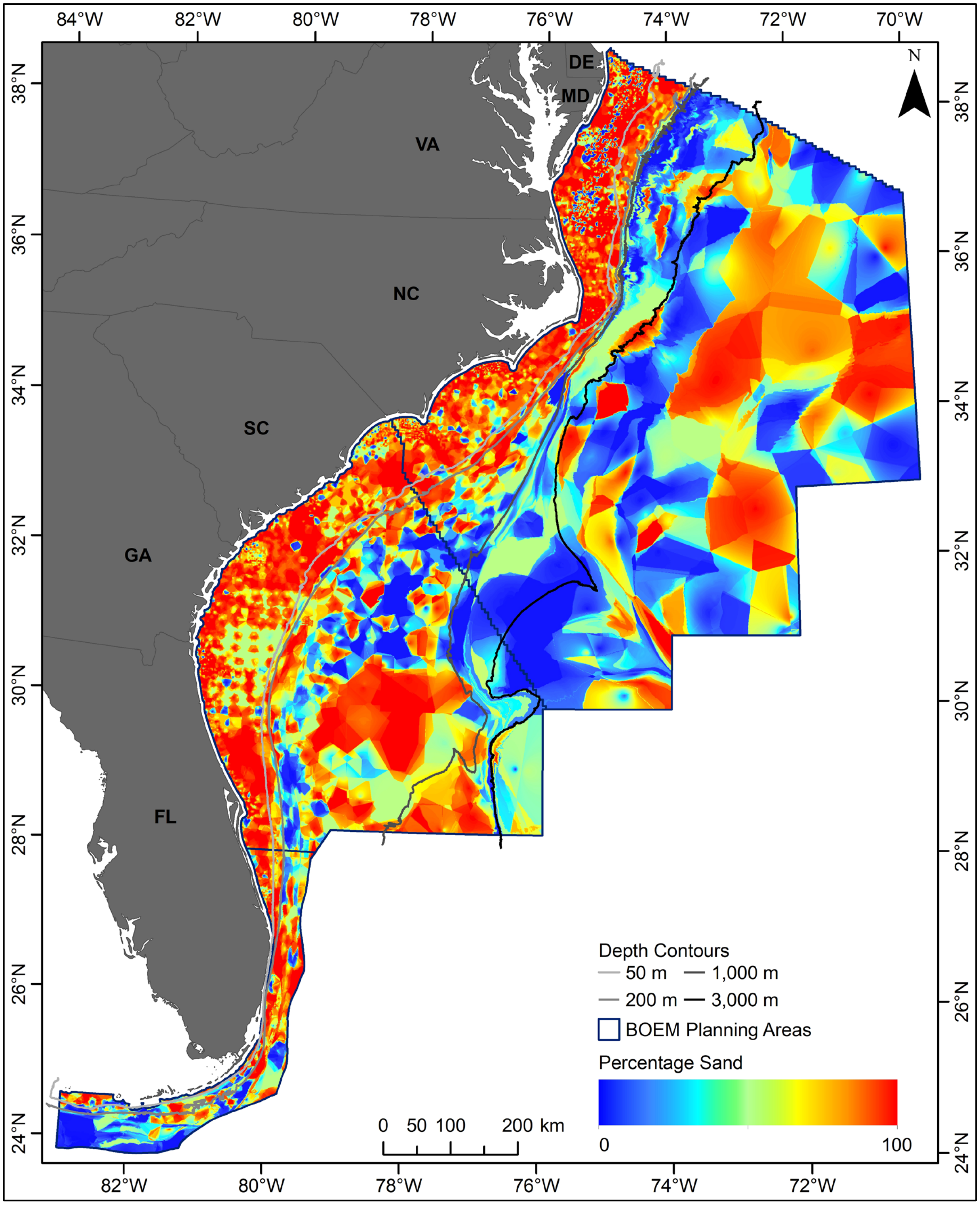

Figure C-8. Surficial sediment percentage sand, 100 x 100 m resolution.

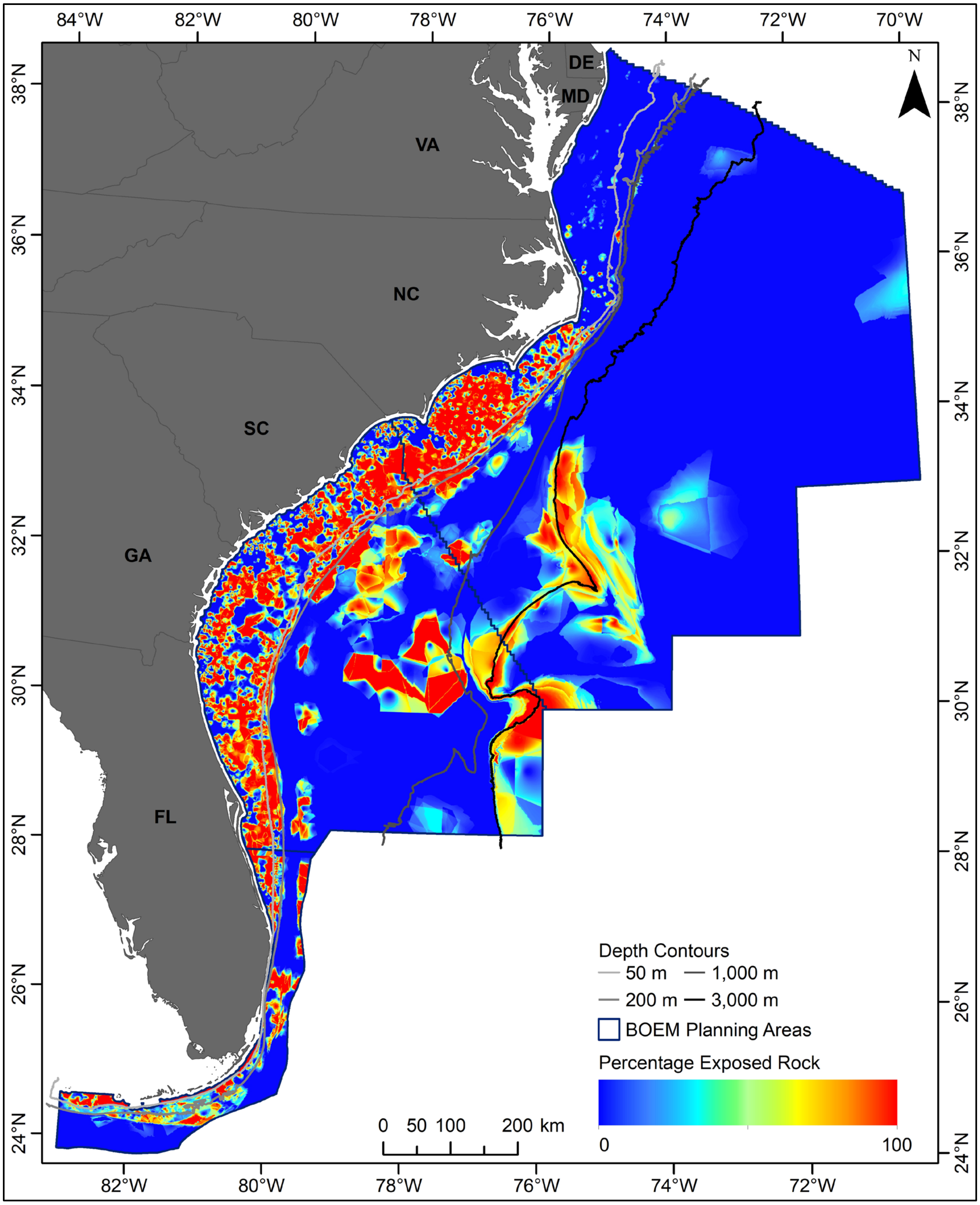

Figure C-9. Percentage of exposed rock on the seafloor, 100 x 100 m resolution.

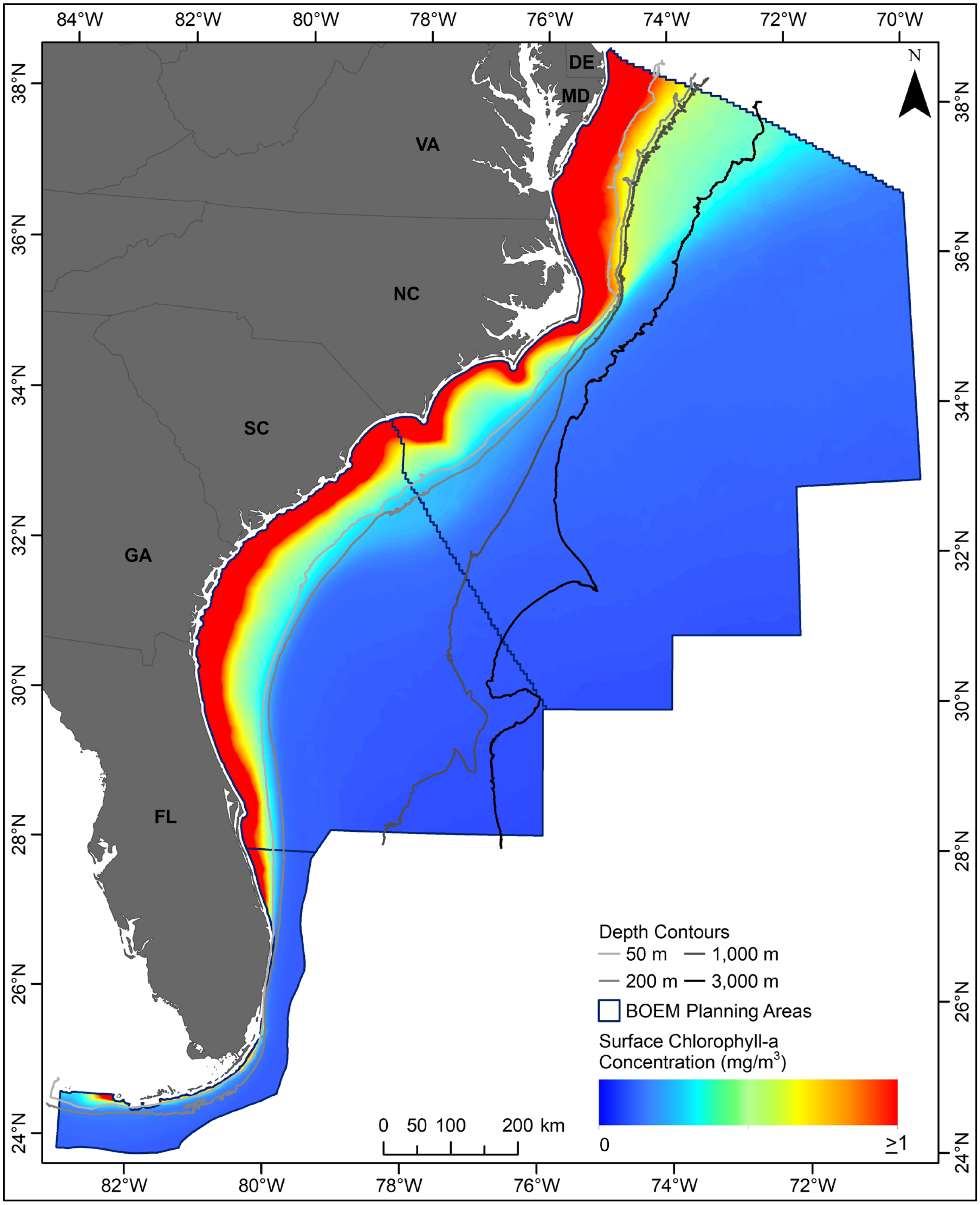

Figure C-10. Annual mean surface chlorophyll-a concentration, 100 x 100 m resolution.

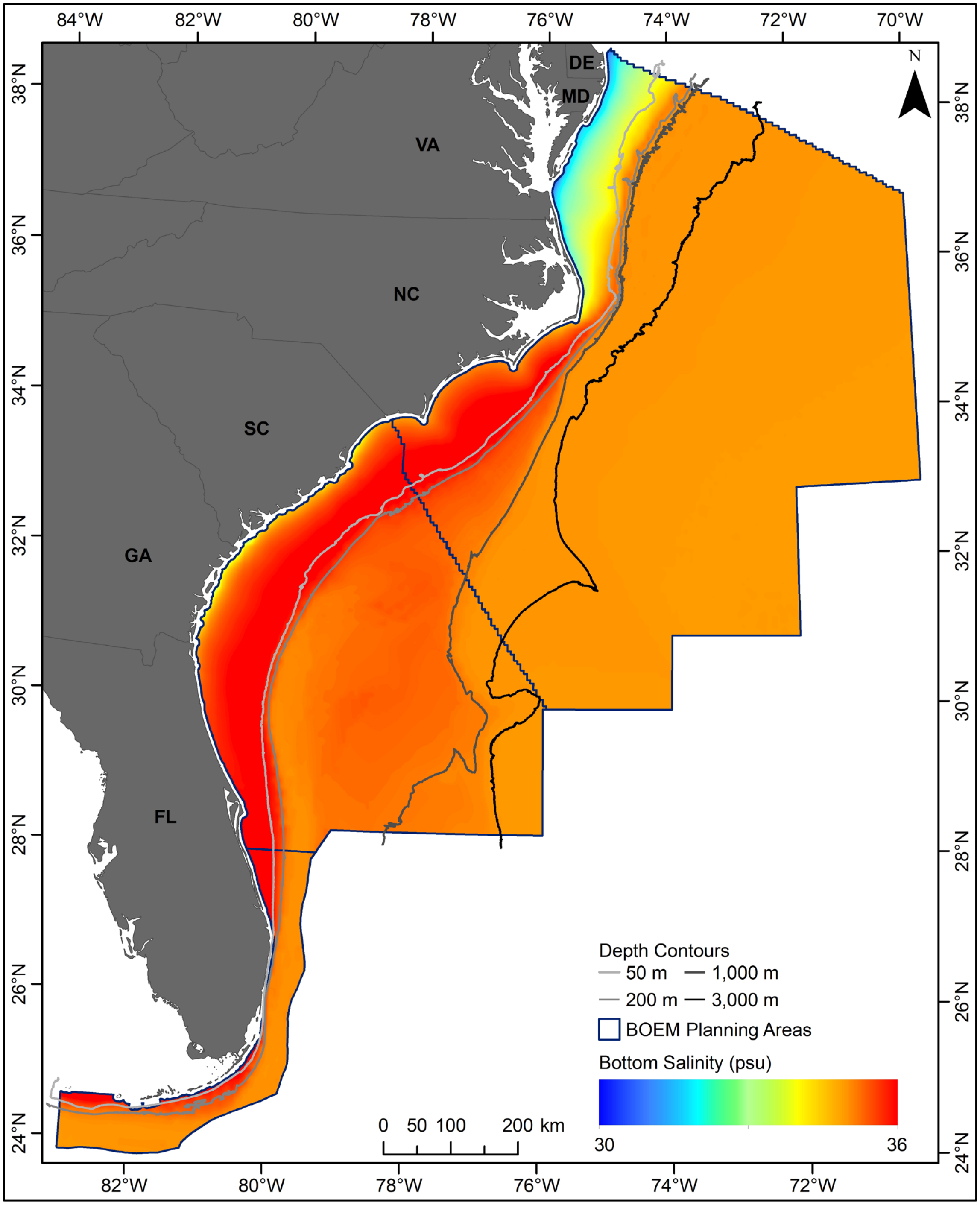

Figure C-11. Annual mean bottom salinity, 100 x 100 m resolution.

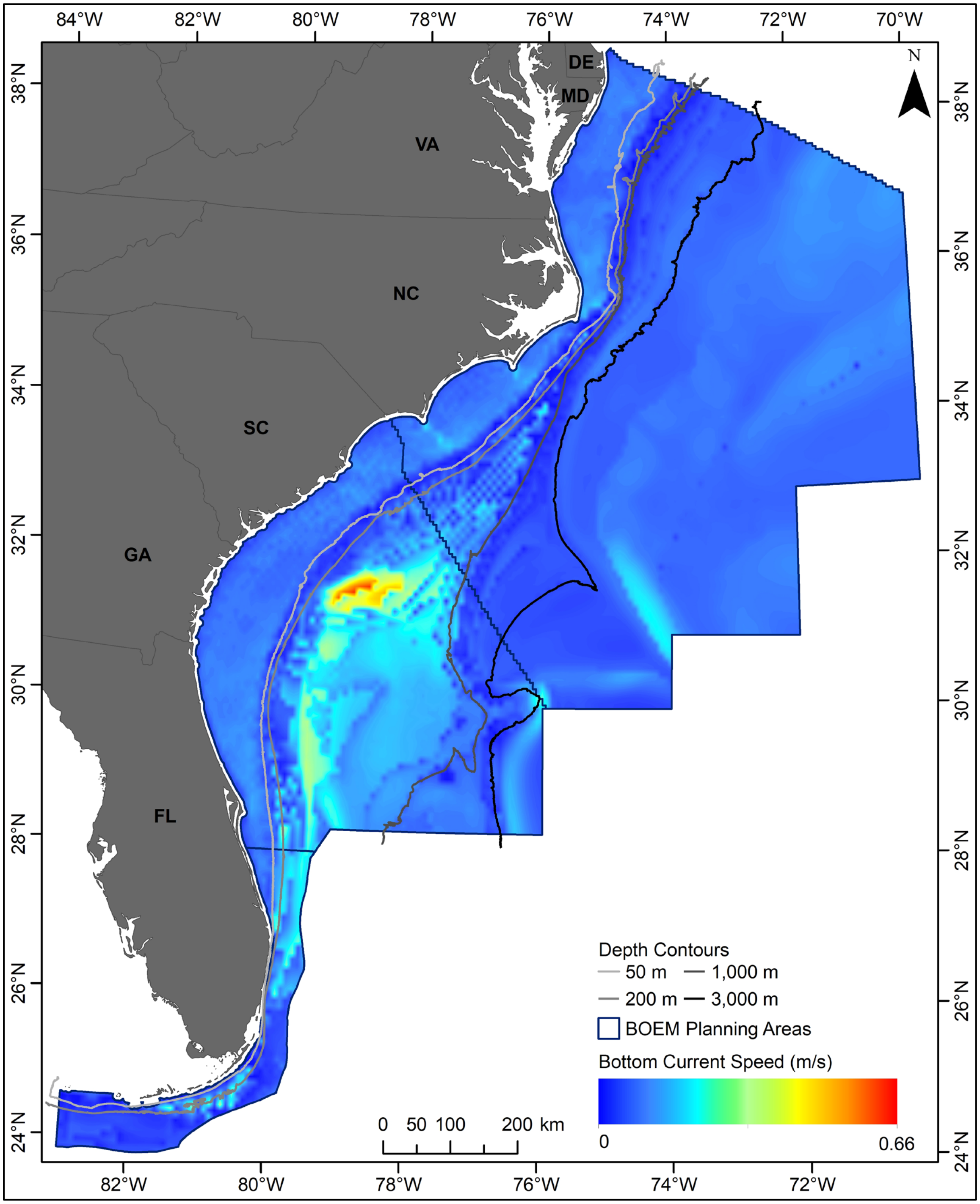

Figure C-12. Annual mean bottom current speed, 100 x 100 m resolution.

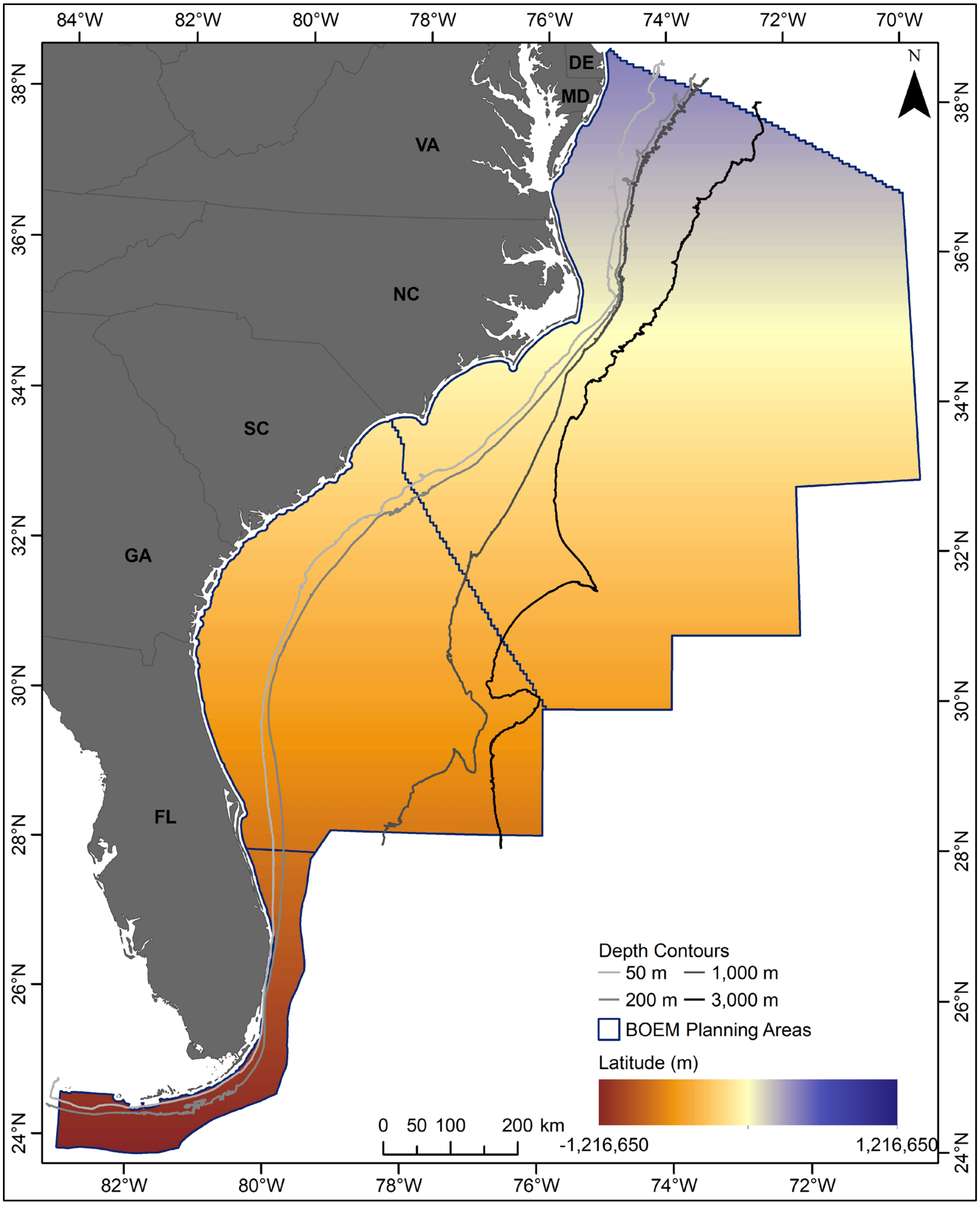

Figure C-13. Latitude (projected), 100 x 100 m resolution.

Appendix D: Maps of the Observed and Predicted Spatial Distributions for Each Deep-sea Coral Taxon

This appendix includes the set of maps produced for each DSC taxon. Values of the median occupancy probability are referred to as very high (0.8–1), high (0.6–0.8), medium (0.4–0.6), low (0.2–0.4), and very low (0–0.2) predicted occurrence for the purpose of facilitating descriptions of the spatial patterns observed. Similarly, values of the CV of occupancy probability are referred to as very high (>25), high (10–25), medium (5–10), low (2–5), and very low (0–2).

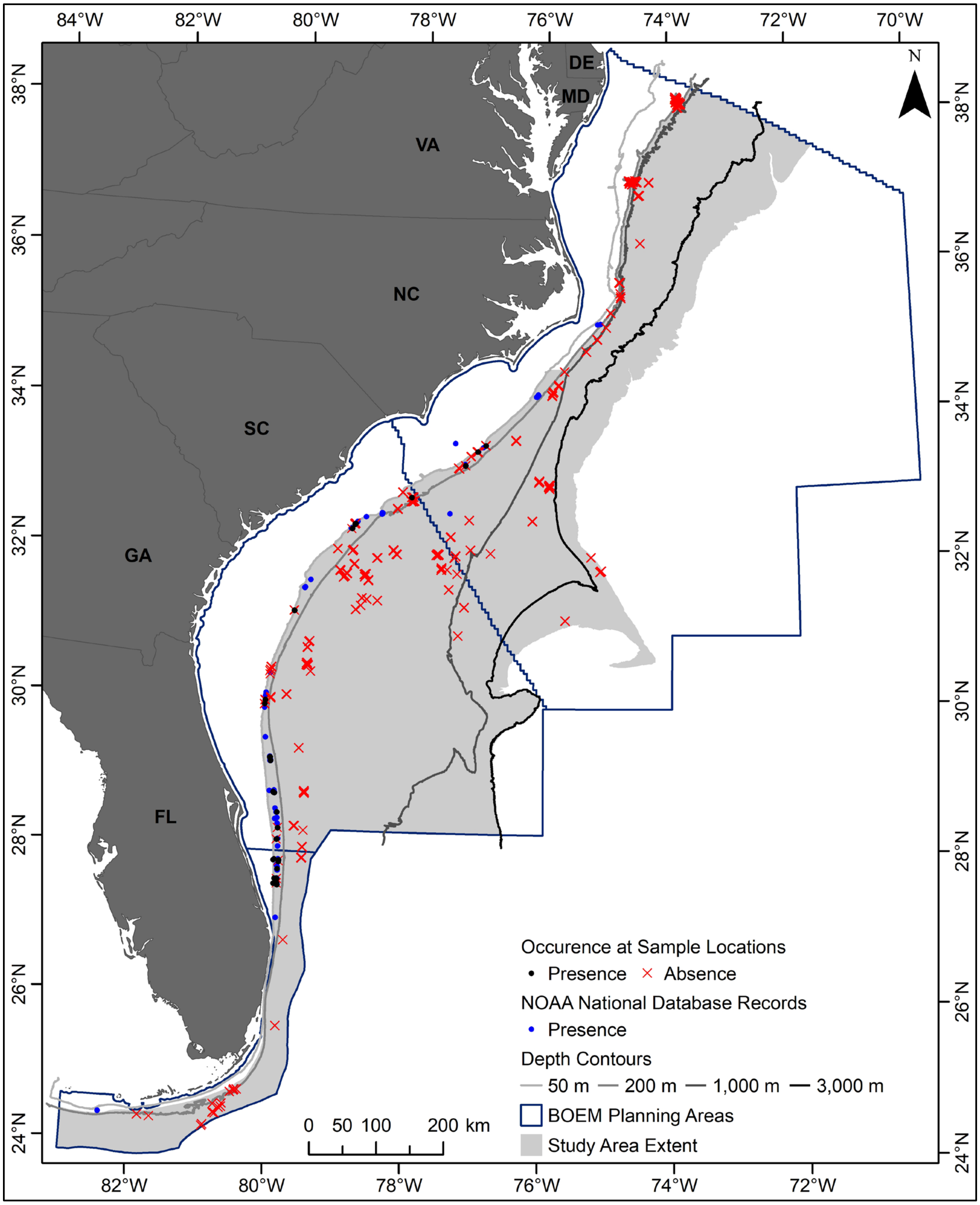

Figure D-1. Occurrence records for the stony coral *Oculina*.
This map shows the observed occurrence (presence-absence) of *Oculina* at sample locations in the presence-absence database compiled for this study. Additional records of occurrence (presence) from the NOAA National Database are also displayed.

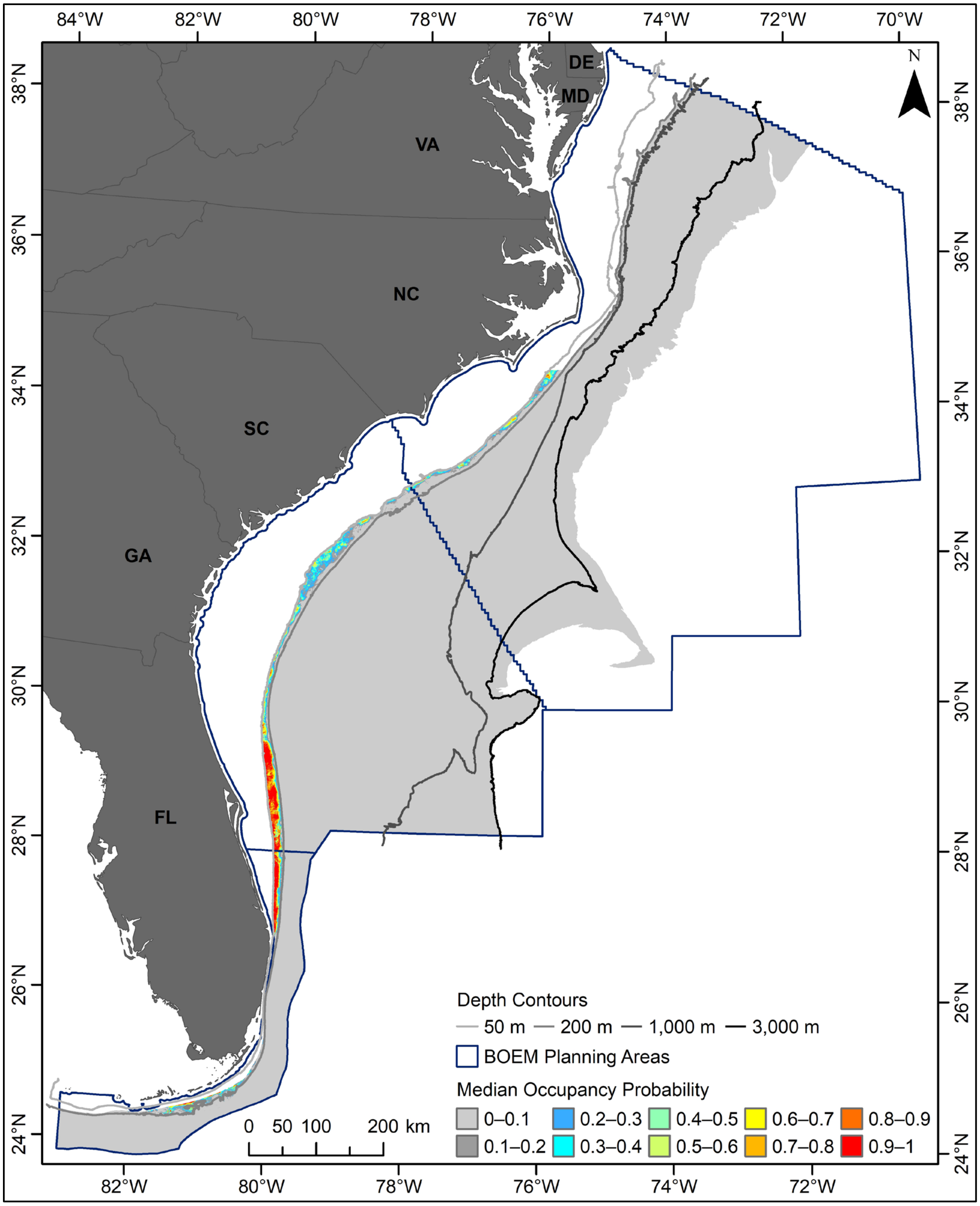

Figure D-2. Predicted occurrence of the stony coral *Oculina*.
This map shows the posterior median occupancy probability for *Oculina* from the multi-taxon model.

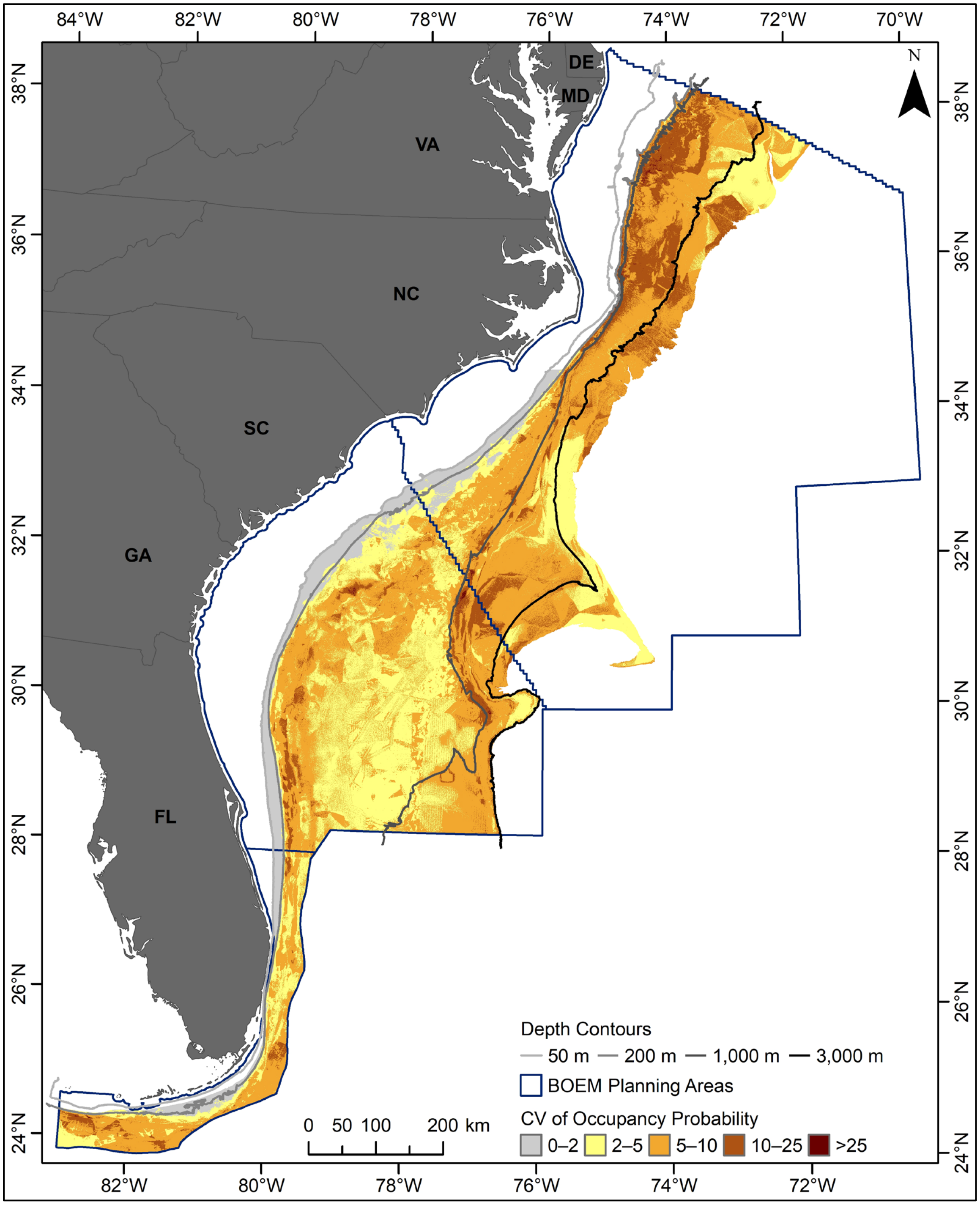

Figure D-3. Variability in the predicted occurrence of the stony coral *Oculina*.
This map shows the posterior coefficient of variation of occupancy probability for *Oculina* from the multi-taxon model.

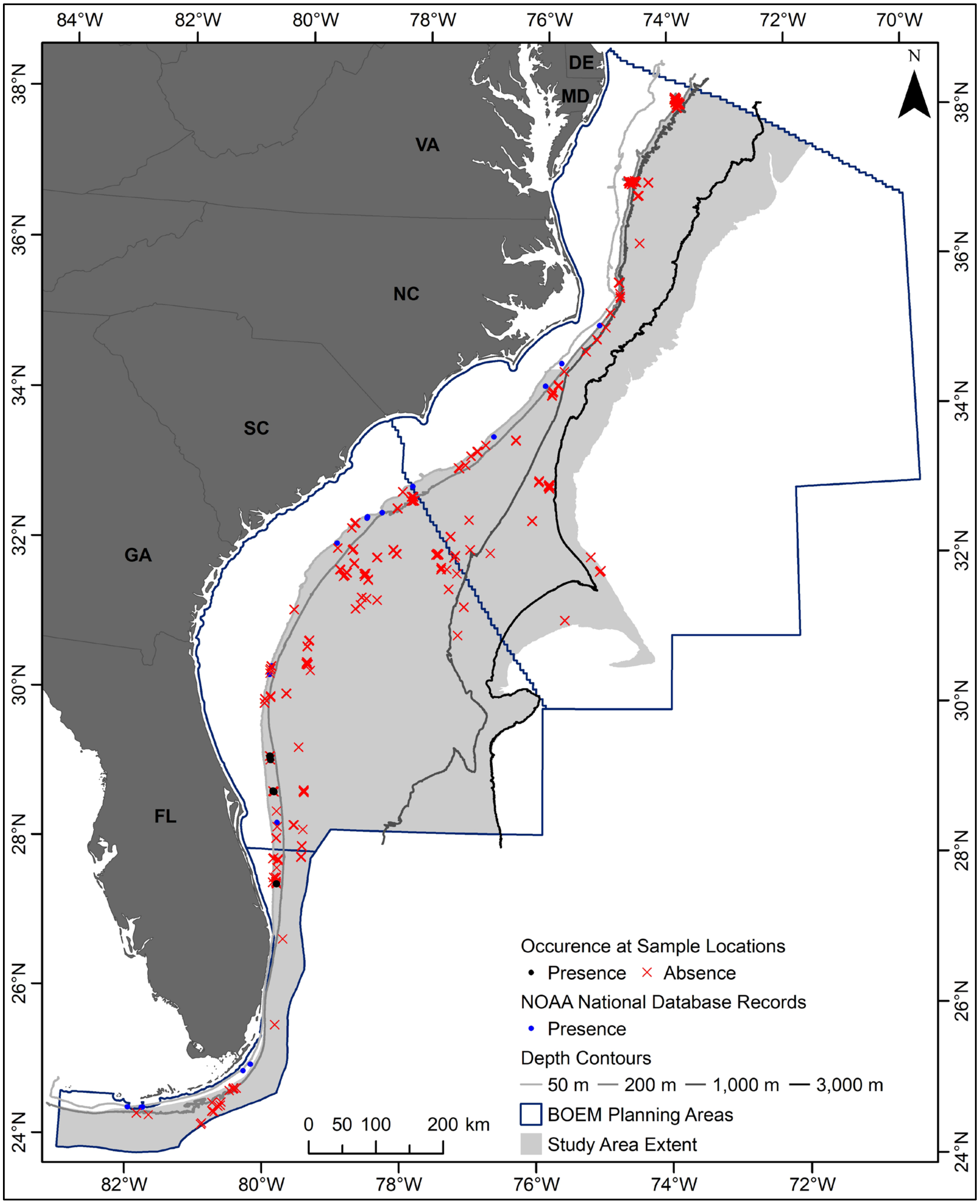

Figure D-4. Occurrence records for the stony coral *Cladocora*.
This map shows the observed occurrence (presence-absence) of *Cladocora* at sample locations in the presence-absence database compiled for this study. Additional records of occurrence (presence) from the NOAA National Database are also displayed.

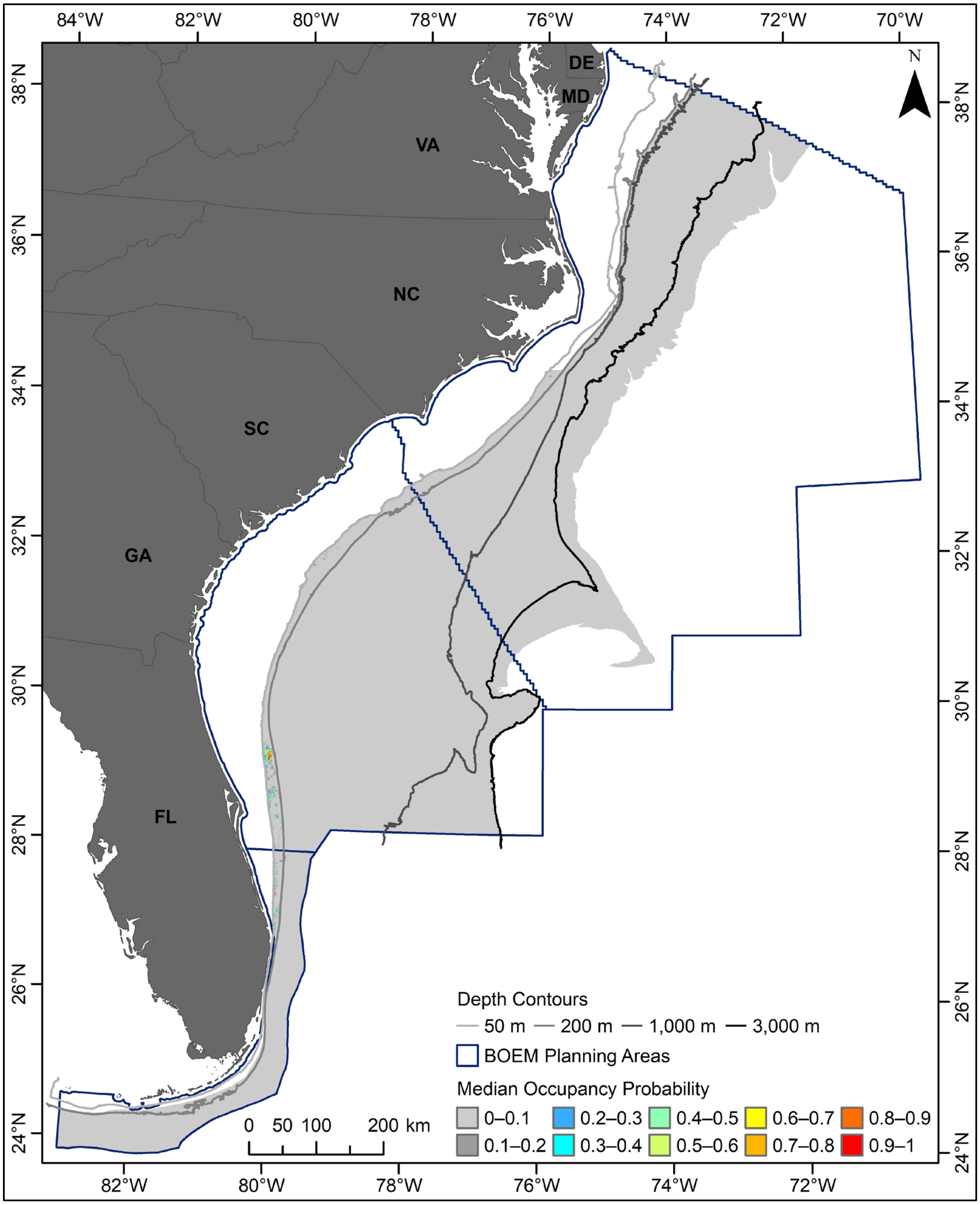

Figure D-5. Predicted occurrence of the stony coral *Cladocora*.
This map shows the posterior median occupancy probability for *Cladocora* from the multi-taxon model.

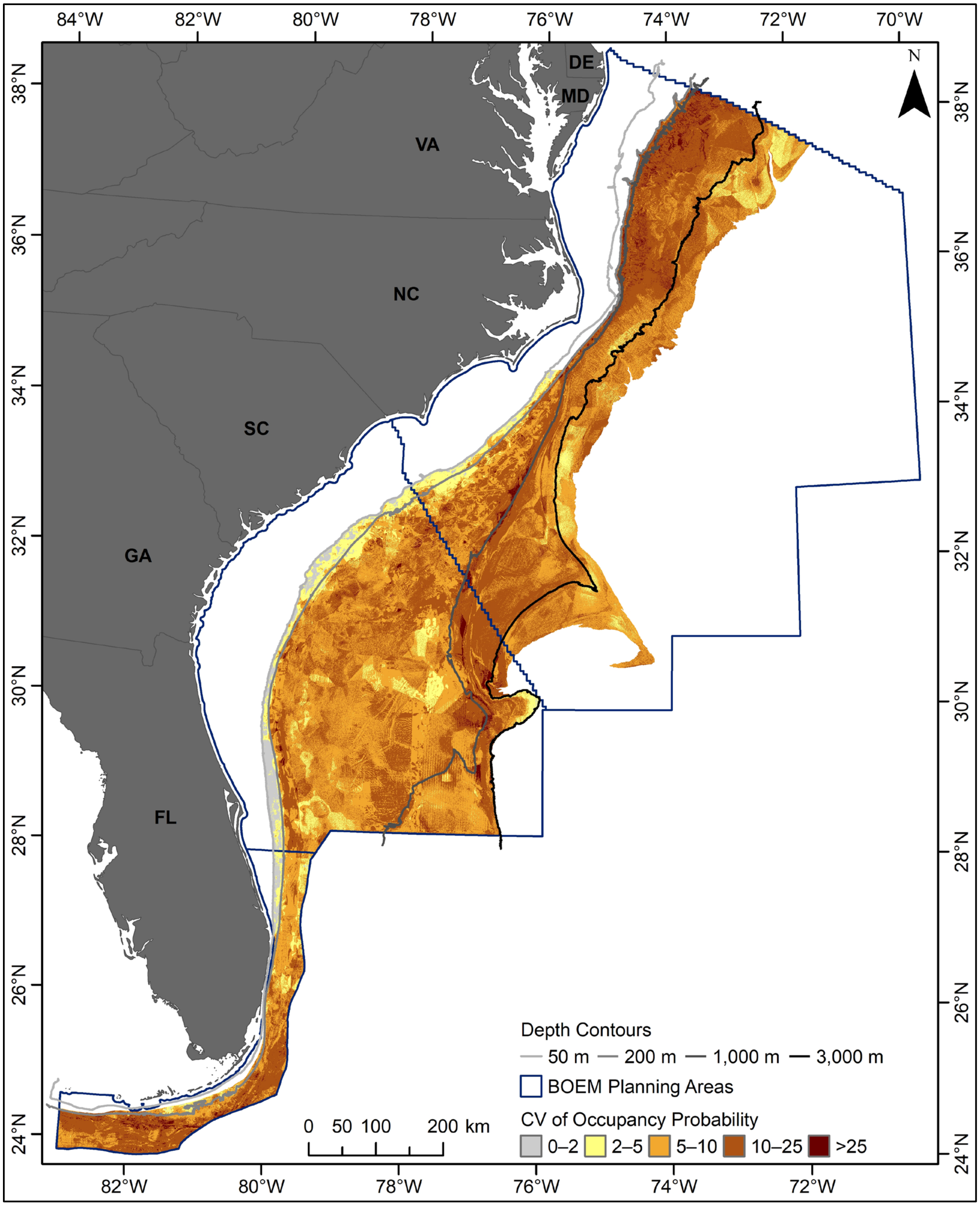

Figure D-6. Variability in the predicted occurrence of the stony coral *Cladocora*.
This map shows the posterior coefficient of variation of occupancy probability for *Cladocora* from the multi-taxon model.

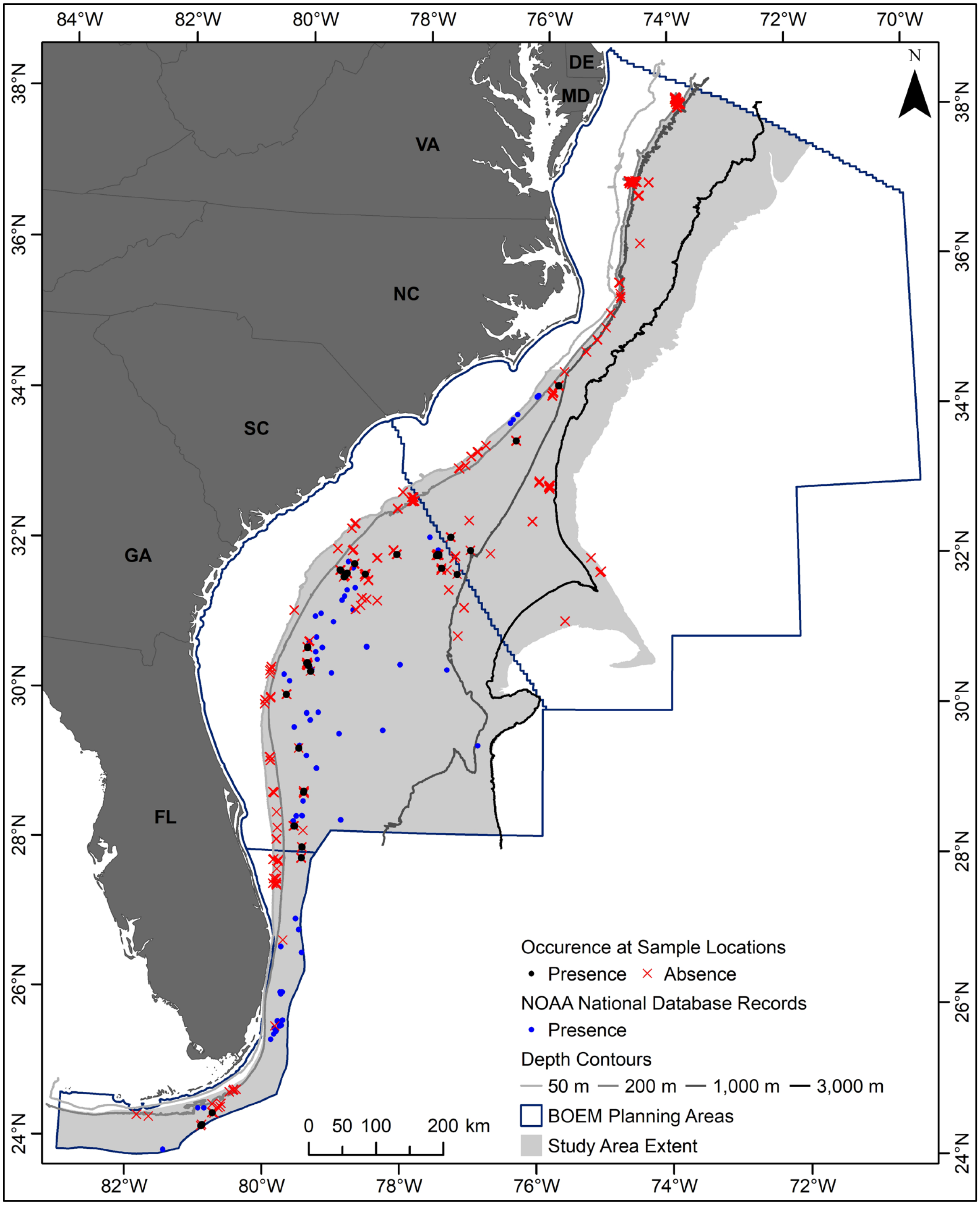

Figure D-7. Occurrence records for the stony coral *Madrepora*.
This map shows the observed occurrence (presence-absence) of *Madrepora* at sample locations in the presence-absence database compiled for this study. Additional records of occurrence (presence) from the NOAA National Database are also displayed.

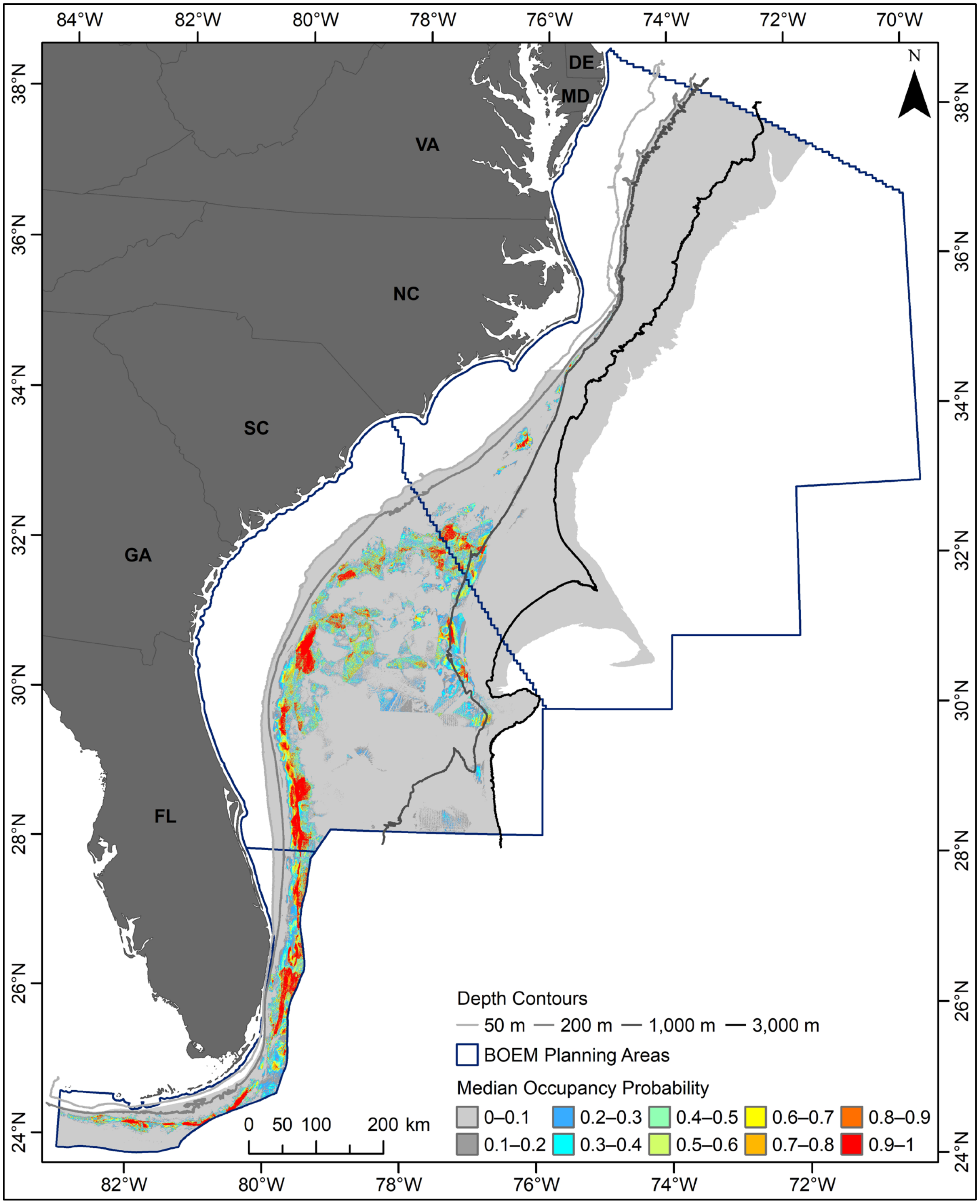

Figure D-8. Predicted occurrence of the stony coral *Madrepora*.
This map shows the posterior median occupancy probability for *Madrepora* from the multi-taxon model.

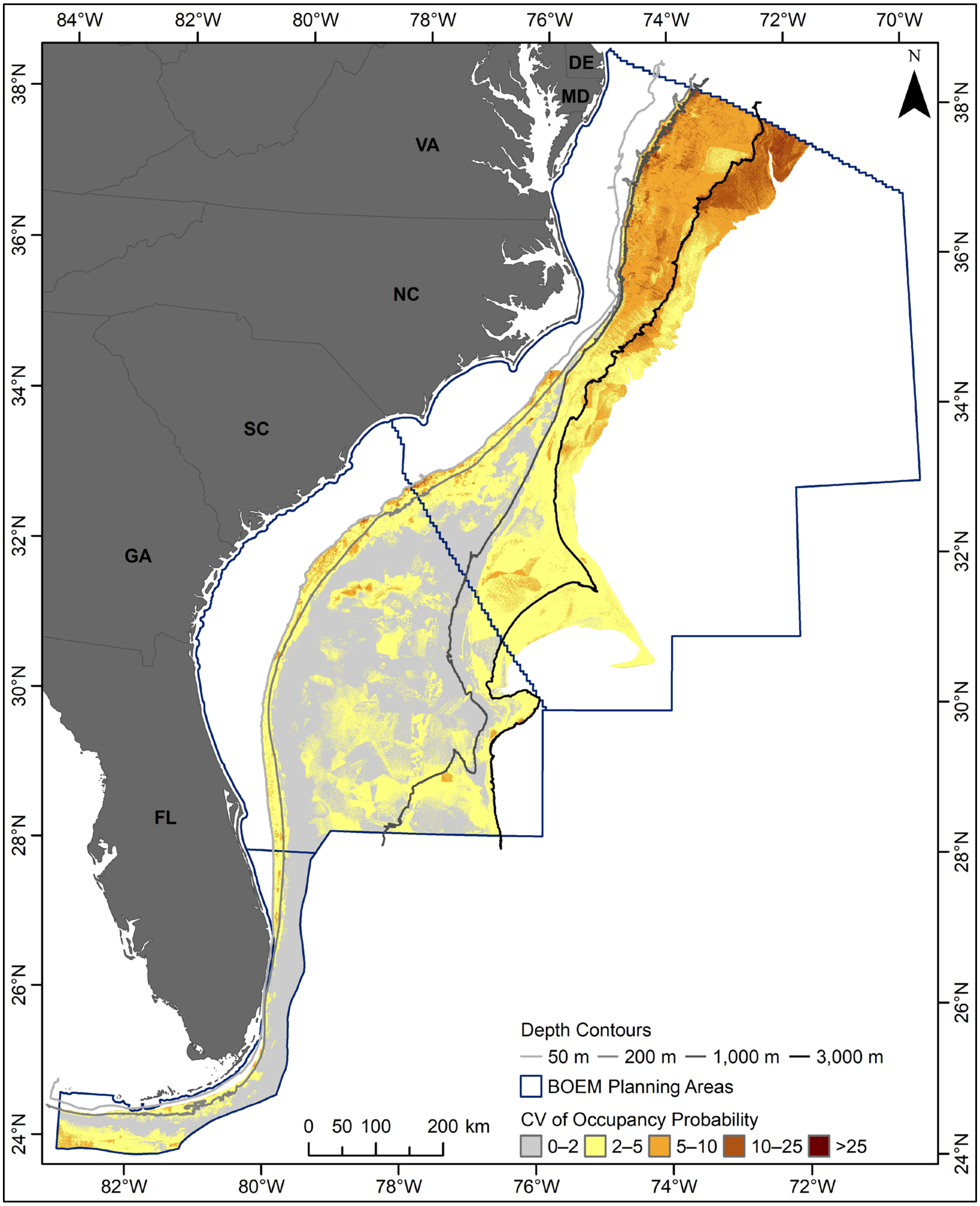

Figure D-9. Variability in the predicted occurrence of the stony coral *Madrepora*.
This map shows the posterior coefficient of variation of occupancy probability for *Madrepora* from the multi-taxon model.

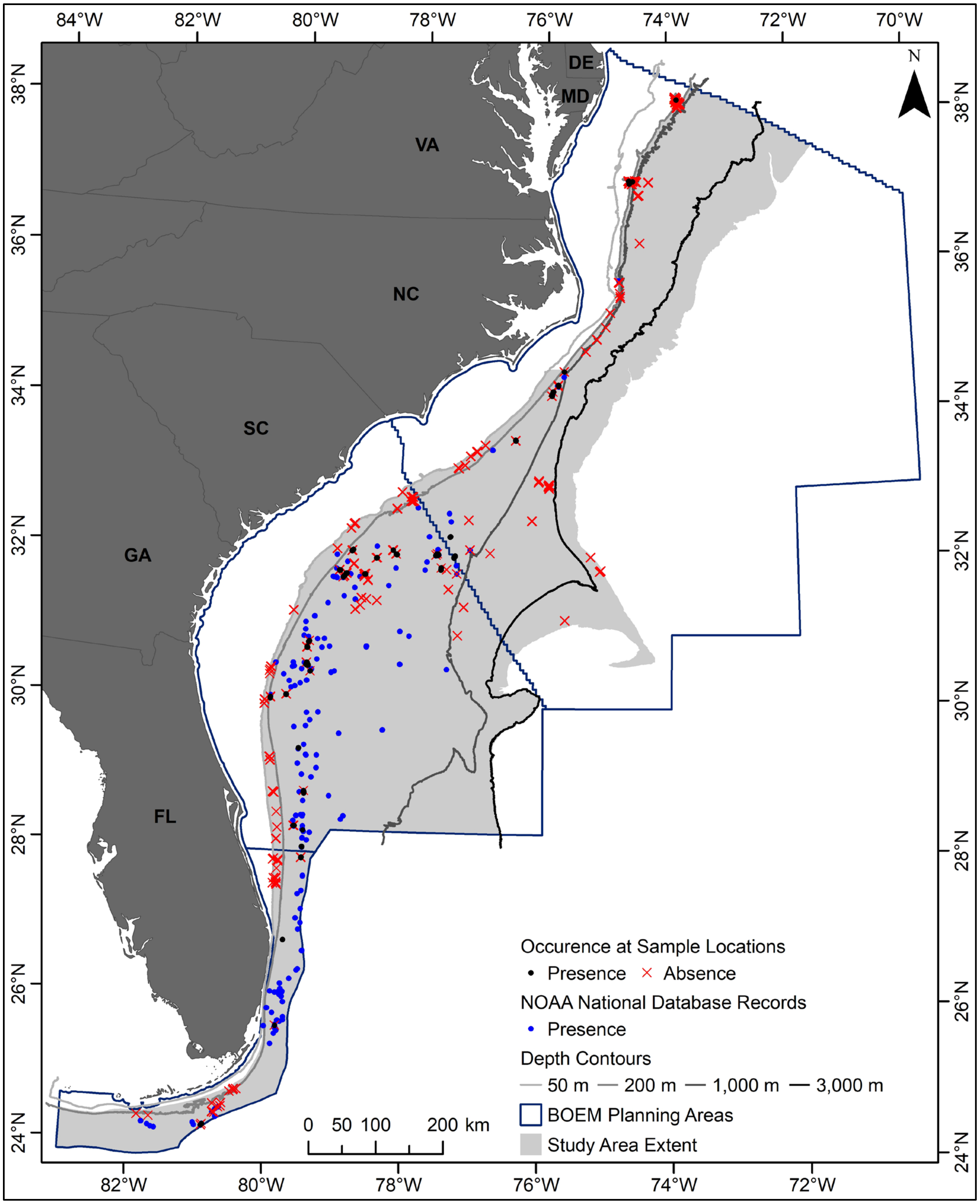

Figure D-10. Occurrence records for the stony coral *Lophelia*.
This map shows the observed occurrence (presence-absence) of *Lophelia* at sample locations in the presence-absence database compiled for this study. Additional records of occurrence (presence) from the NOAA National Database are also displayed.

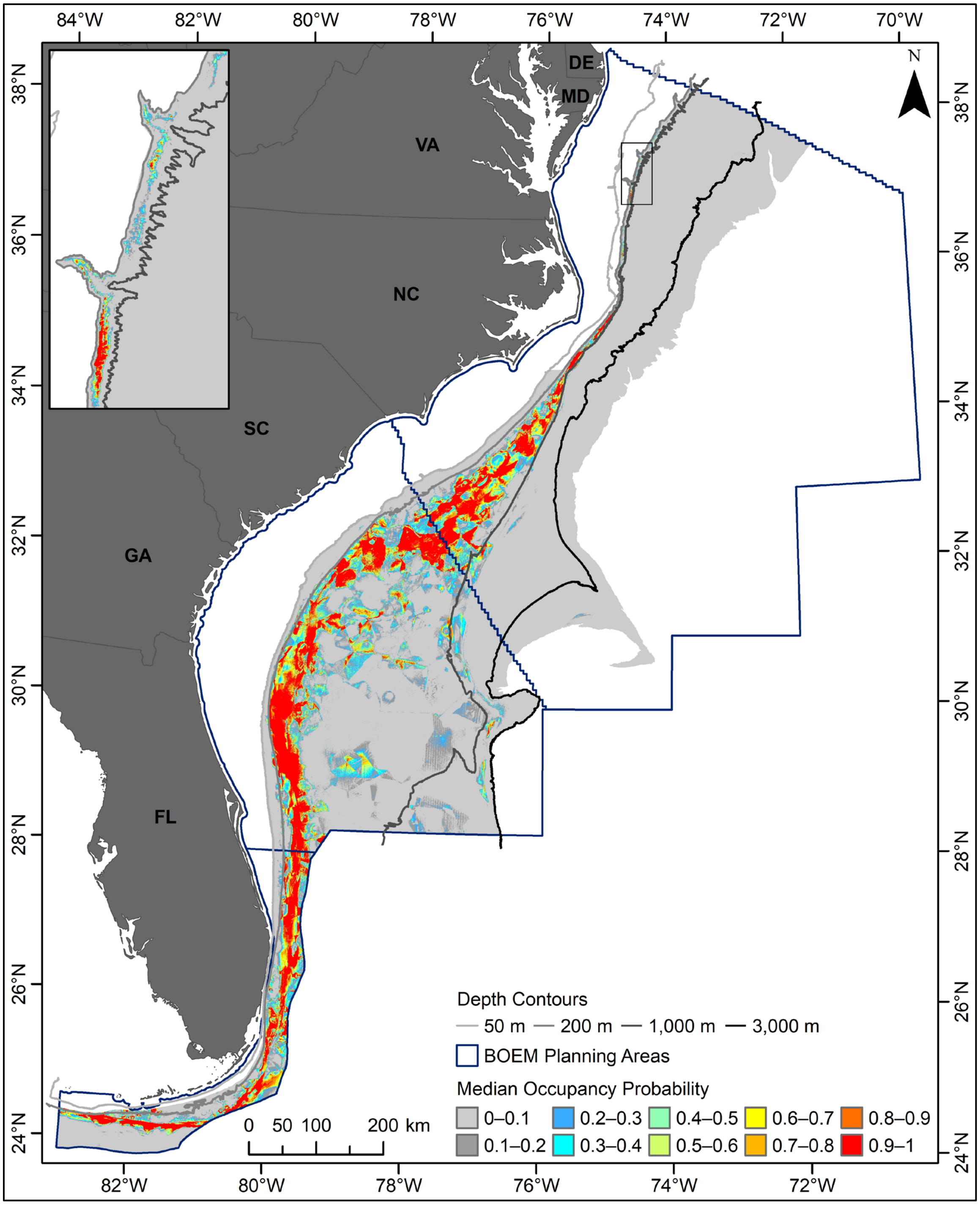

Figure D-11. Predicted occurrence of the stony coral *Lophelia*.
This map shows the posterior median occupancy probability for *Lophelia* from the multi-taxon model.

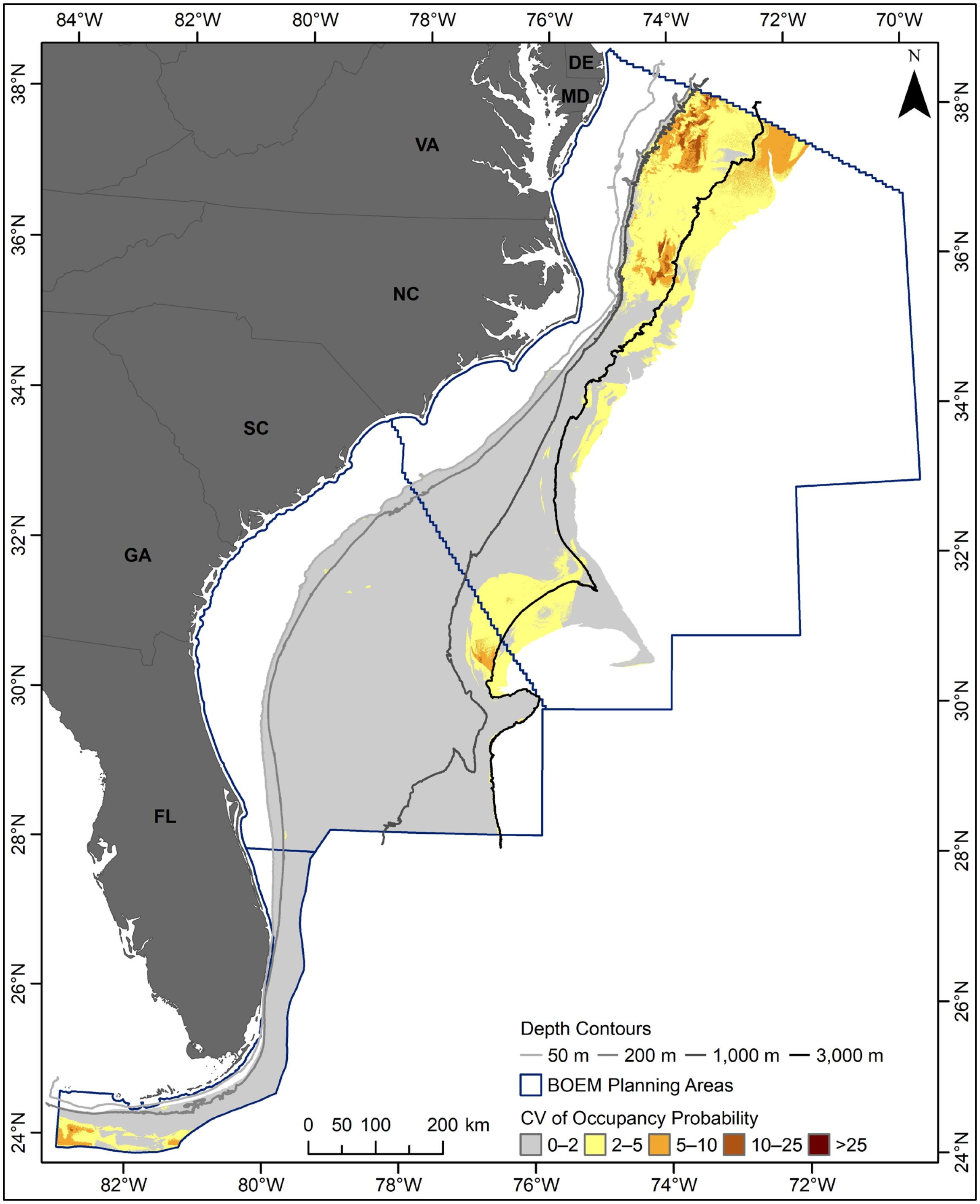

Figure D-12. Variability in the predicted occurrence of the stony coral *Lophelia*.
This map shows the posterior coefficient of variation of occupancy probability for *Lophelia* from the multi-taxon model.

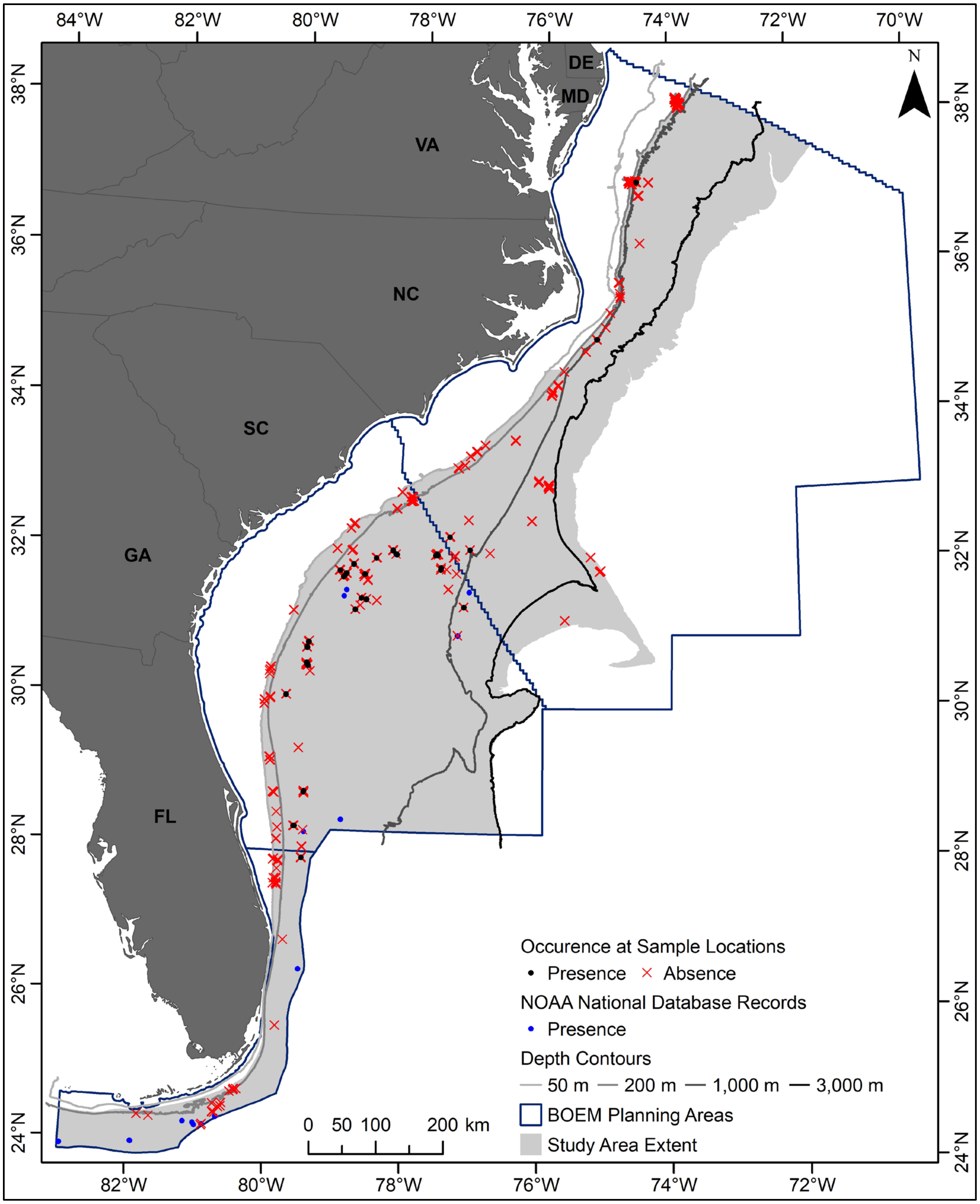

Figure D-13. Occurrence records for the stony coral *Solenosmilia*.
This map shows the observed occurrence (presence-absence) of *Solenosmilia* at sample locations in the presence-absence database compiled for this study. Additional records of occurrence (presence) from the NOAA National Database are also displayed.

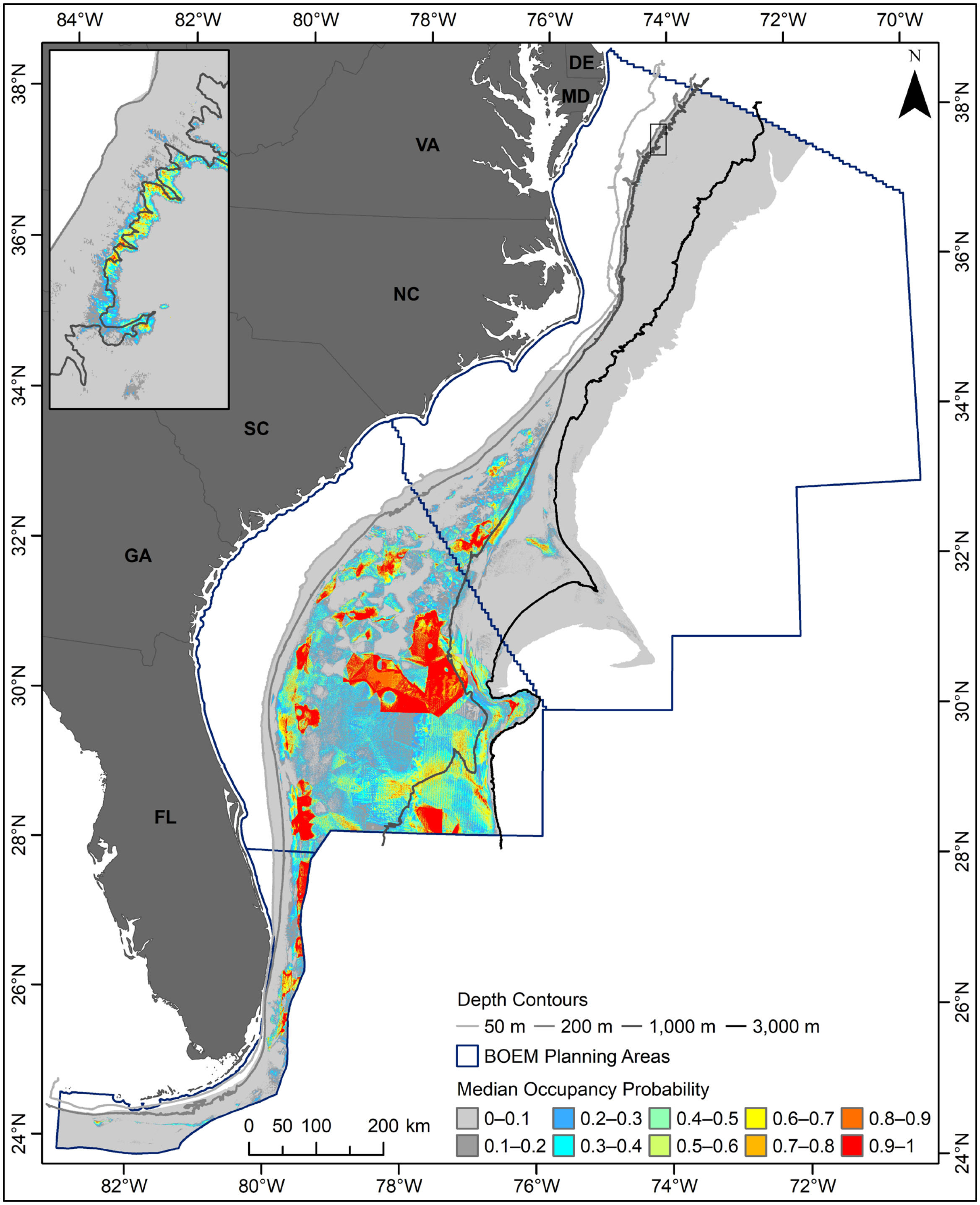

Figure D-14. Predicted occurrence of the stony coral *Solenosmilia*.
This map shows the posterior median occupancy probability for *Solenosmilia* from the multi-taxon model.

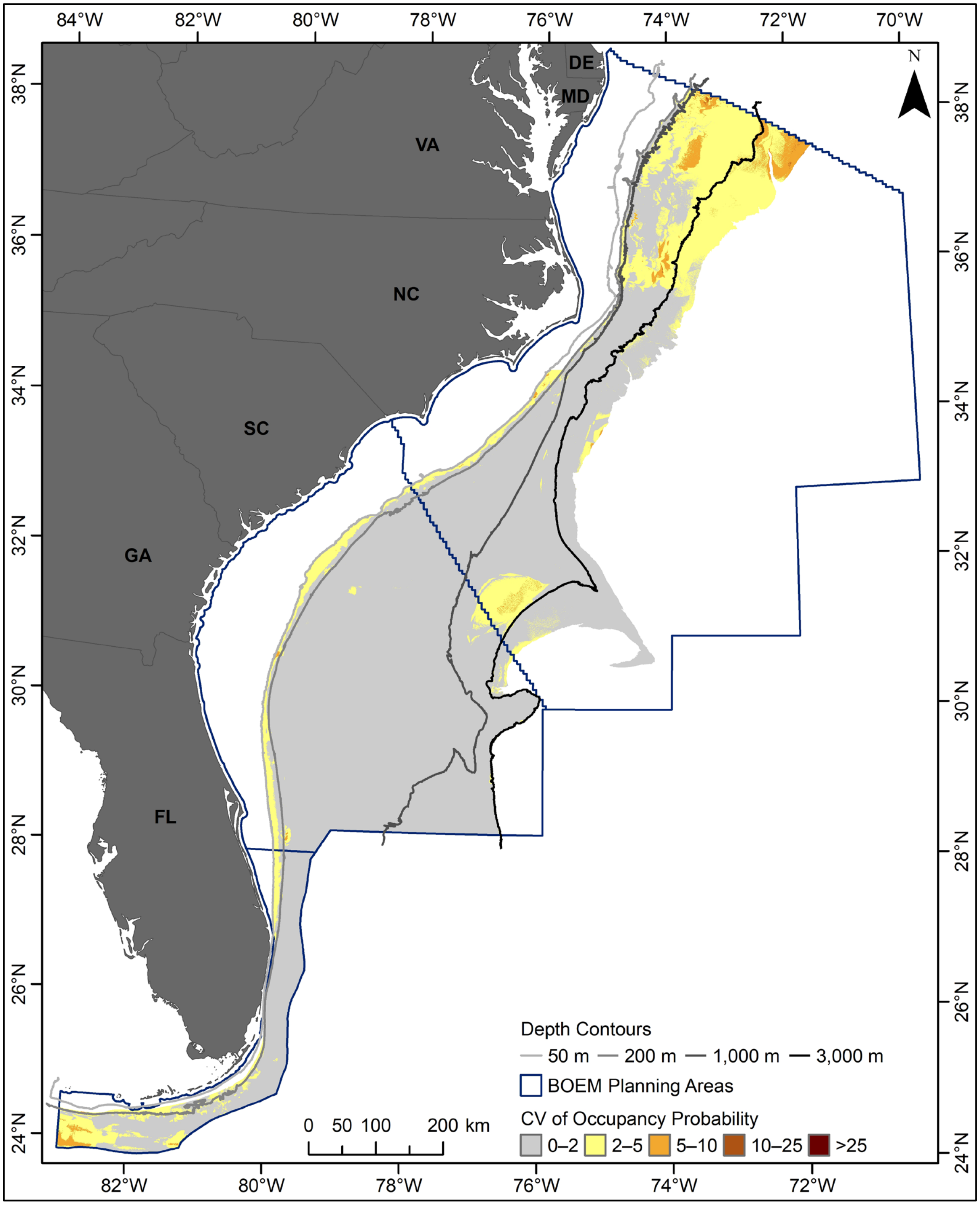

Figure D-15. Variability in the predicted occurrence of the stony coral *Solenosmilia*.
This map shows the posterior coefficient of variation of occupancy probability for *Solenosmilia* from the multi-taxon model.

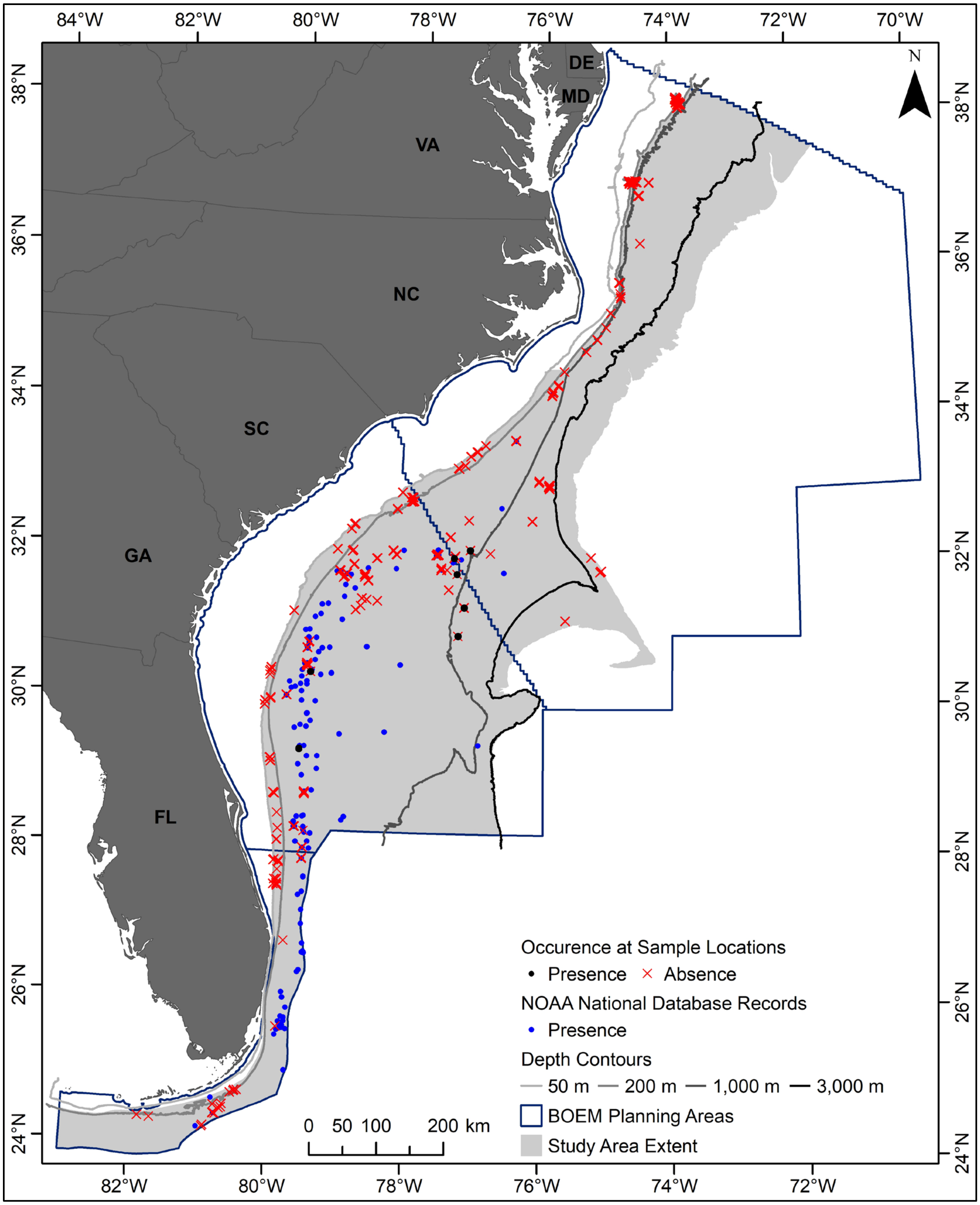

Figure D-16. Occurrence records for the stony coral *Enallopsammia*.
This map shows the observed occurrence (presence-absence) of *Enallopsammia* at sample locations in the presence-absence database compiled for this study. Additional records of occurrence (presence) from the NOAA National Database are also displayed.

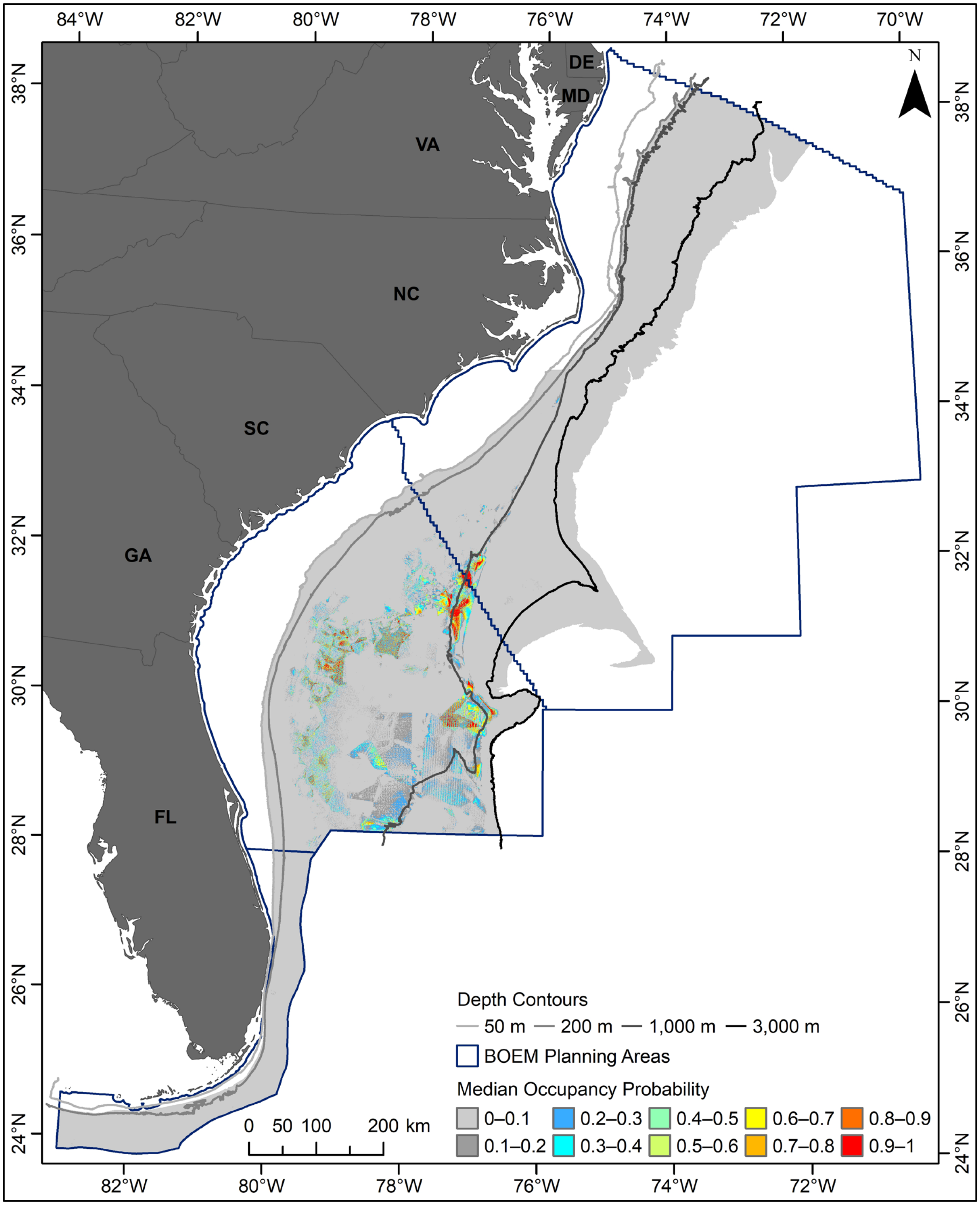

Figure D-17. Predicted occurrence of the stony coral *Enallopsammia*.
This map shows the posterior median occupancy probability for *Enallopsammia* from the multi-taxon model.

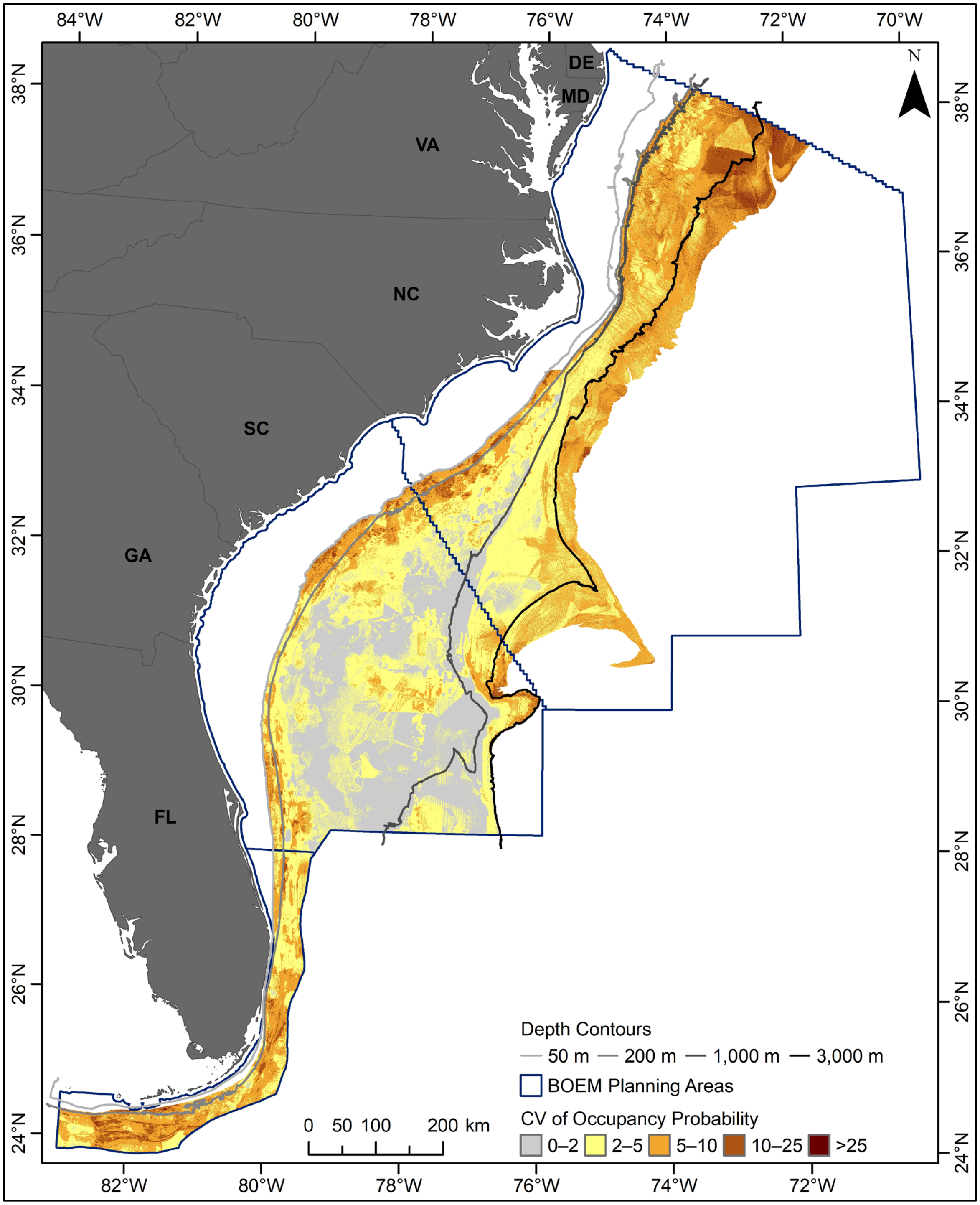

Figure D-18. Variability in the predicted occurrence of the stony coral *Enallopsammia*.
This map shows the posterior coefficient of variation of occupancy probability for *Enallopsammia* from the multi-taxon model.

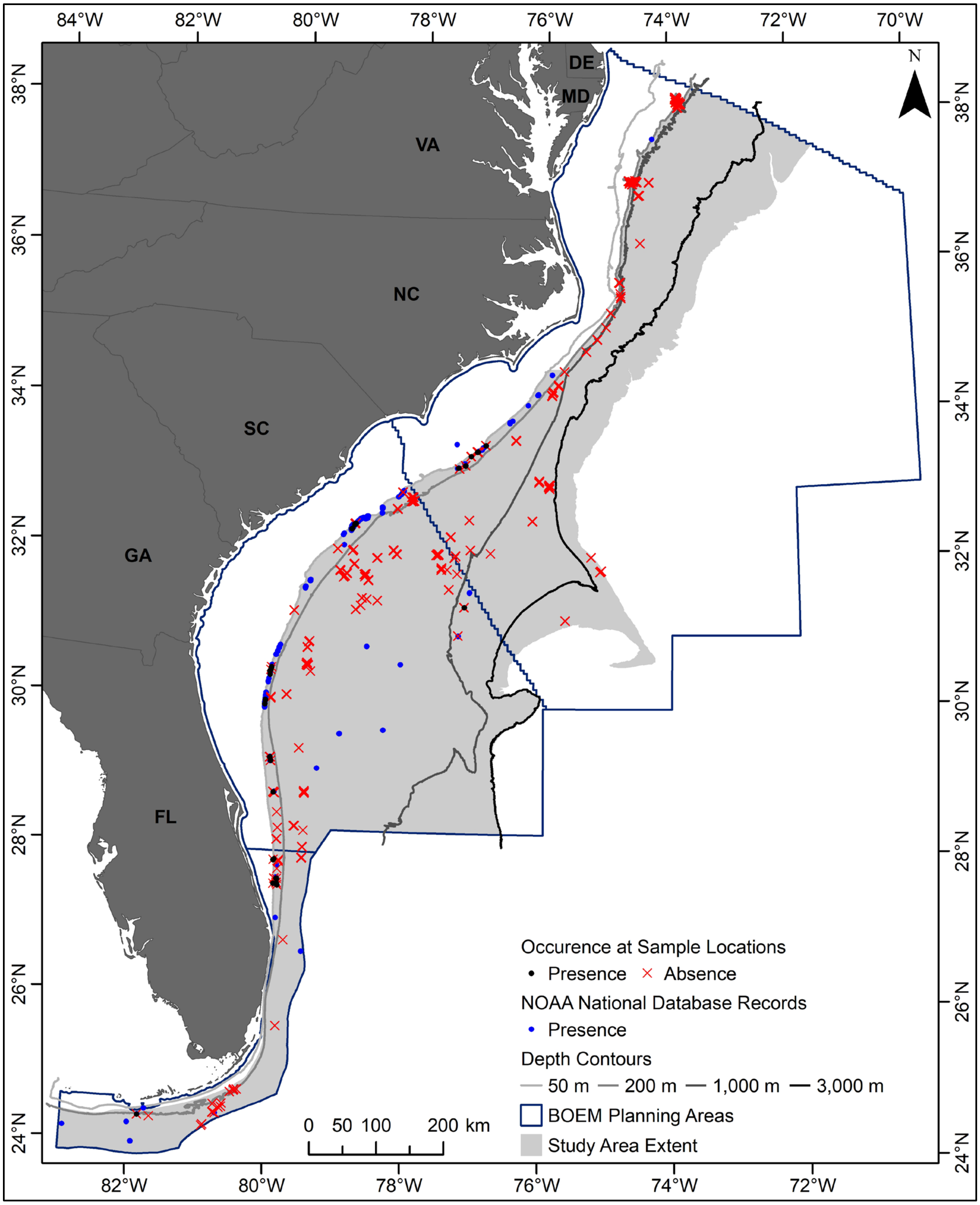

Figure D-19. Occurrence records for the black coral *Stichopathes*.
This map shows the observed occurrence (presence-absence) of *Stichopathes* at sample locations in the presence-absence database compiled for this study. Additional records of occurrence (presence) from the NOAA National Database are also displayed.

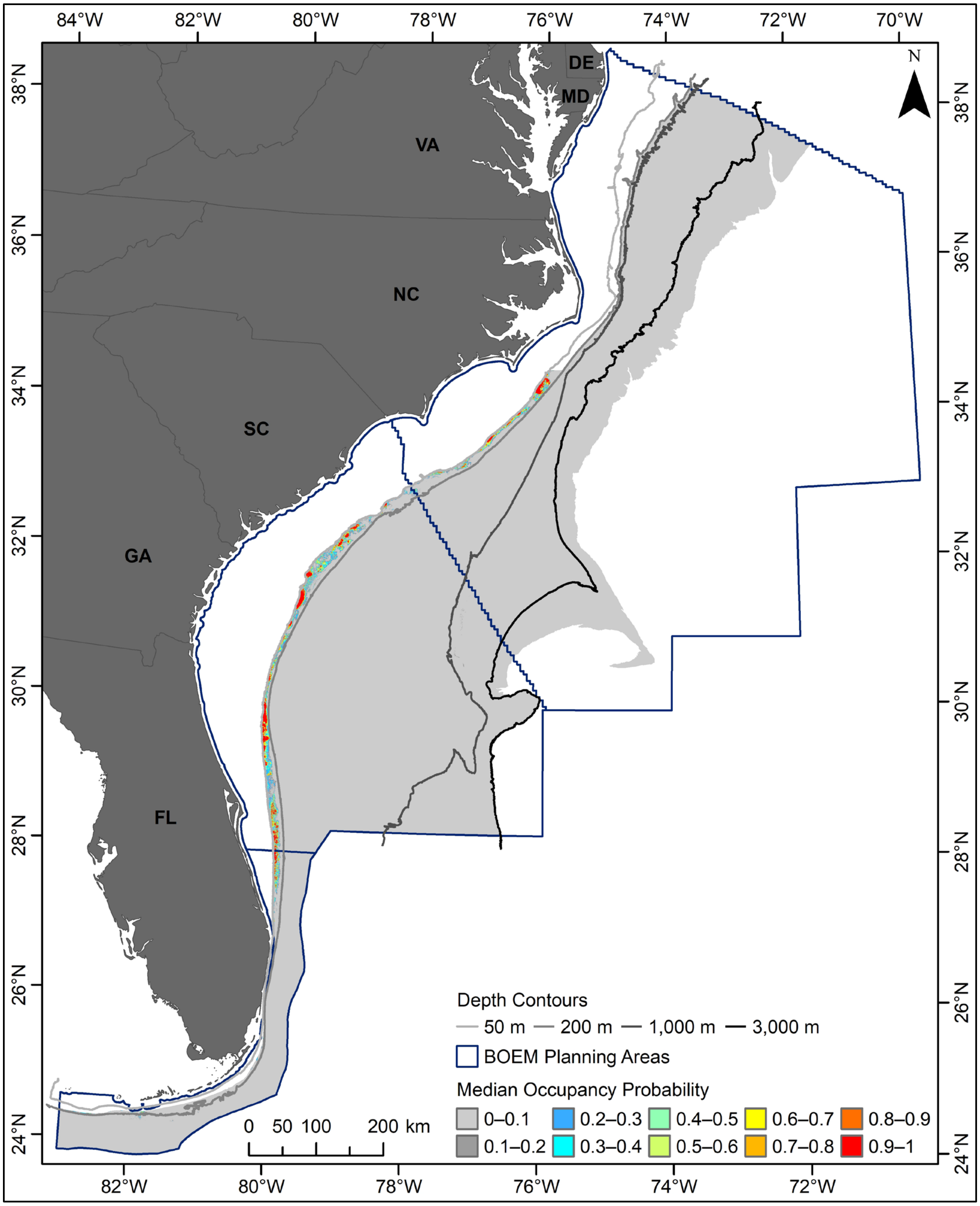

Figure D-20. Predicted occurrence of the black coral *Stichopathes*.
This map shows the posterior median occupancy probability for *Stichopathes* from the multi-taxon model.

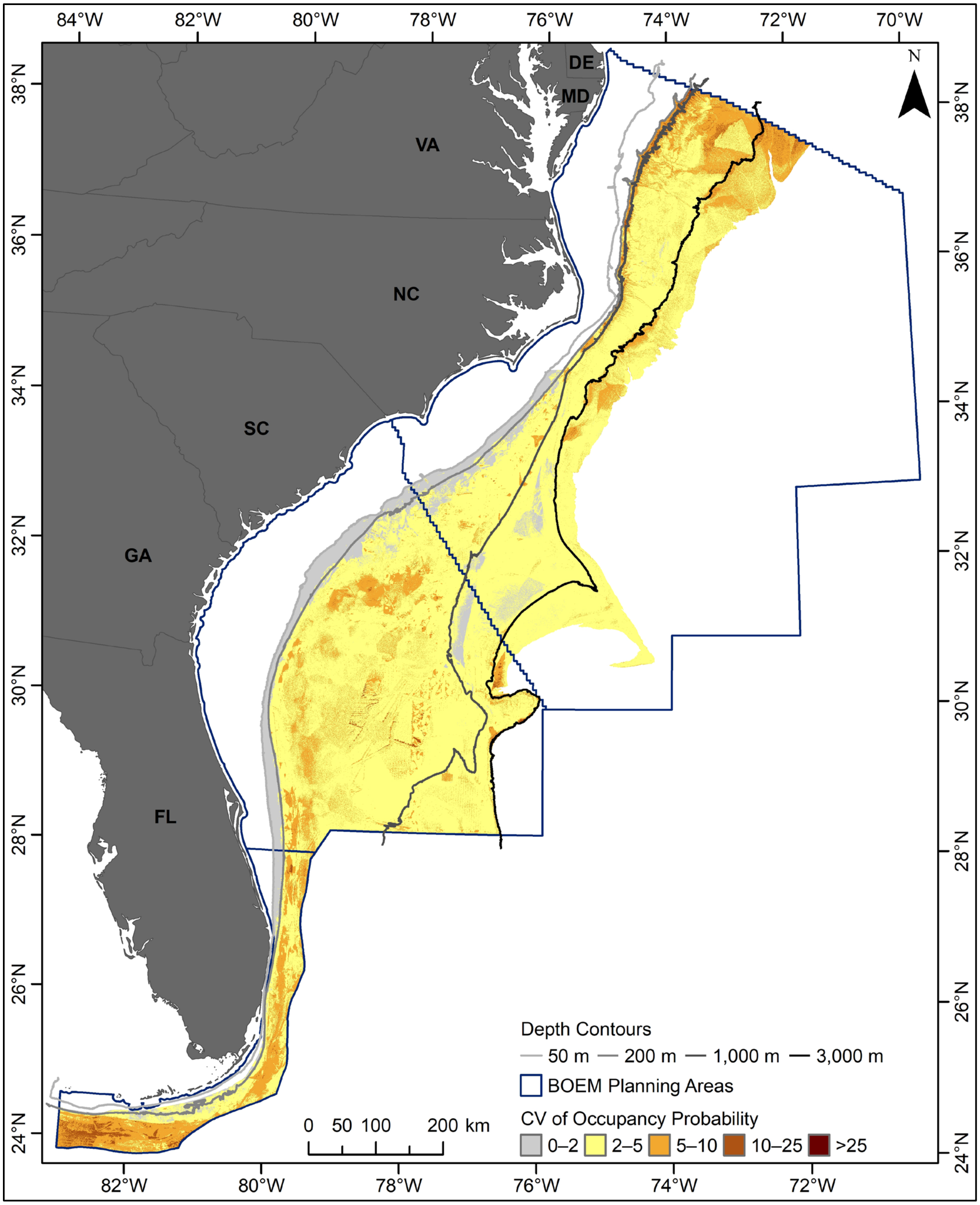

Figure D-21. Variability in the predicted occurrence of the black coral *Stichopathes*.
This map shows the posterior coefficient of variation of occupancy probability for *Stichopathes* from the multi-taxon model.

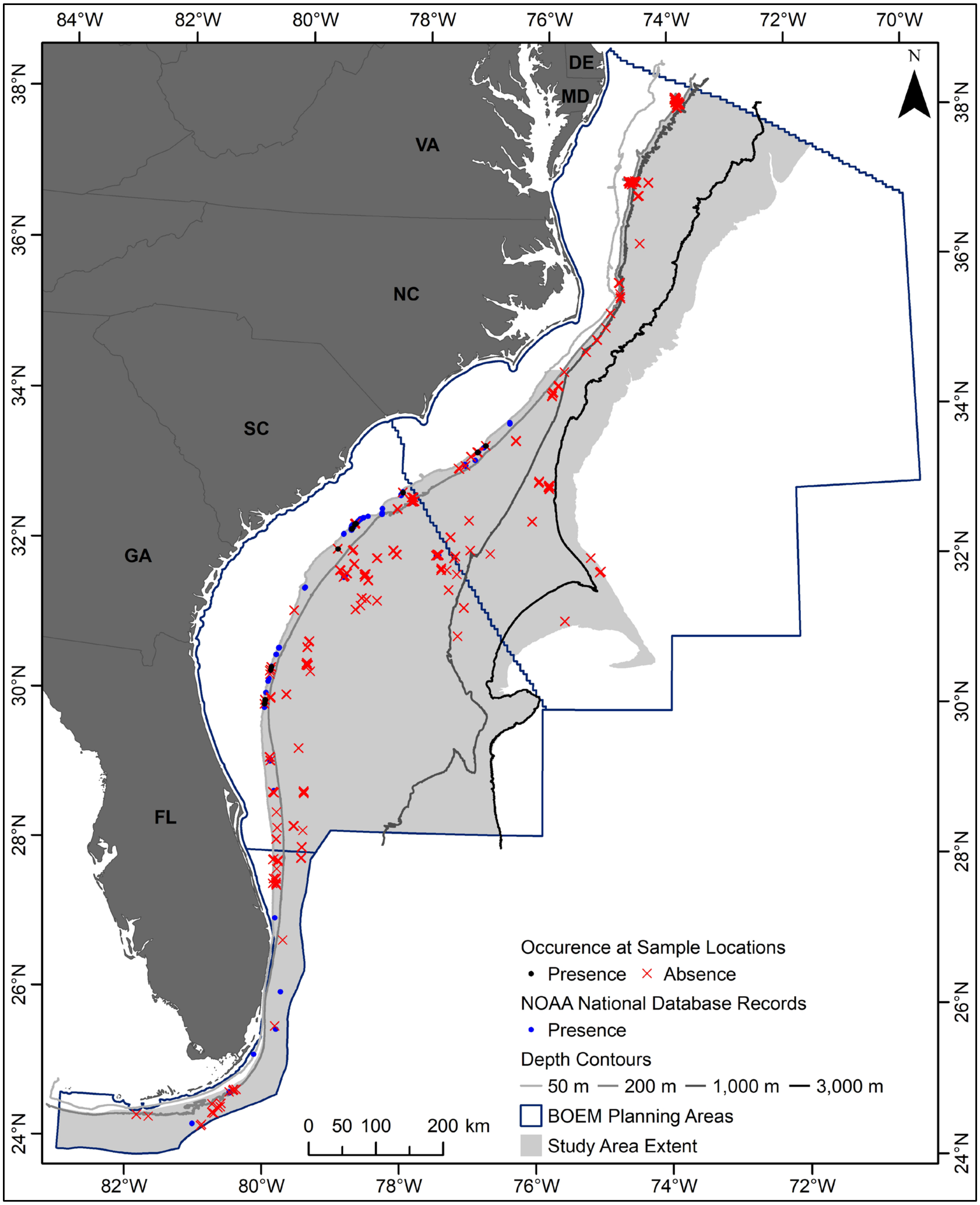

Figure D-22. Occurrence records for the black coral *Antipathes*.
This map shows the observed occurrence (presence-absence) of *Antipathes* at sample locations in the presence-absence database compiled for this study. Additional records of occurrence (presence) from the NOAA National Database are also displayed.

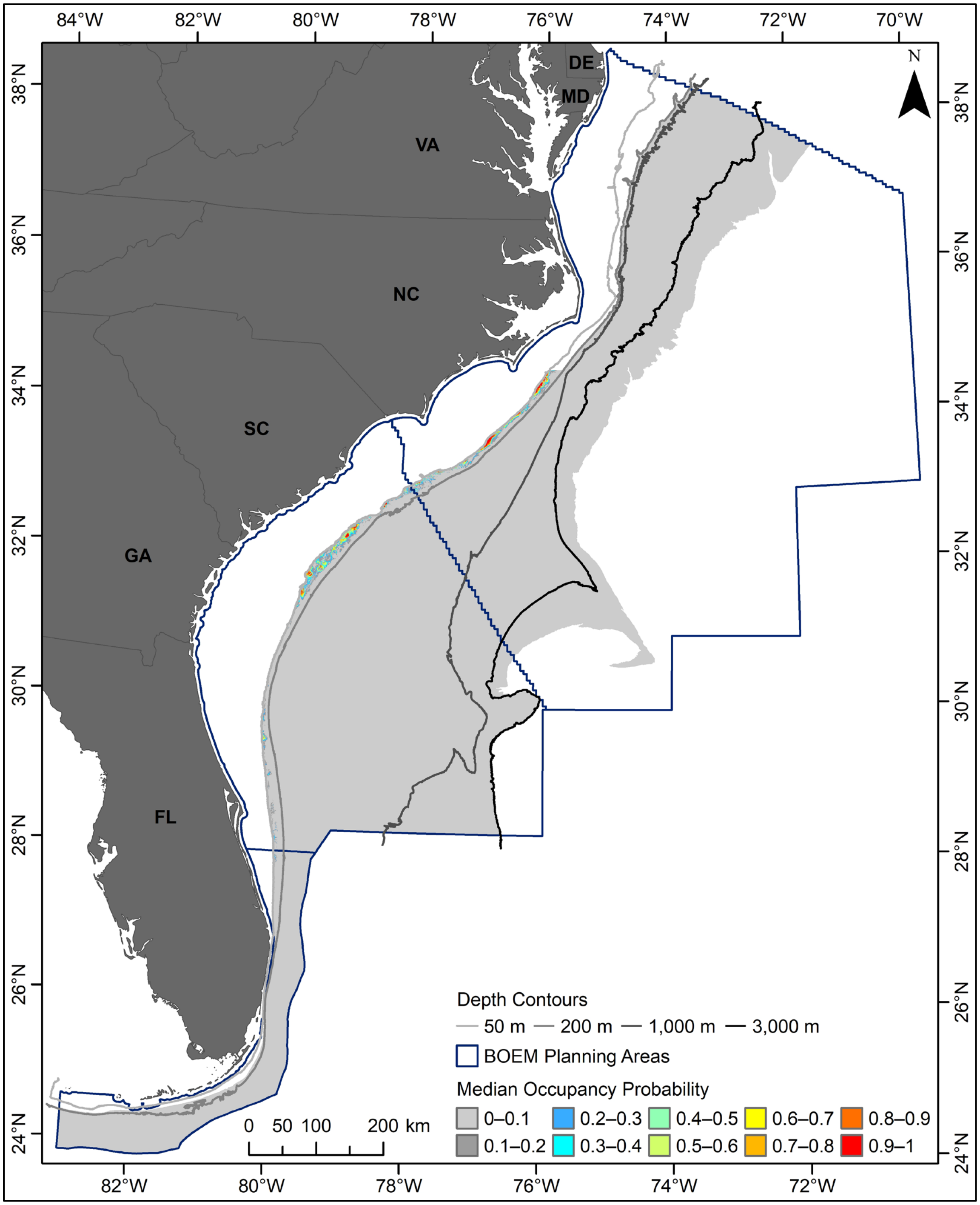

Figure D-23. Predicted occurrence of the black coral *Antipathes*.
This map shows the posterior median occupancy probability for *Antipathes* from the multi-taxon model.

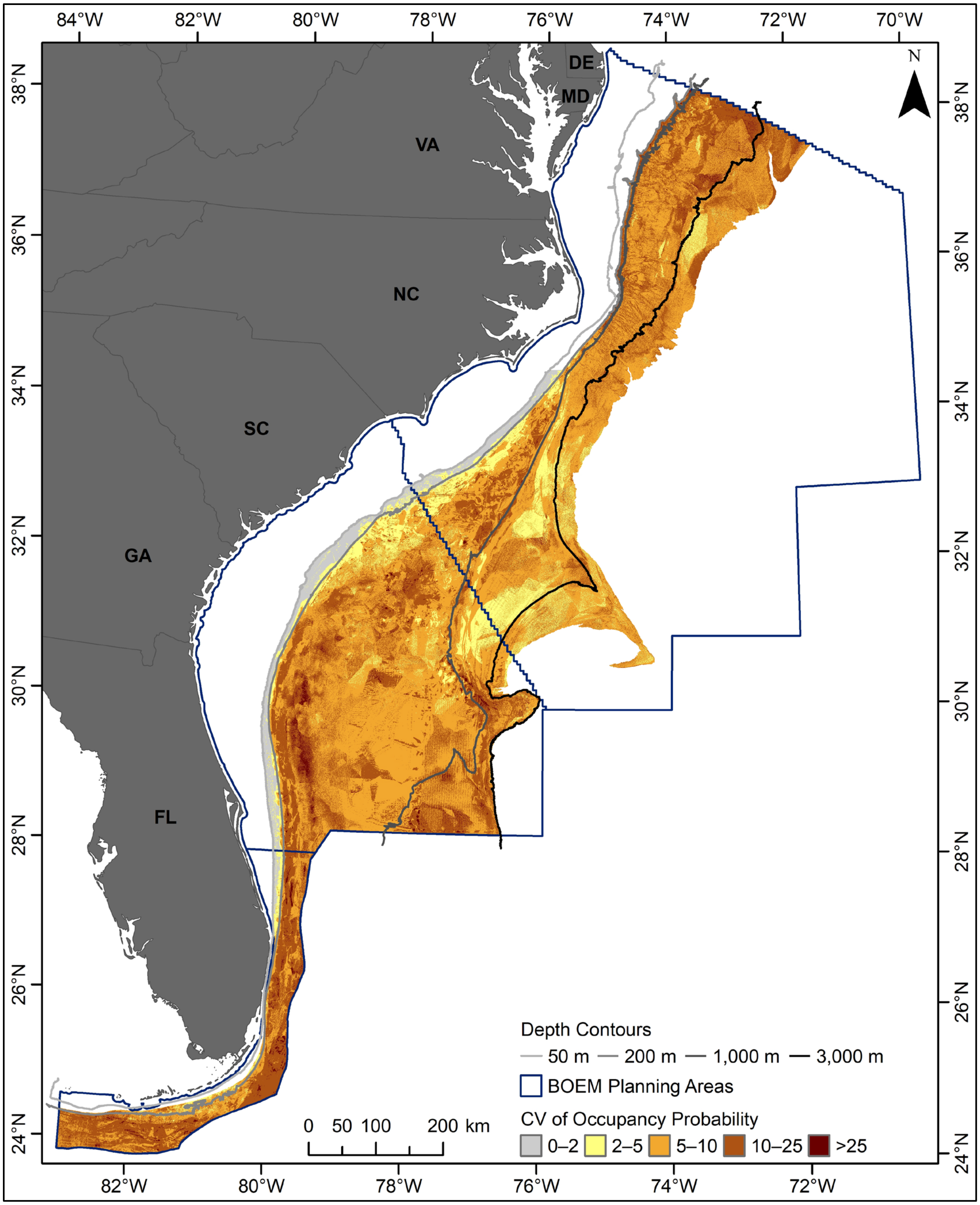

Figure D-24. Variability in the predicted occurrence of the black coral *Antipathes*.
This map shows the posterior coefficient of variation of occupancy probability for *Antipathes* from the multi-taxon model.

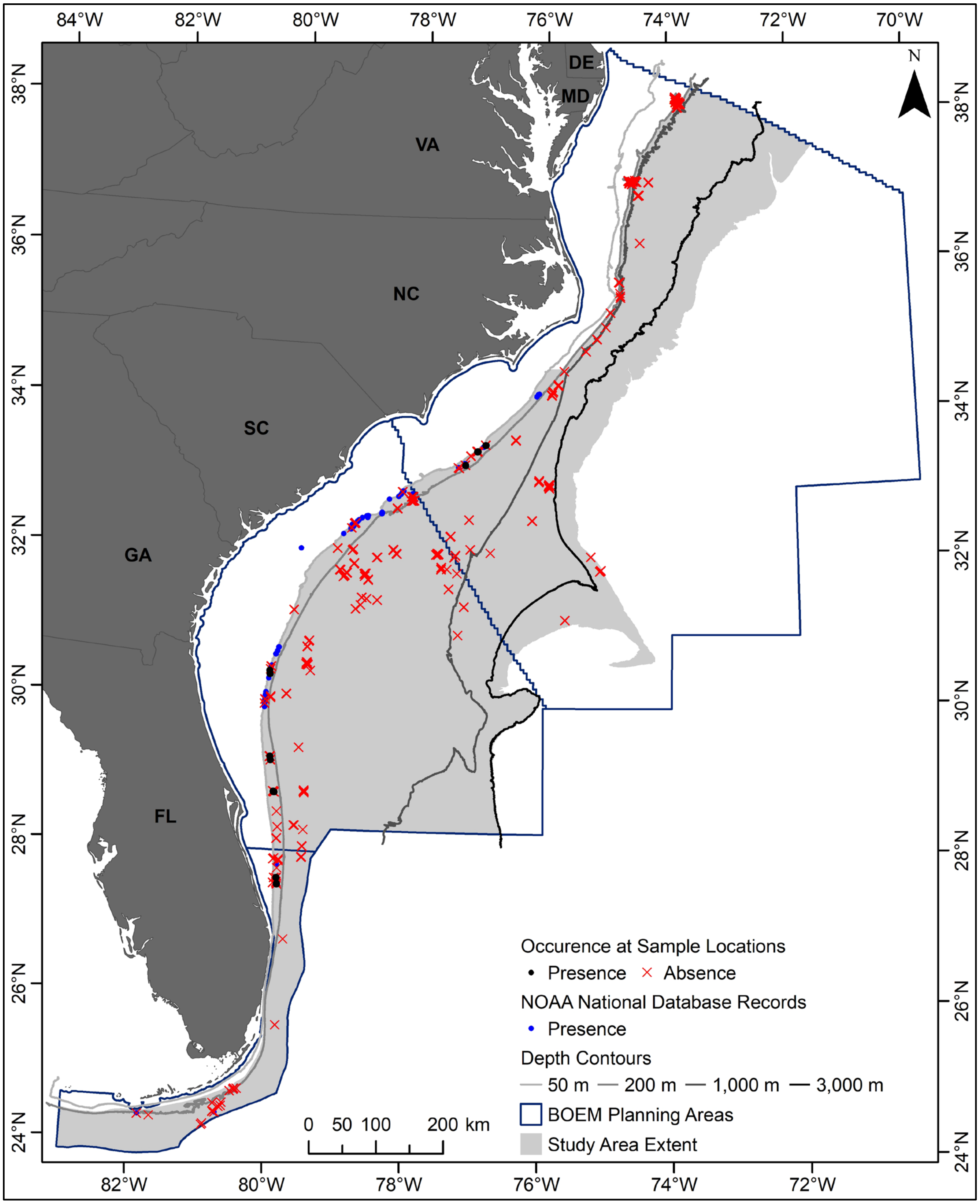

Figure D-25. Occurrence records for the black coral *Tanacetipathes*.
This map shows the observed occurrence (presence-absence) of *Tanacetipathes* at sample locations in the presence-absence database compiled for this study. Additional records of occurrence (presence) from the NOAA National Database are also displayed.

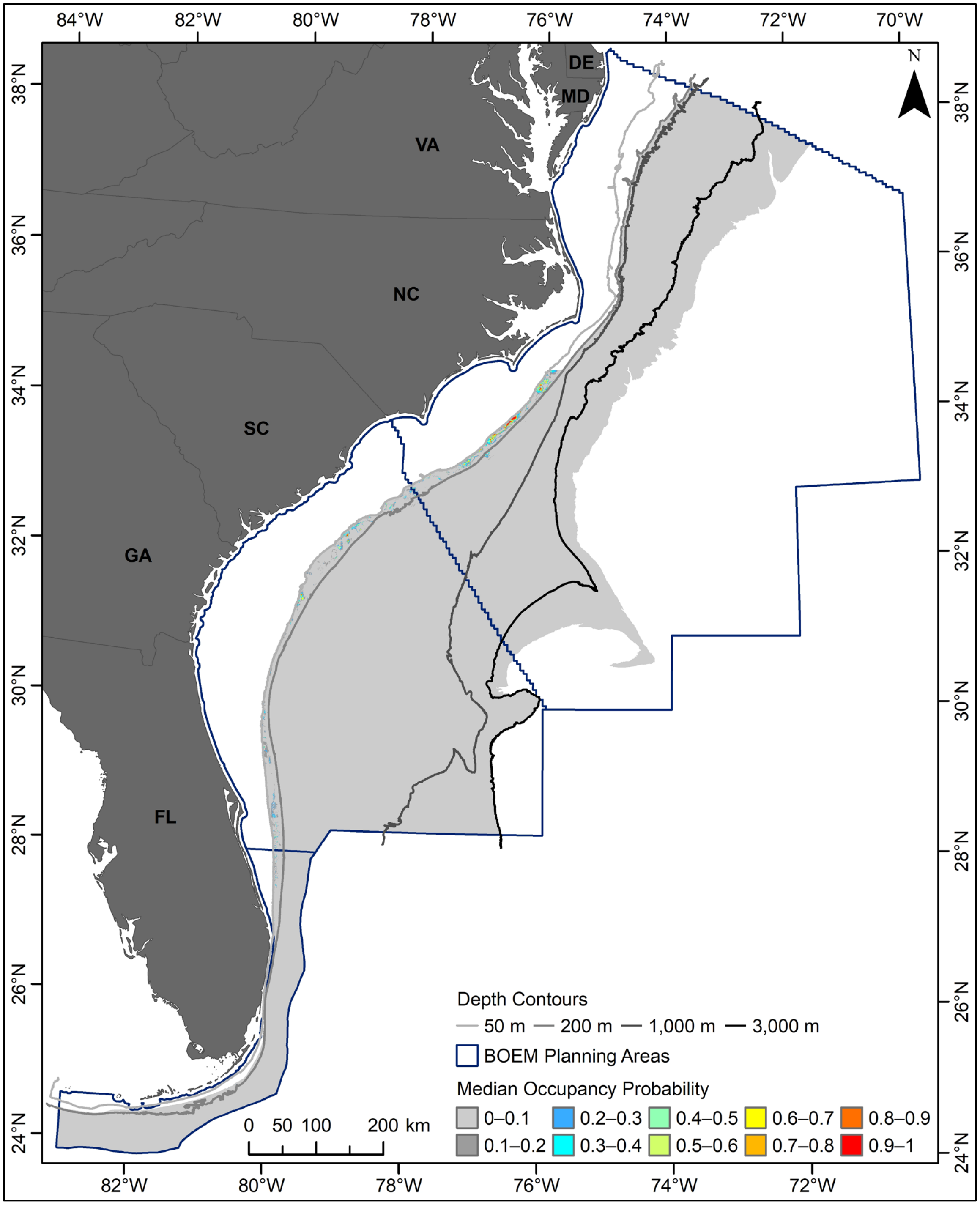

Figure D-26. Predicted occurrence of the black coral *Tanacetipathes*.
This map shows the posterior median occupancy probability for *Tanacetipathes* from the multi-taxon model.

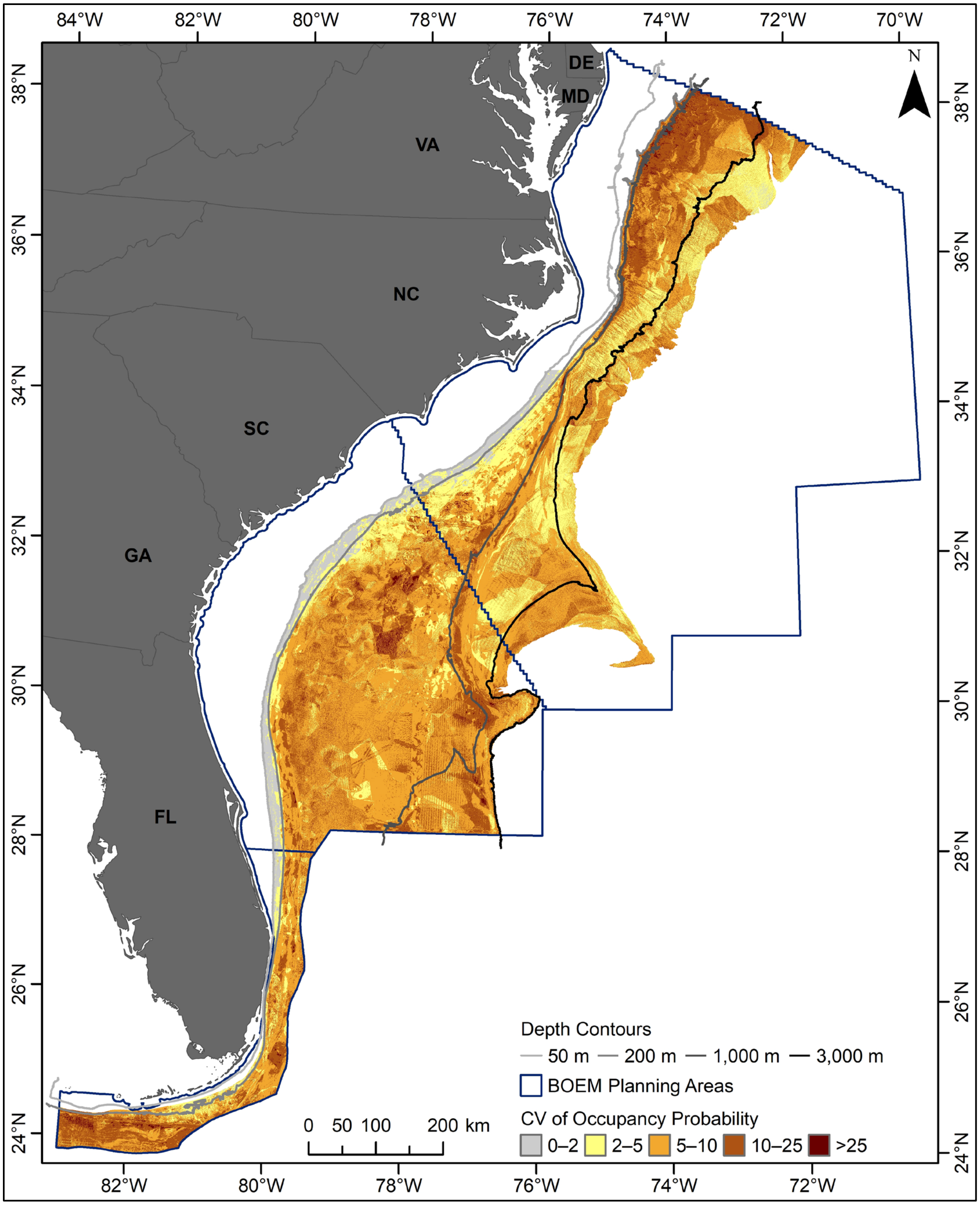

Figure D-27. Variability in the predicted occurrence of the black coral *Tanacetipathes*.
This map shows the posterior coefficient of variation of occupancy probability for *Tanacetipathes* from the multi-taxon model.

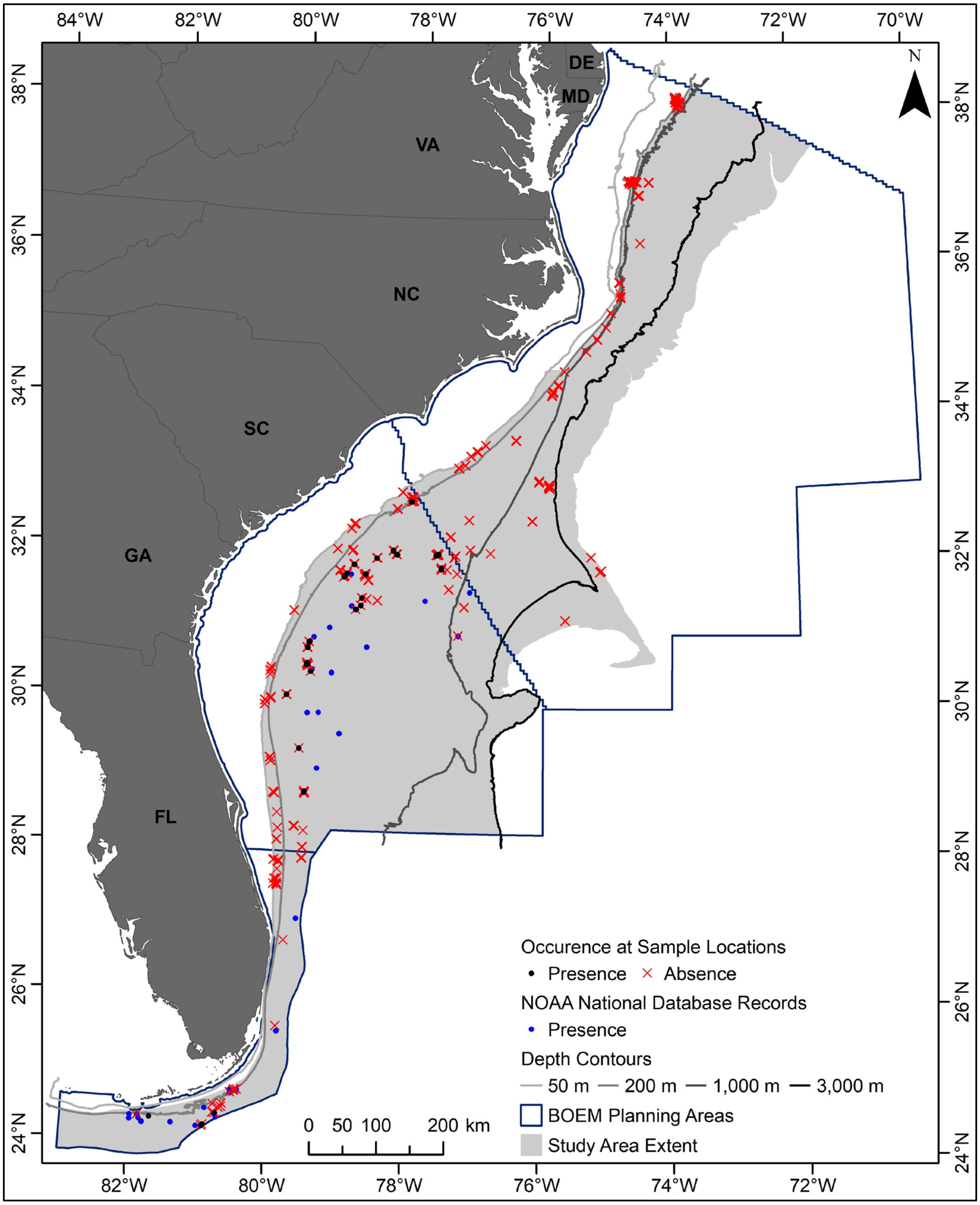

Figure D-28. Occurrence records for the black coral *Leiopathes*.
This map shows the observed occurrence (presence-absence) of *Leiopathes* at sample locations in the presence-absence database compiled for this study. Additional records of occurrence (presence) from the NOAA National Database are also displayed.

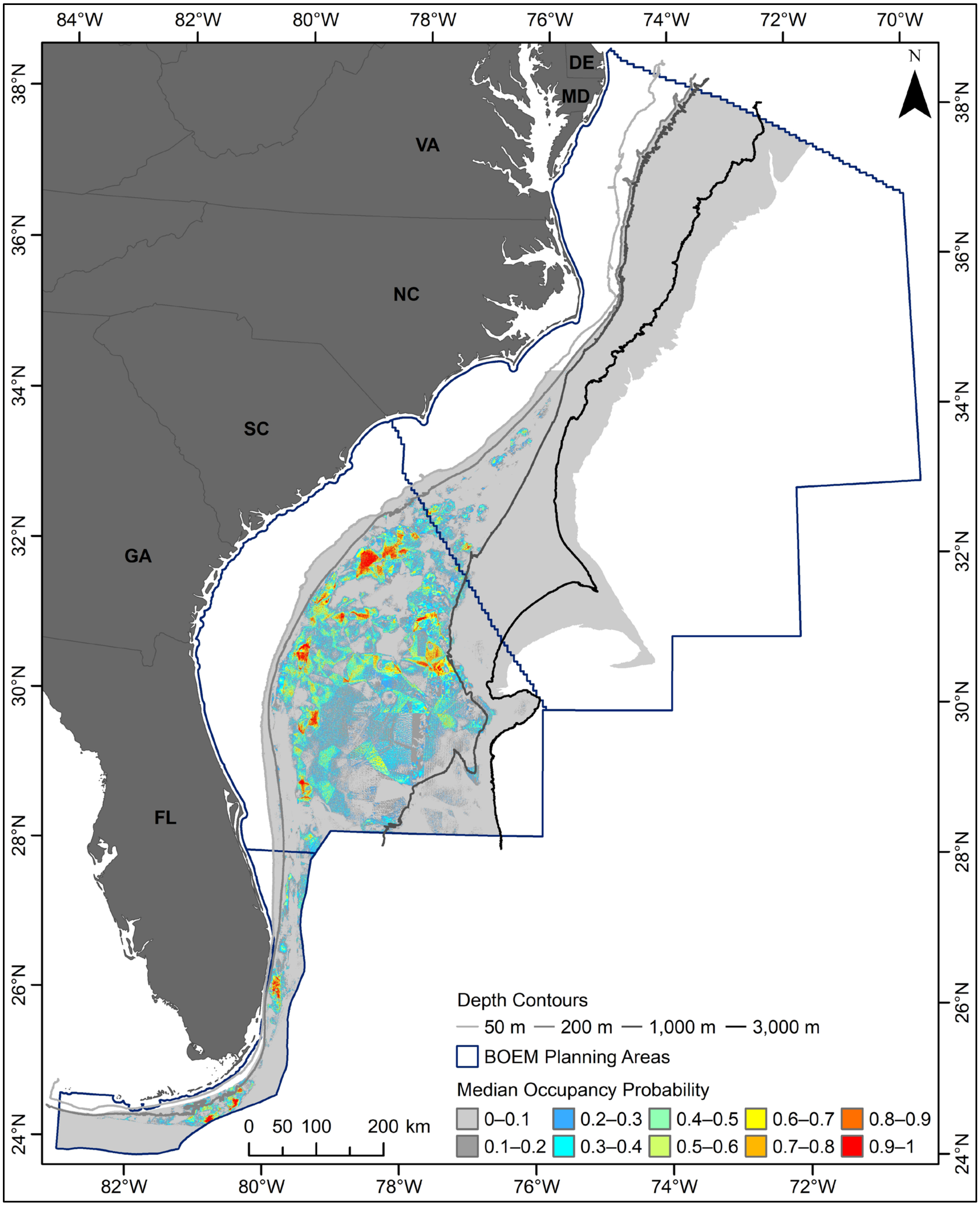

Figure D-29. Predicted occurrence of the black coral *Leiopathes*.
This map shows the posterior median occupancy probability for *Leiopathes* from the multi-taxon model.

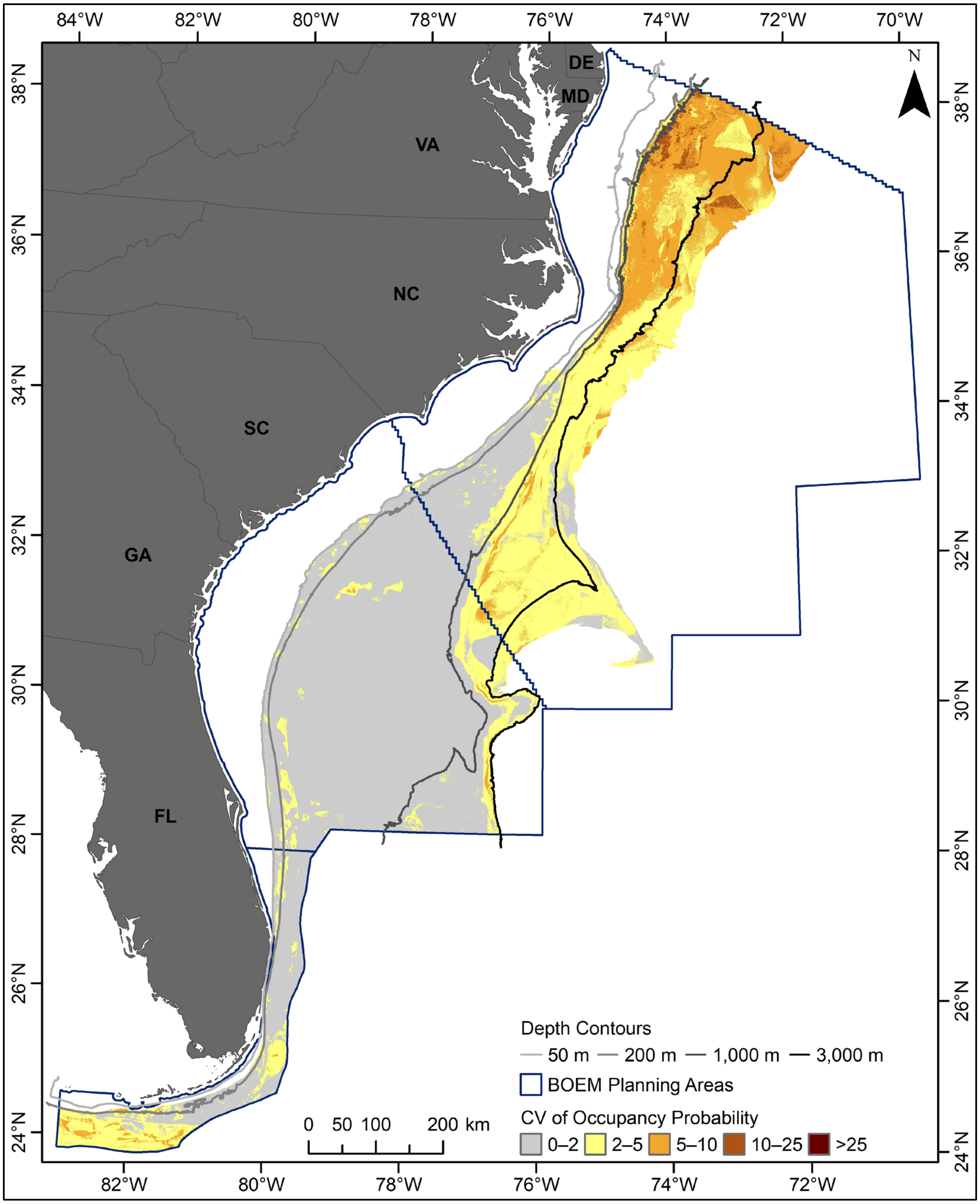

Figure D-30. Variability in the predicted occurrence of the black coral *Leiopathes*.
This map shows the posterior coefficient of variation of occupancy probability for *Leiopathes* from the multi-taxon model.

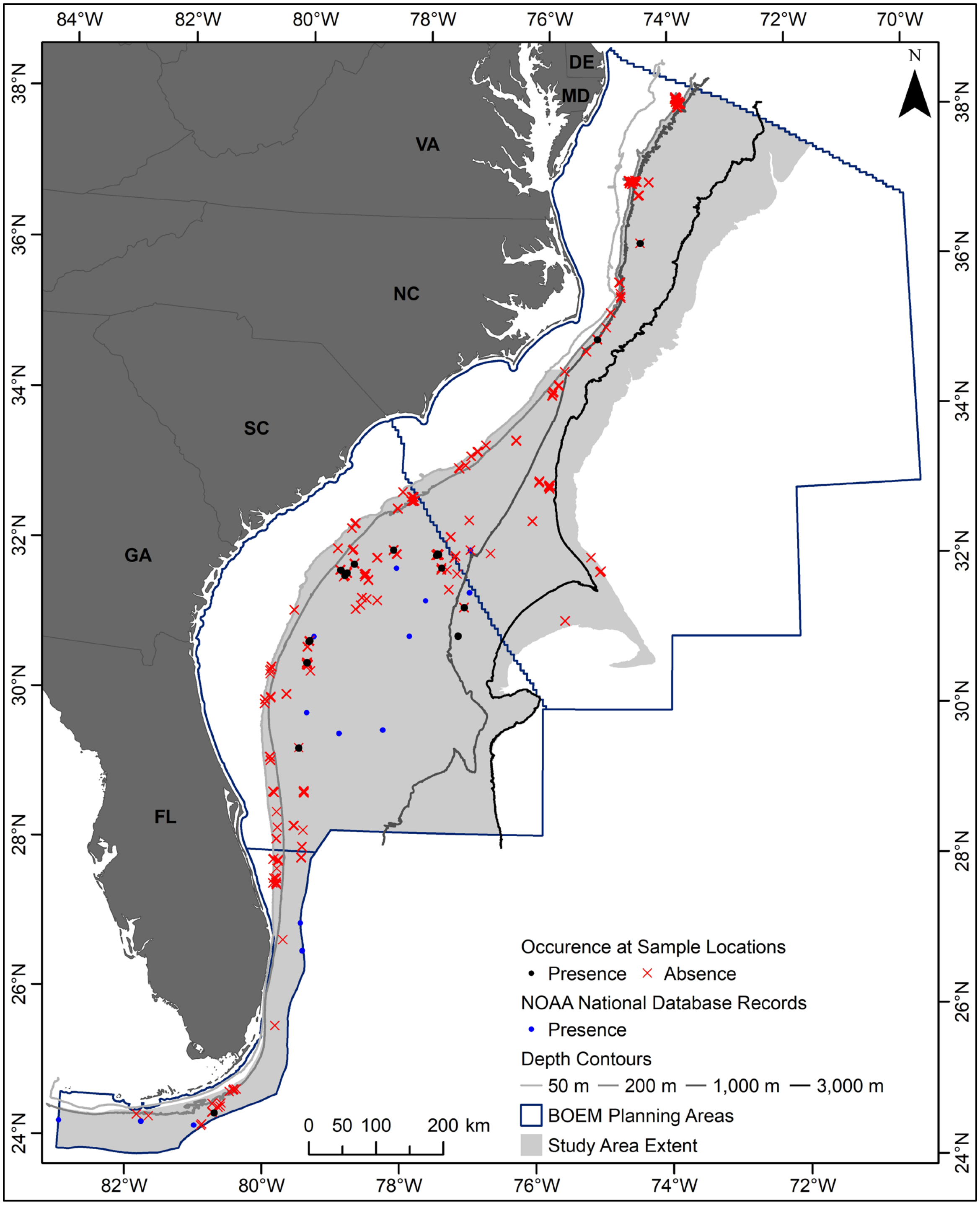

Figure D-31. Occurrence records for the black coral *Bathypathes*.

This map shows the observed occurrence (presence-absence) of *Bathypathes* at sample locations in the presence-absence database compiled for this study. Additional records of occurrence (presence) from the NOAA National Database are also displayed.

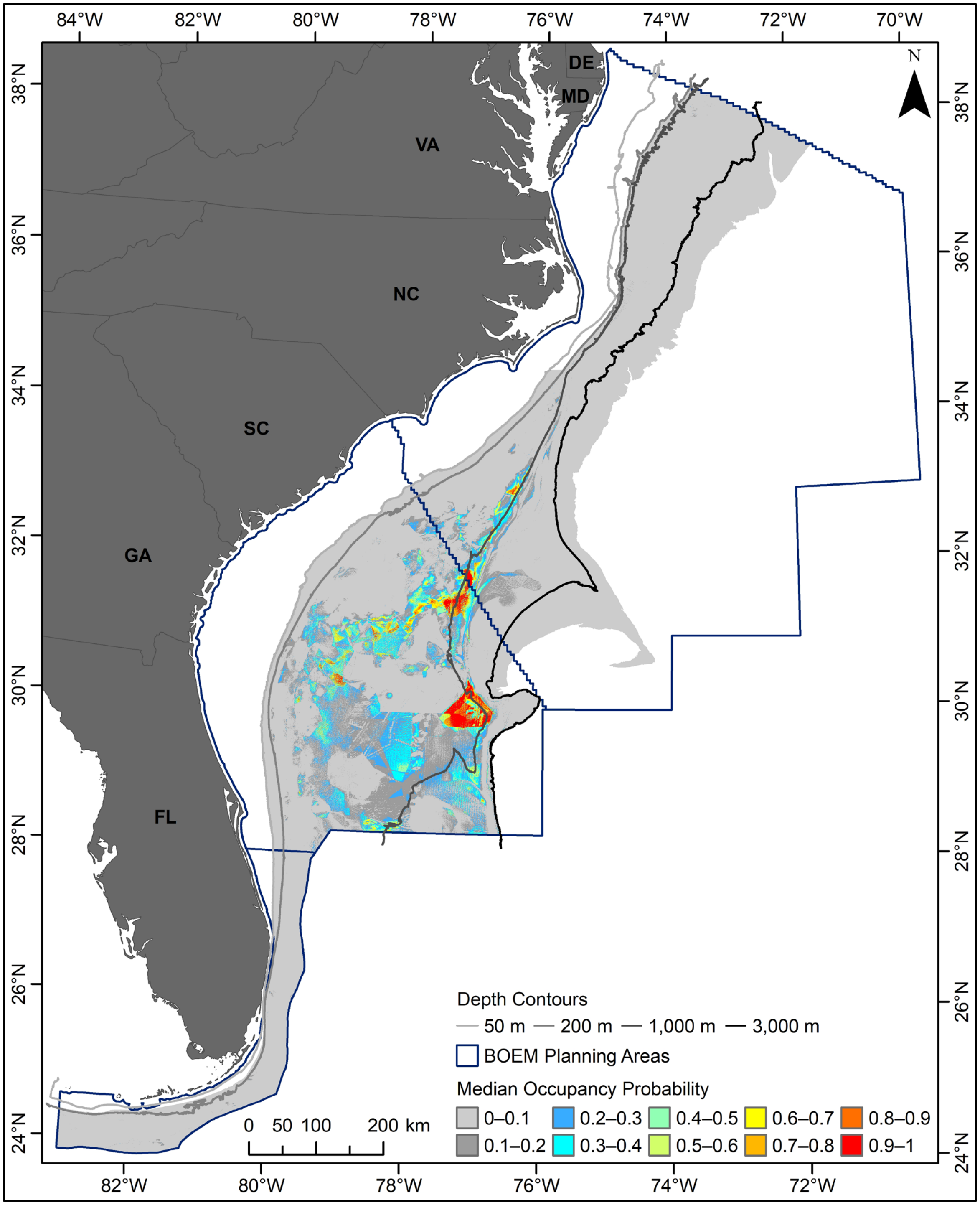

Figure D-32. Predicted occurrence of the black coral *Bathypathes*.
This map shows the posterior median occupancy probability for *Bathypathes* from the multi-taxon model.

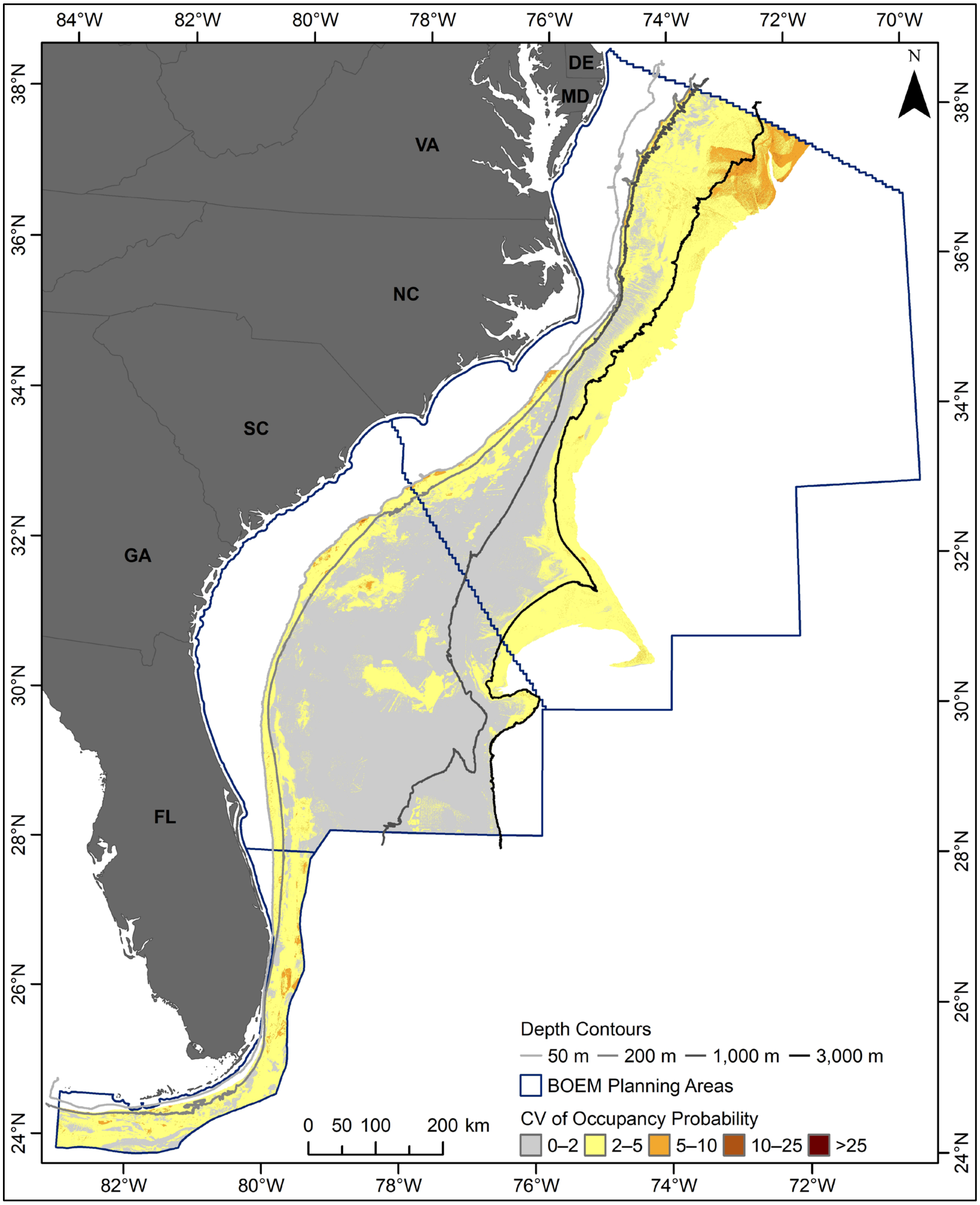

Figure D-33. Variability in the predicted occurrence of the black coral *Bathypathes*.
This map shows the posterior coefficient of variation of occupancy probability for *Bathypathes* from the multi-taxon model.

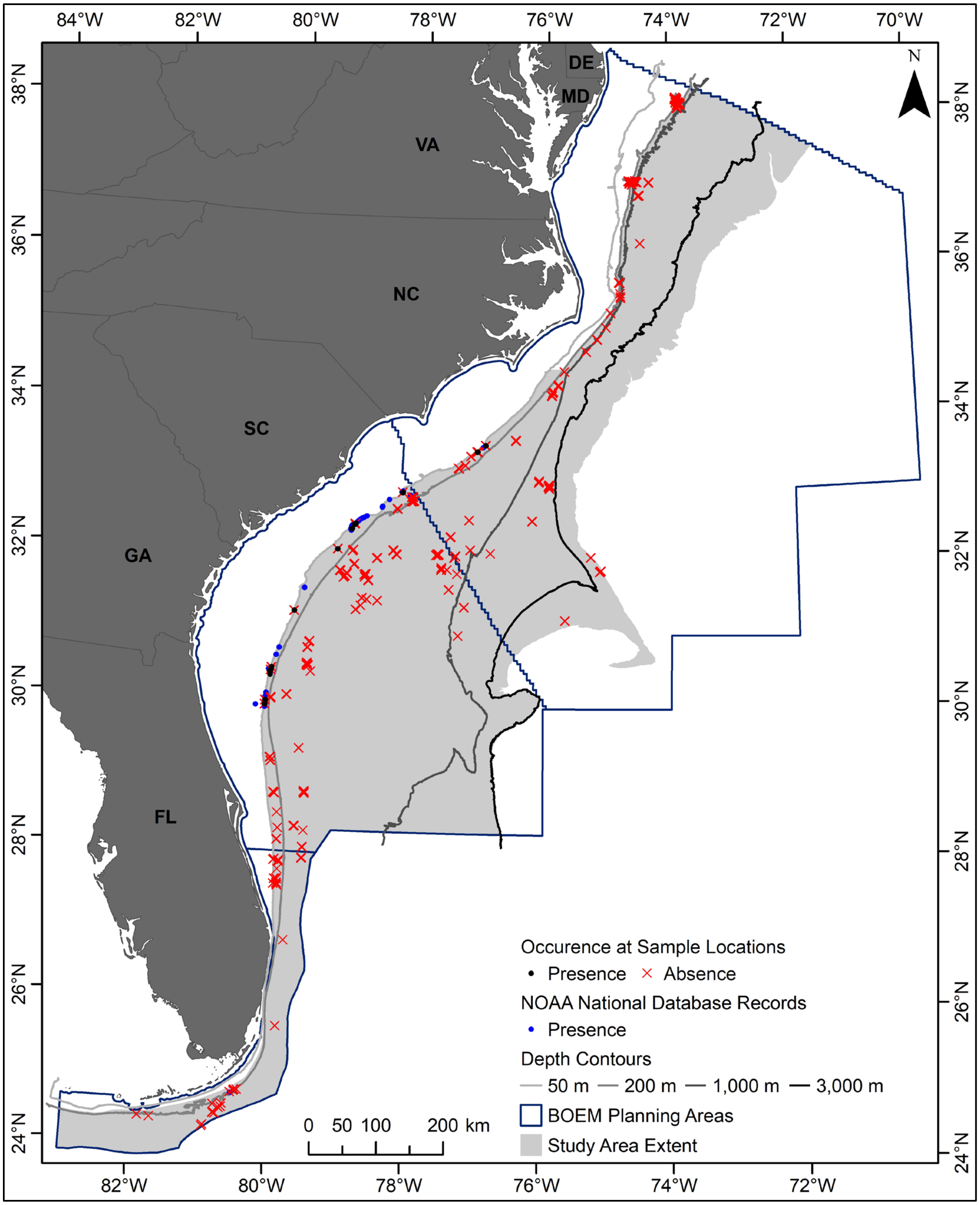

Figure D-34. Occurrence records for the gorgonian coral *Muricea*.
This map shows the observed occurrence (presence-absence) of *Muricea* at sample locations in the presence-absence database compiled for this study. Additional records of occurrence (presence) from the NOAA National Database are also displayed.

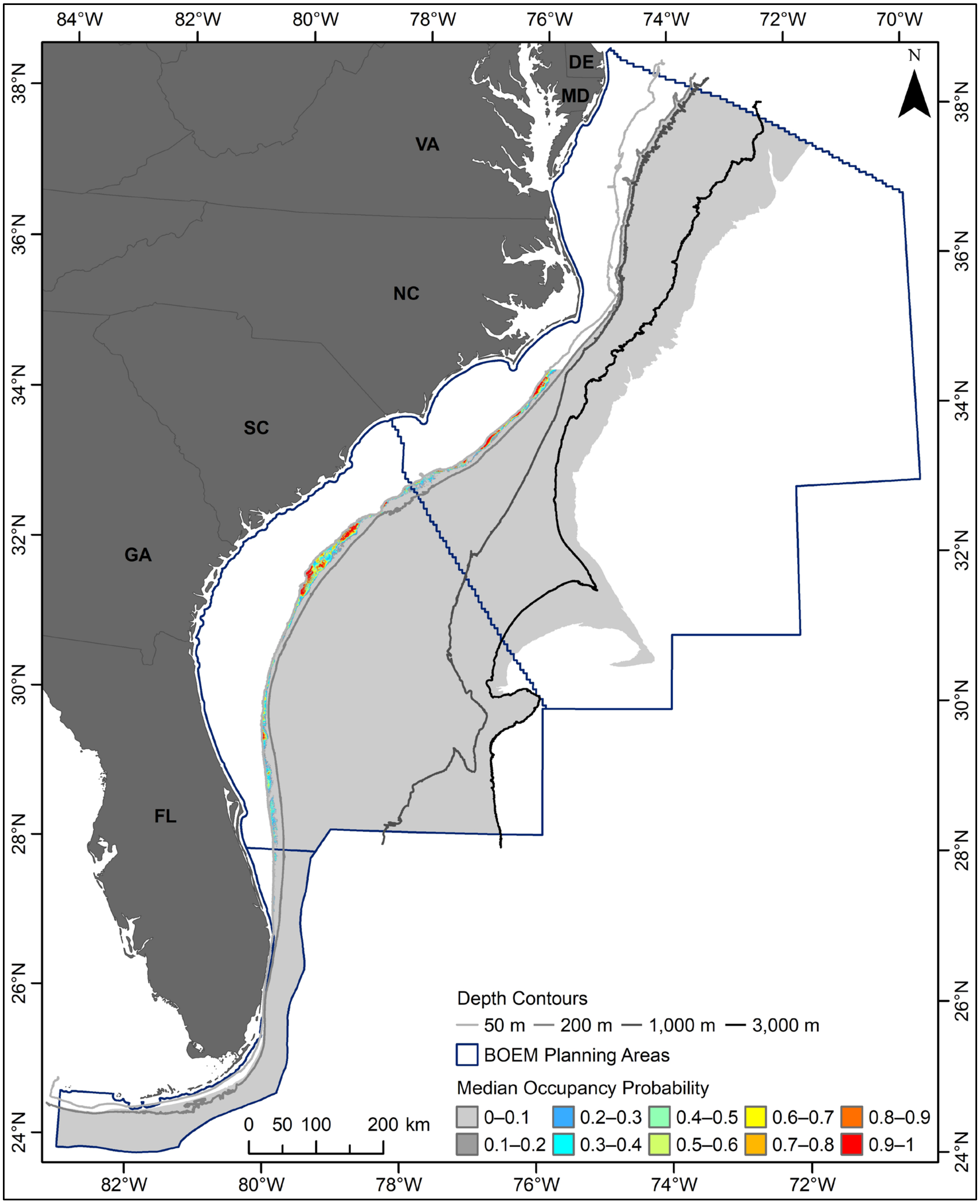

Figure D-35. Predicted occurrence of the gorgonian coral *Muricea*.
This map shows the posterior median occupancy probability for *Muricea* from the multi-taxon model.

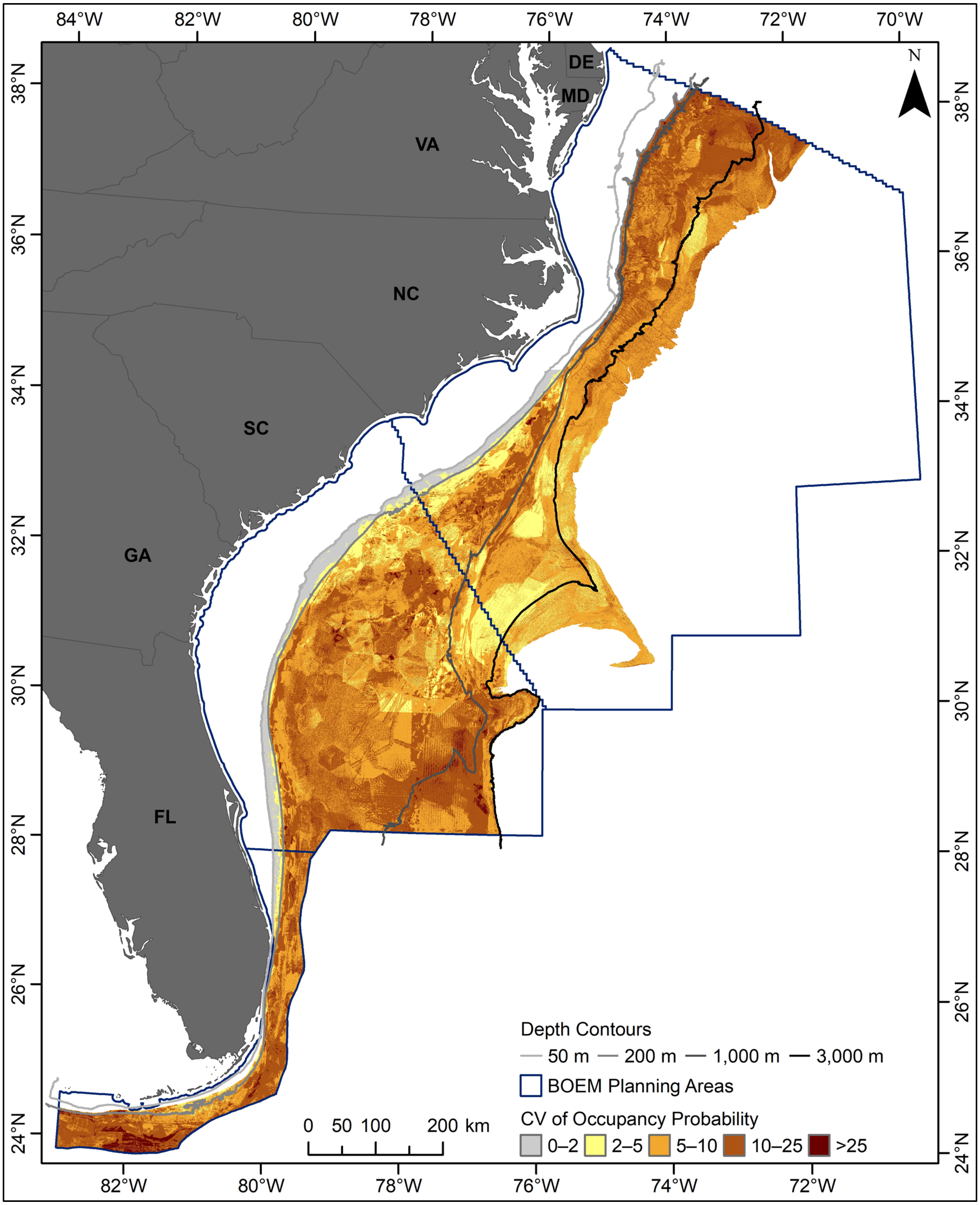

Figure D-36. Variability in the predicted occurrence of the gorgonian coral *Muricea*.
This map shows the posterior coefficient of variation of occupancy probability for *Muricea* from the multi-taxon model.

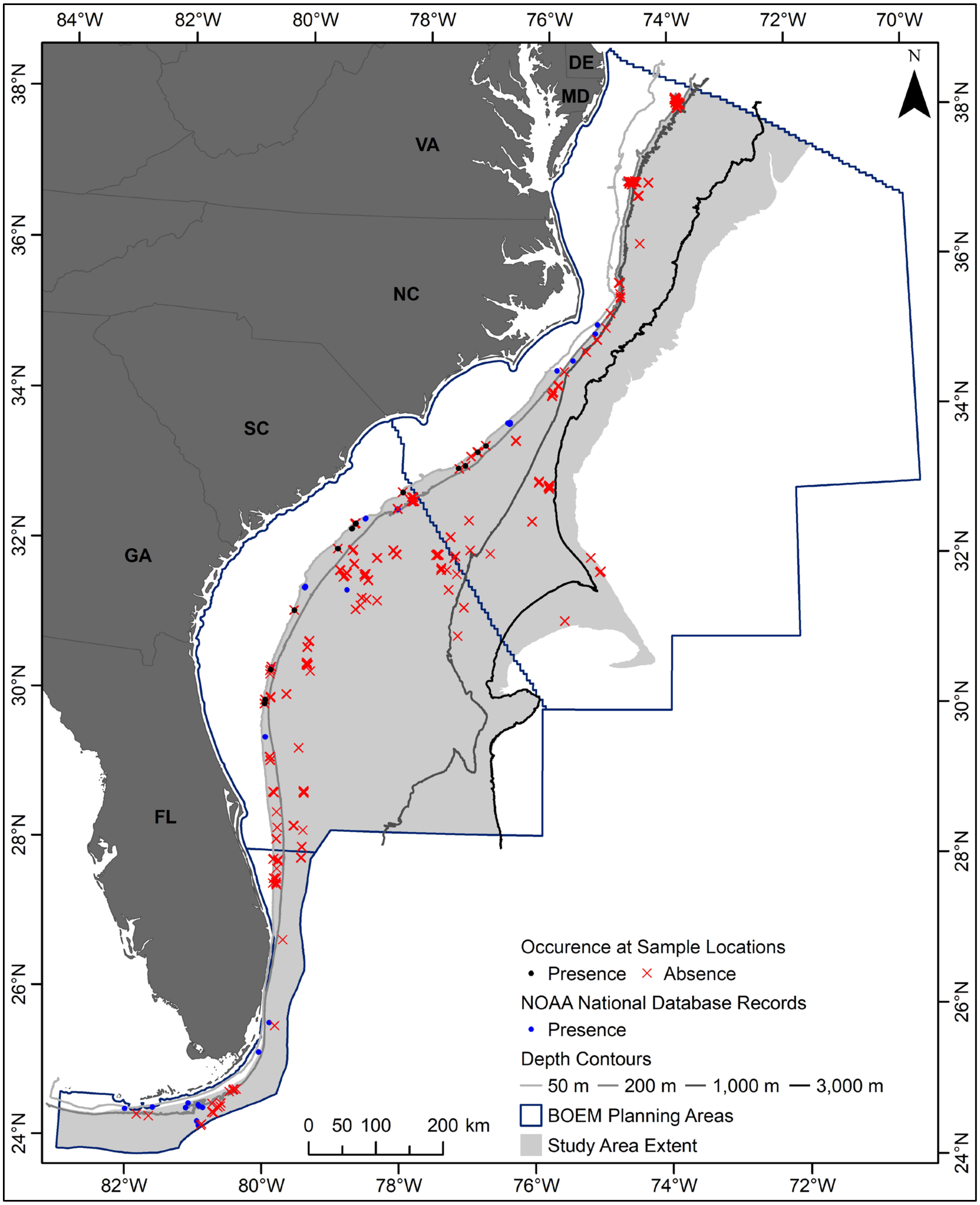

Figure D-37. Occurrence records for the gorgonian coral *Thesea*.
This map shows the observed occurrence (presence-absence) of *Thesea* at sample locations in the presence-absence database compiled for this study. Additional records of occurrence (presence) from the NOAA National Database are also displayed.

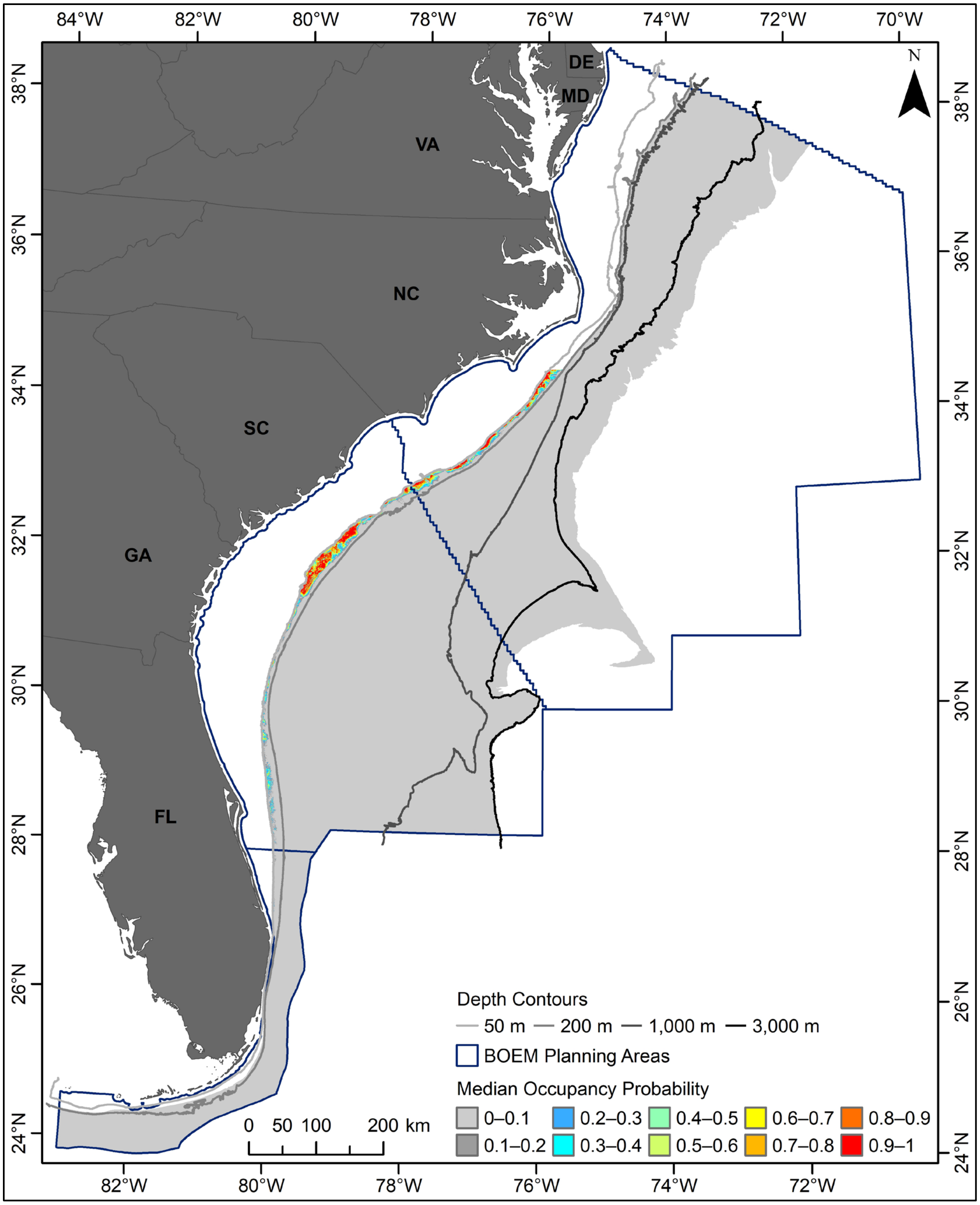

Figure D-38. Predicted occurrence of the gorgonian coral *Thesea*.
This map shows the posterior median occupancy probability for *Thesea* from the multi-taxon model.

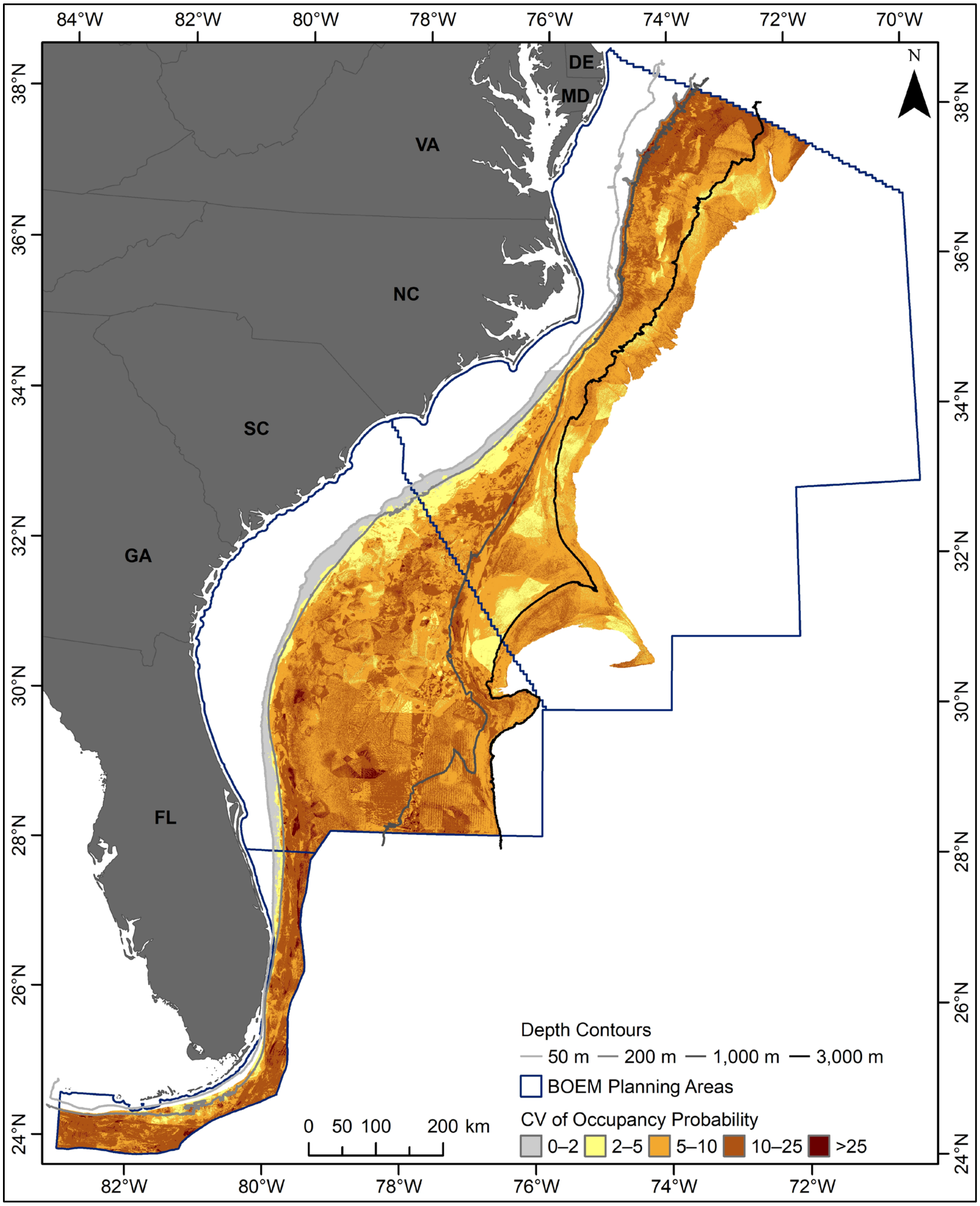

Figure D-39. Variability in the predicted occurrence of the gorgonian coral *Thesea*.
This map shows the posterior coefficient of variation of occupancy probability for *Thesea* from the multi-taxon model.

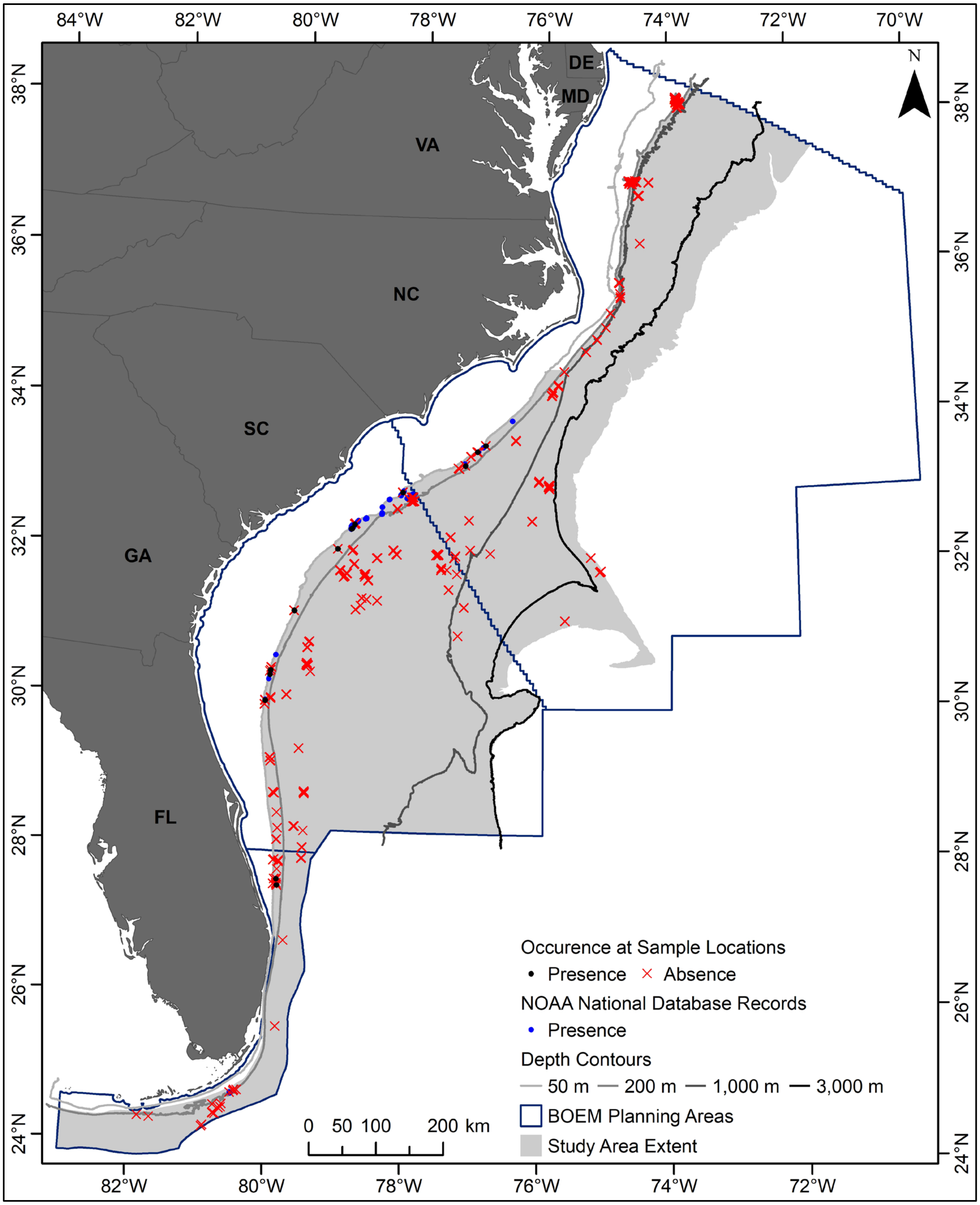

Figure D-40. Occurrence records for the gorgonian coral *Nicella*.
This map shows the observed occurrence (presence-absence) of *Nicella* at sample locations in the presence-absence database compiled for this study. Additional records of occurrence (presence) from the NOAA National Database are also displayed.

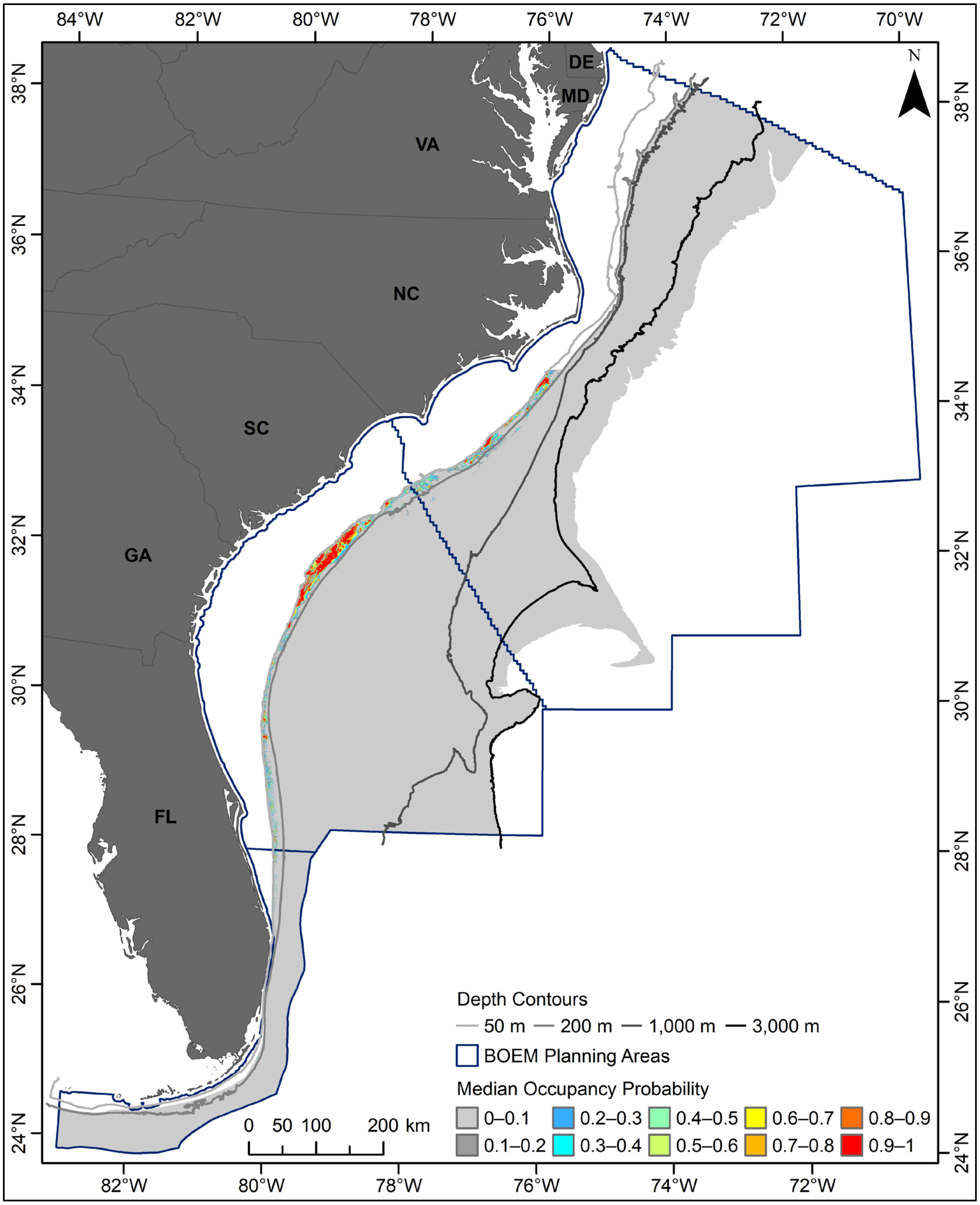

Figure D-41. Predicted occurrence of the gorgonian coral *Nicella*.
This map shows the posterior median occupancy probability for *Nicella* from the multi-taxon model.

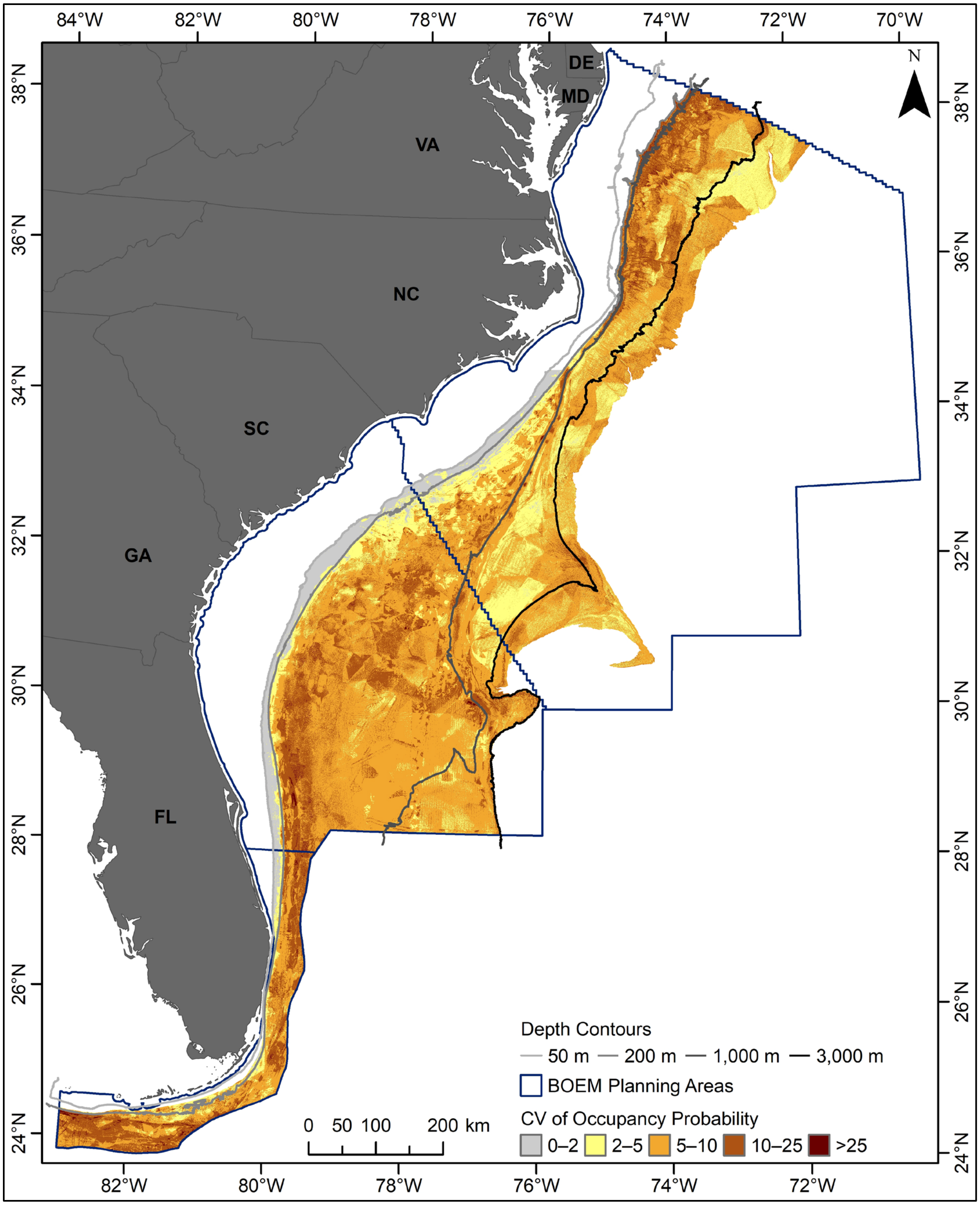

Figure D-42. Variability in the predicted occurrence of the gorgonian coral *Nicella*.
This map shows the posterior coefficient of variation of occupancy probability for *Nicella* from the multi-taxon model.

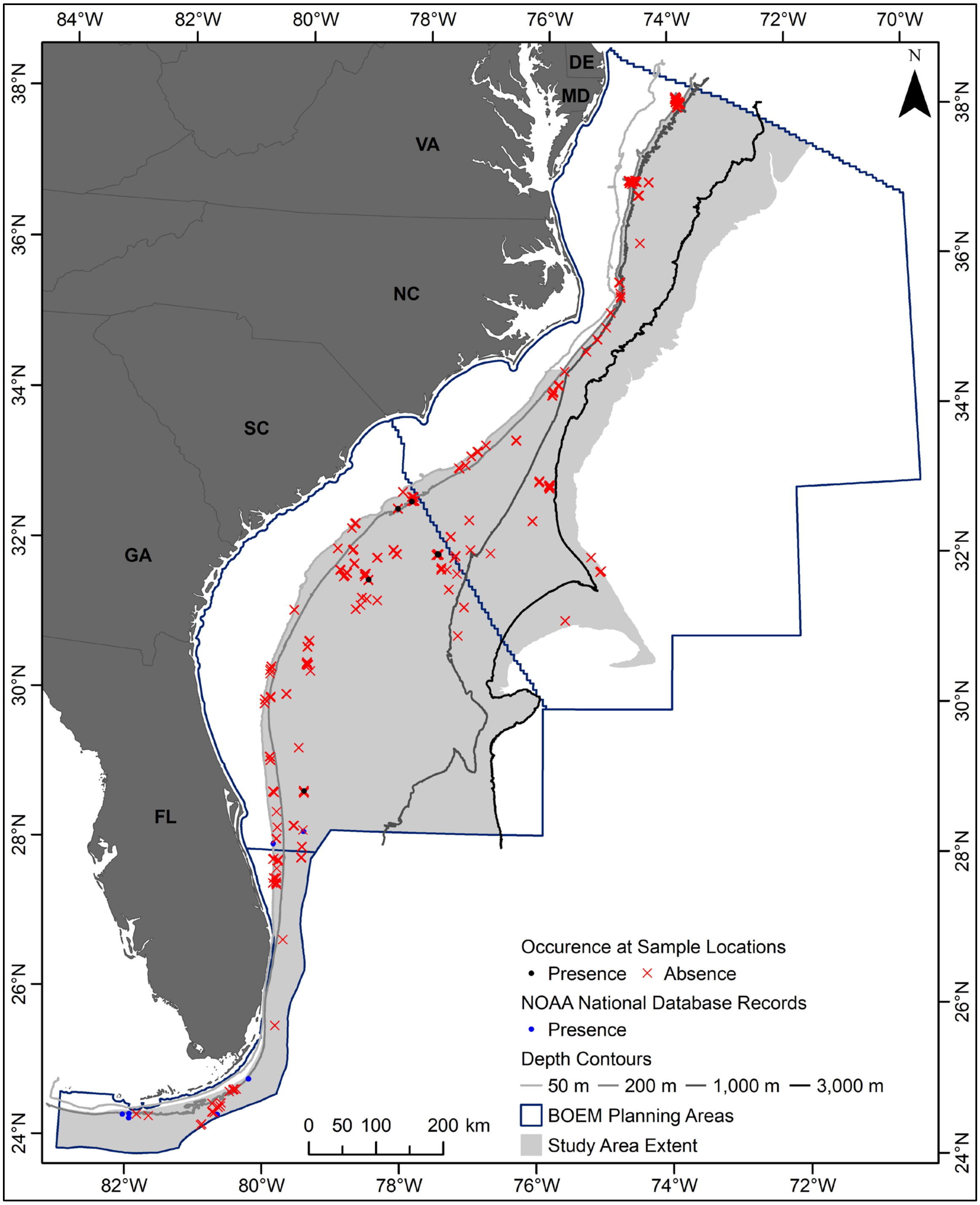

Figure D-43. Occurrence records for the gorgonian coral *Callogorgia*.
This map shows the observed occurrence (presence-absence) of *Callogorgia* at sample locations in the presence-absence database compiled for this study. Additional records of occurrence (presence) from the NOAA National Database are also displayed.

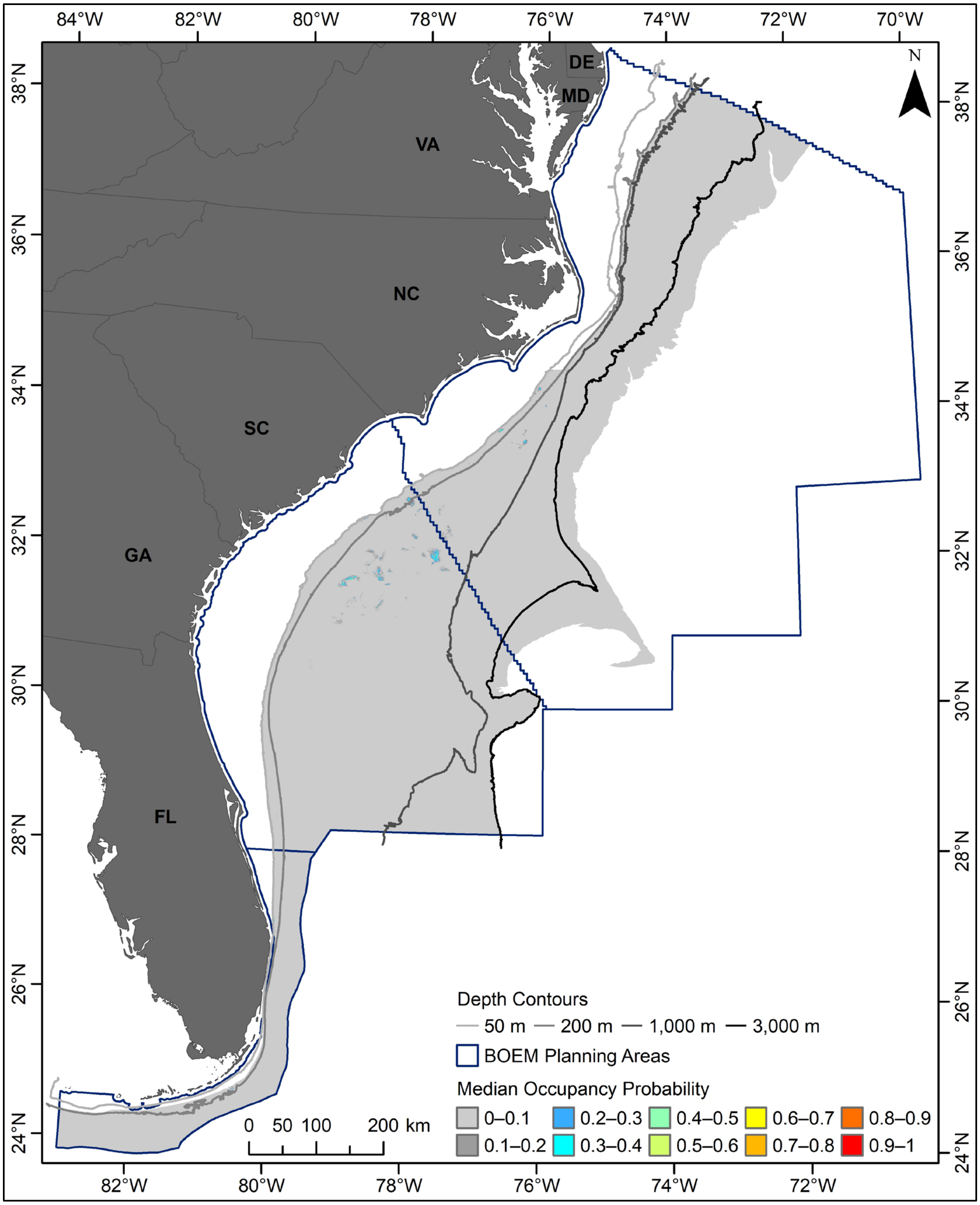

Figure D-44. Predicted occurrence of the gorgonian coral *Callogorgia*.
This map shows the posterior median occupancy probability for *Callogorgia* from the multi-taxon model.

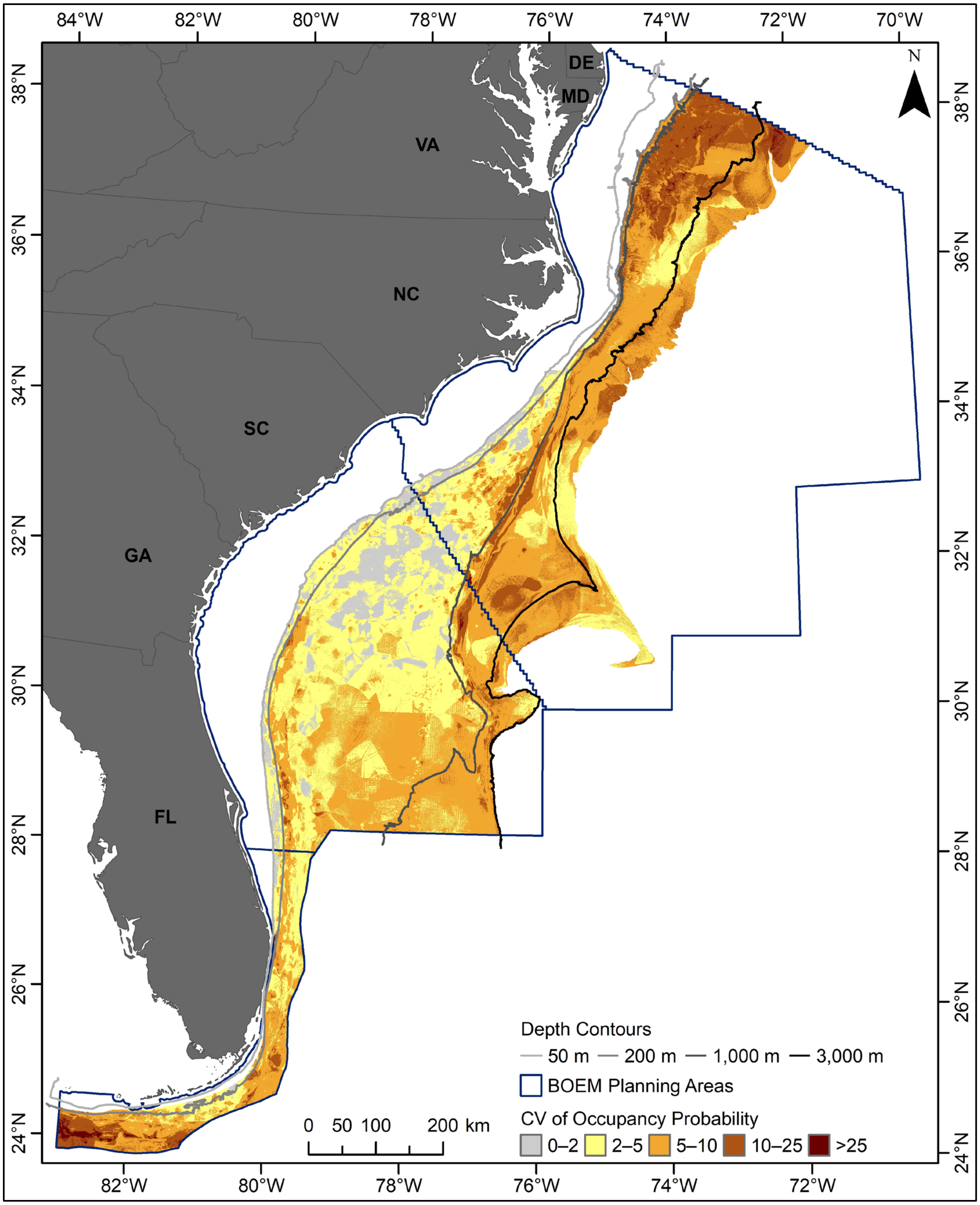

Figure D-45. Variability in the predicted occurrence of the gorgonian coral *Callogorgia*.
This map shows the posterior coefficient of variation of occupancy probability for *Callogorgia* from the multi-taxon model.

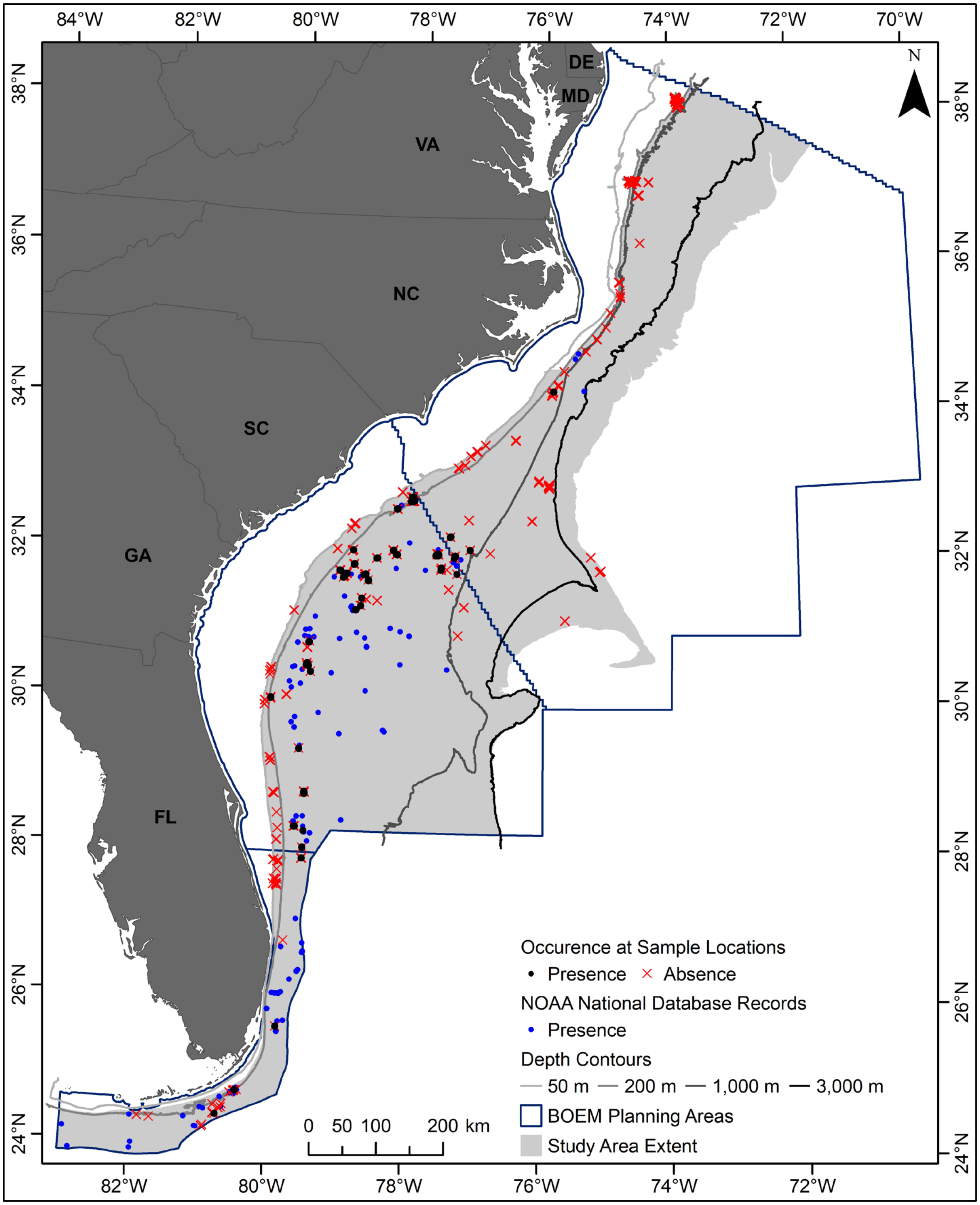

Figure D-46. Occurrence records for the gorgonian coral *Plumarella*.
This map shows the observed occurrence (presence-absence) of *Plumarella* at sample locations in the presence-absence database compiled for this study. Additional records of occurrence (presence) from the NOAA National Database are also displayed.

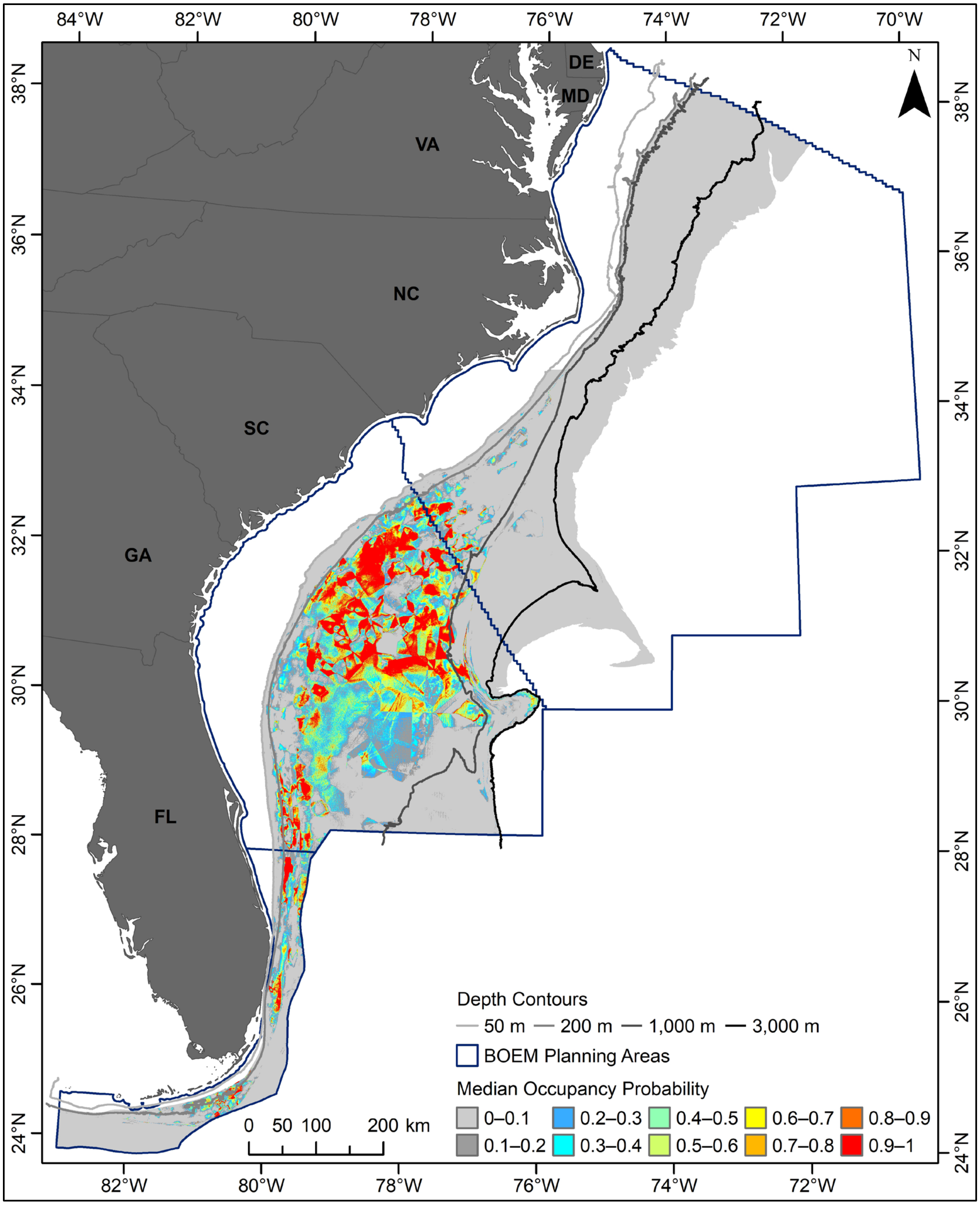

Figure D-47. Predicted occurrence of the gorgonian coral *Plumarella*.
This map shows the posterior median occupancy probability for *Plumarella* from the multi-taxon model.

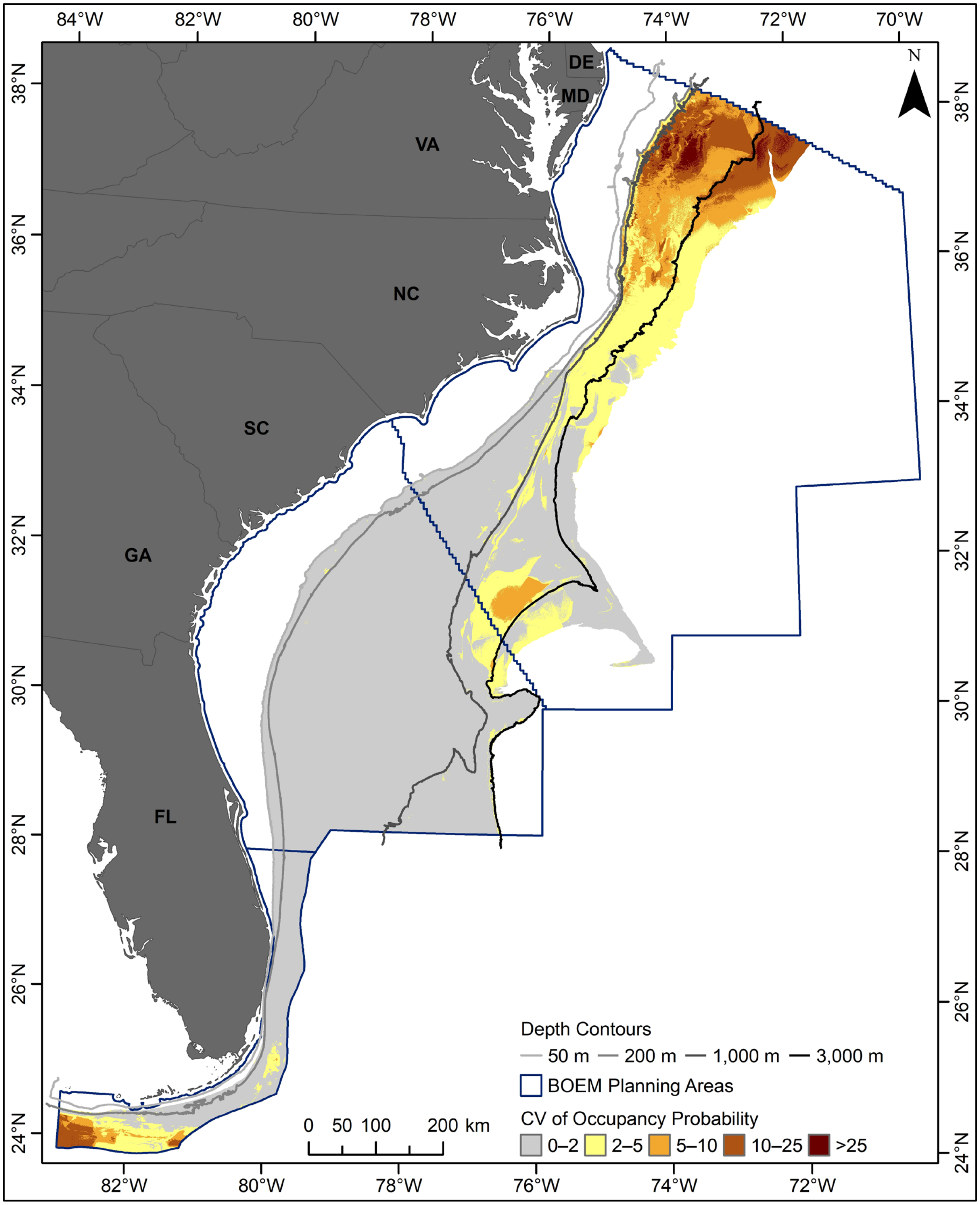

Figure D-48. Variability in the predicted occurrence of the gorgonian coral *Plumarella*.
This map shows the posterior coefficient of variation of occupancy probability for *Plumarella* from the multi-taxon model.

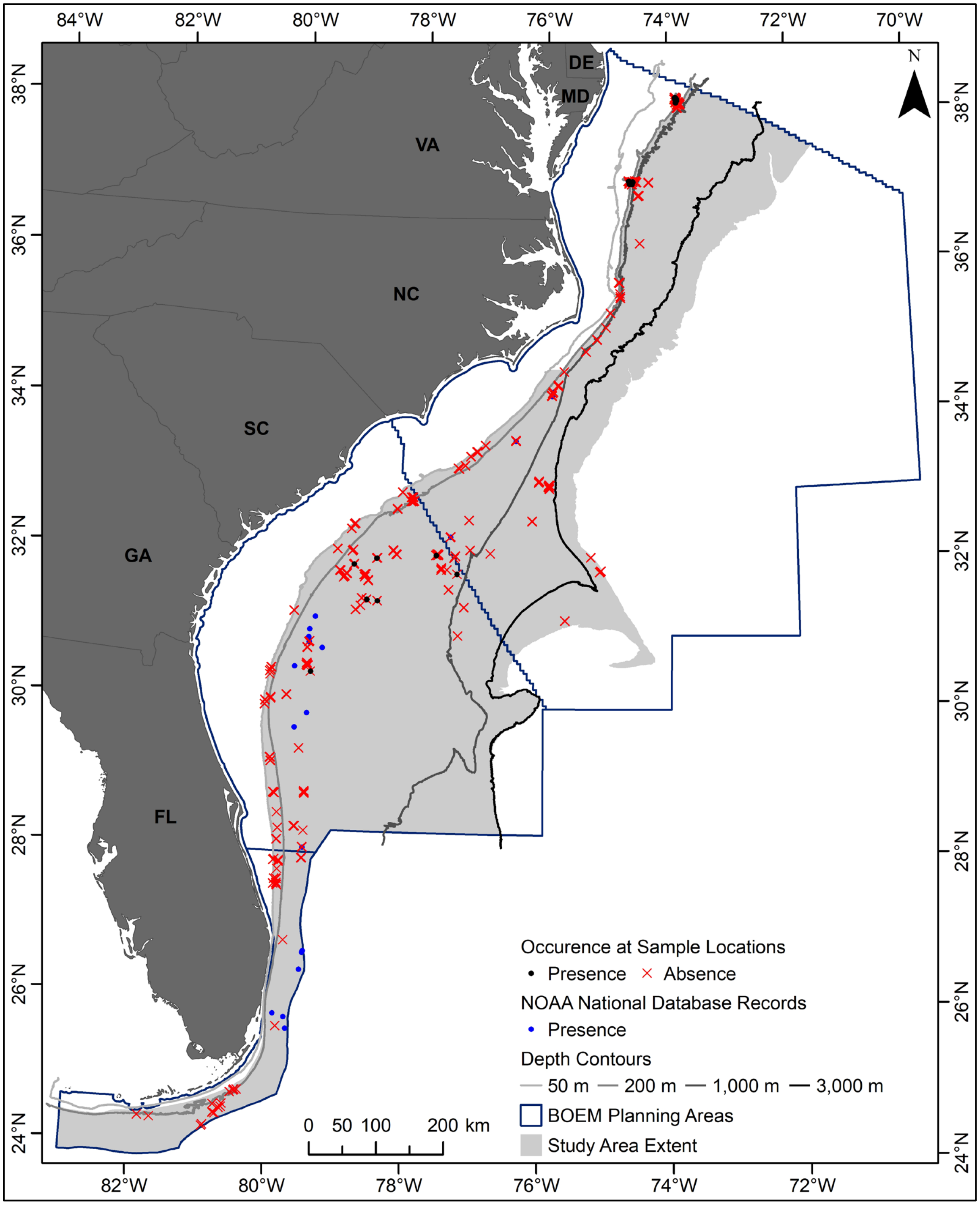

Figure D-49. Occurrence records for the gorgonian coral *Anthothela*.
This map shows the observed occurrence (presence-absence) of *Anthothela* at sample locations in the presence-absence database compiled for this study. Additional records of occurrence (presence) from the NOAA National Database are also displayed.

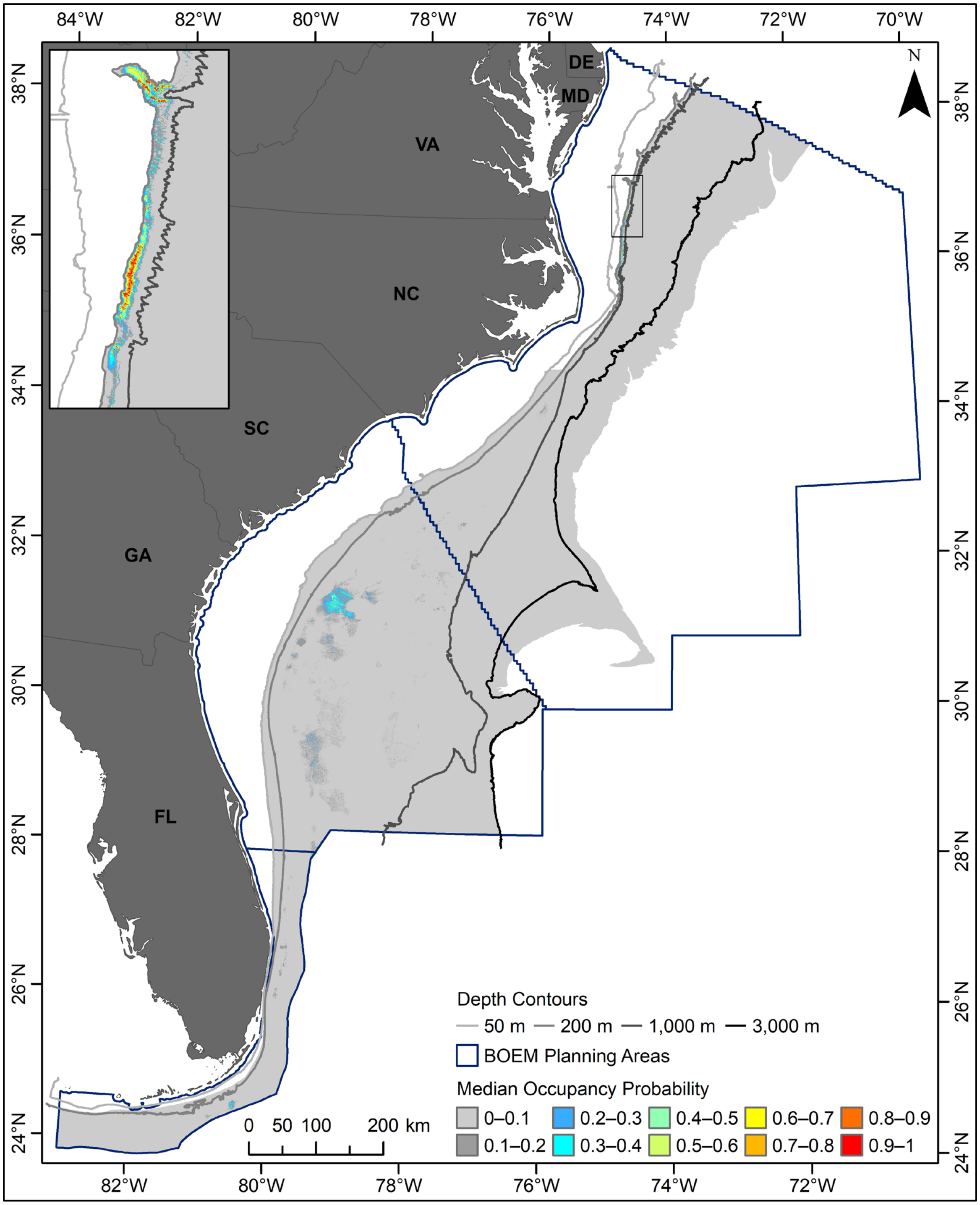

Figure D-50. Predicted occurrence of the gorgonian coral *Anthothela*.
This map shows the posterior median occupancy probability for *Anthothela* from the multi-taxon model.

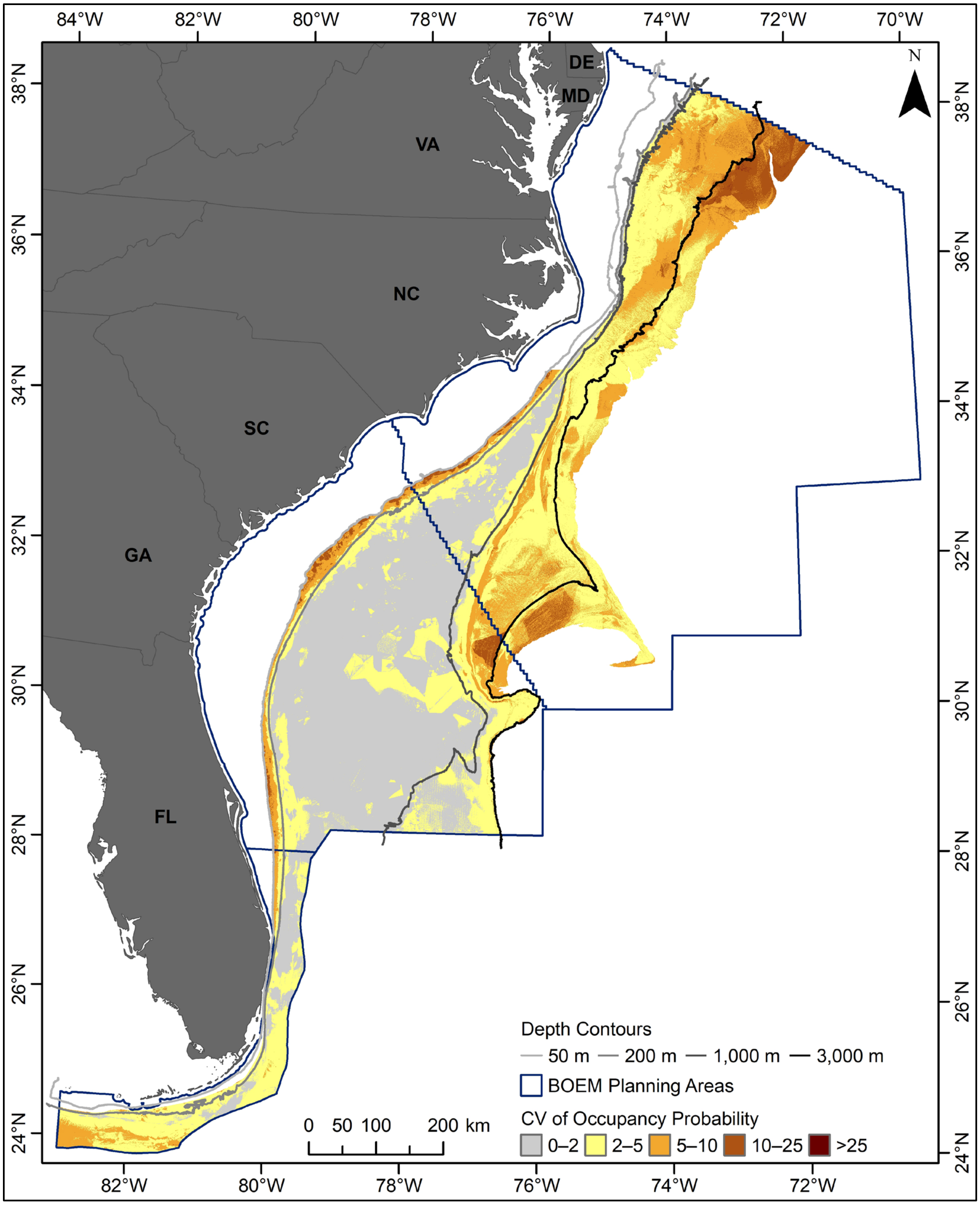

Figure D-51. Variability in the predicted occurrence of the gorgonian coral *Anthothela*.
This map shows the posterior coefficient of variation of occupancy probability for *Anthothela* from the multi-taxon model.

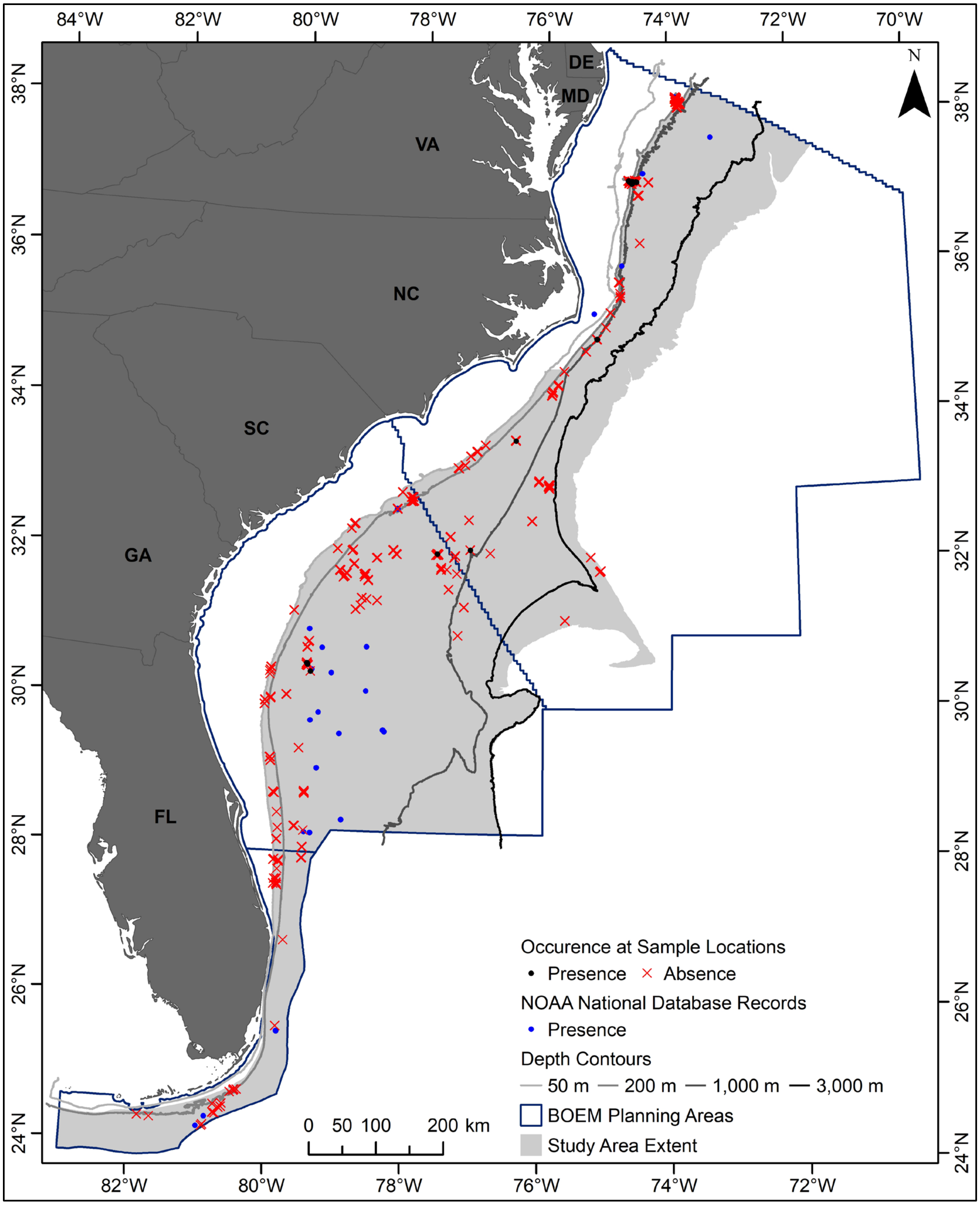

Figure D-52. Occurrence records for the gorgonian coral *Acanthogorgia*.
This map shows the observed occurrence (presence-absence) of *Acanthogorgia* at sample locations in the presence-absence database compiled for this study. Additional records of occurrence (presence) from the NOAA National Database are also displayed.

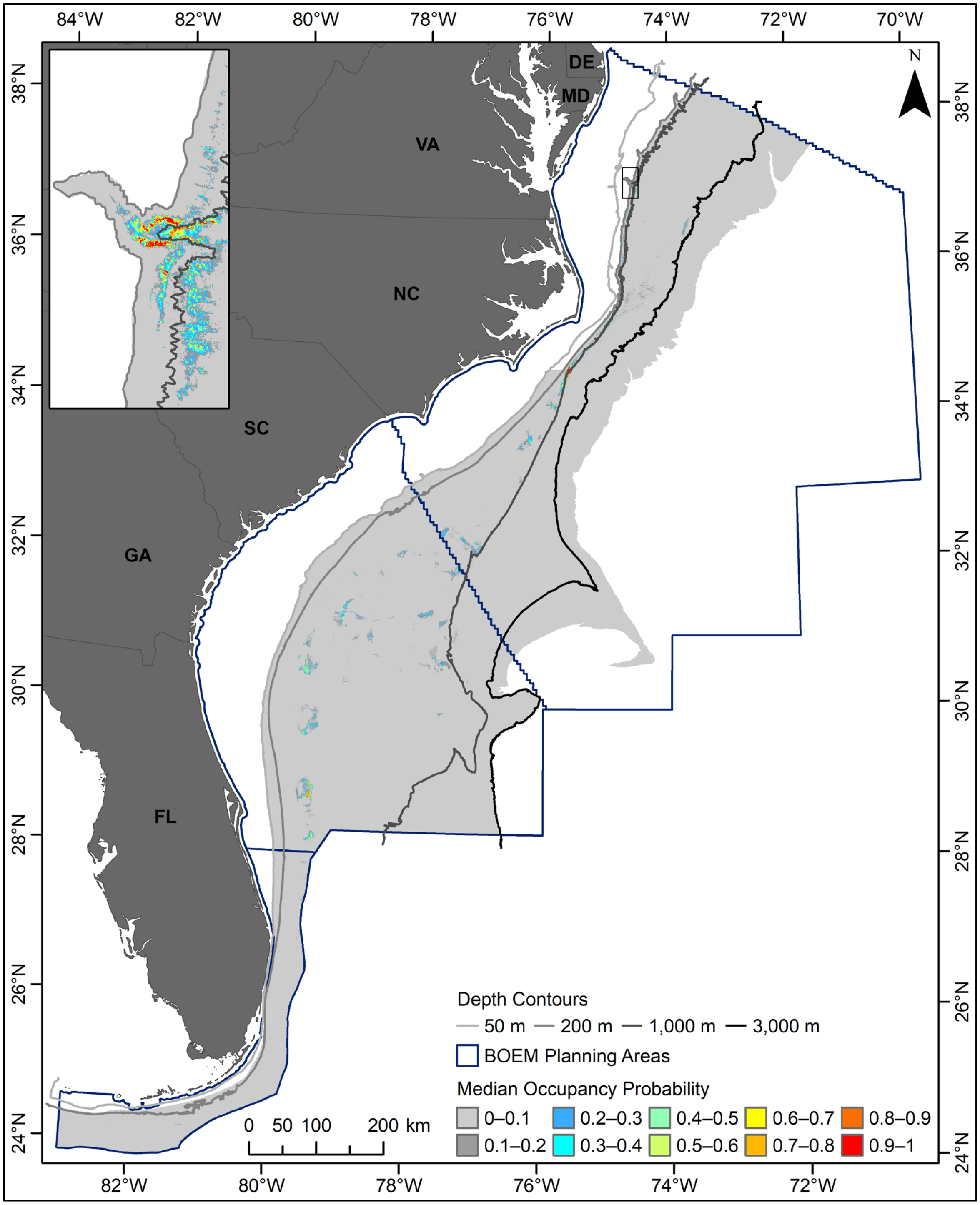

Figure D-53. Predicted occurrence of the gorgonian coral *Acanthogorgia*.
This map shows the posterior median occupancy probability for *Acanthogorgia* from the multi-taxon model.

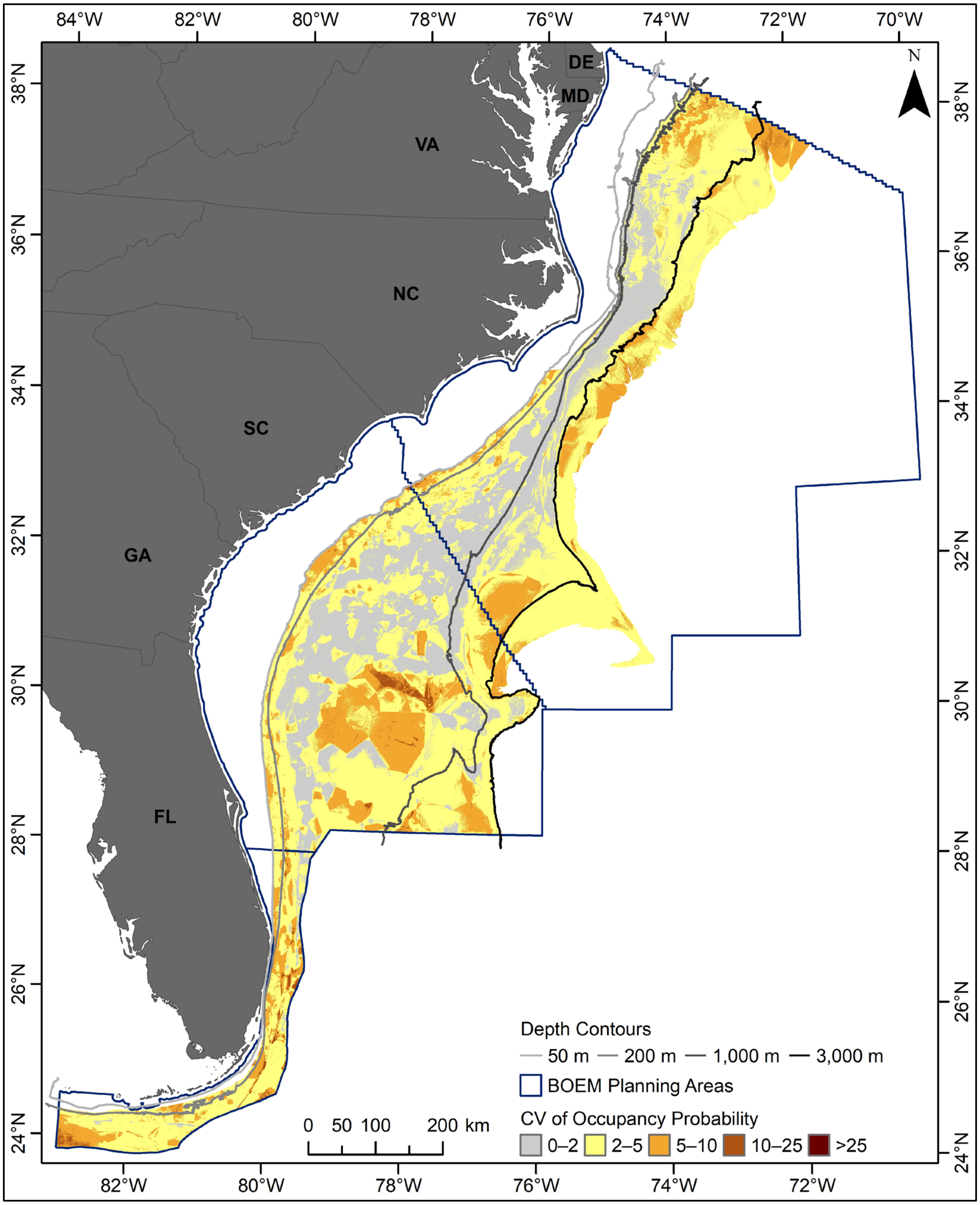

Figure D-54. Variability in the predicted occurrence of the gorgonian coral *Acanthogorgia*.
This map shows the posterior coefficient of variation of occupancy probability for *Acanthogorgia* from the multi-taxon model.

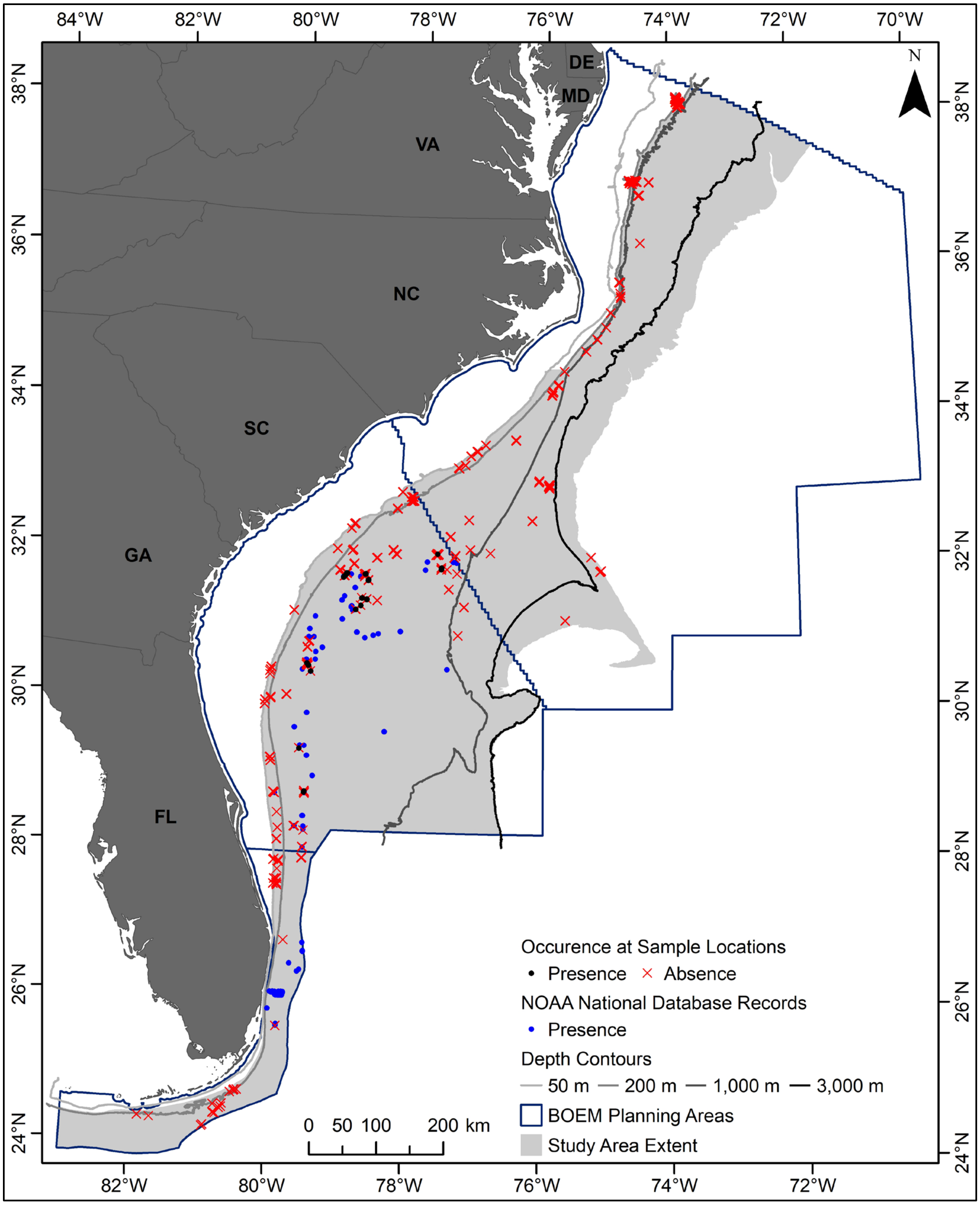

Figure D-55. Occurrence records for the gorgonian coral *Eunicella*.
This map shows the observed occurrence (presence-absence) of *Eunicella* at sample locations in the presence-absence database compiled for this study. Additional records of occurrence (presence) from the NOAA National Database are also displayed.

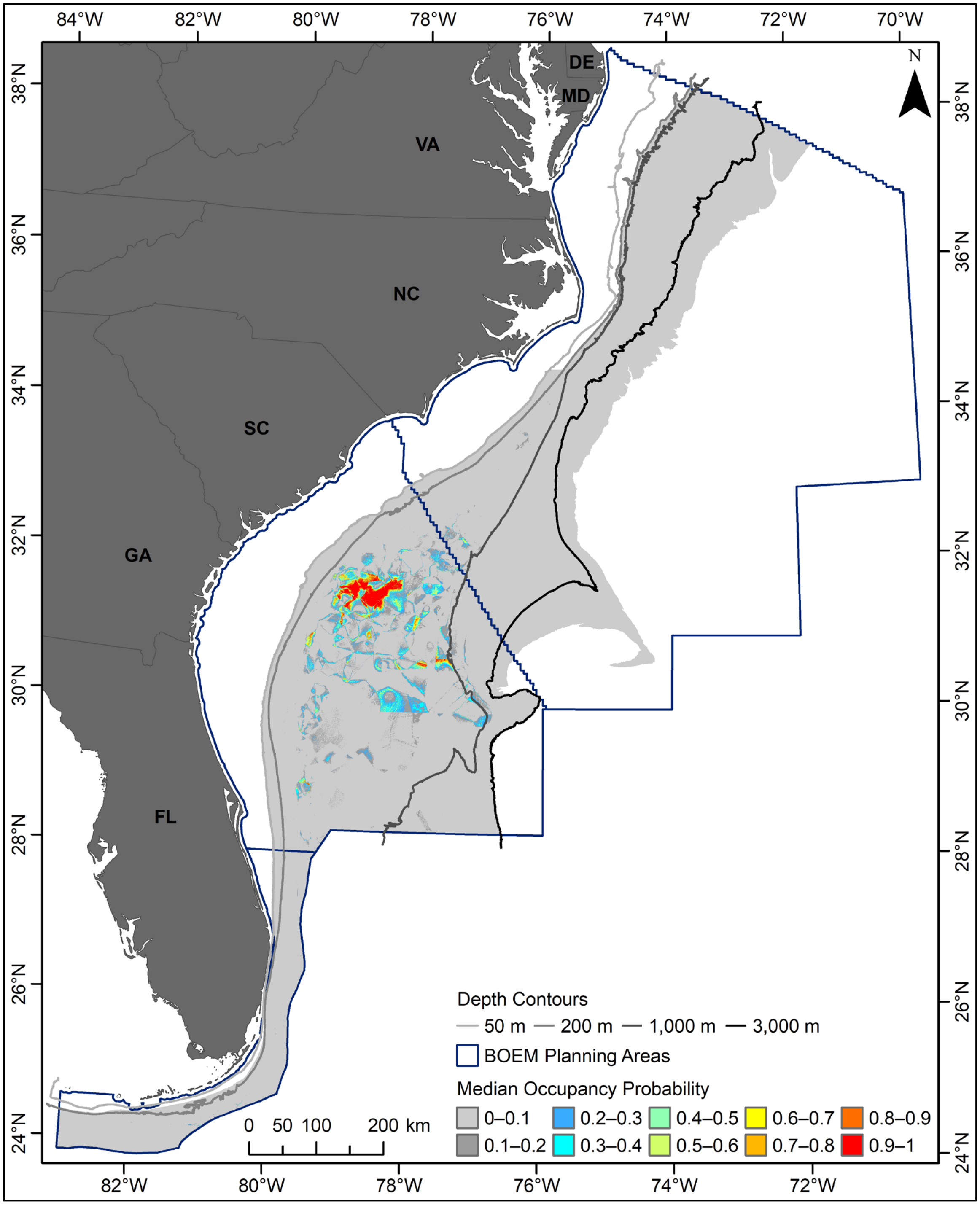

Figure D-56. Predicted occurrence of the gorgonian coral *Eunicella*.
This map shows the posterior median occupancy probability for *Eunicella* from the multi-taxon model.

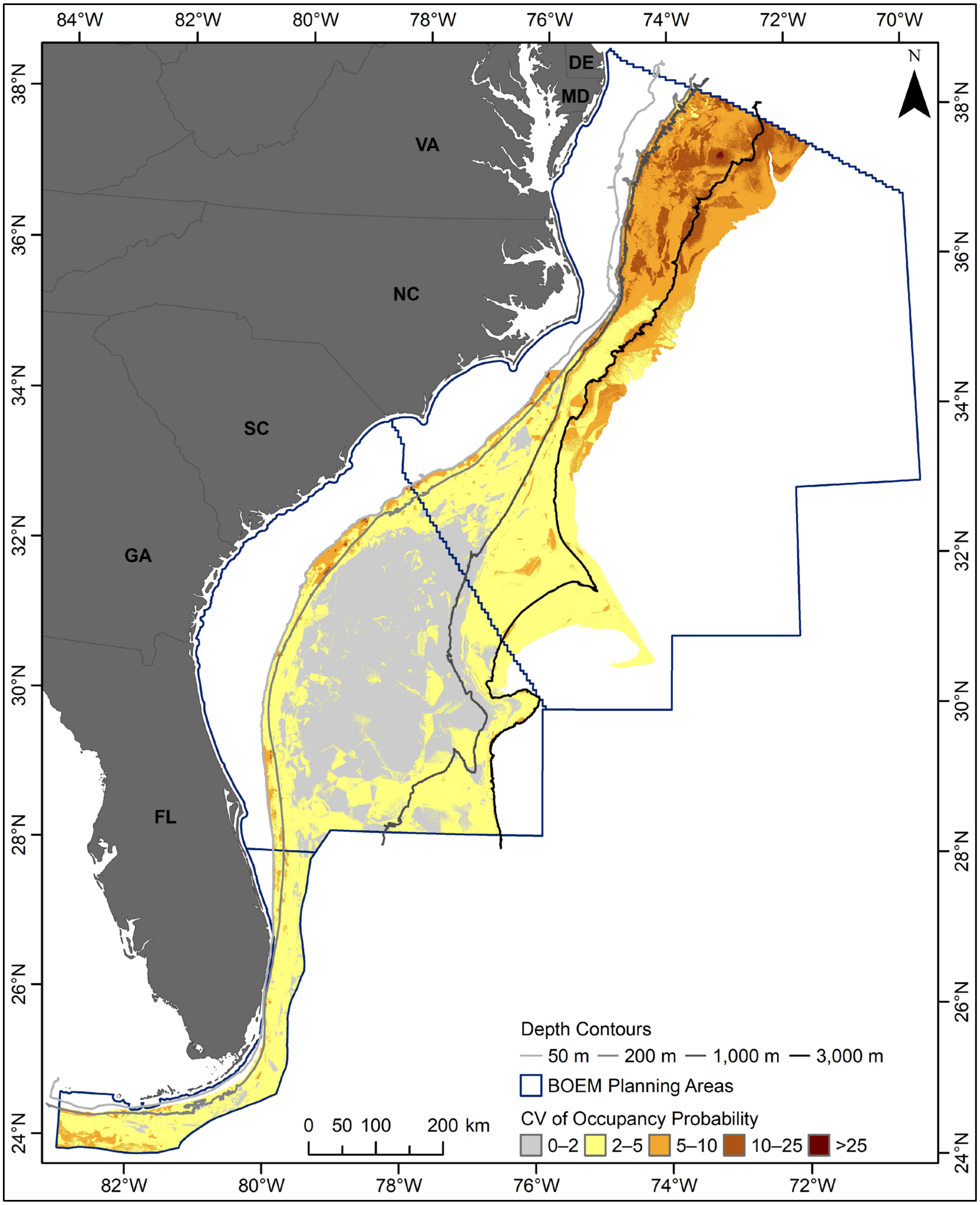

Figure D-57. Variability in the predicted occurrence of the gorgonian coral *Eunicella*.
This map shows the posterior coefficient of variation of occupancy probability for *Eunicella* from the multi-taxon model.

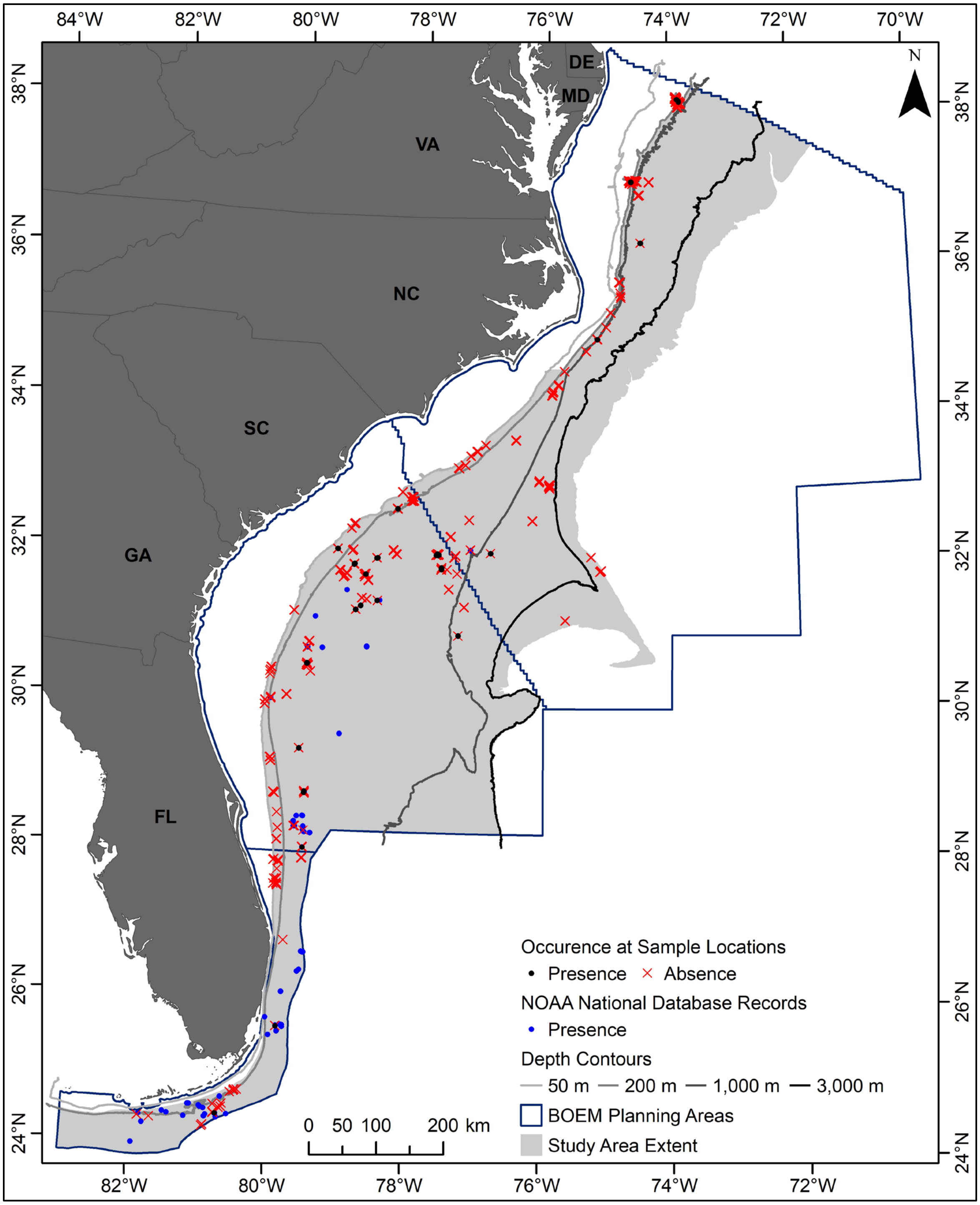

Figure D-58. Occurrence records for the gorgonian coral *Paramuricea*.
This map shows the observed occurrence (presence-absence) of *Paramuricea* at sample locations in the presence-absence database compiled for this study. Additional records of occurrence (presence) from the NOAA National Database are also displayed.

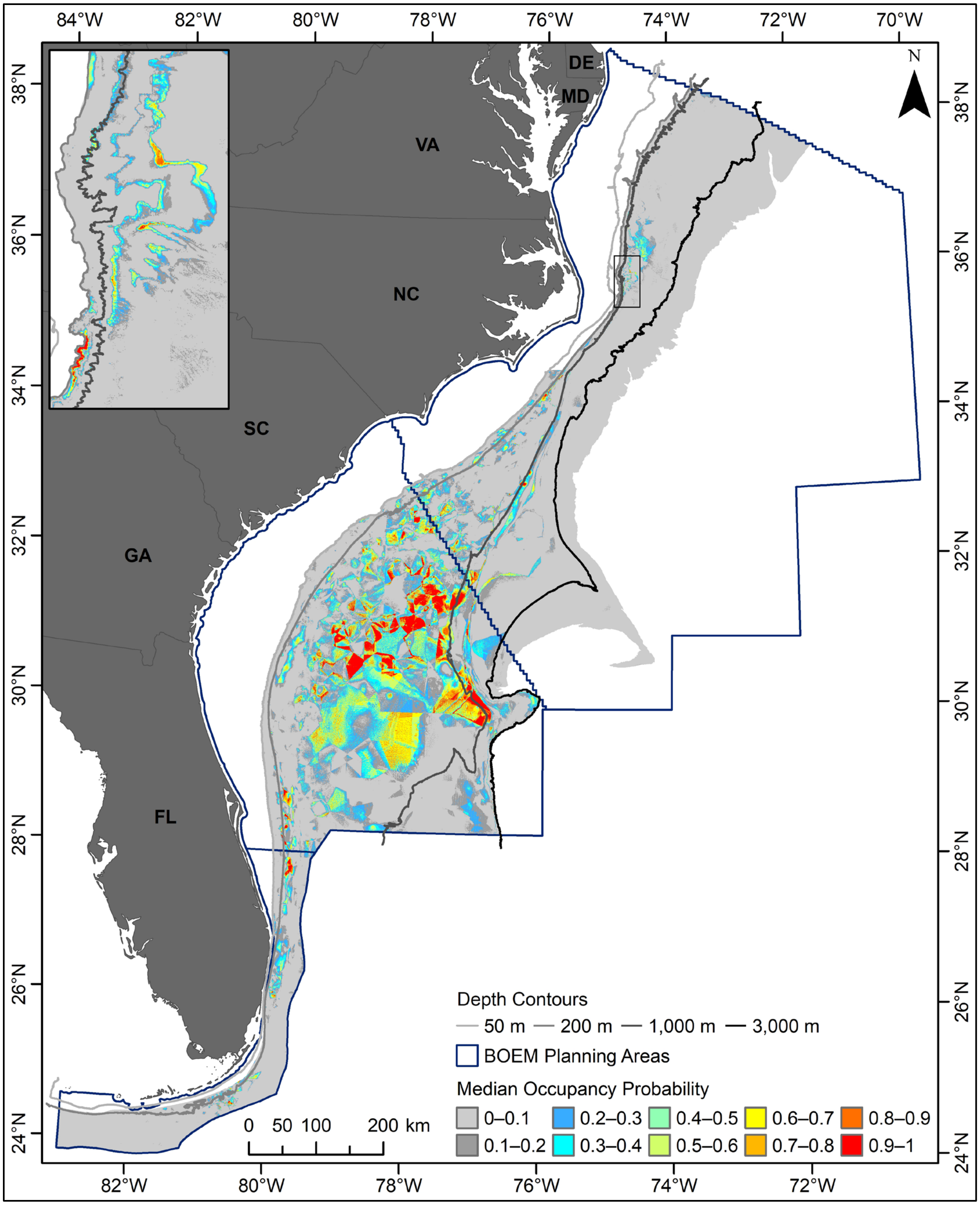

Figure D-59. Predicted occurrence of the gorgonian coral *Paramuricea*.
This map shows the posterior median occupancy probability for *Paramuricea* from the multi-taxon model.

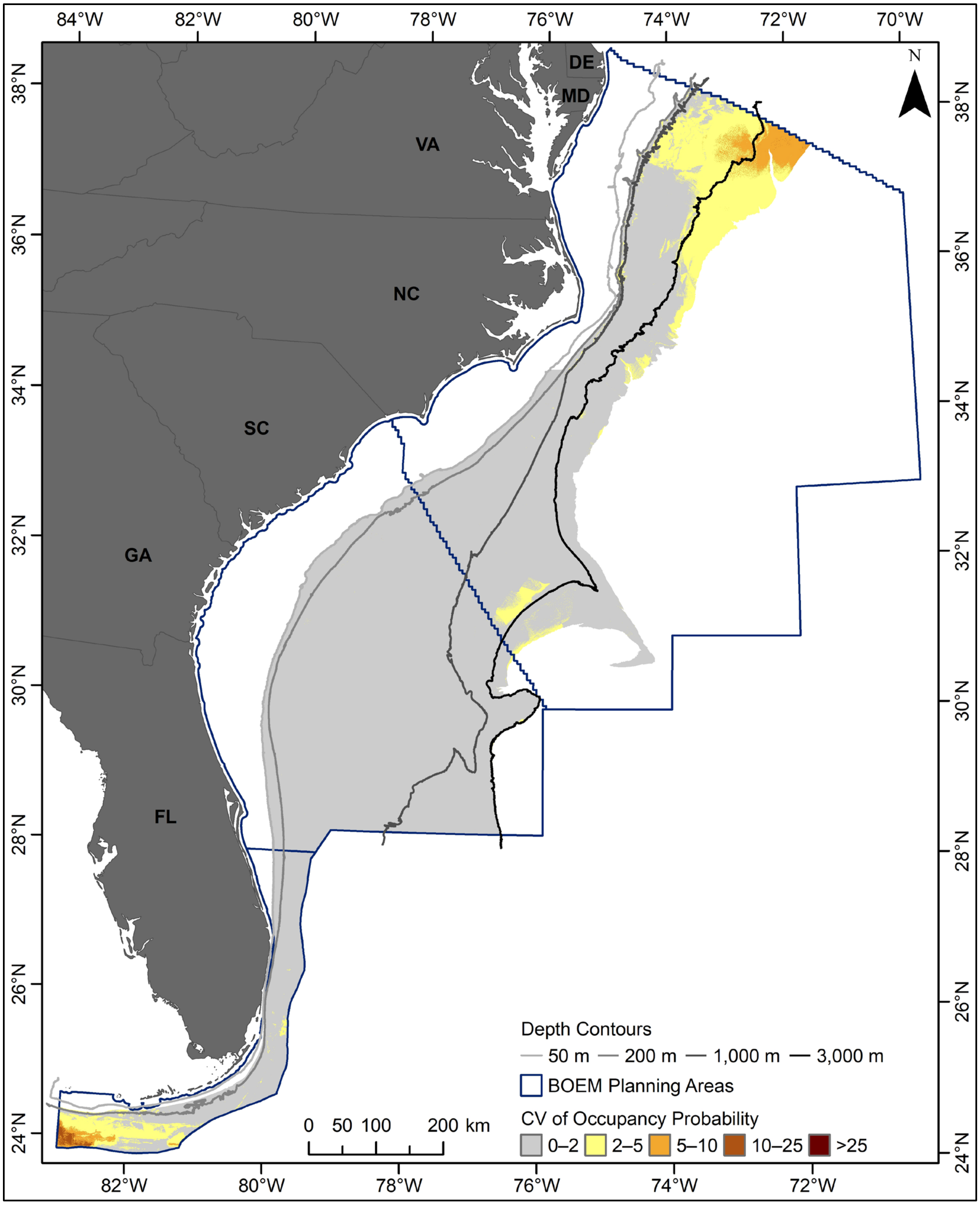

Figure D-60. Variability in the predicted occurrence of the gorgonian coral *Paramuricea*. This map shows the posterior coefficient of variation of occupancy probability for *Paramuricea* from the multi-taxon model.

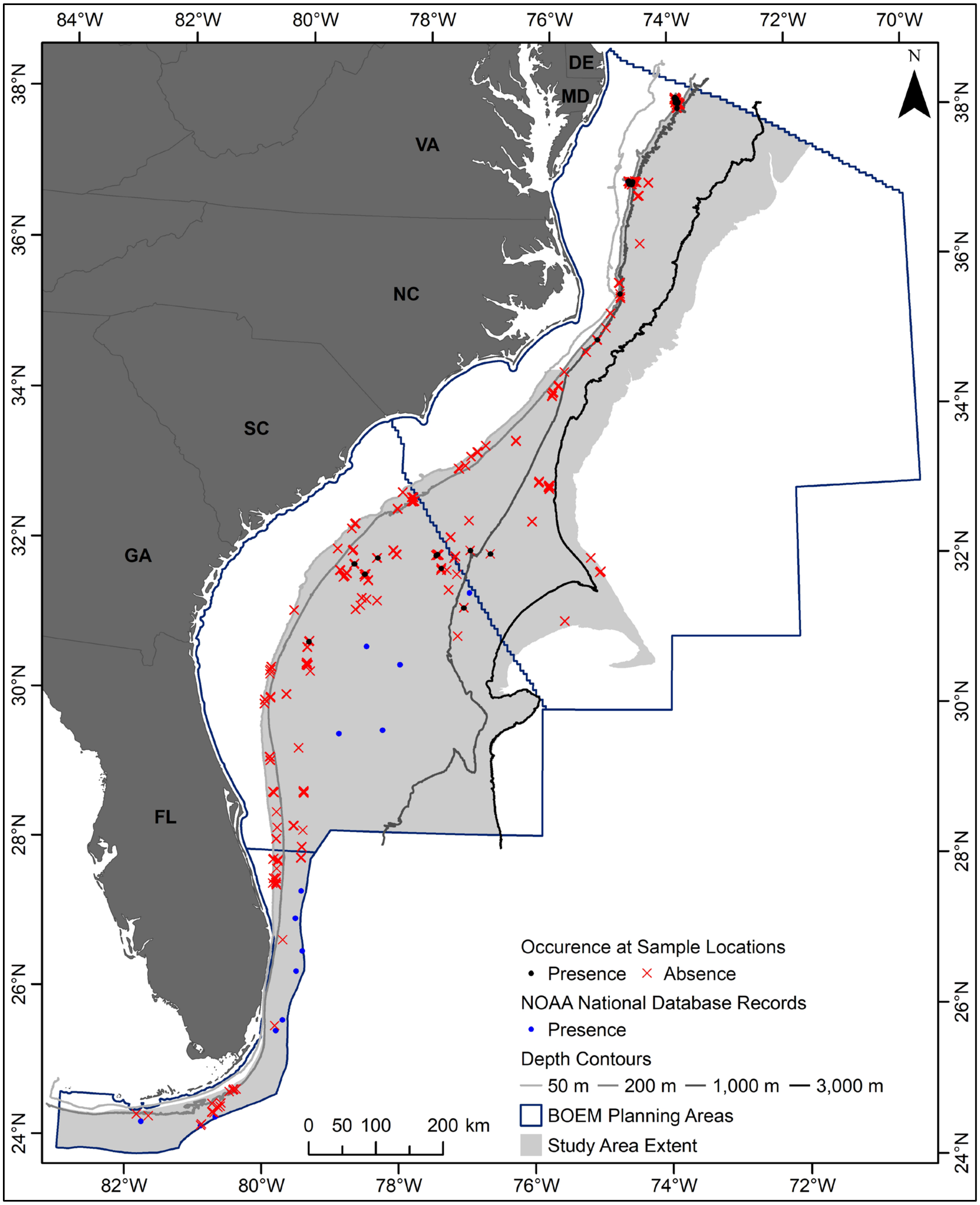

Figure D-61. Occurrence records for the gorgonian coral *Paragorgia*.
This map shows the observed occurrence (presence-absence) of *Paragorgia* at sample locations in the presence-absence database compiled for this study. Additional records of occurrence (presence) from the NOAA National Database are also displayed.

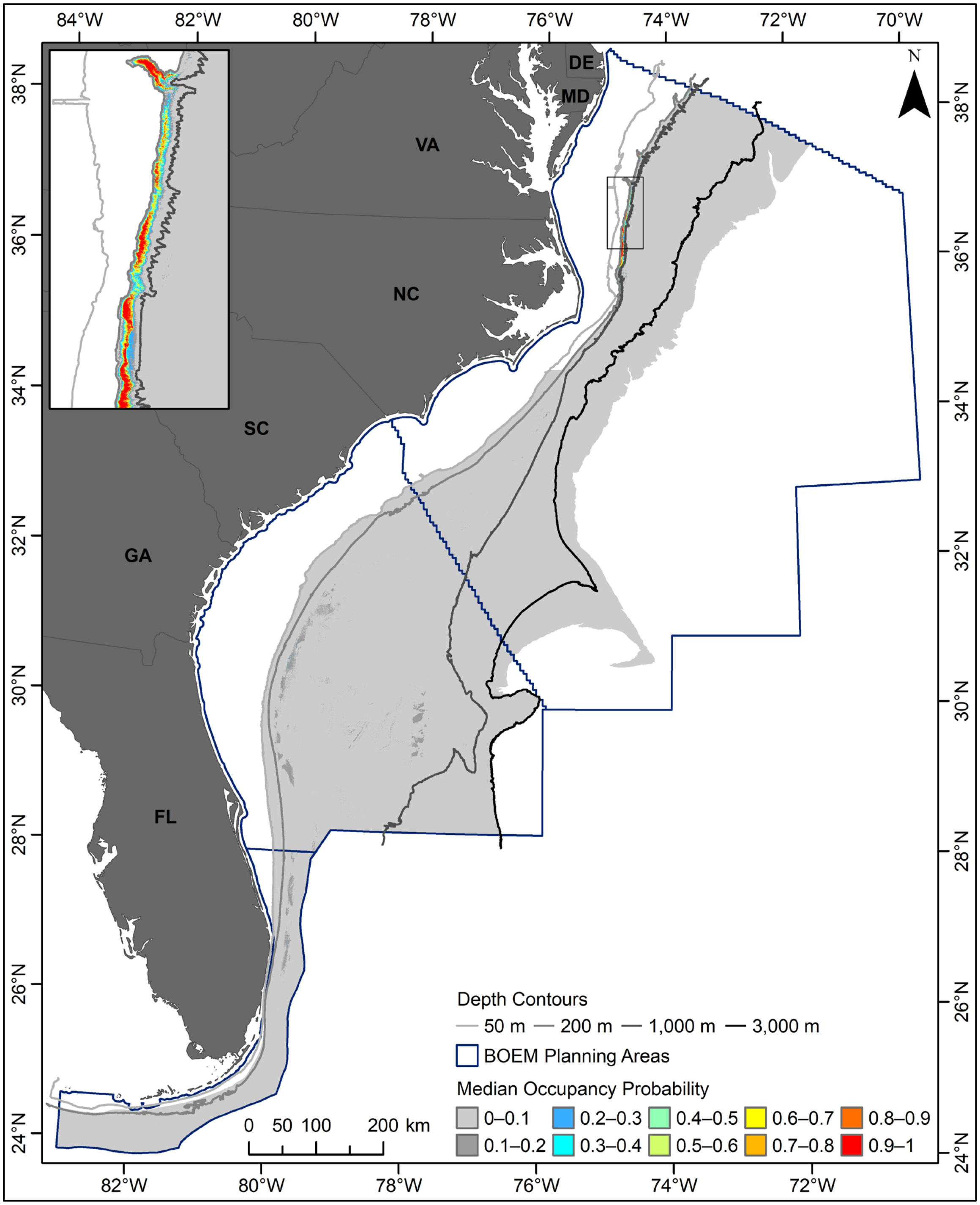

Figure D-62. Predicted occurrence of the gorgonian coral *Paragorgia*.
This map shows the posterior median occupancy probability for *Paragorgia* from the multi-taxon model.

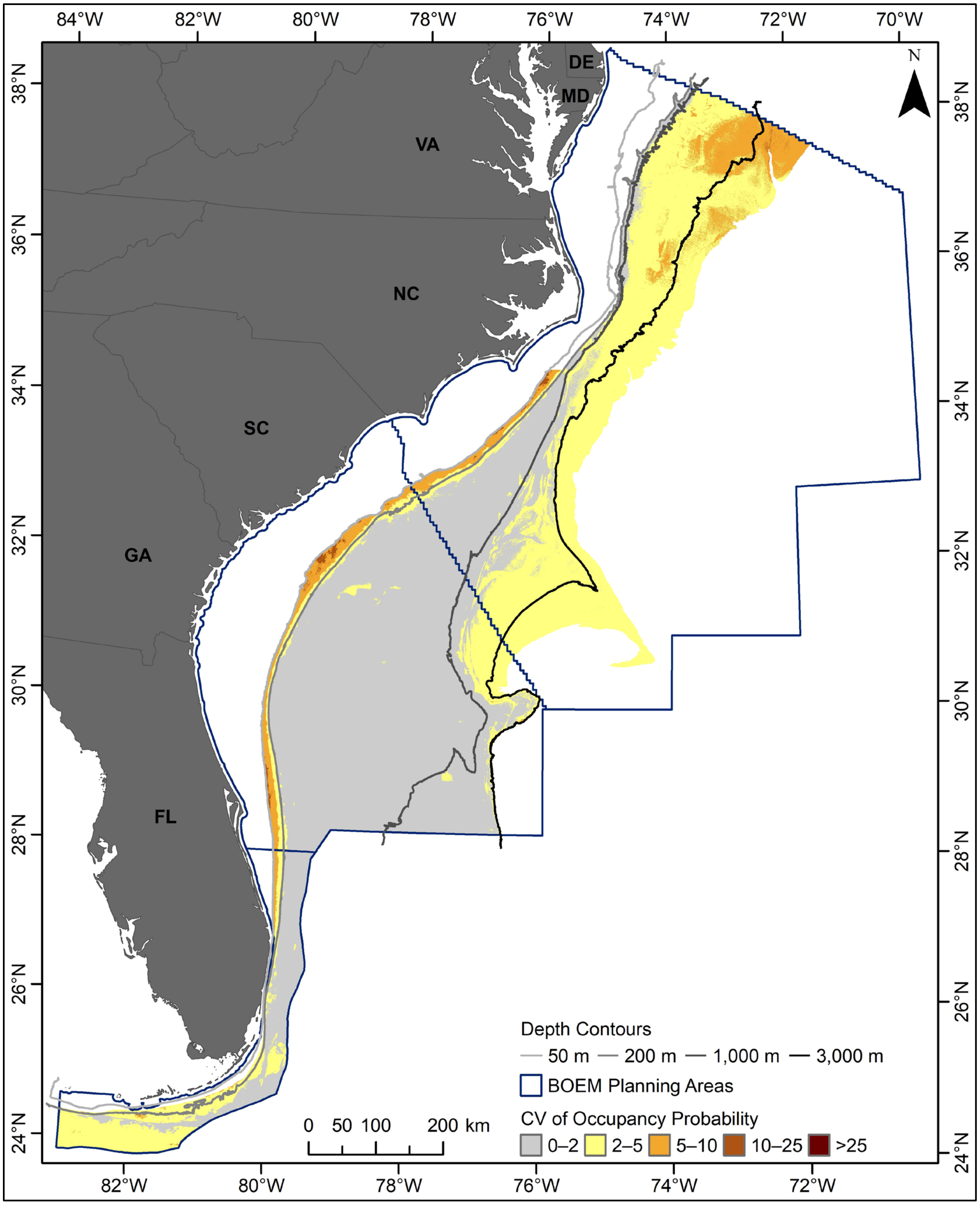

Figure D-63. Variability in the predicted occurrence of the gorgonian coral *Paragorgia*.
This map shows the posterior coefficient of variation of occupancy probability for *Paragorgia* from the multi-taxon model.

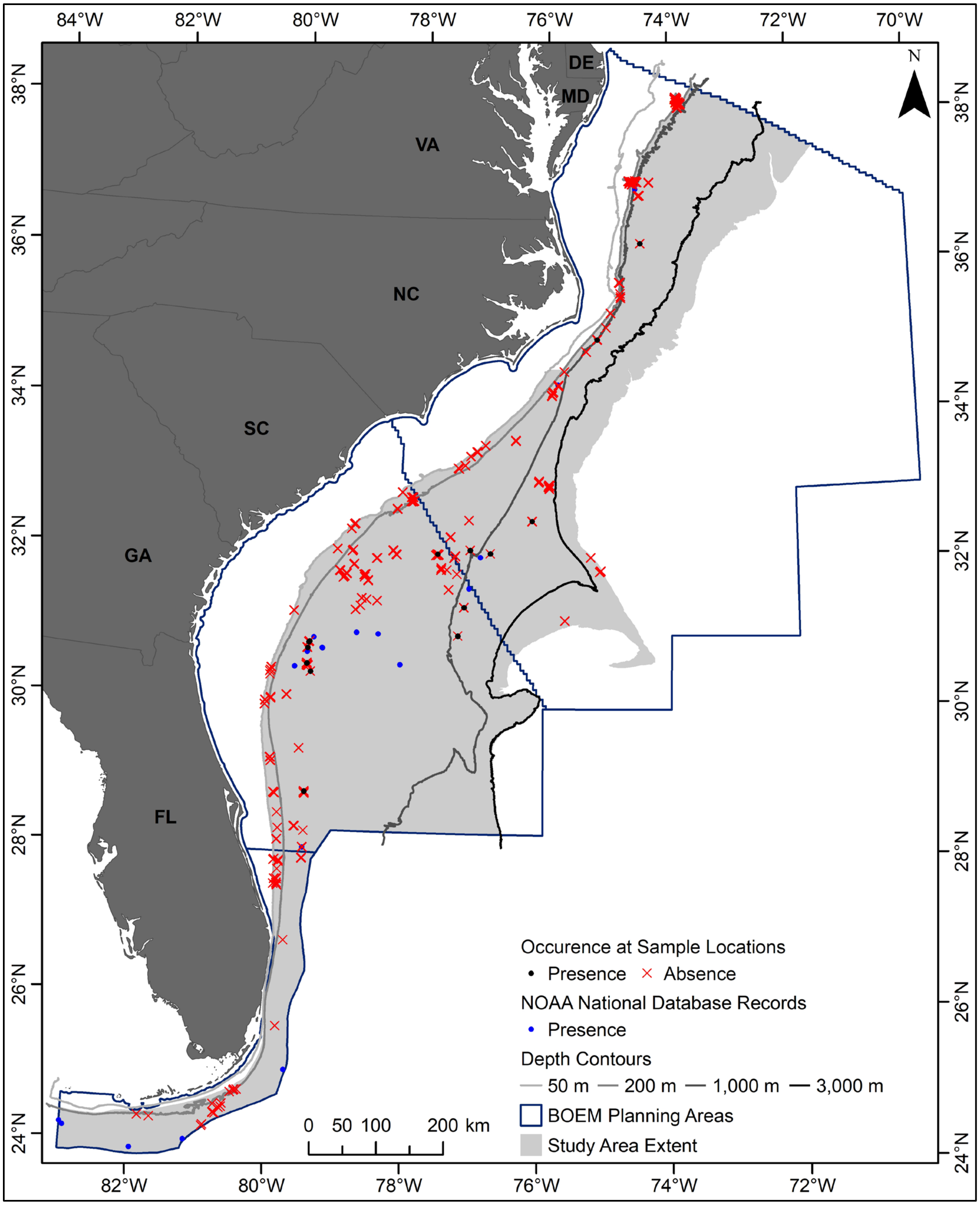

Figure D-64. Occurrence records for the gorgonian coral *Chrysogorgia*.
This map shows the observed occurrence (presence-absence) of *Chrysogorgia* at sample locations in the presence-absence database compiled for this study. Additional records of occurrence (presence) from the NOAA National Database are also displayed.

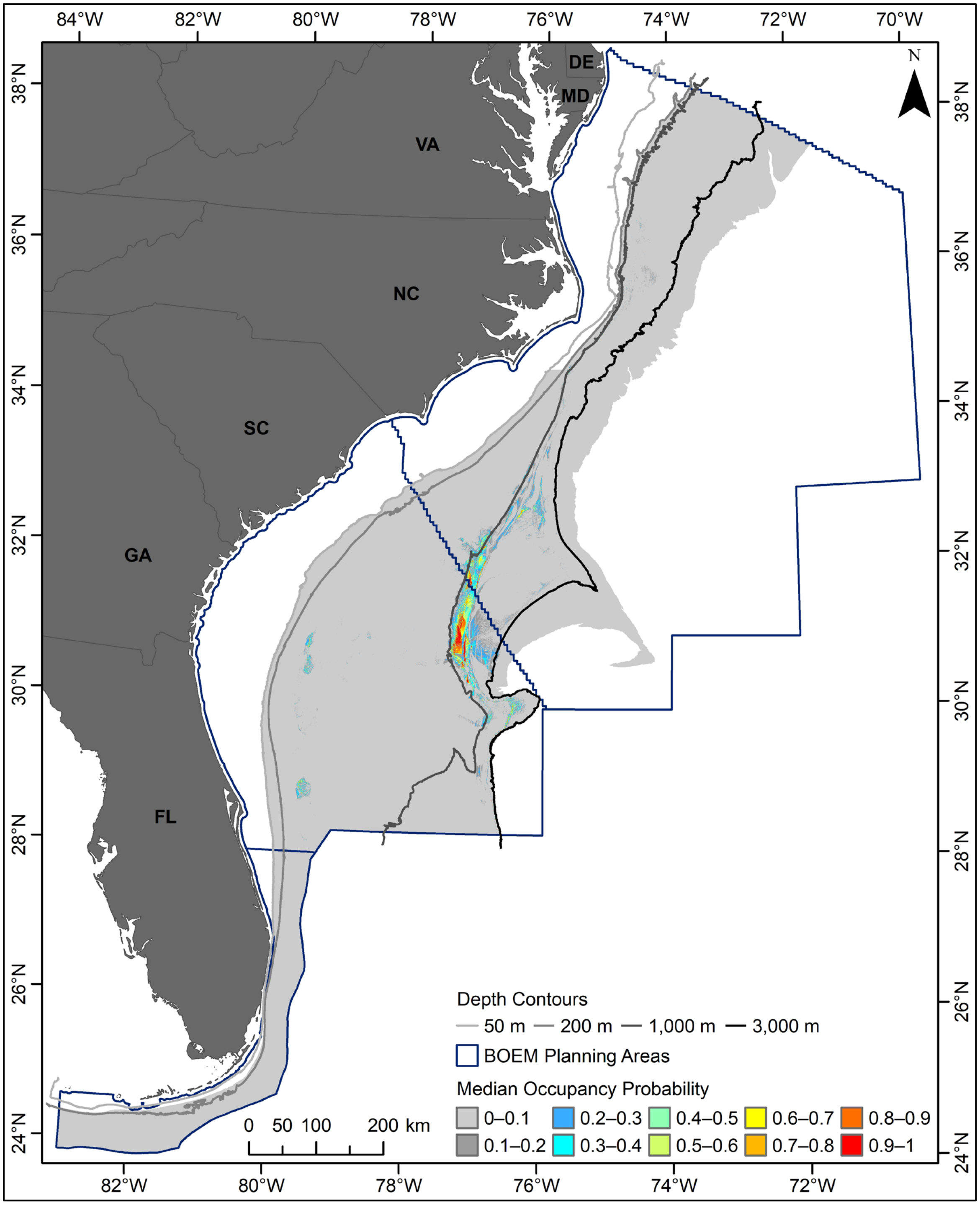

Figure D-65. Predicted occurrence of the gorgonian coral *Chrysogorgia*.
This map shows the posterior median occupancy probability for *Chrysogorgia* from the multi-taxon model.

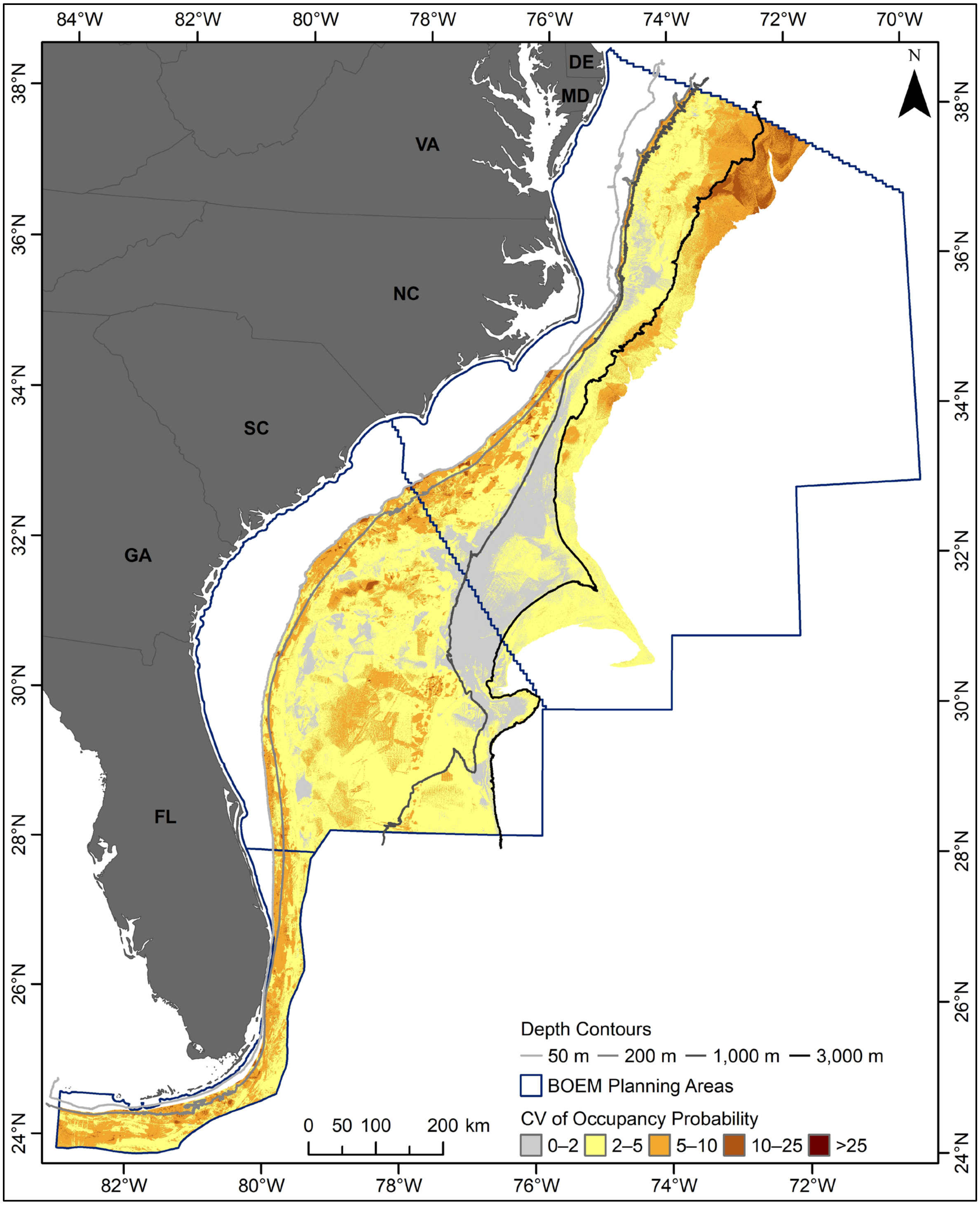

Figure D-66. Variability in the predicted occurrence of the gorgonian coral *Chrysogorgia*.
This map shows the posterior coefficient of variation of occupancy probability for *Chrysogorgia* from the multi-taxon model.

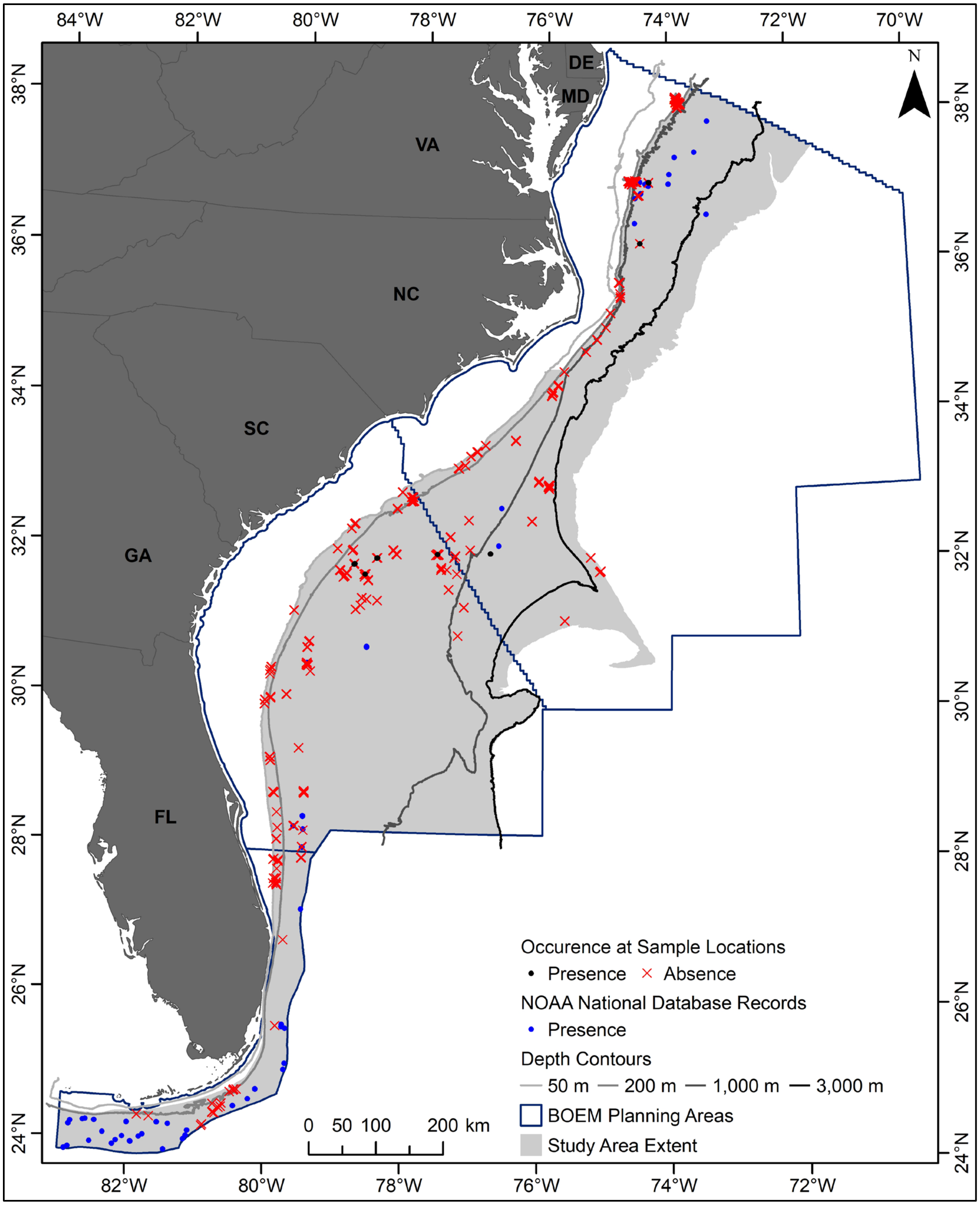

Figure D-67. Occurrence records for the gorgonian coral *Acanella*.
This map shows the observed occurrence (presence-absence) of *Acanella* at sample locations in the presence-absence database compiled for this study. Additional records of occurrence (presence) from the NOAA National Database are also displayed.

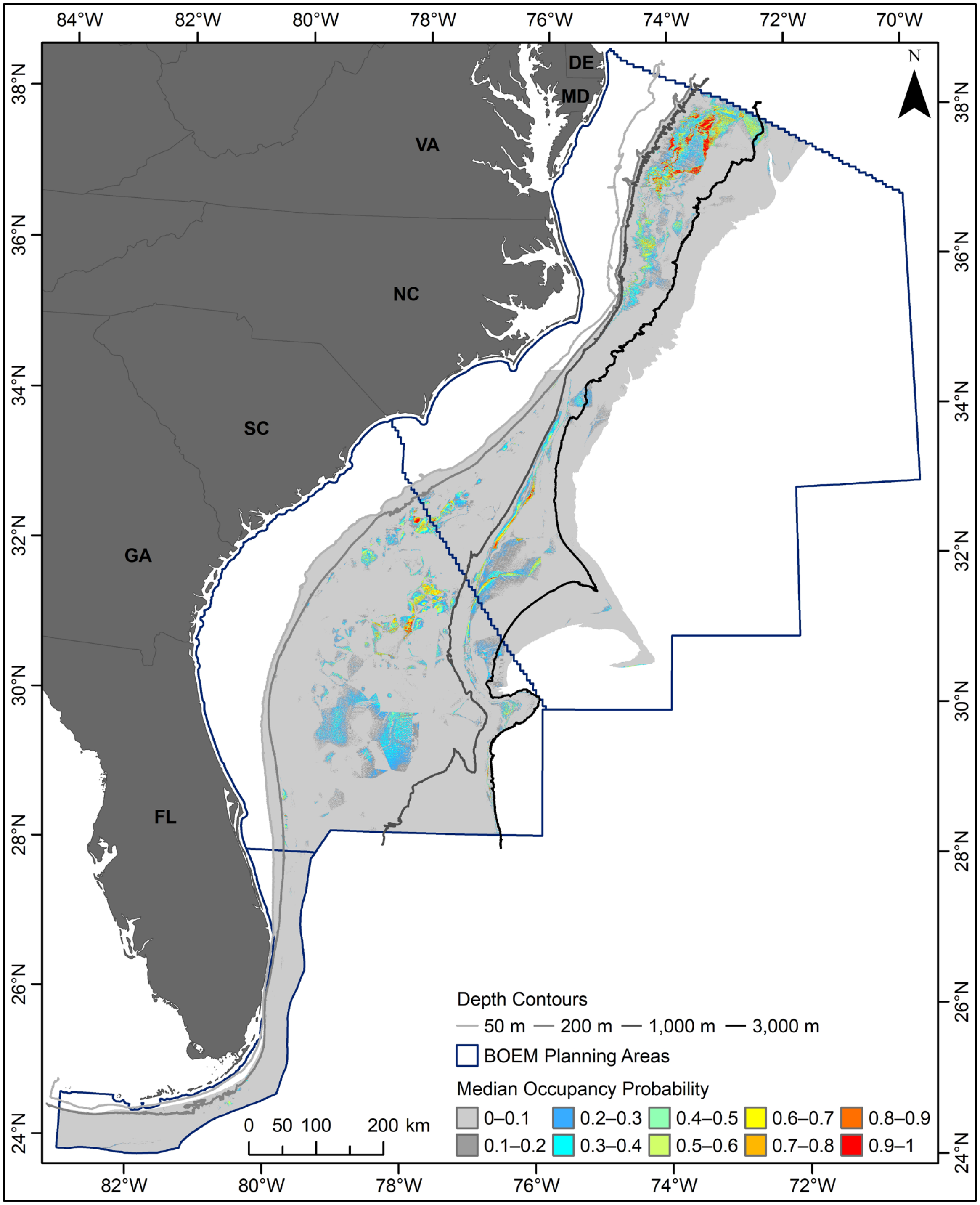

Figure D-68. Predicted occurrence of the gorgonian coral *Acanella*.
This map shows the posterior median occupancy probability for *Acanella* from the multi-taxon model.

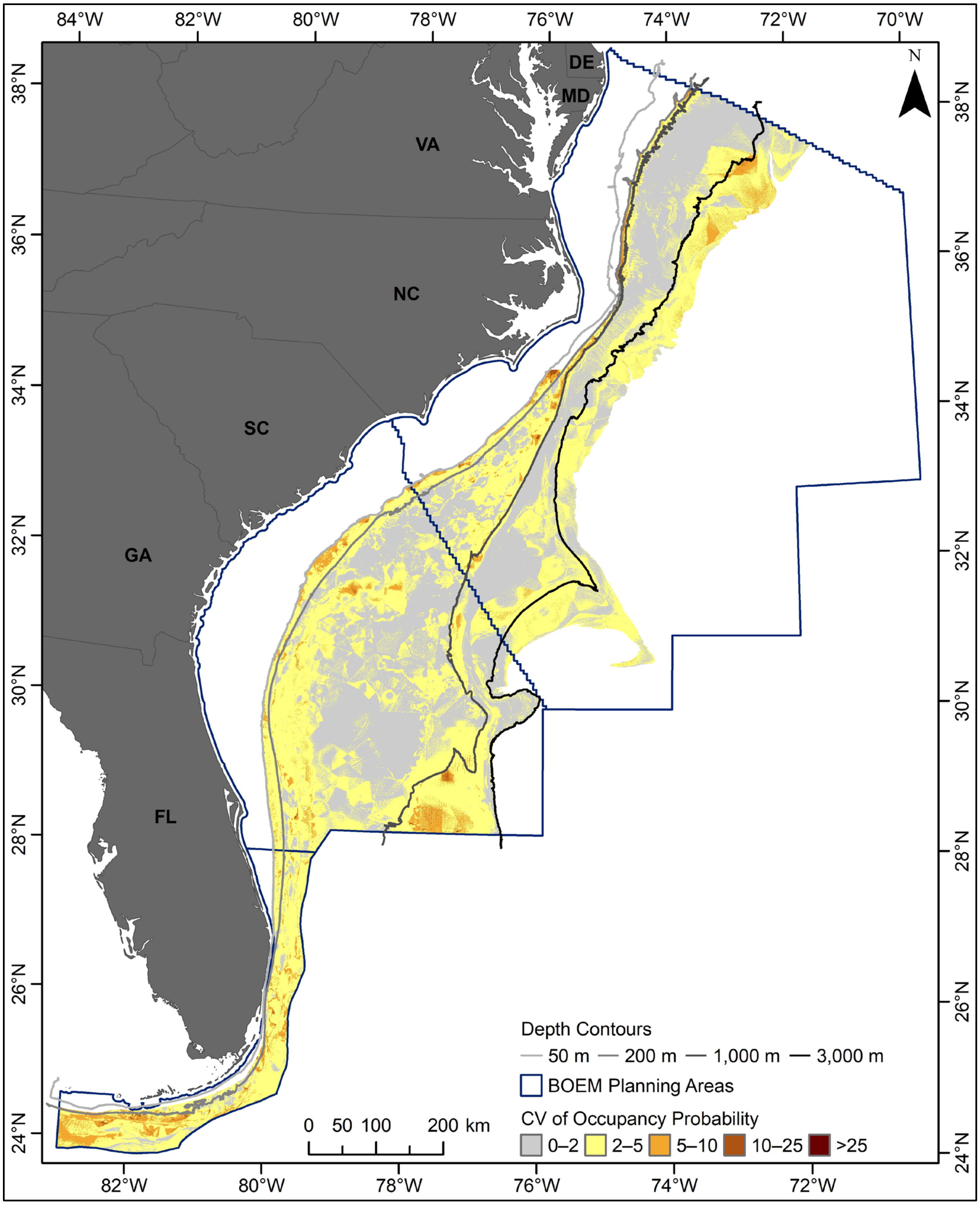

Figure D-69. Variability in the predicted occurrence of the gorgonian coral *Acanella*.
This map shows the posterior coefficient of variation of occupancy probability for *Acanella* from the multi-taxon model.

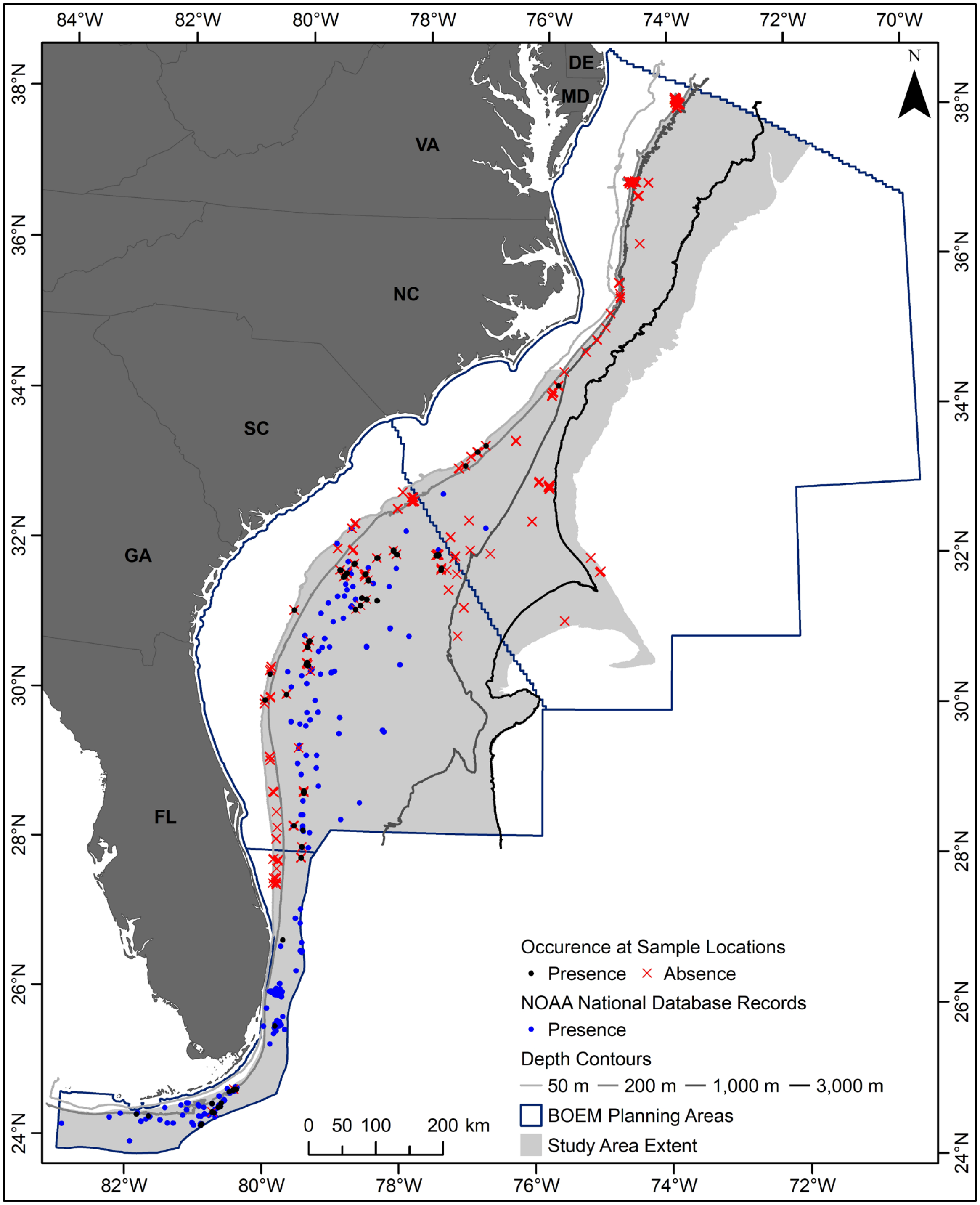

Figure D-70. Occurrence records for the lace coral Stylasteridae.
This map shows the observed occurrence (presence-absence) of Stylasteridae at sample locations in the presence-absence database compiled for this study. Additional records of occurrence (presence) from the NOAA National Database are also displayed.

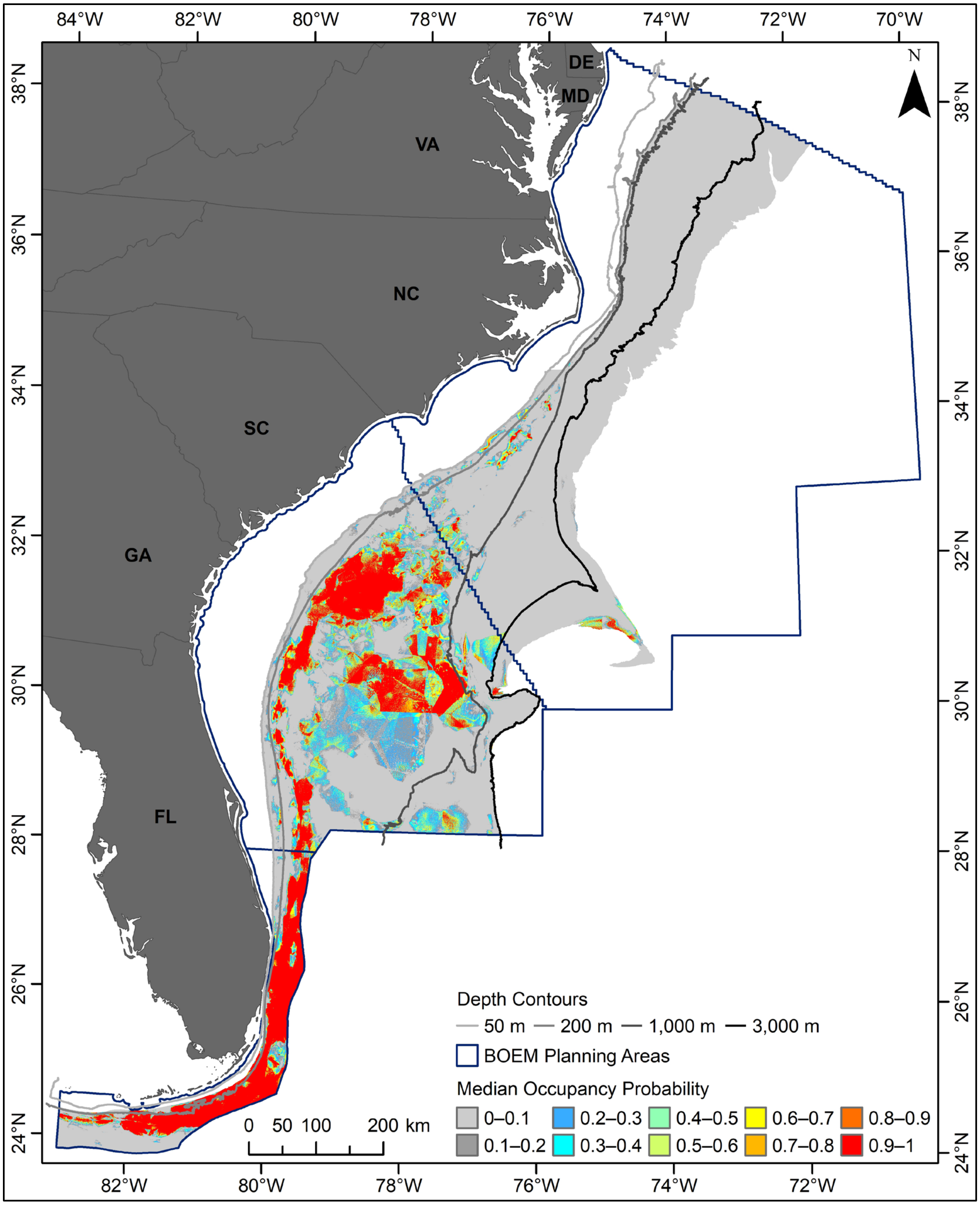

Figure D-71. Predicted occurrence of the lace coral Stylasteridae.
This map shows the posterior median occupancy probability for Stylasteridae.

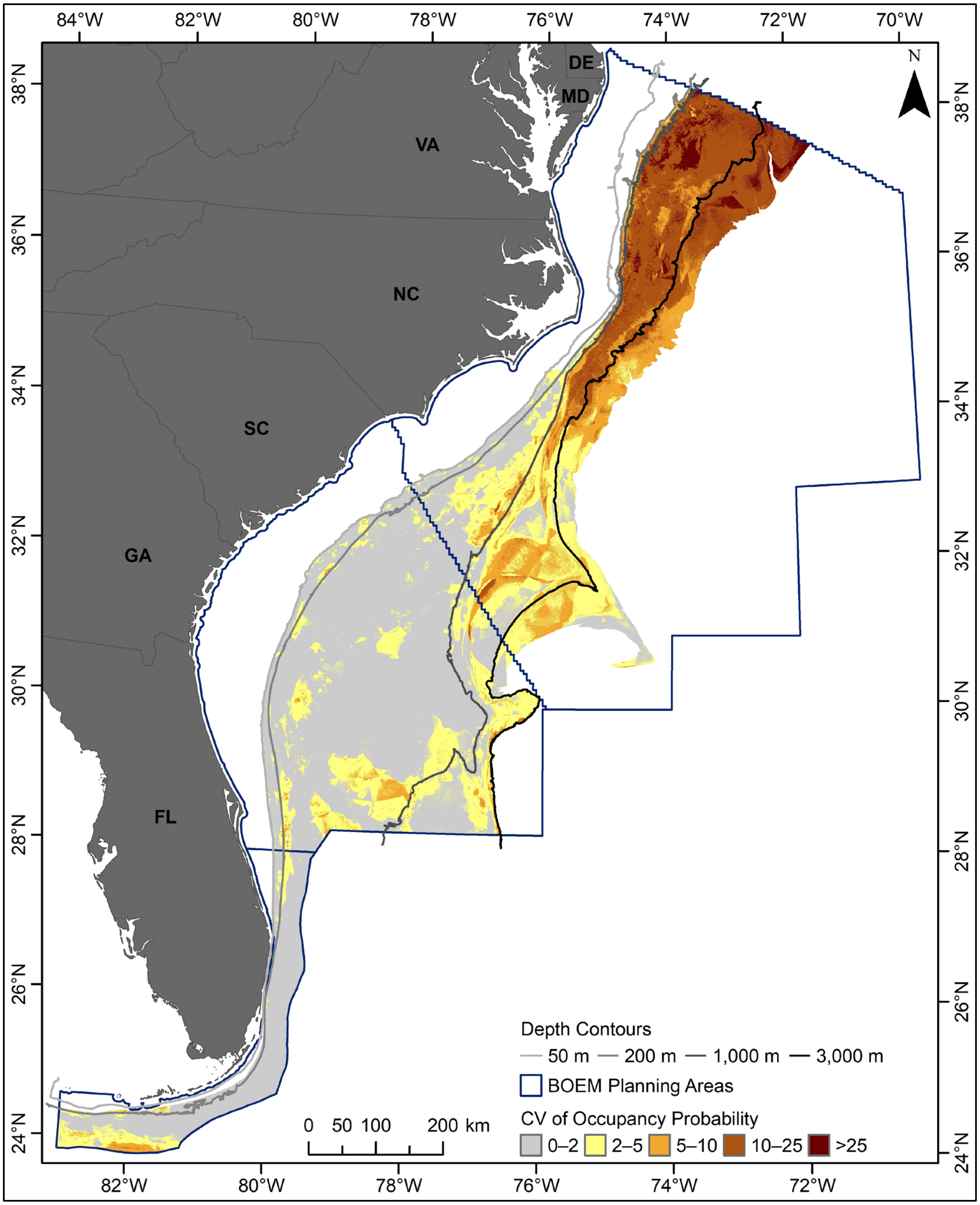

Figure D-72. Variability in the predicted occurrence of the lace coral Stylasteridae.
This map shows the posterior coefficient of variation of occupancy probability for Stylasteridae.

Appendix E: Marginal Effects Plots

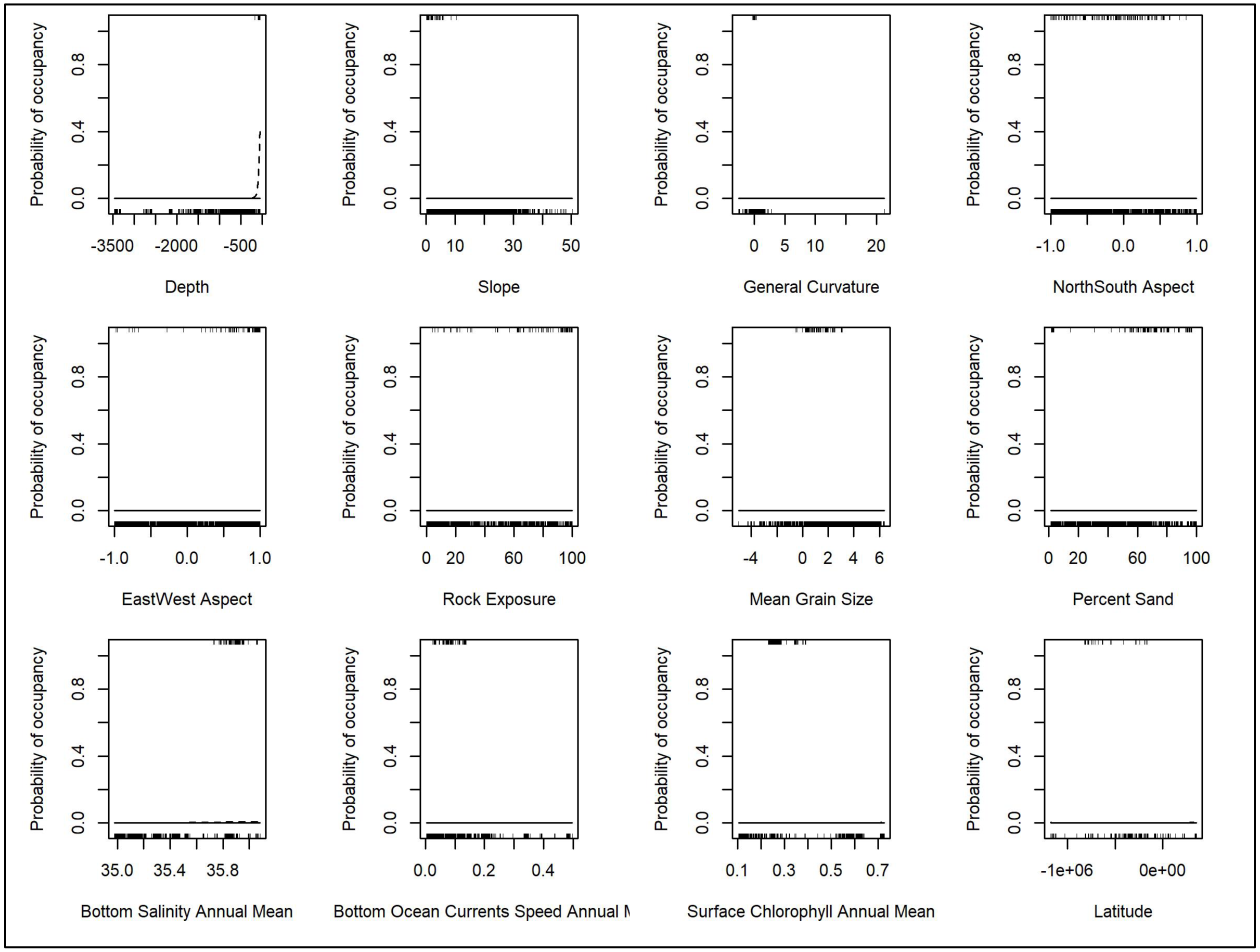

Figure E-1. Marginal effects of the predictors on the predicted occurrence of *Oculina*.
The y-axes show the predicted occurrence for *Oculina* for values of each environmental predictor (the x-axes). The solid line depicts the posterior median occupancy probability, while the dashed lines depict the 95% credible interval. Tick marks at the top and bottom (i.e., rug plots) of each plot indicate the sampled predictor values at which *Oculina* was observed to be present (top) or absent (bottom). The marginal effects plots should be interpreted with caution because they illustrate the estimated effects of each predictor while all others are set at their mean value (i.e., each plot ignores the realized range of effects from all predictors).

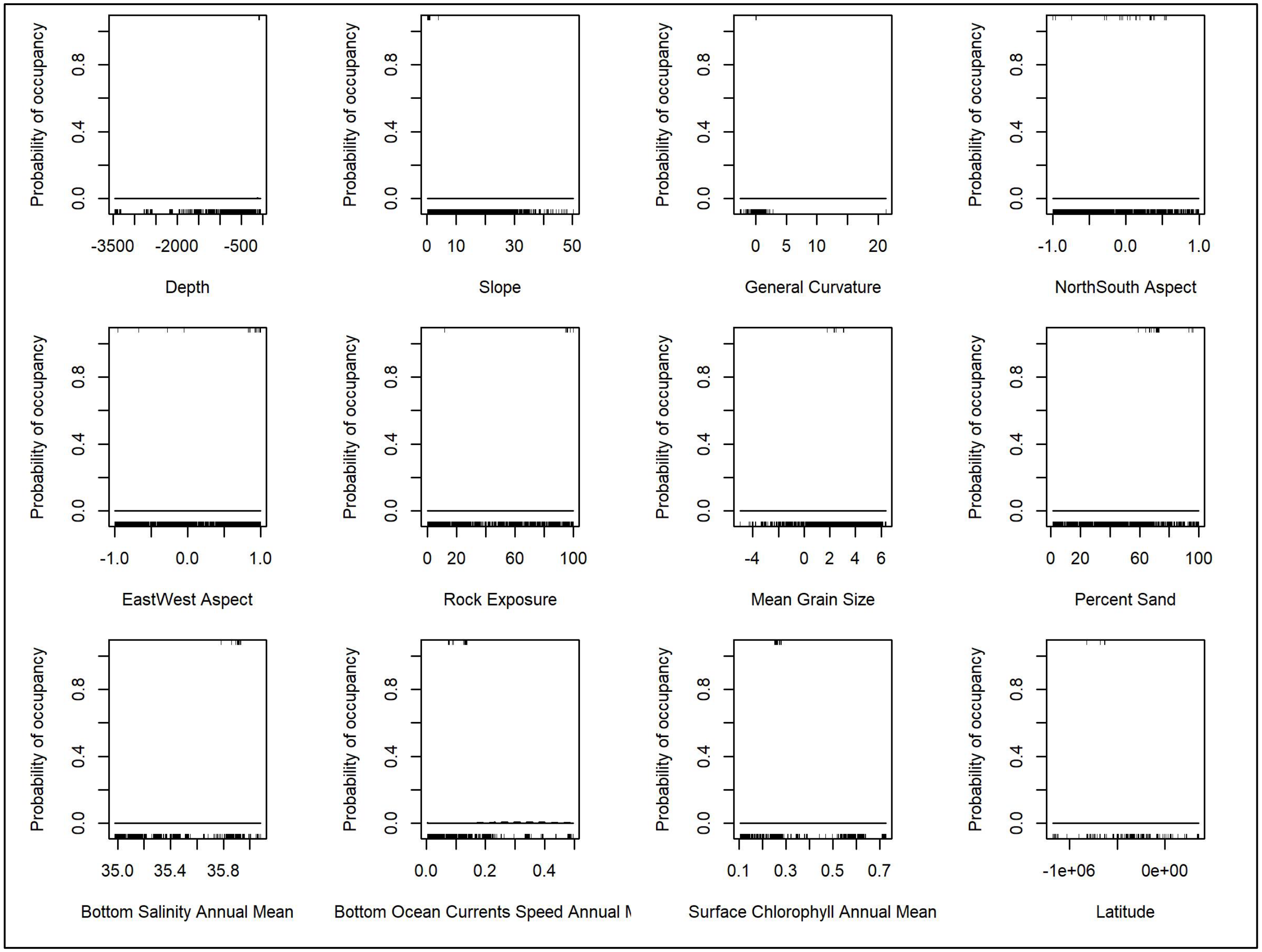

Figure E-2. Marginal effects of the predictors on the predicted occurrence of *Cladocora*.
The y-axes show the predicted occurrence for *Cladocora* for values of each environmental predictor (the x-axes). The solid line depicts the posterior median occupancy probability, while the dashed lines depict the 95% credible interval. Tick marks at the top and bottom (i.e., rug plots) of each plot indicate the sampled predictor values at which *Cladocora* was observed to be present (top) or absent (bottom). The marginal effects plots should be interpreted with caution because they illustrate the estimated effects of each predictor while all others are set at their mean value (i.e., each plot ignores the realized range of effects from all predictors).

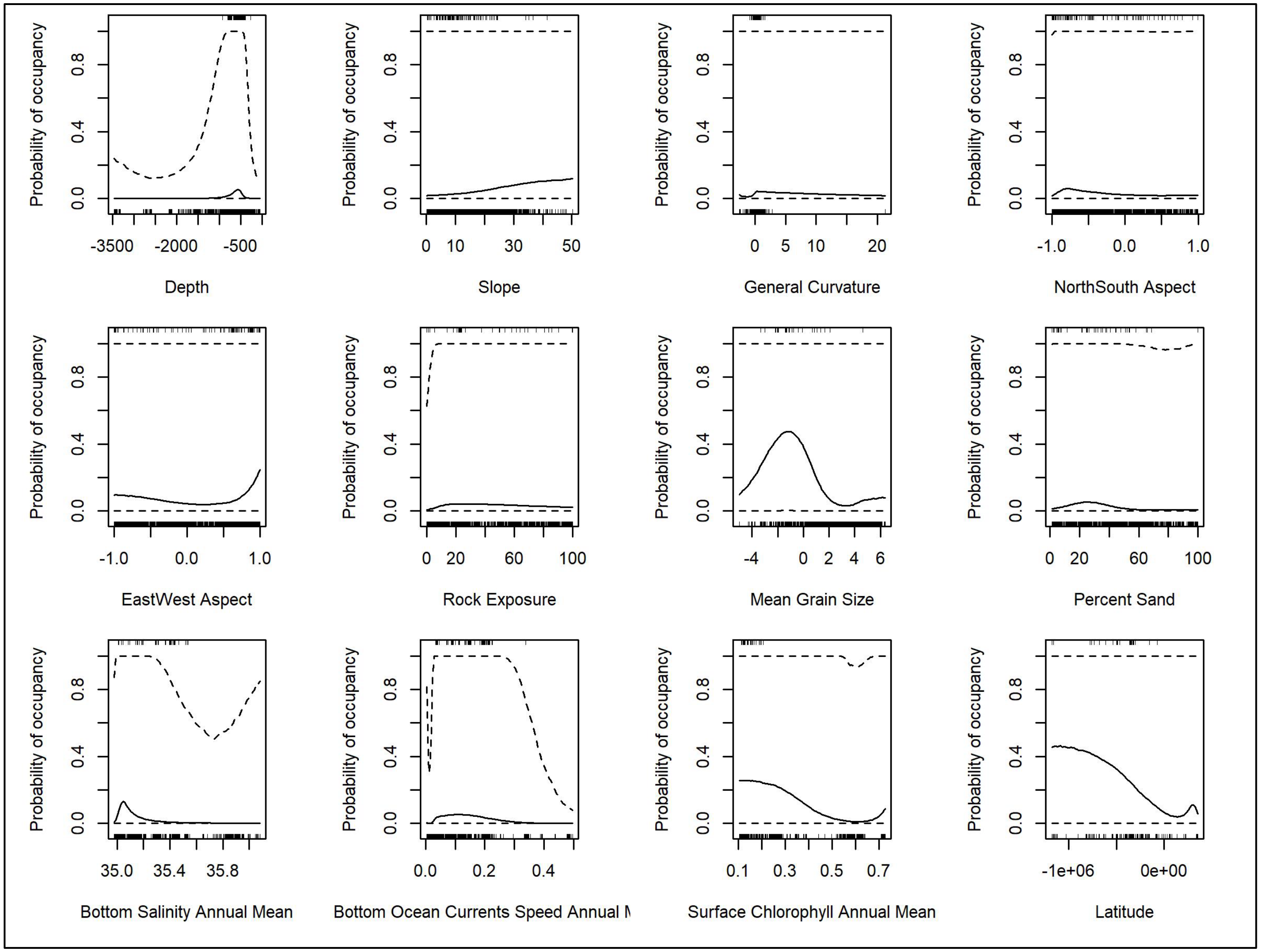

Figure E-3. Marginal effects of the predictors on the predicted occurrence of *Madrepora*.
The y-axes show the predicted occurrence for *Madrepora* for values of each environmental predictor (the x-axes). The solid line depicts the posterior median occupancy probability, while the dashed lines depict the 95% credible interval. Tick marks at the top and bottom (i.e., rug plots) of each plot indicate the sampled predictor values at which *Madrepora* was observed to be present (top) or absent (bottom). The marginal effects plots should be interpreted with caution because they illustrate the estimated effects of each predictor while all others are set at their mean value (i.e., each plot ignores the realized range of effects from all predictors).

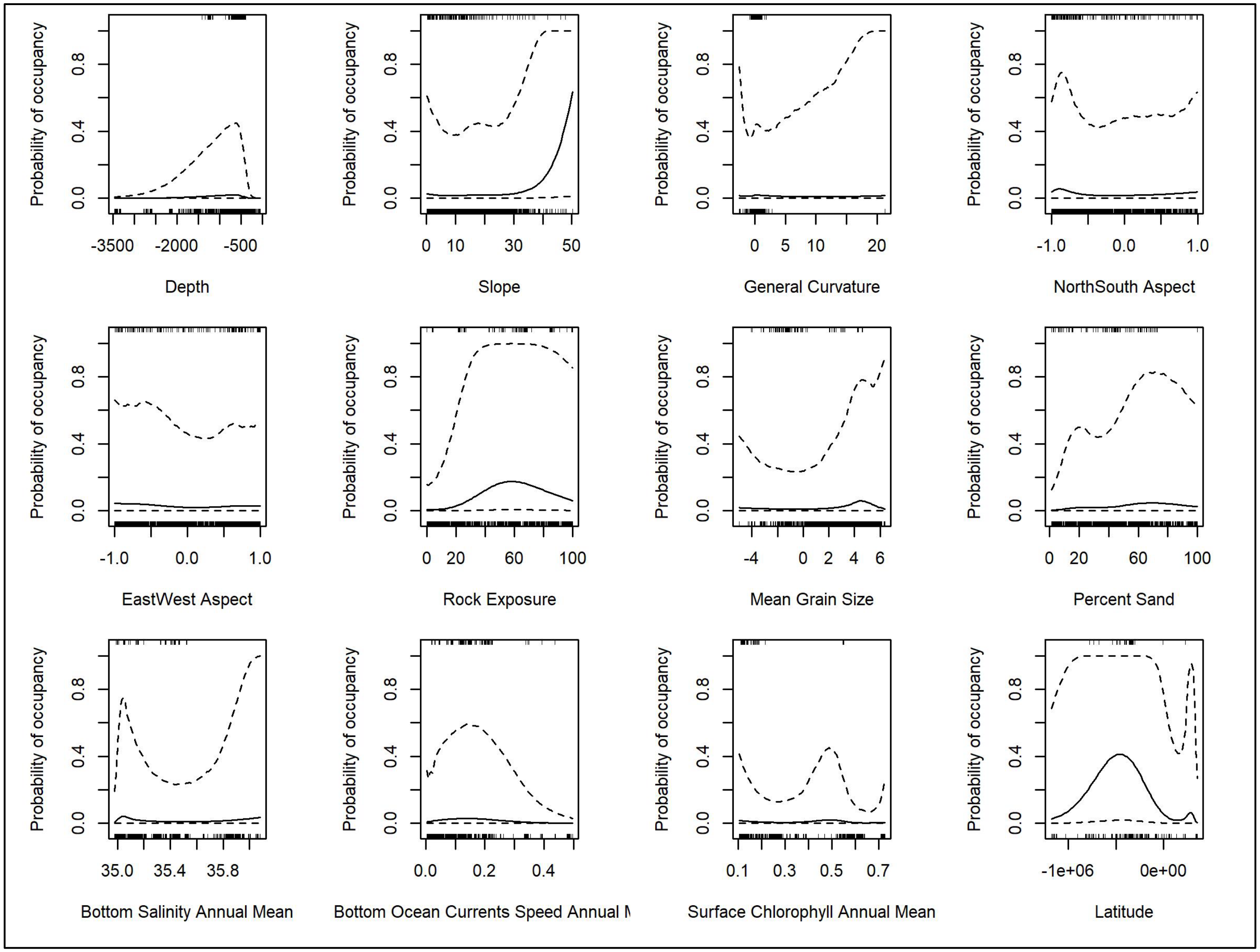

Figure E-4. Marginal effects of the predictors on the predicted occurrence of *Solenosmilia*.
The y-axes show the predicted occurrence for *Solenosmilia* for values of each environmental predictor (the x-axes). The solid line depicts the posterior median occupancy probability, while the dashed lines depict the 95% credible interval. Tick marks at the top and bottom (i.e., rug plots) of each plot indicate the sampled predictor values at which *Solenosmilia* was observed to be present (top) or absent (bottom). The marginal effects plots should be interpreted with caution because they illustrate the estimated effects of each predictor while all others are set at their mean value (i.e., each plot ignores the realized range of effects from all predictors).

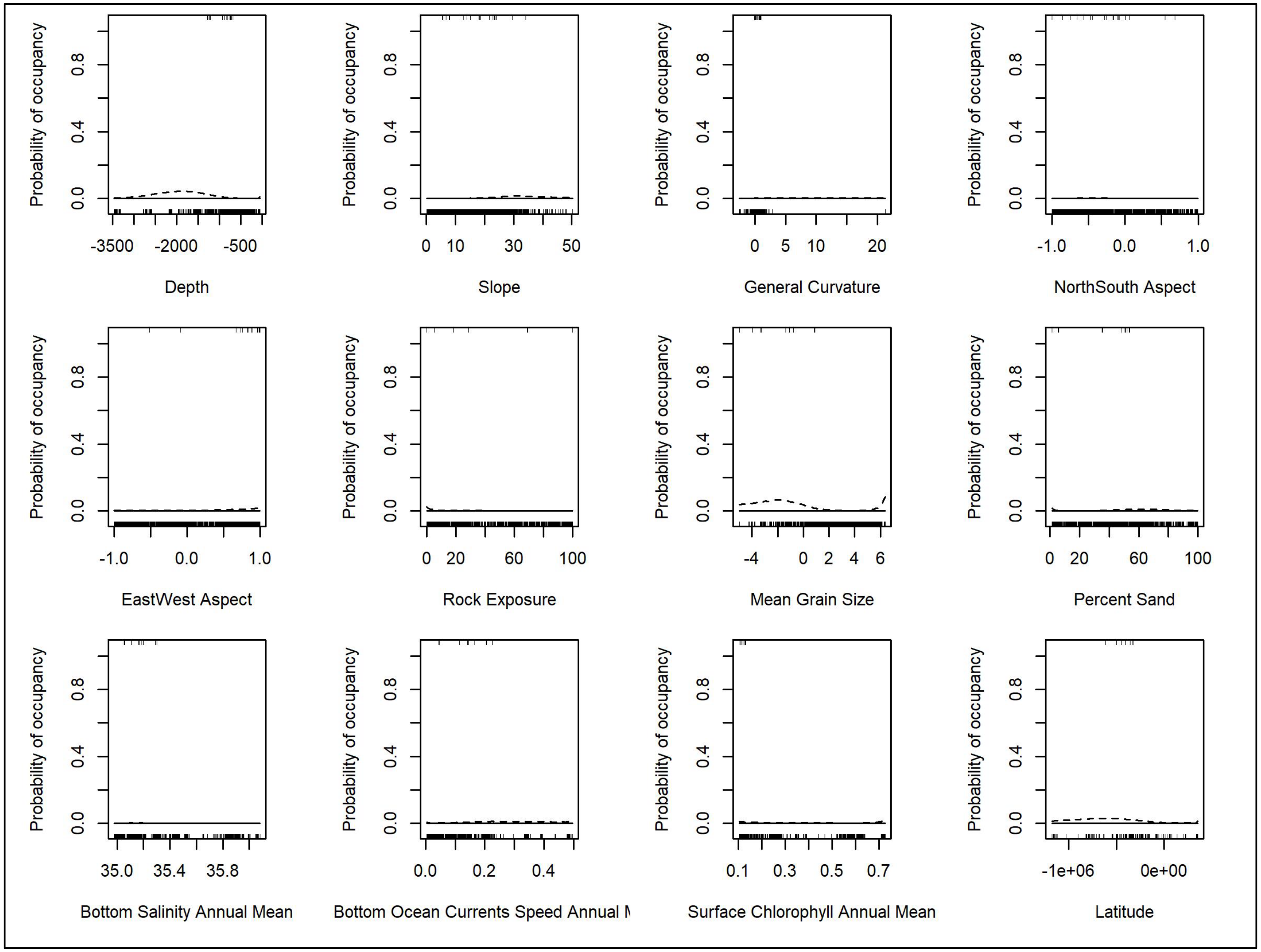

Figure E-5. Marginal effects of the predictors on the predicted occurrence of *Enallopsammia*.
The y-axes show the predicted occurrence for *Enallopsammia* for values of each environmental predictor (the x-axes). The solid line depicts the posterior median occupancy probability, while the dashed lines depict the 95% credible interval. Tick marks at the top and bottom (i.e., rug plots) of each plot indicate the sampled predictor values at which *Enallopsammia* was observed to be present (top) or absent (bottom). The marginal effects plots should be interpreted with caution because they illustrate the estimated effects of each predictor while all others are set at their mean value (i.e., each plot ignores the realized range of effects from all predictors).

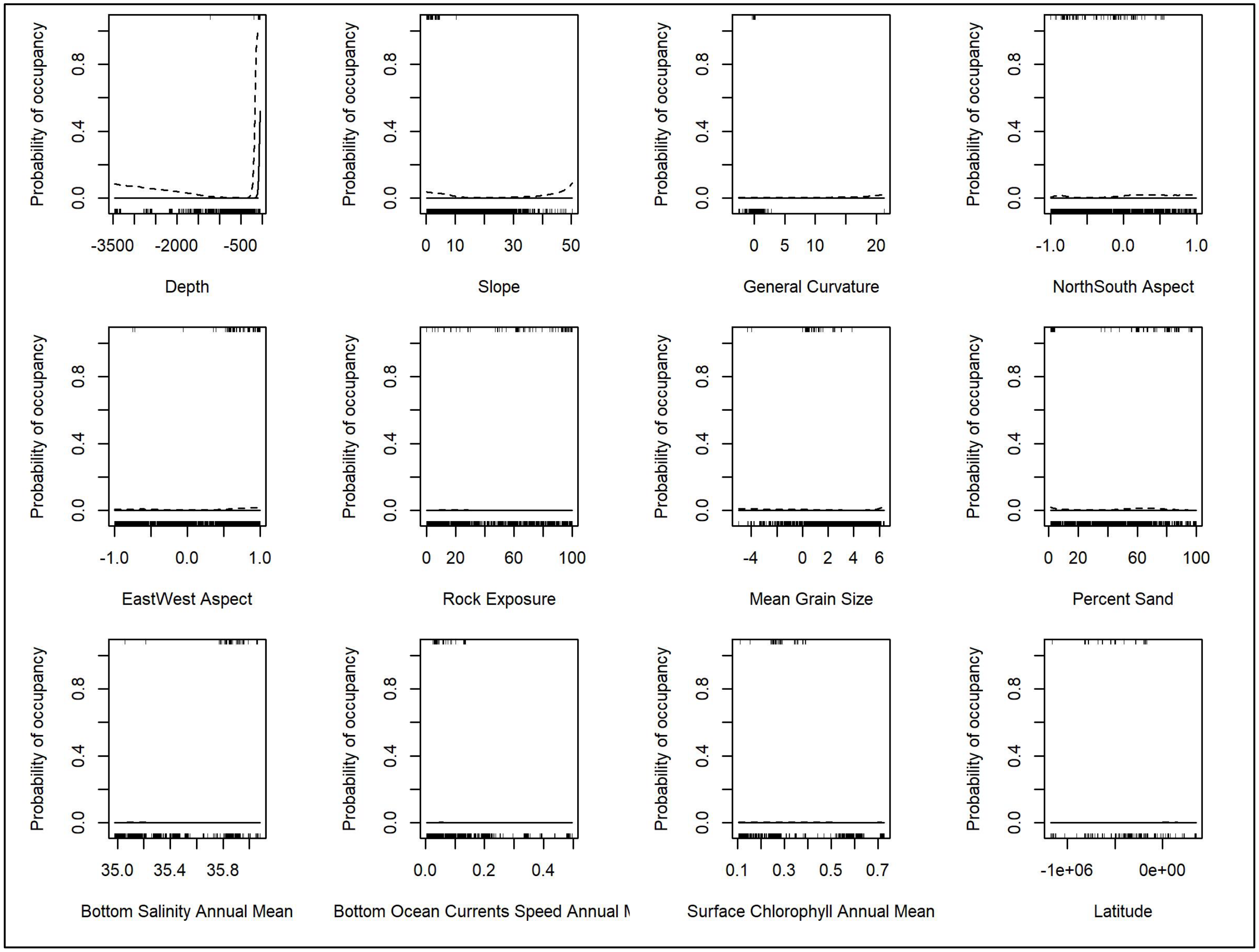

Figure E-6. Marginal effects of the predictors on the predicted occurrence of *Stichopathes*.
The y-axes show the predicted occurrence for *Stichopathes* for values of each environmental predictor (the x-axes). The solid line depicts the posterior median occupancy probability, while the dashed lines depict the 95% credible interval. Tick marks at the top and bottom (i.e., rug plots) of each plot indicate the sampled predictor values at which *Stichopathes* was observed to be present (top) or absent (bottom). The marginal effects plots should be interpreted with caution because they illustrate the estimated effects of each predictor while all others are set at their mean value (i.e., each plot ignores the realized range of effects from all predictors).

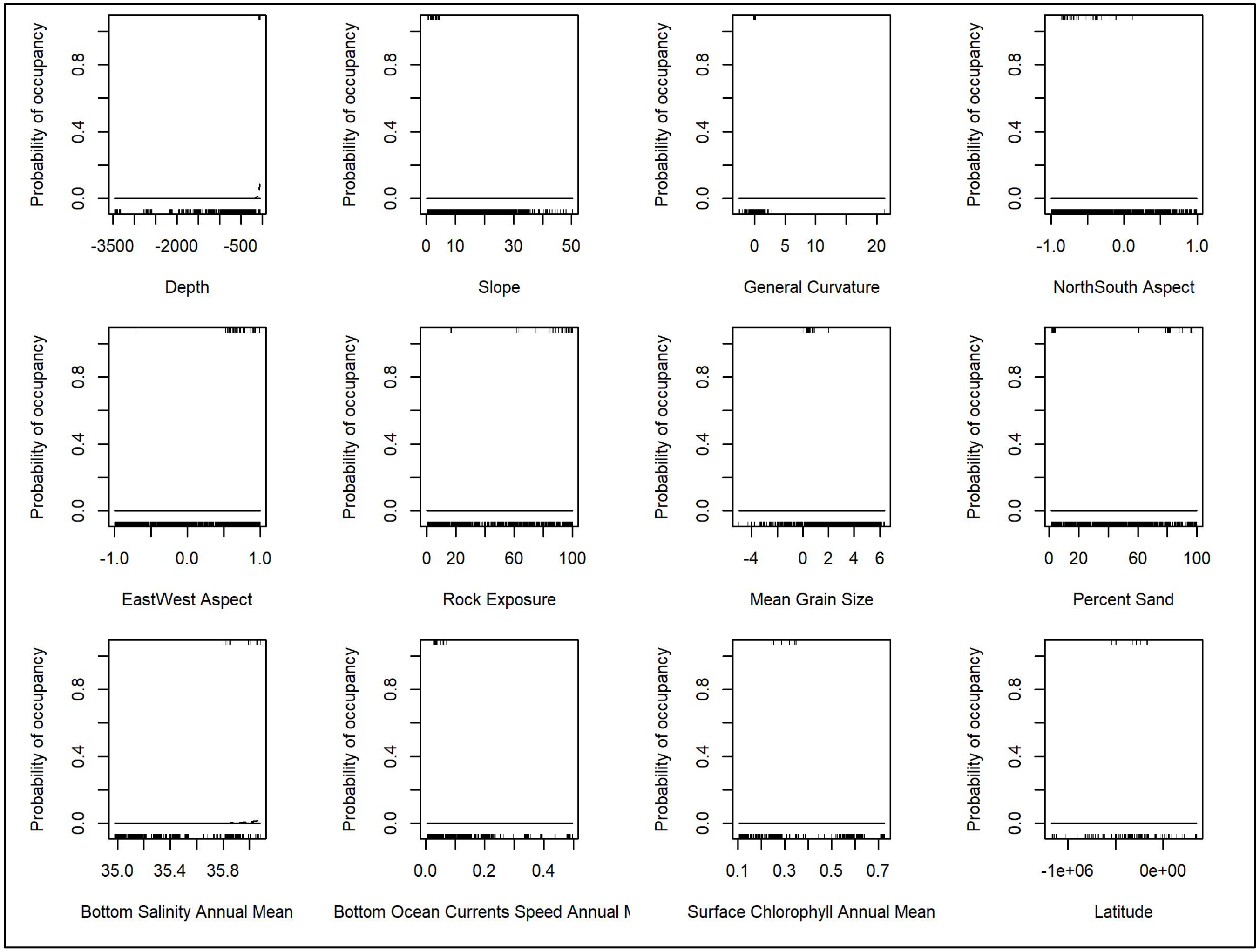

Figure E-7. Marginal effects of the predictors on the predicted occurrence of *Antipathes*.
The y-axes show the predicted occurrence for *Antipathes* for values of each environmental predictor (the x-axes). The solid line depicts the posterior median occupancy probability, while the dashed lines depict the 95% credible interval. Tick marks at the top and bottom (i.e., rug plots) of each plot indicate the sampled predictor values at which *Antipathes* was observed to be present (top) or absent (bottom). The marginal effects plots should be interpreted with caution because they illustrate the estimated effects of each predictor while all others are set at their mean value (i.e., each plot ignores the realized range of effects from all predictors).

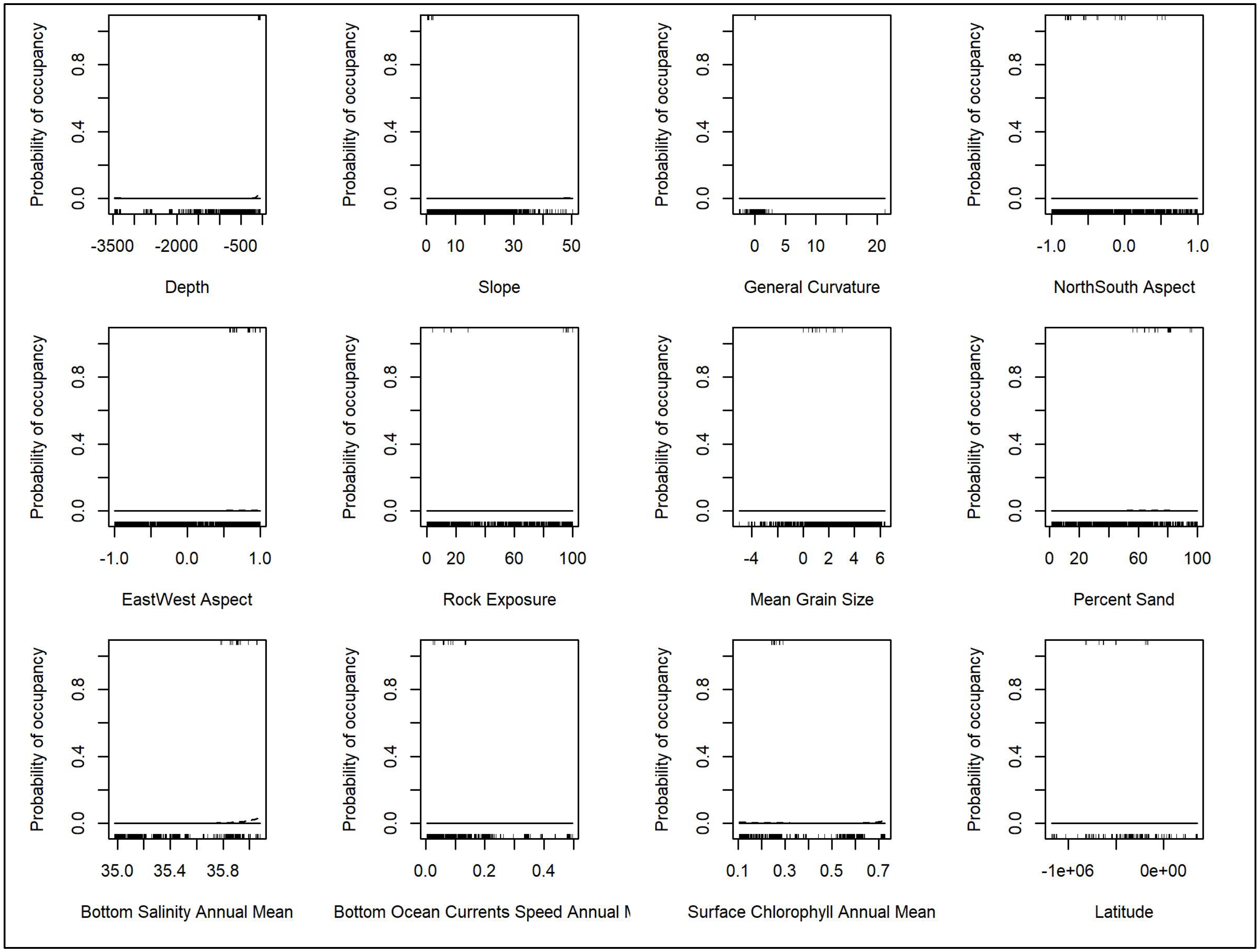

Figure E-8. Marginal effects of the predictors on the predicted occurrence of *Tanacetipathes*.
The y-axes show the predicted occurrence for *Tanacetipathes* for values of each environmental predictor (the x-axes). The solid line depicts the posterior median occupancy probability, while the dashed lines depict the 95% credible interval. Tick marks at the top and bottom (i.e., rug plots) of each plot indicate the sampled predictor values at which *Tanacetipathes* was observed to be present (top) or absent (bottom). The marginal effects plots should be interpreted with caution because they illustrate the estimated effects of each predictor while all others are set at their mean value (i.e., each plot ignores the realized range of effects from all predictors).

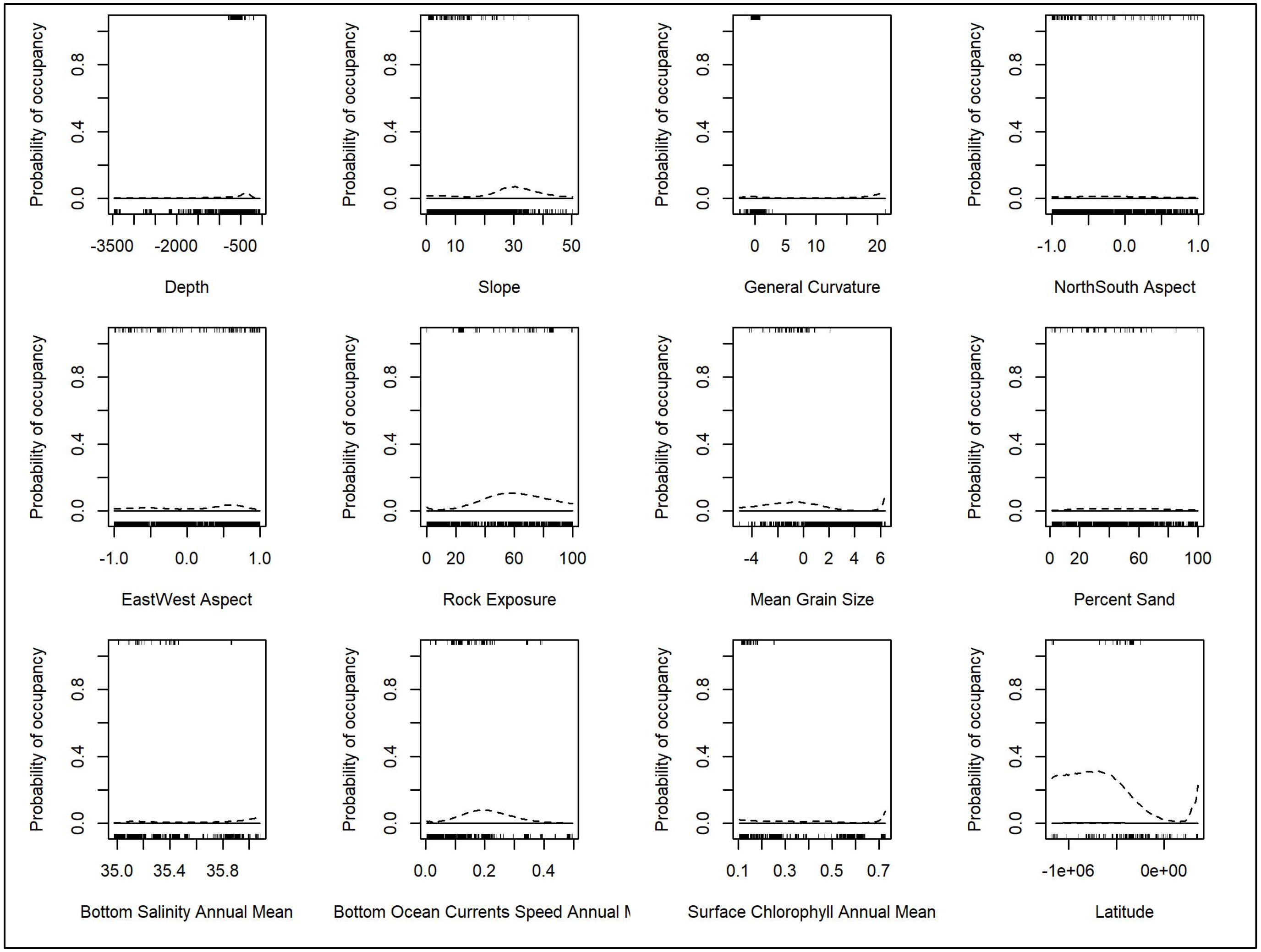

Figure E-9. Marginal effects of the predictors on the predicted occurrence of *Leiopathes*.
The y-axes show the predicted occurrence for *Leiopathes* for values of each environmental predictor (the x-axes). The solid line depicts the posterior median occupancy probability, while the dashed lines depict the 95% credible interval. Tick marks at the top and bottom (i.e., rug plots) of each plot indicate the sampled predictor values at which *Leiopathes* was observed to be present (top) or absent (bottom). The marginal effects plots should be interpreted with caution because they illustrate the estimated effects of each predictor while all others are set at their mean value (i.e., each plot ignores the realized range of effects from all predictors).

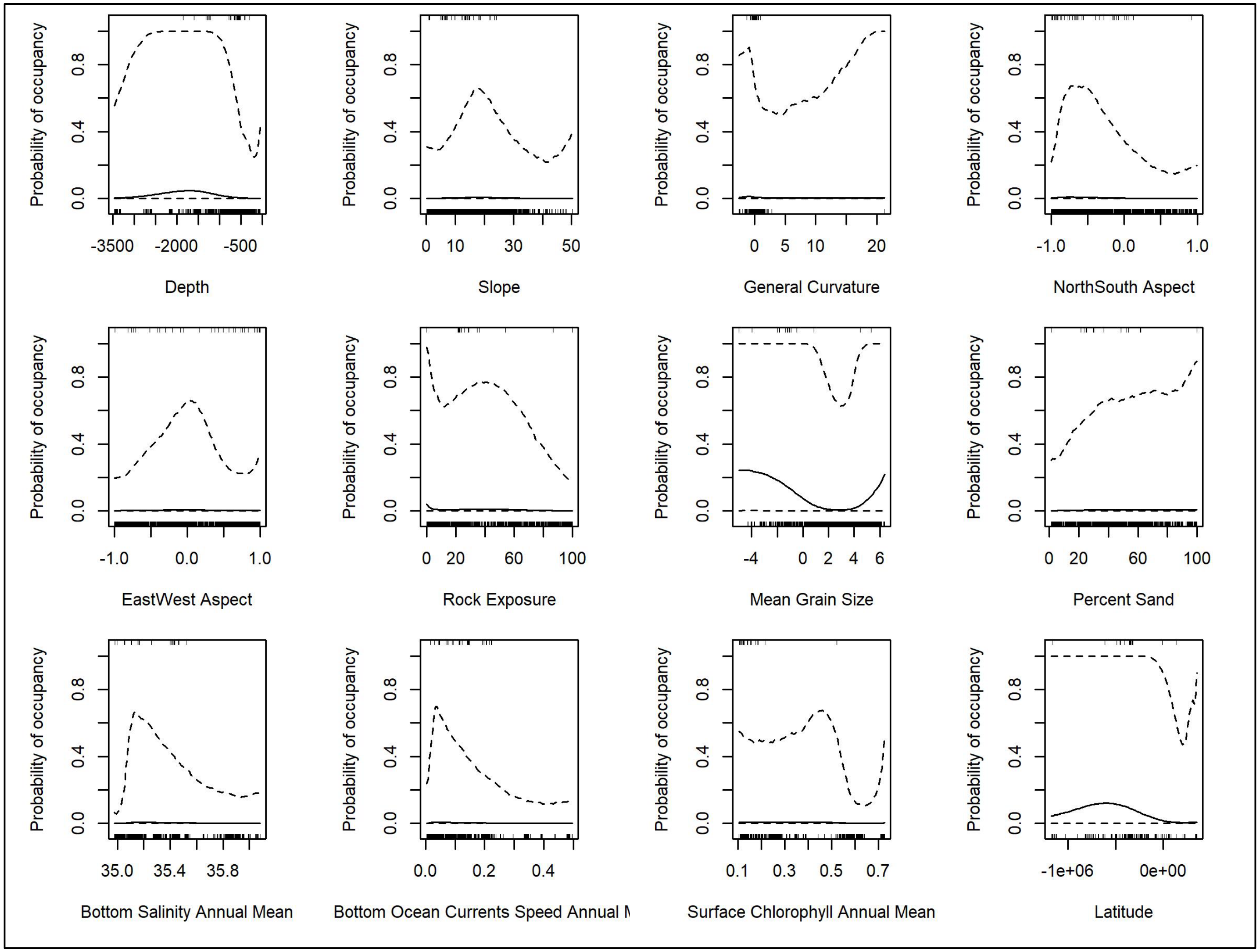

Figure E-10. Marginal effects of the predictors on the predicted occurrence of *Bathypathes*.
The y-axes show the predicted occurrence for *Bathypathes* for values of each environmental predictor (the x-axes). The solid line depicts the posterior median occupancy probability, while the dashed lines depict the 95% credible interval. Tick marks at the top and bottom (i.e., rug plots) of each plot indicate the sampled predictor values at which *Bathypathes* was observed to be present (top) or absent (bottom). The marginal effects plots should be interpreted with caution because they illustrate the estimated effects of each predictor while all others are set at their mean value (i.e., each plot ignores the realized range of effects from all predictors).

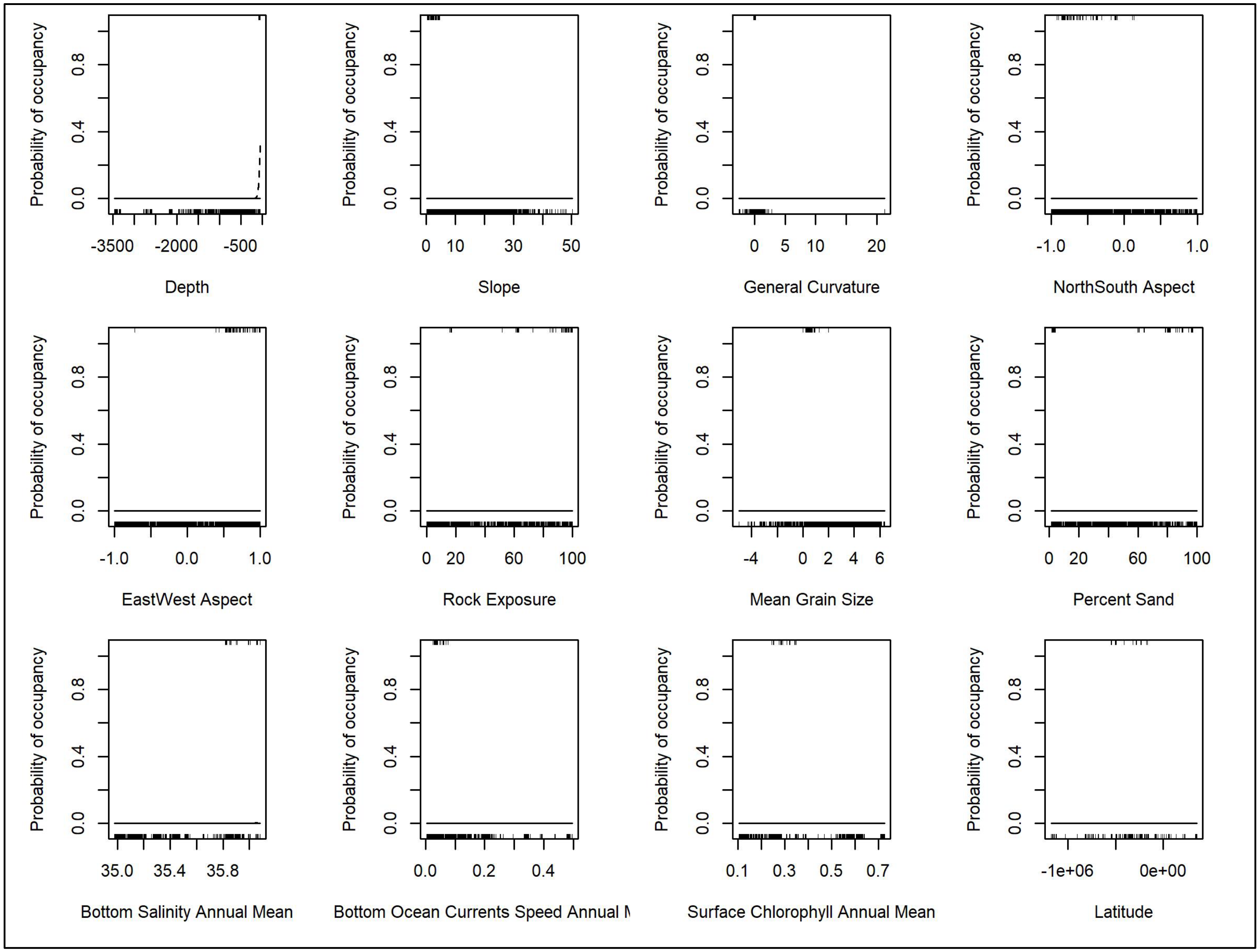

Figure E-11. Marginal effects of the predictors on the predicted occurrence of *Muricea*.
The y-axes show the predicted occurrence for *Muricea* for values of each environmental predictor (the x-axes). The solid line depicts the posterior median occupancy probability, while the dashed lines depict the 95% credible interval. Tick marks at the top and bottom (i.e., rug plots) of each plot indicate the sampled predictor values at which *Muricea* was observed to be present (top) or absent (bottom). The marginal effects plots should be interpreted with caution because they illustrate the estimated effects of each predictor while all others are set at their mean value (i.e., each plot ignores the realized range of effects from all predictors).

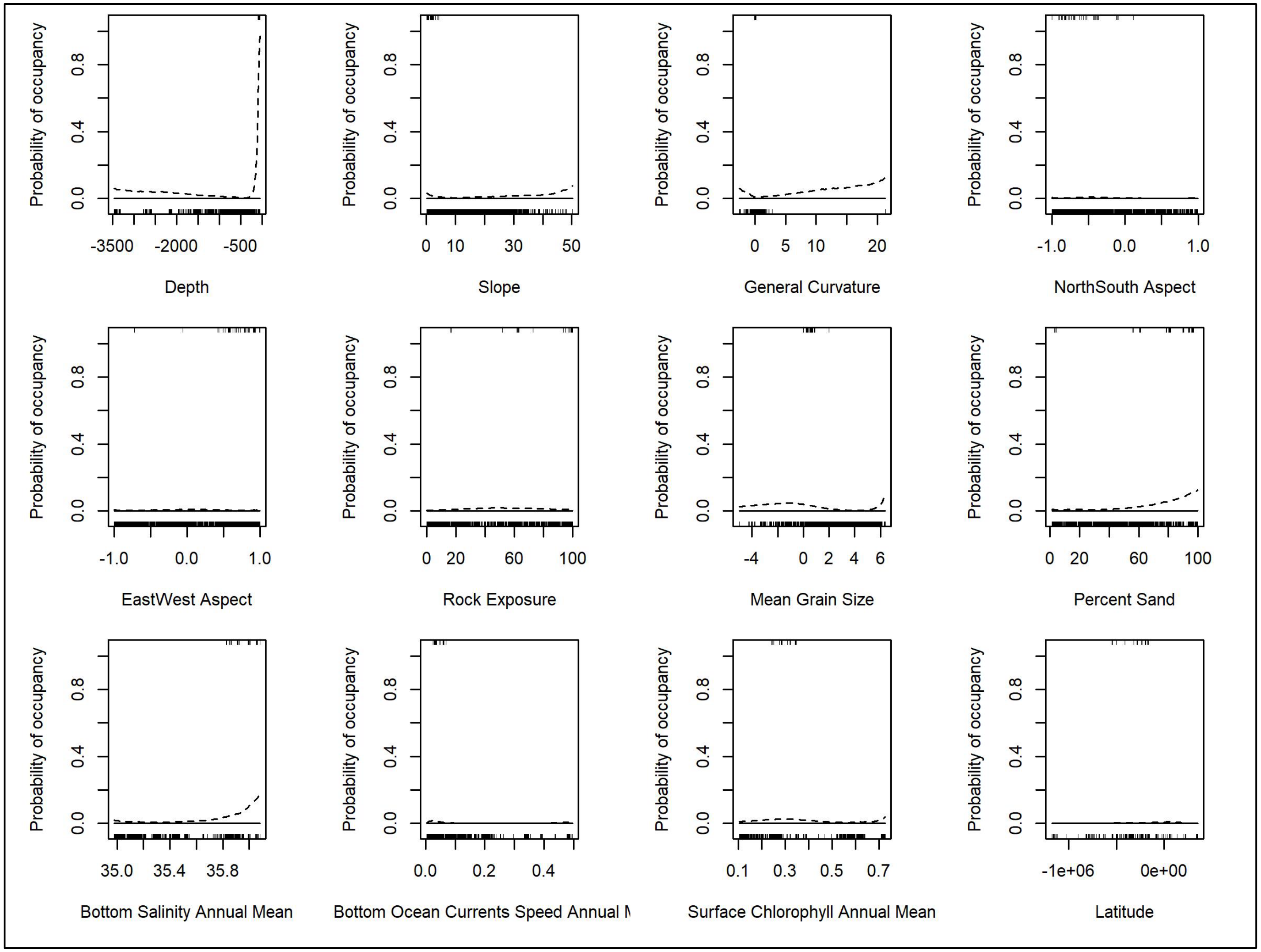

Figure E-12. Marginal effects of the predictors on the predicted occurrence of *Thesea*.
The y-axes show the predicted occurrence for *Thesea* for values of each environmental predictor (the x-axes). The solid line depicts the posterior median occupancy probability, while the dashed lines depict the 95% credible interval. Tick marks at the top and bottom (i.e., rug plots) of each plot indicate the sampled predictor values at which *Thesea* was observed to be present (top) or absent (bottom). The marginal effects plots should be interpreted with caution because they illustrate the estimated effects of each predictor while all others are set at their mean value (i.e., each plot ignores the realized range of effects from all predictors).

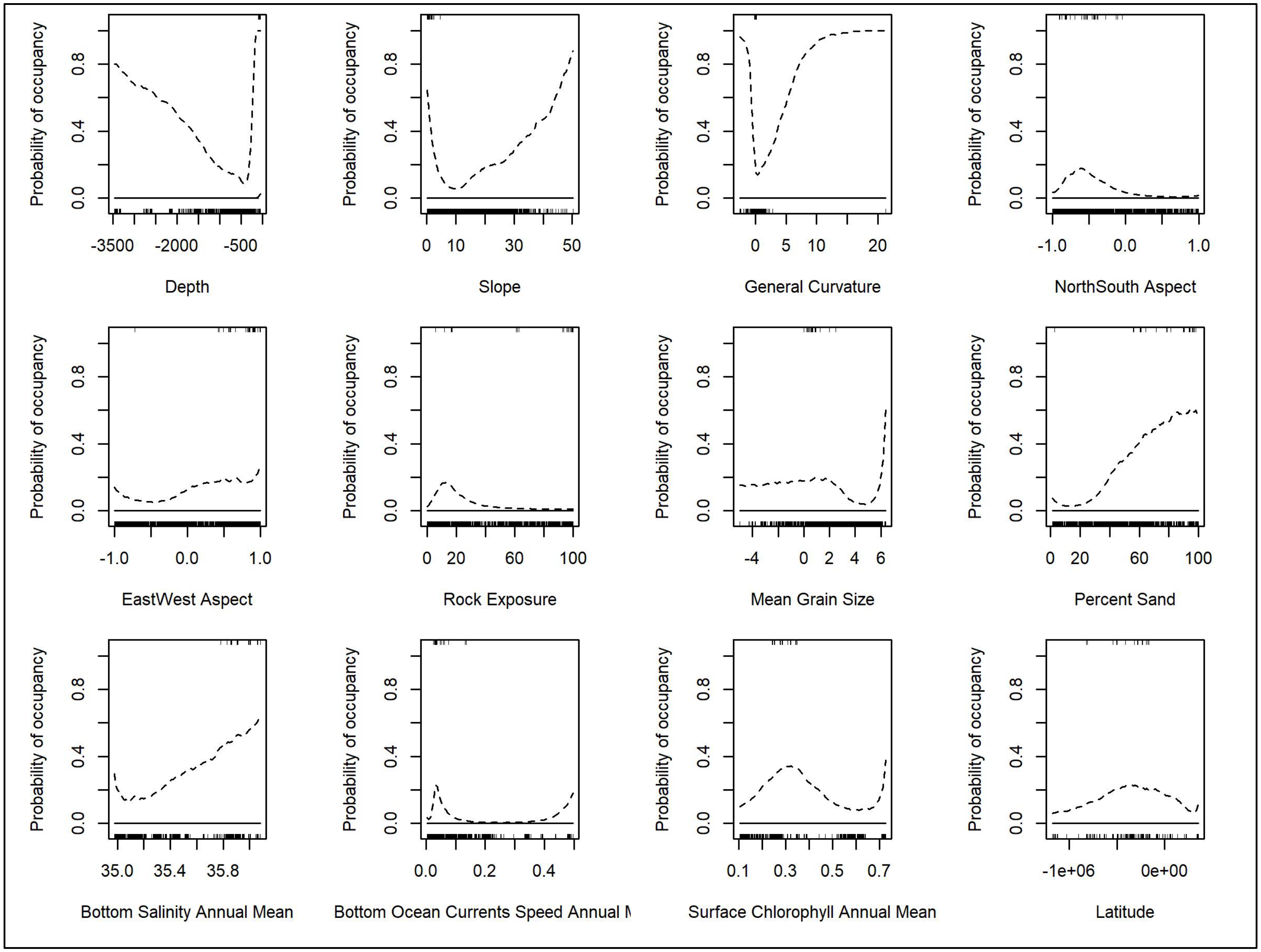

Figure E-13. Marginal effects of the predictors on the predicted occurrence of *Nicella*.
The y-axes show the predicted occurrence for *Nicella* for values of each environmental predictor (the x-axes). The solid line depicts the posterior median occupancy probability, while the dashed lines depict the 95% credible interval. Tick marks at the top and bottom (i.e., rug plots) of each plot indicate the sampled predictor values at which *Nicella* was observed to be present (top) or absent (bottom). The marginal effects plots should be interpreted with caution because they illustrate the estimated effects of each predictor while all others are set at their mean value (i.e., each plot ignores the realized range of effects from all predictors).

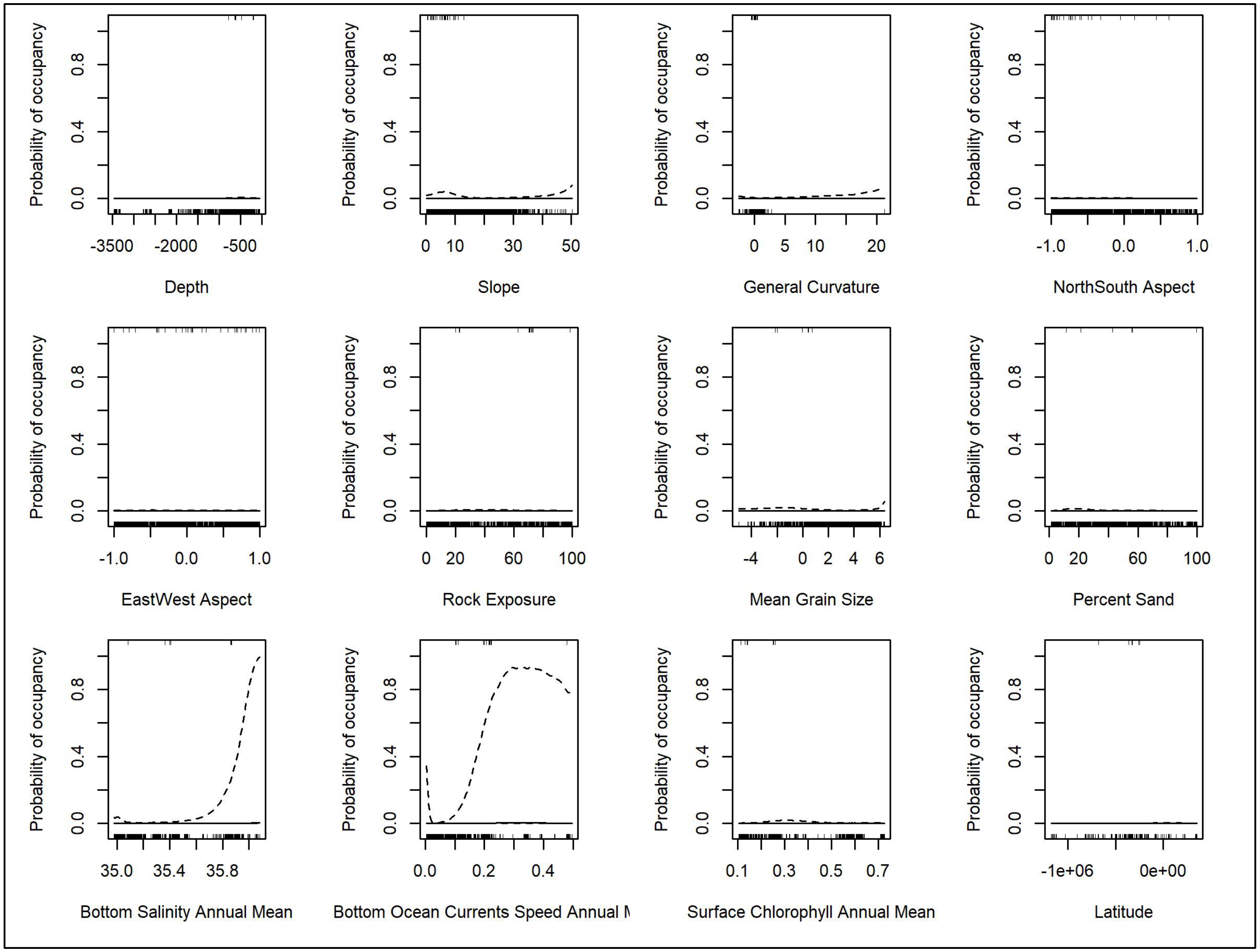

Figure E-14. Marginal effects of the predictors on the predicted occurrence of *Callogorgia*.
The y-axes show the predicted occurrence for *Callogorgia* for values of each environmental predictor (the x-axes). The solid line depicts the posterior median occupancy probability, while the dashed lines depict the 95% credible interval. Tick marks at the top and bottom (i.e., rug plots) of each plot indicate the sampled predictor values at which *Callogorgia* was observed to be present (top) or absent (bottom). The marginal effects plots should be interpreted with caution because they illustrate the estimated effects of each predictor while all others are set at their mean value (i.e., each plot ignores the realized range of effects from all predictors).

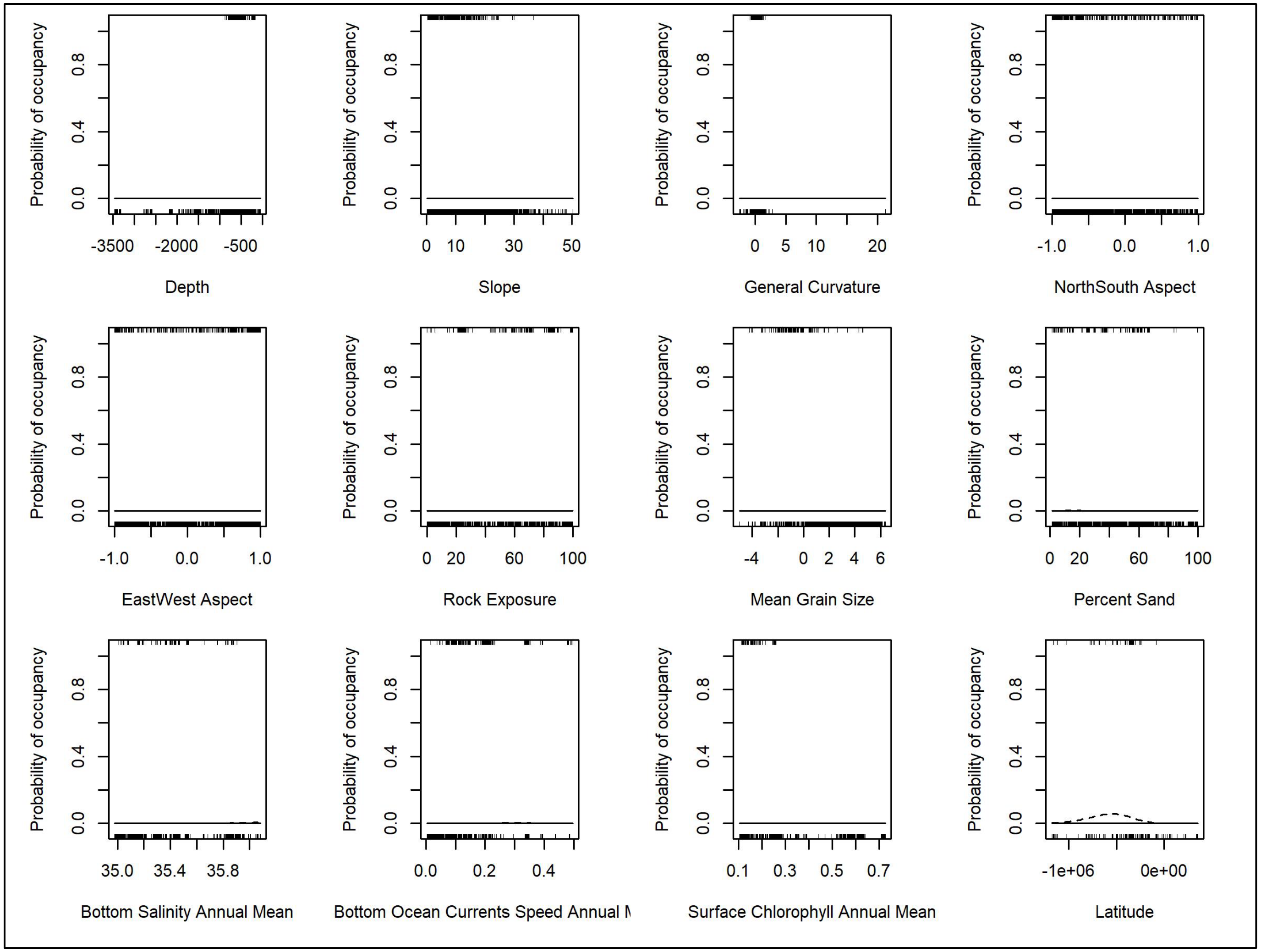

Figure E-15. Marginal effects of the predictors on the predicted occurrence of *Plumarella*.
The y-axes show the predicted occurrence for *Plumarella* for values of each environmental predictor (the x-axes). The solid line depicts the posterior median occupancy probability, while the dashed lines depict the 95% credible interval. Tick marks at the top and bottom (i.e., rug plots) of each plot indicate the sampled predictor values at which *Plumarella* was observed to be present (top) or absent (bottom). The marginal effects plots should be interpreted with caution because they illustrate the estimated effects of each predictor while all others are set at their mean value (i.e., each plot ignores the realized range of effects from all predictors).

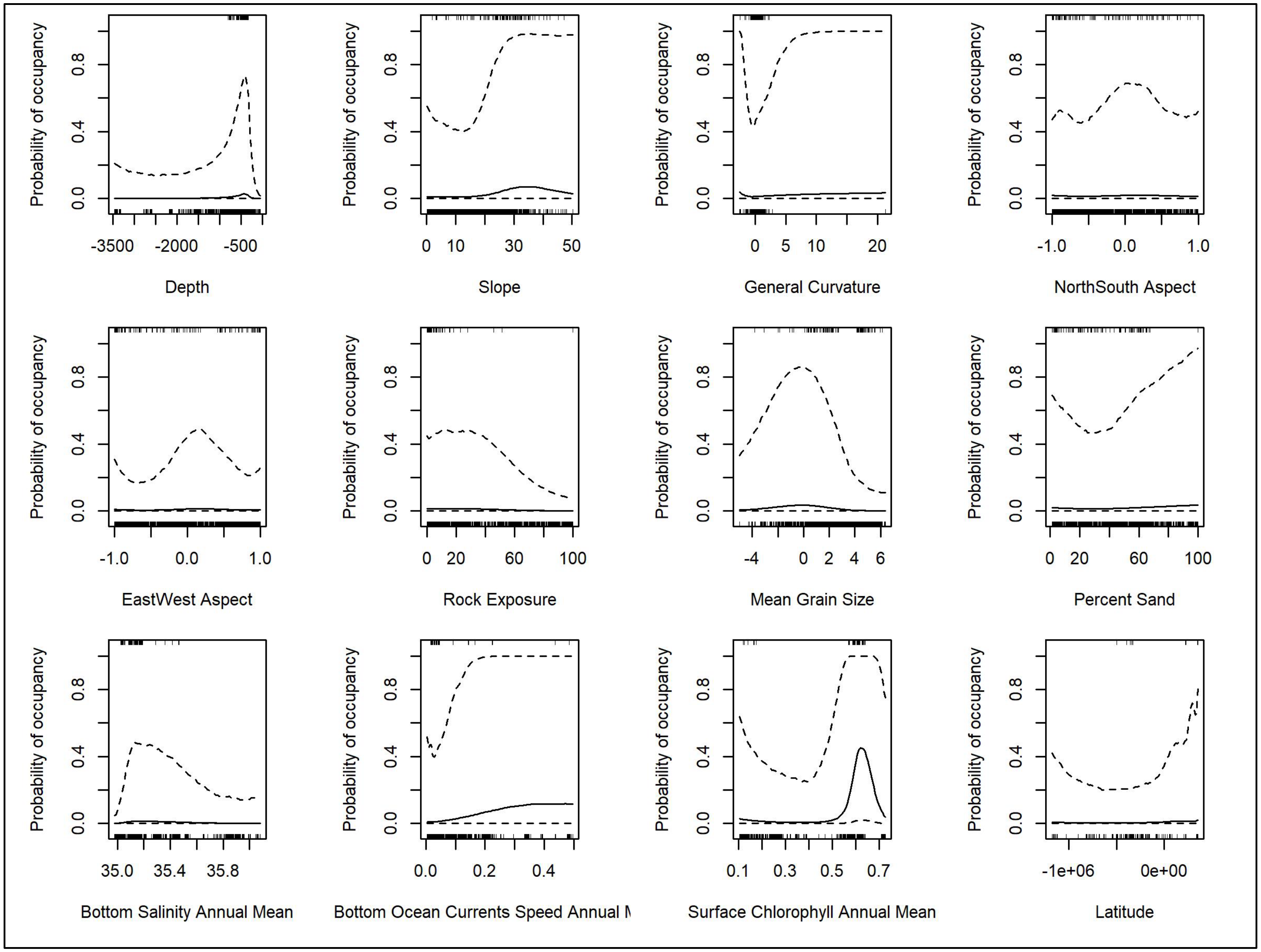

Figure E-16. Marginal effects of the predictors on the predicted occurrence of *Anthothela*.

The y-axes show the predicted occurrence for *Anthothela* for values of each environmental predictor (the x-axes). The solid line depicts the posterior median occupancy probability, while the dashed lines depict the 95% credible interval. Tick marks at the top and bottom (i.e., rug plots) of each plot indicate the sampled predictor values at which *Anthothela* was observed to be present (top) or absent (bottom). The marginal effects plots should be interpreted with caution because they illustrate the estimated effects of each predictor while all others are set at their mean value (i.e., each plot ignores the realized range of effects from all predictors).

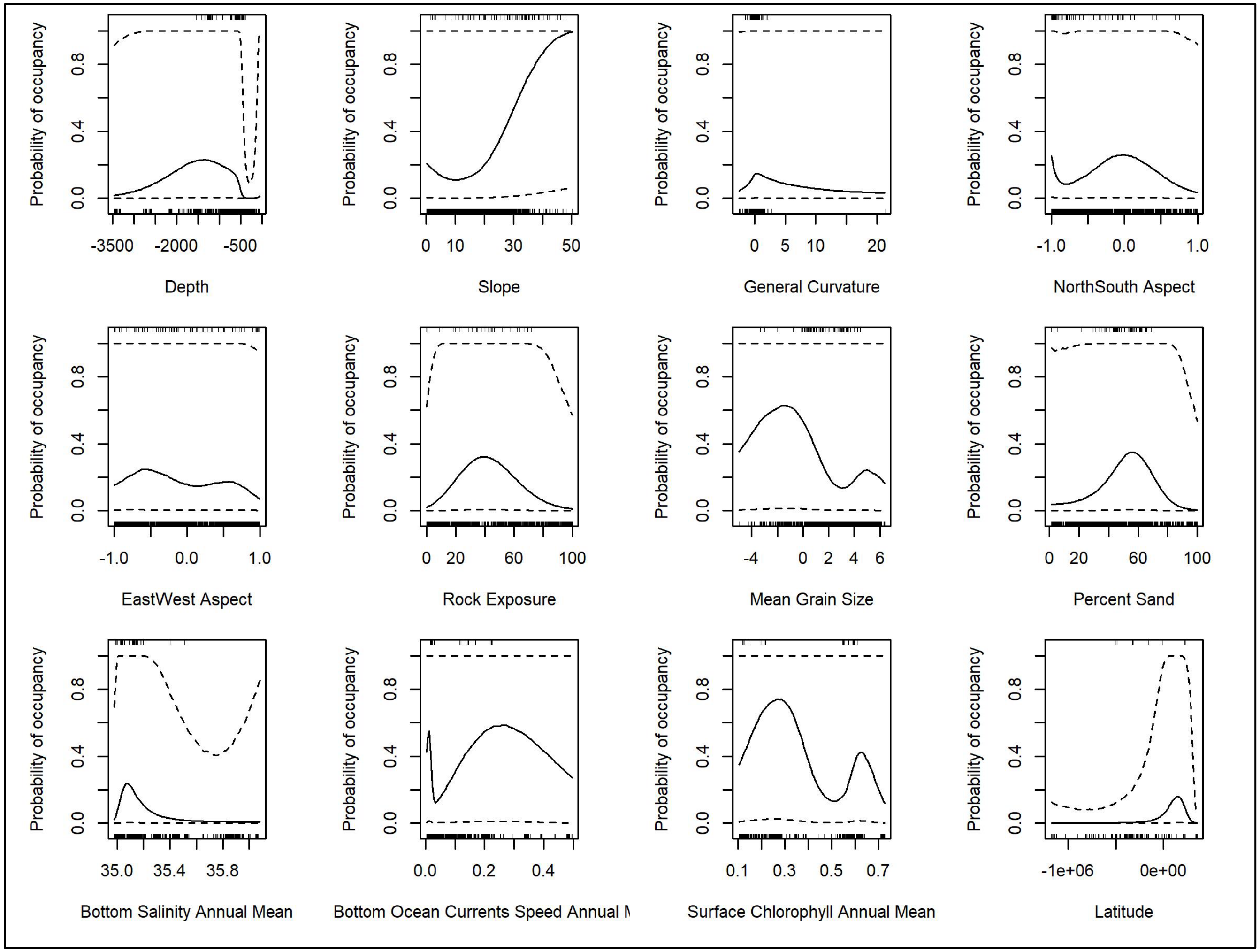

Figure E-17. Marginal effects of the predictors on the predicted occurrence of *Acanthogorgia*.
The y-axes show the predicted occurrence for *Acanthogorgia* for values of each environmental predictor (the x-axes). The solid line depicts the posterior median occupancy probability, while the dashed lines depict the 95% credible interval. Tick marks at the top and bottom (i.e., rug plots) of each plot indicate the sampled predictor values at which *Acanthogorgia* was observed to be present (top) or absent (bottom). The marginal effects plots should be interpreted with caution because they illustrate the estimated effects of each predictor while all others are set at their mean value (i.e., each plot ignores the realized range of effects from all predictors).

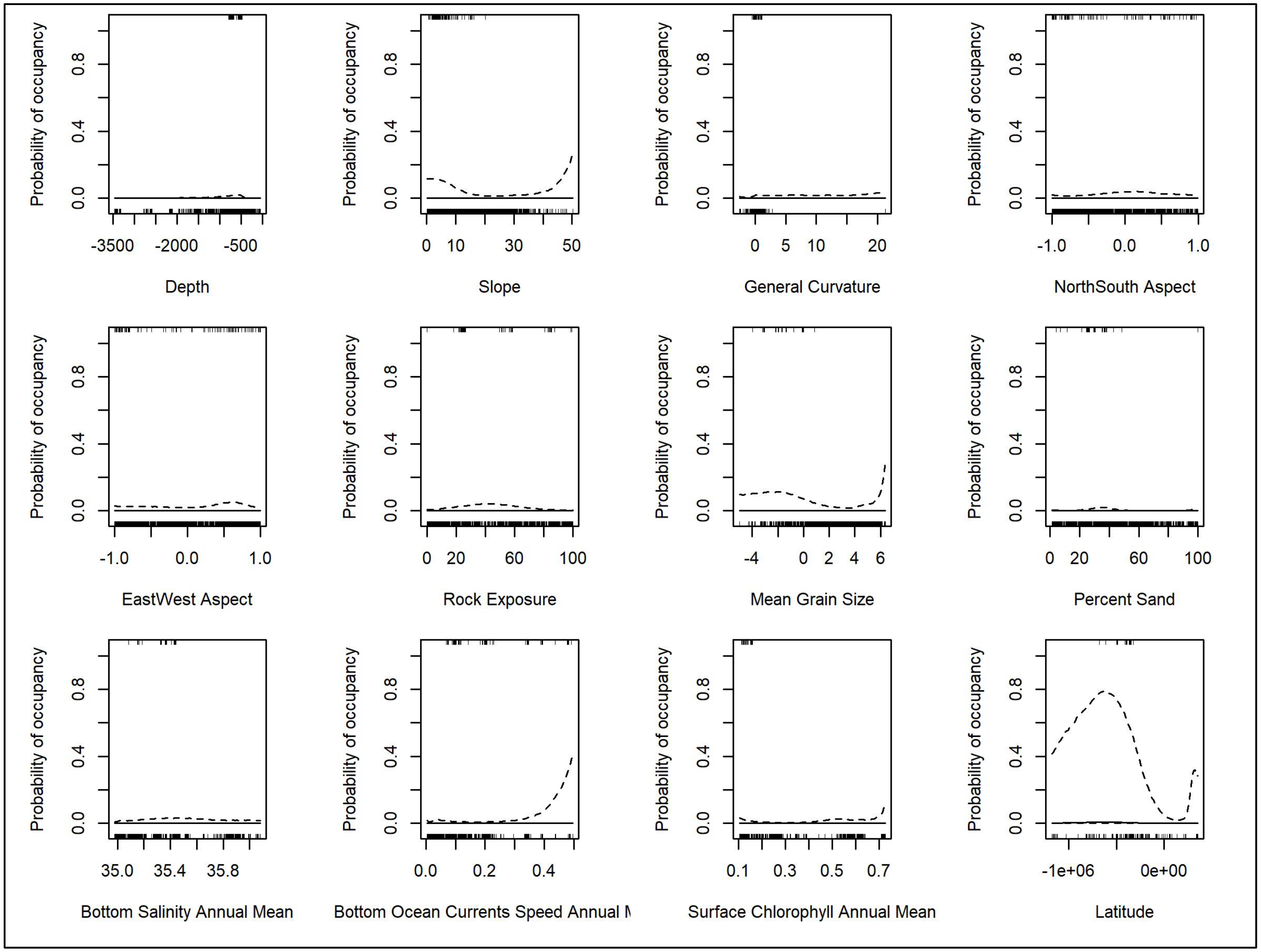

Figure E-18. Marginal effects of the predictors on the predicted occurrence of *Eunicella*.
The y-axes show the predicted occurrence for *Eunicella* for values of each environmental predictor (the x-axes). The solid line depicts the posterior median occupancy probability, while the dashed lines depict the 95% credible interval. Tick marks at the top and bottom (i.e., rug plots) of each plot indicate the sampled predictor values at which *Eunicella* was observed to be present (top) or absent (bottom). The marginal effects plots should be interpreted with caution because they illustrate the estimated effects of each predictor while all others are set at their mean value (i.e., each plot ignores the realized range of effects from all predictors).

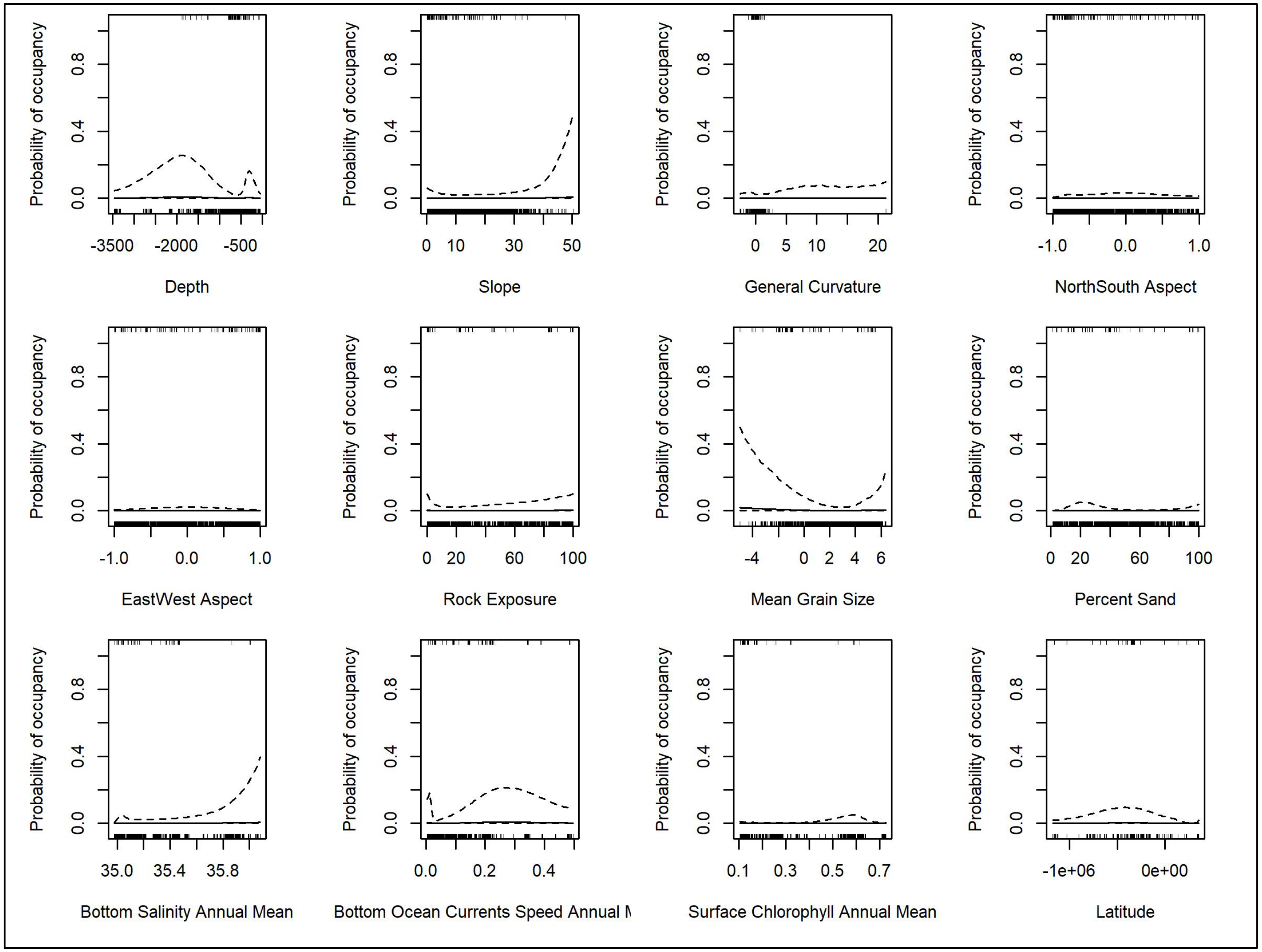

Figure E-19. Marginal effects of the predictors on the predicted occurrence of *Paramuricea*.
The y-axes show the predicted occurrence for *Paramuricea* for values of each environmental predictor (the x-axes). The solid line depicts the posterior median occupancy probability, while the dashed lines depict the 95% credible interval. Tick marks at the top and bottom (i.e., rug plots) of each plot indicate the sampled predictor values at which *Paramuricea* was observed to be present (top) or absent (bottom). The marginal effects plots should be interpreted with caution because they illustrate the estimated effects of each predictor while all others are set at their mean value (i.e., each plot ignores the realized range of effects from all predictors).

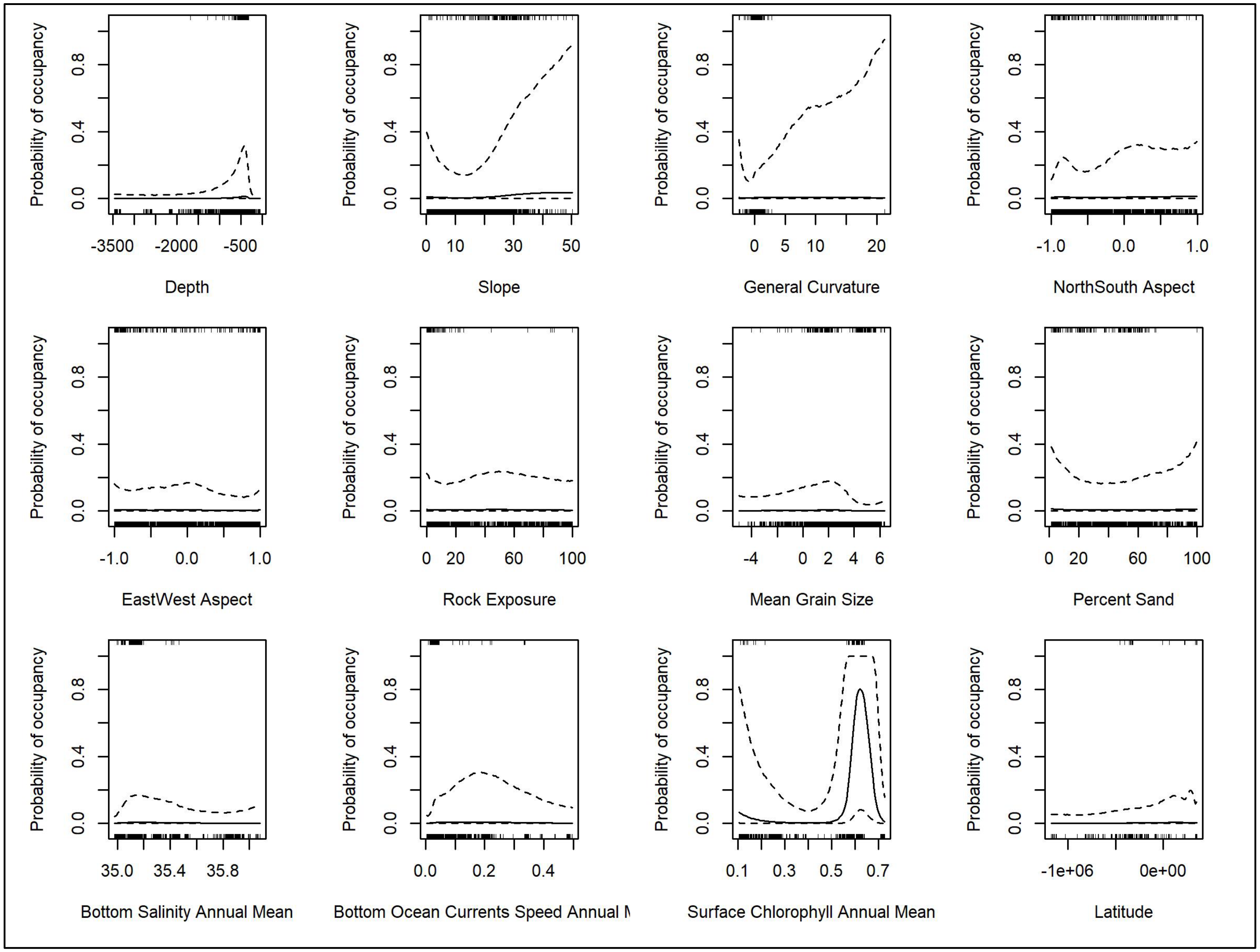

Figure E-20. Marginal effects of the predictors on the predicted occurrence of *Paragorgia*.
The y-axes show the predicted occurrence for *Paragorgia* for values of each environmental predictor (the x-axes). The solid line depicts the posterior median occupancy probability, while the dashed lines depict the 95% credible interval. Tick marks at the top and bottom (i.e., rug plots) of each plot indicate the sampled predictor values at which *Paragorgia* was observed to be present (top) or absent (bottom). The marginal effects plots should be interpreted with caution because they illustrate the estimated effects of each predictor while all others are set at their mean value (i.e., each plot ignores the realized range of effects from all predictors).

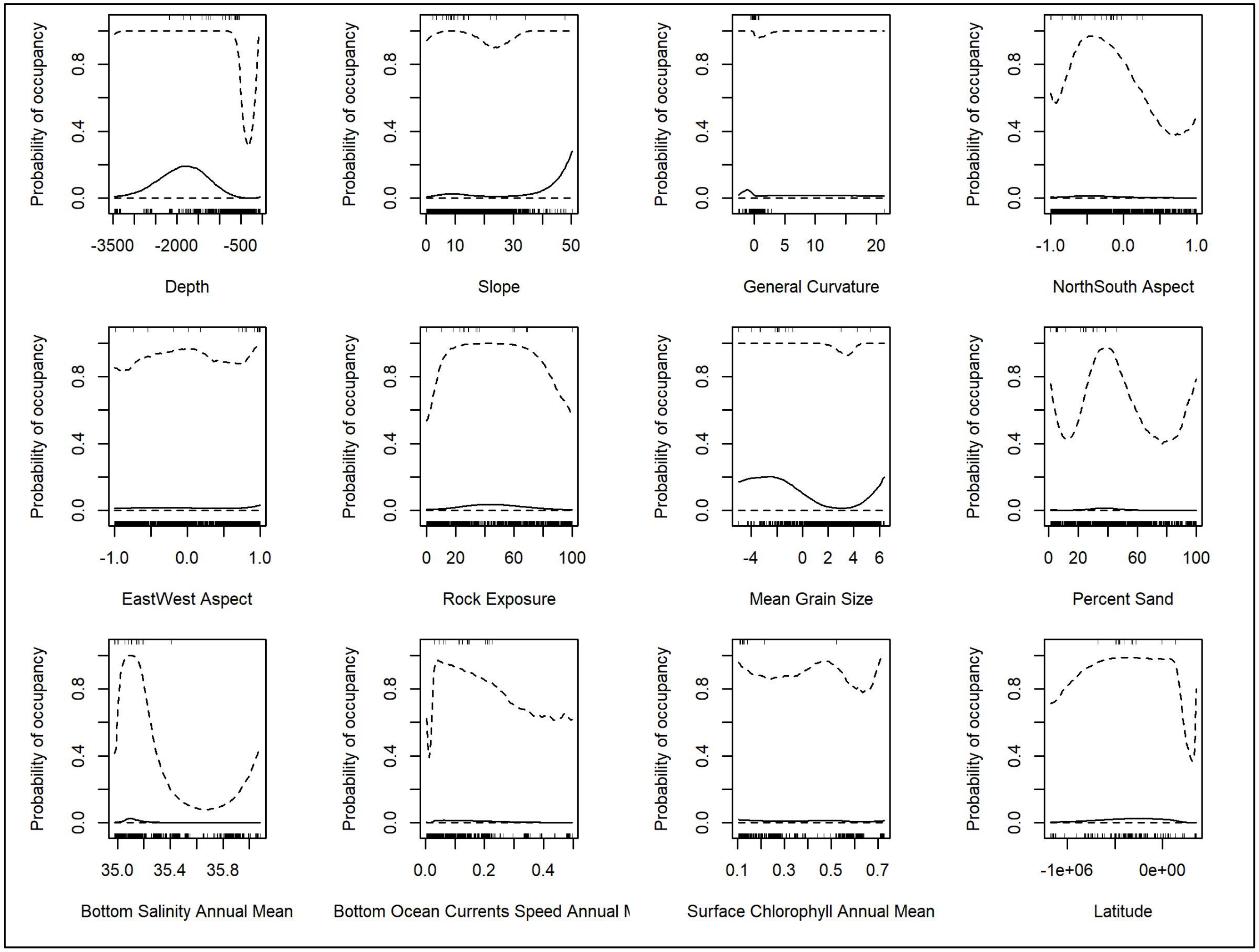

Figure E-21. Marginal effects of the predictors on the predicted occurrence of *Chrysogorgia*.
The y-axes show the predicted occurrence for *Chrysogorgia* for values of each environmental predictor (the x-axes). The solid line depicts the posterior median occupancy probability, while the dashed lines depict the 95% credible interval. Tick marks at the top and bottom (i.e., rug plots) of each plot indicate the sampled predictor values at which *Chrysogorgia* was observed to be present (top) or absent (bottom). The marginal effects plots should be interpreted with caution because they illustrate the estimated effects of each predictor while all others are set at their mean value (i.e., each plot ignores the realized range of effects from all predictors).

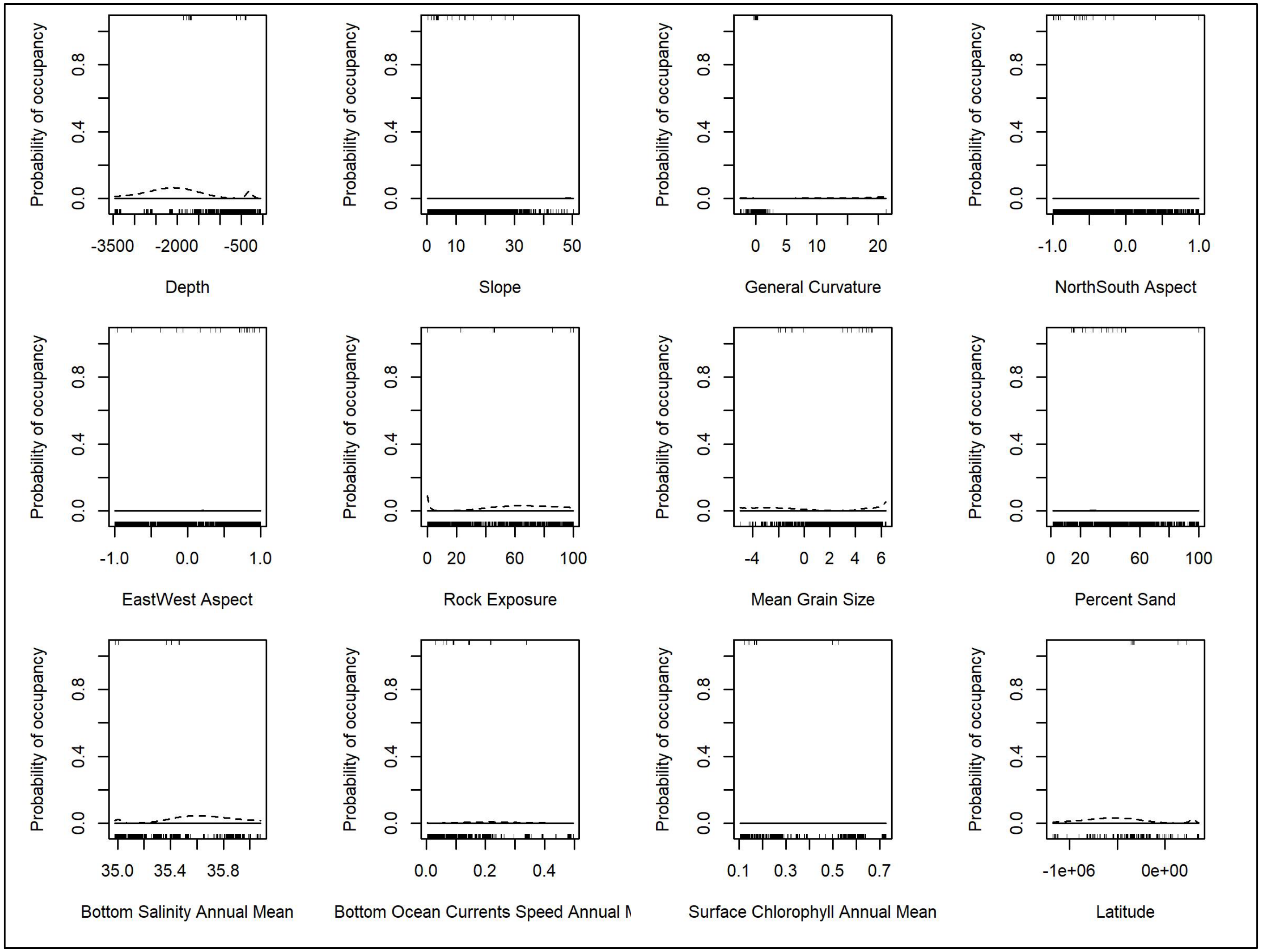

Figure E-22. Marginal effects of the predictors on the predicted occurrence of *Acanella*.
The y-axes show the predicted occurrence for *Acanella* for values of each environmental predictor (the x-axes). The solid line depicts the posterior median occupancy probability, while the dashed lines depict the 95% credible interval. Tick marks at the top and bottom (i.e., rug plots) of each plot indicate the sampled predictor values at which *Acanella* was observed to be present (top) or absent (bottom). The marginal effects plots should be interpreted with caution because they illustrate the estimated effects of each predictor while all others are set at their mean value (i.e., each plot ignores the realized range of effects from all predictors).

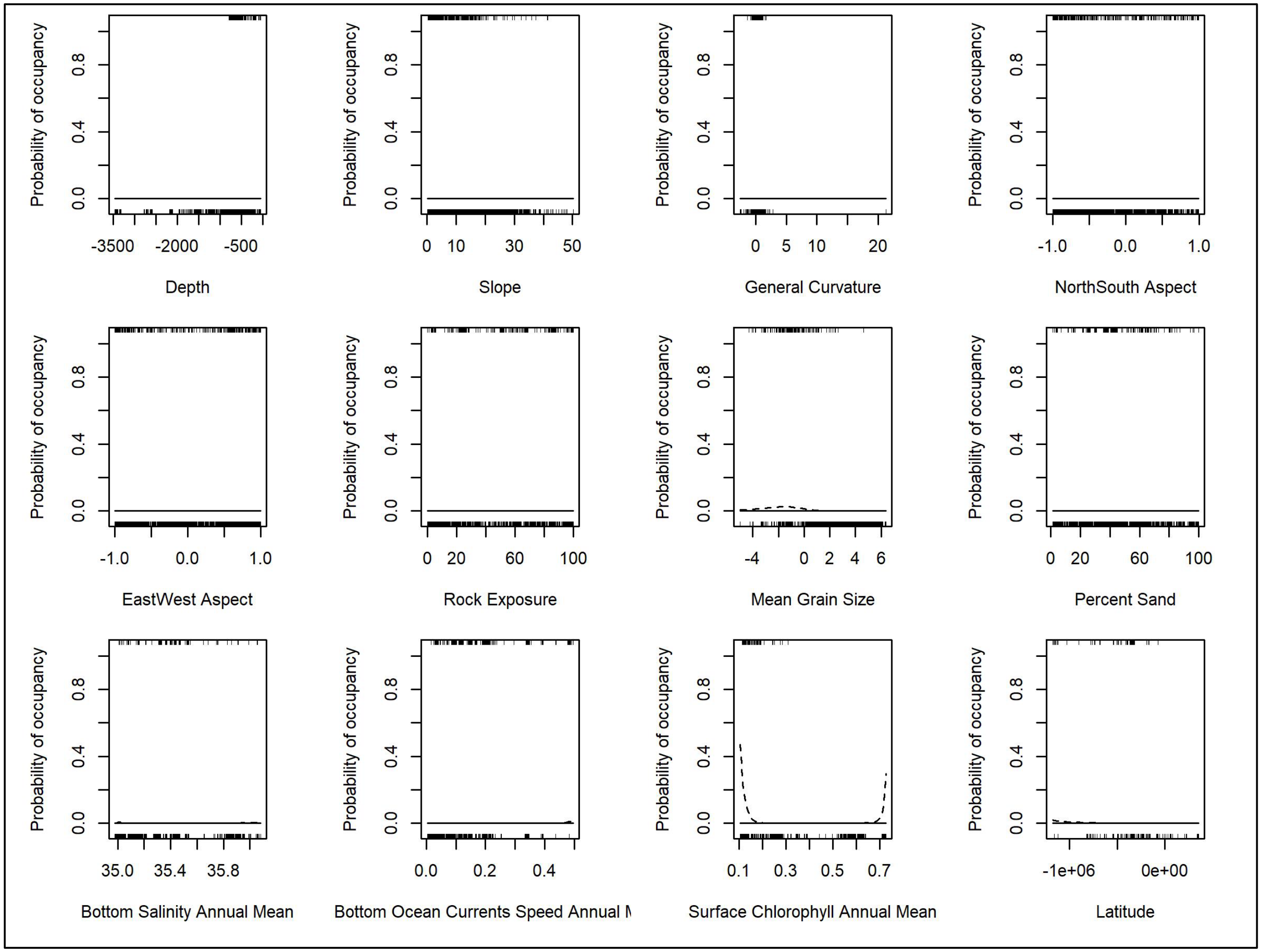

Figure E-23. Marginal effects of the predictors on the predicted occurrence of Stylasteridae.
The y-axes show the predicted occurrence for Stylasteridae for values of each environmental predictor (the x-axes). The solid line depicts the posterior median occupancy probability, while the dashed lines depict the 95% credible interval. Tick marks at the top and bottom (i.e., rug plots) of each plot indicate the sampled predictor values at which Stylasteridae was observed to be present (top) or absent (bottom). The marginal effects plots should be interpreted with caution because they illustrate the estimated effects of each predictor while all others are set at their mean value (i.e., each plot ignores the realized range of effects from all predictors).

U.S. Department of the Interior (DOI)
DOI protects and manages the Nation's natural resources and cultural heritage; provides scientific and other information about those resources; and honors the Nation’s trust responsibilities or special commitments to American Indians, Alaska Natives, and affiliated island communities.

Bureau of Ocean Energy Management (BOEM)
BOEM’s mission is to manage development of U.S. Outer Continental Shelf energy and mineral resources in an environmentally and economically responsible way.

BOEM Environmental Studies Program
The mission of the Environmental Studies Program is to provide the information needed to predict, assess, and manage impacts from offshore energy and marine mineral exploration, development, and production activities on human, marine, and coastal environments. The proposal, selection, research, review, collaboration, production, and dissemination of each of BOEM’s Environmental Studies follows the DOI Code of Scientific and Scholarly Conduct, in support of a culture of scientific and professional integrity, as set out in the DOI Departmental Manual (305 DM 3).